Visual Adaptations and Behavioural Strategies to Detect and Catch Small Targets

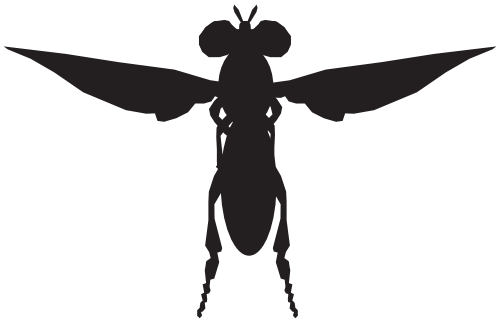

Samuel T Fabian

Physiology Development and Neuroscience
University of Cambridge

This dissertation is submitted for the degree of
Doctor of Philosophy

Clare College July 2019

Declaration

This dissertation is the result of my own work and includes nothing which is the outcome of work done in collaboration except as declared in the Preface and specified in the text.

It is not substantially the same as any that I have submitted, or, is being concurrently submitted for a degree or diploma or other qualification at the University of Cambridge or any other University or similar institution except as declared in the Preface and specified in the text. I further state that no substantial part of my dissertation has already been submitted, or, is being concurrently submitted for any such degree, diploma or other qualification at the University of Cambridge or any other University or similar institution except as declared in the Preface and specified in the text.

It does not exceed the prescribed word limit for a PhD thesis in biology (60000 words).

Samuel T Fabian
July 2019

Acknowledgements

First and foremost, I would like to thank my supervisor, Paloma Gonzalez-Bellido. It's a great honour to be your first PhD student and a pleasure to watch the new lab grow and develop into a close, productive, and supportive family. I am extremely grateful for the opportunity you have given me and look forward to our collaborations in the future. Great thanks are also due to Trevor Wardill for his patience and technical expertise, which underpinned much of the apparatus and procedures I used to record data.

Thank you to Mary Sumner for every day spent sweating through Pennsylvania summers and being a companion throughout the most trying moments of field research. I also could not have asked to be joined by finer nestmates than Jack Supple, Rachael Feord, and Sergio Rossoni, who's company through every up and down, I miss more every day. Milly Sharkey and Kate Feller have both been irreplaceable sources of scientific and career advice, and I thank them also for their patience.

I would like to thank the US Air Force Office for Scientific Research for funding my PhD. I would also like to thank those within Nature-Inspired Flight Technologies and Ideas (NIFTI) group for their insightful discourse.

I would like to thank every member of Clare College MCR who have made my time in Cambridge overwhelmingly enjoyable. I hope I leave an impression on more than just an armchair. I would also like to thank all at Street Farm, for their patience and kindness; I could not have written up in a more idyllic location.

Lastly, I would like to thank my family. This is especially to my mum and dad, without whose tireless intellectual curiosity, academic advice, love and support, not one word of my thesis would ever have been written. Thank you for choosing a house with a pond in the back garden; for me, this all started by its edge.

Abstract

Predatory behaviours are ideal for studying the limits of performance and control within animals. Predation naturally creates a competition between the sensors and physiology of predator and prey. Aerial predation demonstrates the greatest feats of physical performance, demanding the highest speeds and accelerations whilst both predator and prey are free to pitch, yaw, and roll. These high speeds and degrees of rotational freedom make control a complex problem. However, from the perspective of the researcher attempting to decipher the control laws that underpin predator guidance, the question is made more soluble by the predator's fixation on its target. The goal of the pursuer is clear, to contact the target, and thus their systems are focused on the optimization of that action. This is as opposed to more mundane activities, where conflicting interests compete for the attention and behavioural response of the animal.

In order to study the necessary trade-offs that underpin aerial predation, this thesis will focus on the hunting behaviour of two fly species. The first is a robber fly, *Holcocephala fusca*, on which the majority of the first two chapters focus. Secondarily, work with the killer fly *Coenosia attenuata* will be included in the latter two chapters as a direct contrast to results from *Holcocephala*. Both are miniature dipteran predators, but not closely related. The structure of this thesis is broken into six chapters, summarised in the following list:

1. The compound eye of insects generally has much poorer resolution than that of camera-type eyes. Poor resolution is exacerbated in smaller insects that cannot commit the resources required for eyes with large lenses that facilitate high spatial resolution. *Holcocephala* has developed a small number of facets into a forward-facing acute zone where the spatial acuity is reduced to ~0.28°, rivalling the very best resolution of any compound eye. The only compound eyes with a comparable spatial resolution belong to dragonflies, in excess of an order of magnitude larger than *Holcocephala*.

2. Numerous potential targets may be airborne within the visual range of a predator. Not all of these may be suitable. Chasing unsuitable targets may waste energy or result in direct harm should they turn out to be larger than the predator can overcome. It is thus

a strong imperative for a predator to filter the targets it takes after. Targets silhouetted against the sky display a paucity of cues that a predator could use to determine their size. *Holcocephala* displays acute size selectivity towards smaller targets. This selectivity goes beyond heuristic rules and size/speed ratios. Instead, *Holcocephala* appears able to determine absolute size and distance of targets.

3. Both *Holcocephala* and *Coenosia* intercept targets, heading for where the target is going to be in the future rather than its current location. Both species plot trajectories in keeping with the guidance law of proportional navigation, an algorithm derived for modern guided missiles. There are key differences evident in the internal physiological constants applied to the control system between the species. These differences are likely linked to the specific environmental conditions and visual physiologies of the flies, especially the range at which targets are attacked.

4. Stemming from the use of the proportional navigational framework, this chapter dives into the intricacies of gain and the weighting of the navigational constant, and the geometric factors that underpin the control effort and eventual success of the control system.

5. "Falcon-diving" can be found in killer flies dropping from their enclosure ceiling, in which they miss targets after diving towards them. Through proportional navigation, it can be demonstrated that the navigational system combined with excessive speed results in acceleration demands the body cannot match.

6. *Holcocephala* is capable of evading static obstacle whilst intercepting targets. Application of proportional navigation and a secondary obstacle-evasive controller can demonstrate where the fly is combining multiple inputs to guide its heading.

Table of contents

List of Figures

Preface

Fundamental Questions

Speed and control of movement are iconic features of animal life. Few other groups of organisms can sustain as high a speed of movement, nor so effect their direction and destination as multicellular animals. Within animals, there is tremendous variation in the medium and method of travel. These include the near-passive planktonic drifting of many marine animals [1], through to the 30,000 km round trip migration of bar-tailed godwits from Alaska to New Zealand [2]. Animals swim, walk, crawl, swing, jump, glide, and fly. Out of these, it is flight that covers the greatest distances [2], acquires the greatest speed [3], and, arguably, is the hardest to achieve.

Powered flight is difficult. To push oneself through the air has some of the highest (sustained) power requirements of any form of transport [4], although for the distance covered, it is more energetically favourable than running [5]. Unlike in water, animals cannot counteract their weight through buoyancy, there are no neutrally buoyant species in air due to its near 3 orders of magnitude lower density. Instead animals must generate lift by passing themselves or parts of their anatomies (i.e. flapping) through the air with enough speed that they generate pressure imbalances and vortices, using the motion of the air to counteract their own weight. The challenges involved in flight make it an uncommonly derived trait, evolving in only 4 separate lineages [6]. Nevertheless, the extant examples of these lineages, birds, bats, and insects, have proliferated into extremely diverse groups and major players within near every terrestrial ecosystem. Insects were the first animals to evolve powered flight, and currently have the most species of any class of multicellular life, by no small margin, with estimates of the currently described species number at near 1 million [7] and the estimates of the true insect diversity condensing around 5 times this value [8]. While much unrecorded insect diversity may still lie within the flightless group of springtails (Collembola) [9], the vast majority of insect species have flight as an integral part of the their adult lifestyle [10].

It is not trivial to attribute flight as the sole cause of the proliferation of insect species, though its importance is frequently made [4, 11, 12]. Insects' small size, tough waterproof cuticles, and adaptable chewing mouthparts have all clearly played their role. However, flight is a primary trait that distinguishes (most) insects from all other arthropod groups [6], none of which are capable of powered flight. Only ballooning spiders are capable of being suspended in the air column for extended periods of time, albeit as aerial plankton [13, 14]. Insects occupy a characteristic set of conditions within flight due to their small size, with intermediate Reynolds numbers ($10<Re<1000$) [15] which affect the flow patterns of the air around them. Insects, most frequently, would be unable to support themselves under conventional steady-state flight, instead relying on unsteady leading-edge vortices amongst other effects that enable them to maintain high lift-to-drag ratios at high angles of attack [4, 16–19]. This, along with their relatively light wings, leads to particular prevalence of flight behaviours such as true hovering [20] and effects the manner of flight manoeuvring and control within insects [21, 6].

Flight not only presents a biomechanical challenge, but also a sensory one. When anchored to the ground, an animal can use the stability of its points of contact to maintain as a cue by which to orient its navigation. Navigating the environment is also broadly simplified by adherence to a surface plane, when walking, running, or jumping. A flying insect must be able to navigate throughout 3 spatial dimensions, remaining both flight stable and navigating to objectives. By taking to the air, insects have three axes along which they can freely rotate without anchor; roll, pitch, and yaw, and the unstable nature of the flight of most insects requires constant feedback as to their rotation around each of these [6, 6]. It is therefore unsurprising that insects have developed multiple sensory systems, each with their own dynamic ranges to sense their environment, their place in it, and the objects that surround them [22]. The primary sense for flight navigation and stability, in insects, is vision. Image forming vision is for almost all insects, mediated by compound eyes [23]. Within Chapter 1 of this thesis, we will see that insects face a trade off between physical eye size, resolution, sensitivity, and field of view. Secondly, in Chapter 2, we will see how insects small size again potentially restricts them in the information that can be gained about distant objectives.

On top of this, most regularly flying insect species have an additional set of eyes called ocelli, but these are 'camera' type eyes that each have a single lens to transmit light onto a retina of multiple photoreceptors below [24]. These eyes are generally grouped in threes, with one medial and two latera. Ocelli are not generally image forming, instead they act as extremely fast light-level sensors. Their function is in quickly sensing the insect's rotation by detecting the visual movement of the brightest regions of the visual field, which should generally correlate with the sky above [25, 26]. There are many other means of sensing

rotation in flight, for instance, the wide-field optic flow across the retina of the compound eyes [27], or the torsion on wings encoded by small strain sensors called sensilla [28]. In the true flies (Diptera) and adult male Strepsiptera, one of the wing pairs (hindwings in Diptera, forewings in Strepsiptera) are reduced to clubs called halteres that beat counterphase with the wings [29]. These clubs have sensilla that enable them to detect the flexion along the club's length due to Coriolis forces created by the club beating back and forth while the body is rotating [29, 30]. Chapters 3 & 4 will show why rotation detection has importance that stretches beyond maintaining flight stability, into target navigation and obstacle avoidance.

The nature of the objective that a flyer is navigating to will affect the requirements of its navigational systems. For some groups, such as the majority of the beetles (Coleoptera), flight is used as a means of transfer between disparate terrestrial or arboreal resources (e.g. food items etc.) or for dispersal. However, for many groups of aerial insects, their objectives are other aerial insects. Either through the maintenance of a territory (chasing off rivals) [31], the pursuit of potential mates [32], or the interception and consumption of prey [33, 34]. While for the first two of these tasks, merely following a target may be sufficient to achieve the goal, aerial predation fundamentally requires the animal to not only track the target, but also to outperform it. They can do this by either travelling faster or taking a shorter path to a collision point. This is not only represented in the biomechanical supremacy of predator over prey, for instance in manoeuvrability [35, 36], but also in the necessary consequences for the demands of the predators sensory systems, such as visual systems tuned for higher spatial resolution rather than sensitivity [37]. Predation meditated by chasing is the pinnacle of selective pressures for extreme locomotive and sensory performance, potentially second only to agonistic conspecific competition in which adaptations are closely mirrored by competing individuals. For one animal to catch and kill another, they must pit their quest for a meal against the prey items "desire" to survive and reproduce.

The challenges involved can be dissected into being of three distinct levels; target detection, target selection and target interception. These are, of course, artificial separations but they do follow the rough chronology of a predatory interaction. Initially, a predator needs to separate out the presence of a potential target from the patterns of its environment. After a distinct object of interest has been identified within the environment, further filters and assessments are carried out on the received signal to assess whether the target is a suitable one to attack. Finally, there is the question of how a predator must direct its movement to bring about contact with the prey, reacting to the prey's deviations and evasive manoeuvres.

Thesis Scope

The aim of the work discussed in this thesis is to understand the mechanisms underlying aerial predation. Specifically, the three-part target interception challenge, of detection, selection, and approach, using two distinct species of aerial predatory insects. Both species are extremely small (<7mm body length), and thus their aerial behaviour operates under physical conditions distinct from those more frequently studied (i.e. in birds, bats, and larger insects such as dragonflies). To be successful at the task, the animal's physiology must meet this three-part challenge. Detection is dependent on sensor sensitivity. Selection may be dependent on a simple trait (i.e. target size [38]), on identity (i.e. fly vs wasp [39]), or it may take into account energy trade-offs between cost and value of the prey (i.e. optimal diet theory [40]). In every case, an active selection process must result from the computations within the predator's neuronal circuitry. Finally, the challenge of approach is answered by the bio-mechanisation of a pursuit or interception algorithm that uses relative positioning of the target to direct and moderate the velocity of the predator. This work aims to find how these challenges have been resolved by the minute predatory robber fly *Holcocephala fusca*. To do so we have investigated the visual acuity, visual cues, and interception algorithms that this species uses to attack prey. Additionally, we have also conducted a comparative approach where possible, using the muscoid killer flies *Coenosia attenuata*.

Findings on the visual acuity and target selection criteria for *Coenosia* have already been published by other researchers, facilitating a comparative framework across the three key questions raised already. By comparing between these two species, a fine grain variation of environment and tactics can be examined. Meanwhile, comparison of findings from these species to published work on larger animals or human engineered applications will be used to highlight both analogy and divergence due to the specific restrictions and conditions of small size.

Such pairwise comparisons can be used to suggest potential underlying selective pressures and reasons for divergence. Therefore, these comparisons are intended to stimulate routes for discussion and further research. However, it is important to note that comparison between two or even a few species, may not have the power in themselves to conclusively demonstrate the myriad optimality criteria that underpin the research species' solutions to the task of catching aerial prey. By studying a species individually, we can see how its physiology has been adapted. By studying across species, it is hoped we can suggest why the tuning of their physiological parameters are advantageous compared with alternative states.

Biology of Research Species

The Robber Fly, *Holcocephala fusca*

Holcocephala fusca is a minute true fly (Diptera) and belongs to the family Asilidae, termed the robber flies. The robber flies are a group of predatory flies with in excess of 5000 species currently described. *Holcocephala* is a genus with currently at least 40 described species, all of which are, compared with other asilids like *Laphria* or *Microstylum*, small in size (*Holcocephala fusca* body length, 6mm). Across the eastern seaboard of north America, there are three hyper-abundant species [41]: *Holcocephala calva*, *Holcocephala abdominalis*, and *Holcocephala fusca*. *Holcocephala calva* coexist closely with either of the other two species, which are not readily distinguishable [42]. *Holcocephala abdominalis* is the older classification of both species which were split based on the distinction that some samples "appear darkened in colouration" as well as featuring more "slender antennae and legs" [42]. However, given that the separation between the two species is not readily clear, there may be considerable crossover in the literature concerning either species, and they may be synonyms of regional variations of the same species. Qualitative descriptions of the behaviour and habits of *Holcocephala abdominalis* are indistinguishable from observations of the behaviour of *Holcocephala fusca*. In contrast, *Holcocephala calva* are larger, matte grey rather than brown, and sit on perches using a different posture. Within this thesis, the species of robber fly will be referred to as *Holcocephala fusca* or simply by the genus name *Holcocephala*, though references to general behaviours may include papers that discuss *Holcocephala abdominalis*. By referring to the species by its generic name, it is not intended that the results obtained from *H. fusca* here are representative of the genus as a whole. Even between *H. fusca* and the coexisting *H. calva*, there are extensive differences in the ethology of their predatory activity, perch choice, and prey selection [42].

Fig. 1 In both images, the robber fly *Holcocephala fusca* sits in typical posture, looking upwards at the sky above. **(left)** *Holcocephala* in profile, consuming a small rove beetle (Staphylinidae) that has been caught on the wing. **(Right)** *Holcocephala* head on, without prey.

The exact perch selection by *Holcocephala fusca* has not been determined experimentally, however some general observations from time spent in the field are salient. *Holcocephala fusca* occurs in extremely high abundances, in particular open, riparian, environments, to the point at which they occupy a major proportion of the possible perches (i.e. low-lying shrubs or plant tips) within some areas and will compete and knock each other off in order to take over a perch. While *Holcocephala* back-light their targets against the open sky, they tend to find perches where they are in shade [41] and during the middle sections of the day, during which time shade may be scarce, they are far less abundant, returning to their perches again as the shadows begin to lengthen throughout the afternoon [42] (for timings see **Fig. 2**).

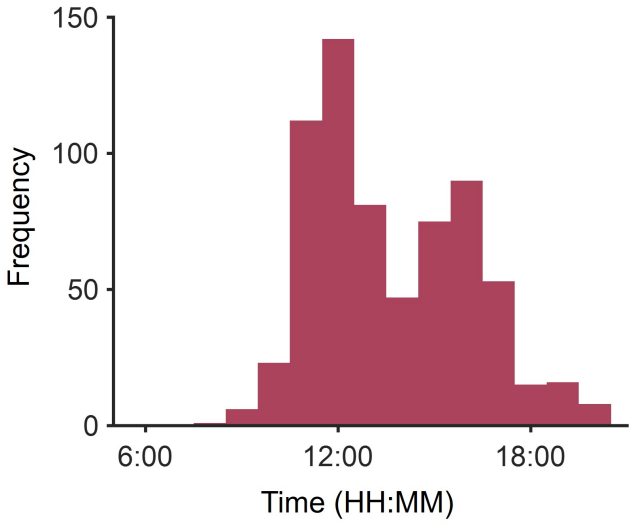

Fig. 2 The frequency of recorded predatory behaviours is compiled against the time of day for 669 recordings (including those that could subsequently not be reconstructed).

Holcocephala generally perch facing diagonally upwards towards the bright sky and fly vertically up towards targets that fly overhead. As objects fly overhead, the flies head-flick with a sharp saccadic movement (i.e. the head jerks to look at the target, covering the intervening angular space rapidly) followed by a slow "tracking motion", extremely similar to those described in dragonflies [43]. These head-cocks may or may not be followed by a take-off.

As with other asilids, the legs and particularly the tarsi are large and bristled. Prey are snatched from the air with the legs and then manipulated in the air so that they can be pierced with the stout proboscis. Asilids are venomous liquid feeders, firstly injecting a concoction of different compounds through their proboscis, some of which have neurotoxic effects, immobilizing prey [44]. Secondly, the asilids are suggested to switch to injecting proteins with enzymatic function to liquify and externally digest the prey before consumption. *Holcocephala* visibly manipulate prey with all six legs whilst hovering, and will drop some targets immediately after they are caught, particularly coleoptera [42], potentially representing difficulty in getting through the tough beetle cuticle.

The sexual behaviour of *Holcocephala* is of importance when considering their predatory behaviour, as interactions with conspecifics have different constraints and incentives than predatory interactions. Fortunately, the courtship within *Holcocephala* radically differs from their predatory interceptions. Instead of males pursuing females that fly past, males take to the wing and fly from plant to plant. Once near prospective perches, the male *Holcocephala*

will hover and "scan" them, oscillating from side to side and working through the branches until a perched individual is located. Once another *Holcocephala* is located, the male will surge forward and attempt to grapple with it. Males were observed performing this behaviour to both males and females of their own species, but also males and females of *Holcocephala calva*, suggesting they cannot readily identify the recipient of their advances. *Holcocephala fusca* have a characteristic behaviour to advances from behind, which Scarbrough [42] suggests are due to the sensation of air-flow from behind. Scarbrough was able to elicit the behaviour by blowing onto the flies from behind through a small pipe. *Holcocephala* will hug tightly to or retreat down from the tip of their perch, kick with the large back legs and occasionally splay their wings, which are dark and opaque, should the stimulus continue. If the males are unsuccessful in their attempts, they will either abandon the target altogether or retreat on the wing before surging forwards again. If they are successful in coupling to the tip of a female abdomen with their clasping hypopygium, they will then hang backwards and upside down from the back of the female abdomen. Females can fly with males in this arrangement, though their flight is clumsy, short, and generally only in response to disturbance. There have been no observed cases of cannibalism between conspecifics, though they are subject to predation from other, larger asilids as well as the potential threat of wasps such as *Vespula* and *Dolichovespula* that were observed searching the perches frequented by *Holcocephala* and will elicit escape responses from the flies.

Fig. 3 **(Left)** A female *Holcocephala* kicks her back legs while feeding on a minute hymenopteran, a behaviour frequently observed when individuals were approached from the rear. **(Right)** A male *Holcocephala* hangs upside down and backwards from a female, coupled through the clasping terminal segment of his abdomen.

Holcocephala is abundant between from June until the beginning of September. Despite the frequency in which the adults are encountered, almost nothing is yet known about the sites where eggs are deposited, where the larvae are located, or what they eat until they become adults. Preliminary searches of the surrounding area, including soil and dead wood have yet to produce any asilid larvae. This missing step prevents *Holcocephala* from being reared in a laboratory environment and is thus why all behavioural trials are under field conditions. Those adults taken indoors failed to be persuaded to intercept presented targets, however throughout the experiments of this thesis, they were not put into a dedicated flight arena.

The Killer Fly, *Coenosia attenuata*

While the primary focus of this thesis is on *Holcocephala fusca*, it will be contrasted against another small, distantly related, predatory dipteran, the killer fly *Coenosia attenuata* (body length 4mm). Killer flies belong to the large group occasionally termed tiger flies of the genus *Coenosia*, with more than 300 described species [45]. Members of this genus are predatory both as larvae and as adults and are non-specific generalists, predating of a diverse array of

different prey organisms. *Coenosia attenuata* has attracted the most academic interest of these species. This is in part due to its near global distribution, presumed to have expanded out of its native southern Europe by hitchhiking on human trade goods such as live plants and soil, and deliberately introduced for its effects as a biocontrol agent against common greenhouse species such as whitefly [46–48].

The predatory behaviour of *Coenosia* is generally similar to *Holcocephala*, in that they sit on a perch and wait for prey items to fly past them, at which point they may take-off and fly to intercept the target, catching it on the wing. Unlike *Holcocephala*, *Coenosia* do not head-cock to targets as they fly over, nor do they always return to the same perch in order to consume the prey, frequently directing themselves to either the nearest perch, flat surface, or to fall to the ground with the prey. The other major difference between *Coenosia* and *Holcocephala* is in their choice of habitat and perch. While *Holcocephala* is highly selective, perching at the tips and upper surfaces of plants, facing upwards towards the sky, *Coenosia* tends to sit on the flat surfaces of stems and leaves, and also tends to sit with the longitudinal axis of the body facing downwards, away from the sky.

Fig. 4 Both images feature a female killer fly *Coenosia attenuata*, in profile **(left)** and head on **(right)**.

The sexual behaviour of *Coenosia* is not well documented. Females are considerably larger than the males and in greater abundance within natural environments [48]. One

potential reason for the sex-ratio imbalance is that *Coenosia* are readily and frequently cannibalistic, flying to intercept conspecifics in much the same manner they would any other prey item. Given that males are smaller, they are likely less able to fend off conspecific grappling. How they avoid capture in order to copulate is not clear, but for the purposes of analysing predatory behaviour of the species, it simplifies the problem. All flights after a target can be considered predatory in nature, as females clearly do not alter their behaviour when directed towards males.

Chapter 1

Object Detection

Abstract

This chapter concerns the vision of *Holcocephala fusca*. This includes measurement and analysis of optics, sensory cells, and the visual behaviour of *Holcocephala*. Experimentally, the maximal focal length (~190 μm) and minimal receptor spacing (~1.15 μm) are resolved and consequently confirm that *Holcocephala* has an exceptional optical resolution (~0.28°) for an animal of its size, rivalling the best of all compound eyes. The behavioural implications of this exceptional resolution were then tested, both in terms of the minimal angular size of a discriminable target (0.10°) and the ability of *Holcocephala* to hunt in crepuscular conditions or against cluttered backgrounds.

Some of the aspects of this chapter involving the optical properties of *Holcocephala's* eye have been published in the following article: "*Wardill, T. J., *Fabian, S. T., Pettigrew, A. C., Stavenga, D. G., Nordström, K., & Gonzalez-Bellido, P. T. (2017). A novel interception strategy in a miniature robber fly with extreme visual acuity. Current Biology, 27(6), 854-859."

**Joint first authorship.*

1.1 Introduction to Form Vision in Insects

Body size not only has profound implications for insect flight dynamics, but also in their vision. The image forming and target detection aspects of vision in adult insects are conducted by the compound eyes (in contrast to their non-image forming camera-type ocelli).

Compound eyes are an array of multiple lenses (up to 30000 in large dragonflies [49]) to focus light onto a bank of receptors below. Within insects, there are four general compound eye designs: Apposition, optical superposition, neural superposition, and multi-eyelet.

In apposition eyes, typically used by diurnal insects, screening pigments shield off individual units of the eye into ommatidia. An ommatidium comprises a single lens from the array that abuts a crystalline cone that transmits the light down and onto a small grouping of 8 photoreceptors (**Fig. 1.1**). For most insects, these photoreceptors are physically united such that each group can be treated as a single pixel.

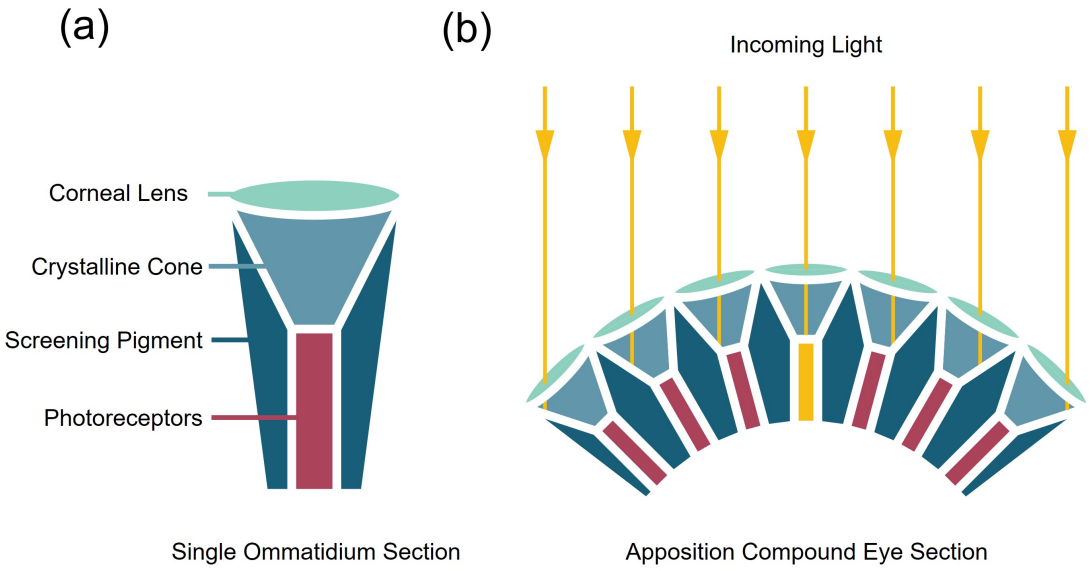

Fig. 1.1 **(a)** A single subunit of a compound eye, an ommatidium, is represented. Light enters the corneal lens and is refracted, transmitting into and down the crystalline cone and onto the light-sensitive photoreceptor tips that lie at the bottom. These convert light photons into nervous action potentials. **(b)** the apposition compound eye is composed of many neighbouring ommatidial subunits, each shielded by screening pigments. Parallel light enters from a point source, entering multiple lenses but only reaching the photoreceptors that are on-axis with the light-source. Elsewhere, the off-axis light is absorbed by the screening pigments, preventing optical cross-talk.

Apposition eyes are typically found in diurnal animals, and optical superposition in nocturnal ones (exceptions to both exist), but flies have successfully broken this dichotomy through the evolution of neural superposition. Neural superposition is considered a more advanced adaptation and is present only in the Diptera [50, 51]. An alternative optical superposition is potentially present in the square-latticed dorsal eye region of male mayflies

may achieve both refracting and reflecting superposition termed parabolic superposition [52–54]. Multi-eyelets are present only in the short-lived parasites of Strepsiptera and feature a small number of lenses (12 – 150) that individually focus light onto the distinct retinae of that lie behind each lens [55, 56] (**Fig. 1.2**).

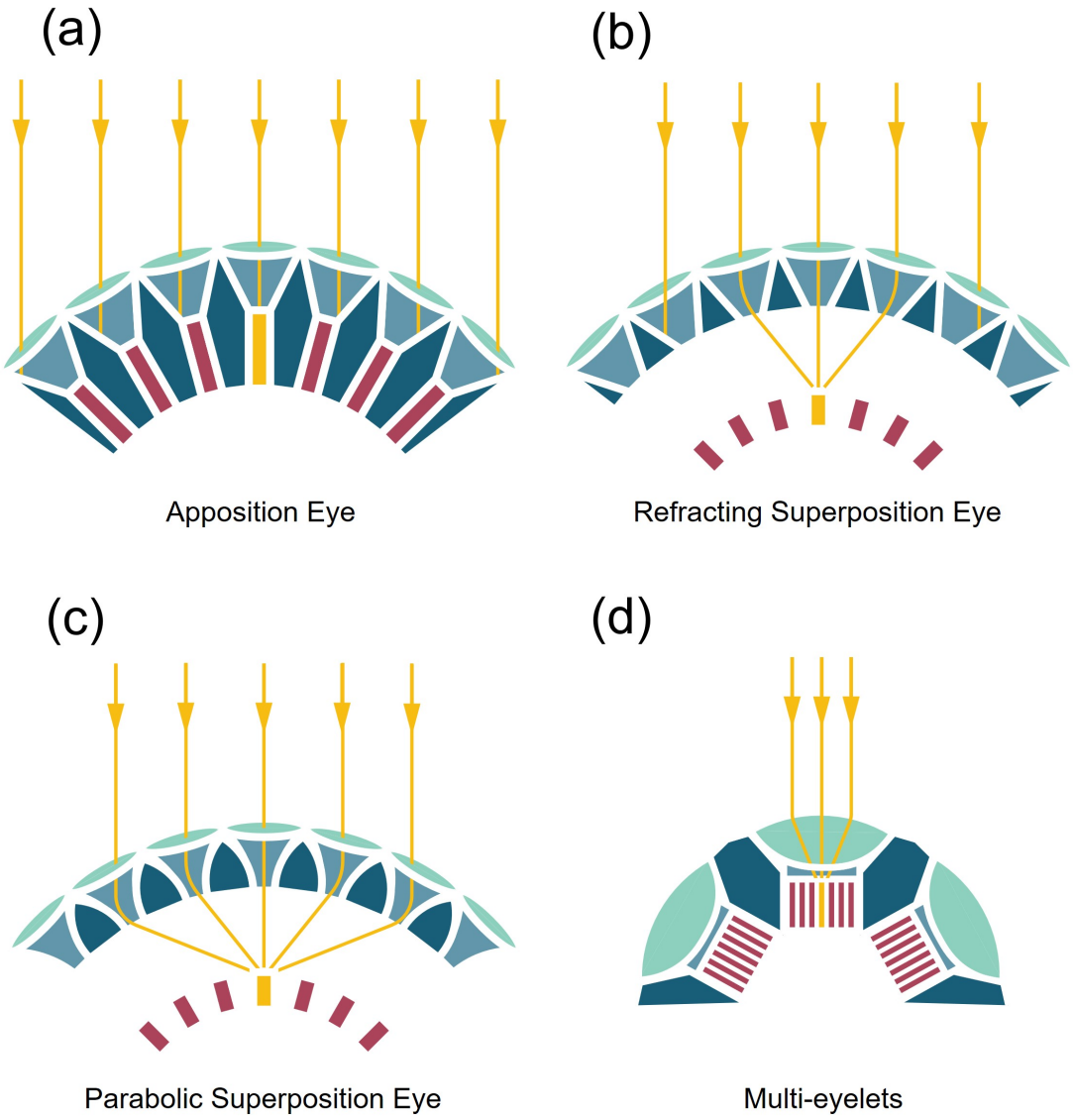

Fig. 1.2 A diagrammatic ray tracing of light entering different types of insect eye. These include: **(a)** the apposition eyes of most diurnal insects, **(b)** the refracting superposition eyes of many nocturnal insects, **(c)** the parabolic superposition eyes of male mayflies, and **(d)** the multi-eyelets of male Strepsiptera.

Many species of true flies (Diptera) spatially separate their photoreceptors into “open” rather than “fused” rhabdoms [51], leaving gaps between the microvilli and associated

photosensitive pigments of each cell (**Fig. 1.3**). By spatially separating the receptors at the bottom of an ommatidium, each cell samples a different region of visual space, bar cells R7 & R8 which are stacked one on top of the other [50]. This turns each individual ommatidium from a single pixel, to a tiny image, comprising 7 pixels. The reason that 7 is significant, is that there is neural summation between the photoreceptors of neighbouring ommatidial units. Ommatidia, when of equal size, stack into a hexagonal lattice, meaning that each unit has 6 near neighbours. The distribution means that there is 1 central photoreceptor and then 6 surrounding, and the information from each of the surrounding receptors is summed with the central receptor of the ommatidium on the opposite side (opposite as in across the central axis of the focal ommatidium, see **Fig. 1.3**) [57]. The arrangement of the photoreceptors in "advanced" Brachyceran flies (the sub-order that includes both *Coenosia* and *Holcocephala* along with many other genera) forms a trapezoid, with the photo receptors of R1-6 not corresponding to the nearest 6 neighbours, but 5 of the nearest neighbours and a nearest-but-one neighbour (see **Fig. 1.3b**). Neural superposition maintains the relatively high resolution of a conventional apposition eye, but with increased sensitivity [50, 58].

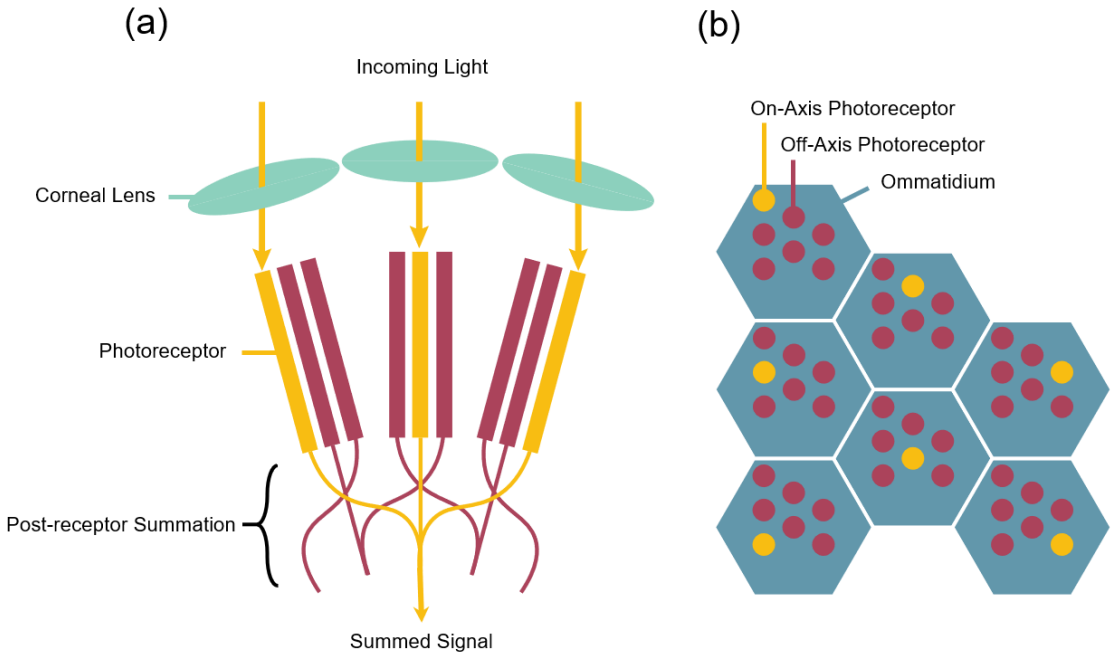

Fig. 1.3 **(a)** The physical separation of photoreceptor units at the base of the fly eye results in them sampling distinct visual axes within each ommatidium. The nearest neighbours of an ommatidium will feature photoreceptors that are on the same axis, whose neural signals are secondarily summated onto a single cartridge of the lamina of fly's optic lobe. **(b)** A transverse section through a hexagonal lattice of ommatidia within a fly's compound eye. Photoreceptors highlighted in gold signify those that will all be on the same visual axis, and thus summated together.

Where size presents a problem is in the visual resolution of the eye. The arrangement of an apposition or neural superposition compound eye requires a single lens for every pixel. The only way in which a compound eye can locally increase its resolution over a visual area (add more pixels/ommatidia per angular unit) is either to increase the radius of curvature of the eye, or to reduce the size of the ommatidia so that more can be packed together. For an eye of fixed resources, increasing the radius of optical curvature necessitates either restricting the field-of-view of the eye as a whole, or at least reducing the resolution of other eye regions as space and resources are diverted away. Increasing the radius of curvature over the entire eye is equivalent to building a larger eye, that comes with the necessary energetic investment of growth, upkeep, and in weight. There is also a packing limit to lenses on a region of fixed curvature.

One key characteristic of the resolution of the compound eye is the inter-ommatidial angle ($\Delta\phi$) (**Fig. 1.4**). This angle is defined by the central axis of a photoreceptor and those of

its nearest neighbours [59] (see **fig. 1.3**). The smaller the inter-ommatidial angle, the greater the possible acuity of the eye. This is not the only consideration; in order for this highest acuity to be reached, neighbouring ommatidia must also sample distinct regions of space, and thus light from a single axis, received anywhere across the eye, should stimulate only a single ommatidial axis. In reality, the edges of the receptive fields of ommatidia overlap to account for reduced sensitivity at the periphery of each ommatidia's field-of-view and provide a contiguous visual field (and in dipteran eyes, neural superposition means that this single axis may correspond to photoreceptors in neighbouring ommatidia that are secondarily summated (**see Fig. 1.3**). Allowing multiple ommatidial axes to sample the light from a single axis may lower the spatial resolution of the eye, but would also increase its sensitivity through oversampling [60].

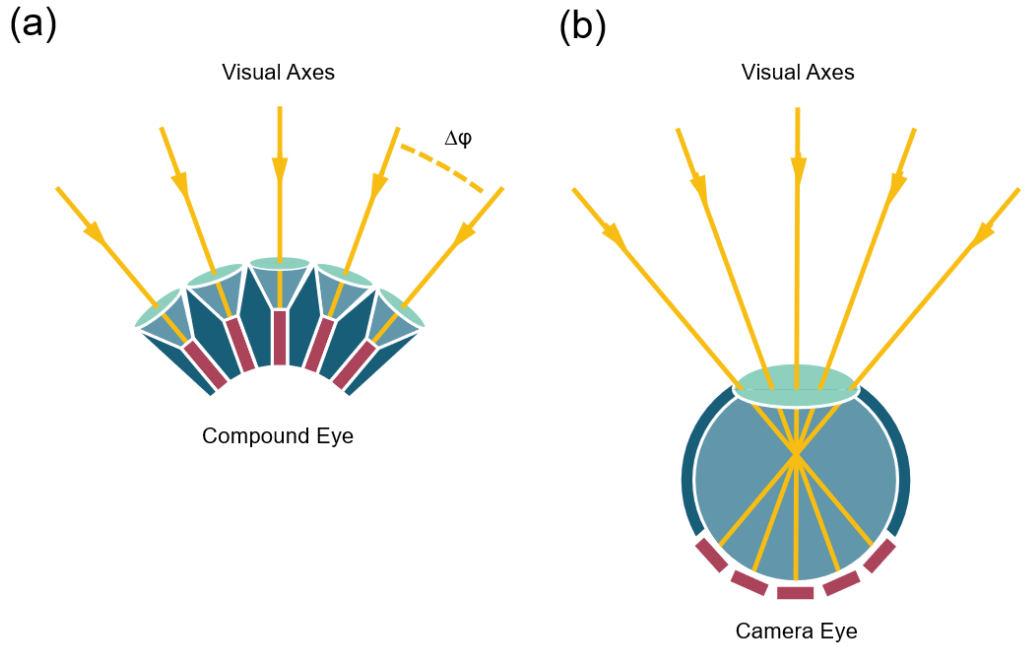

Fig. 1.4 **(a)** A compound eye with visual axes of the ommatidia demarked. The visual axes of each ommatidia are separated by the inter-ommatidial angle ($\Delta\phi$). **(b)** A camera-type eye is shown with equivalent visual axes, demonstrating the analogy of its function.

The resolution that can be transmitted through any lens is restricted by its diameter. This is given by the airy disk function that describes the spreading of a point of light on an image, related to the ratio of the aperture size (i.e. width of lens) and wavelength of the light [60]. Passing light through a smaller and smaller aperture increases the radius of the airy disk as the lens aperture width nears the wavelength of the light, increasing the diffraction (as diffraction of waves is greatest as the width of the diffracting aperture approaches the

wavelength). Doing so worsens the resolution by increasing blur. For vertebrate camera-type eyes, the diffraction limit is extremely small due to the large size of the lens in proportion to the wavelength of light. Yet for small insects attempting to reduce their lens size, this becomes a strong restriction, leading to some insects having diffraction-limited eyes that see at the resolution that the airy-disk function caps them to [61].

One way to circumvent this limitation in a small animal is the application of non-uniform resolution across the eye, and the use of an acute zone. An acute zone is a region of the eye that samples the visual surroundings at an increased resolution. For a compound eye with equal optical curvature across its surface (i.e. all facets survey equal portions of visual space), increasing the resolution (pixels per solid angle) reduces the field-of-view of the eye (total solid angle surveyed by the eye). For an eye with variable optical curvature, the cost can be to the peripheral visual resolution. Within a compound eye, an acute zone is typified by larger ommatidial lenses and flatter curvature than the rest of the eye (although larger lens size may also be indicative of greater light gathering for sensitivity rather than always spatial resolution per se) [62].

1.2 Detection and Object Distance

All objects take up a limited solid angle within the visual field of an observer. This angle, and their contrast against the background are the limiting factors affecting the detection of an object [60]. The solid angle is defined by the physical size of the target and its distance from the observer. Their contrast relative to the background depends on multiple factors of both the target and its background such as their spectral reflectance, the position and nature of light sources, the ambient light intensities etc. The eye has a certain visual resolution, which may vary across the visual scene. This means that each of the effective “pixels” of the eye are sampling a set solid angle of the world.

The “pixels” of an insect’s vision are not truly a hexagonal lattice of blocks of visual space, where each block represents equal sensitivity to a point light-source across its width. Instead the lattice is of individual ommatidial acceptance angles, which have differential angular sensitivities across their width. The ommatidial acceptance angle (effectively the region of visual space observed by an ommatidium) is a product of the rhabdomeric width, the optical image blurring due to the lens, and the waveguide mode in which light travels down the rhabdomeres once it has entered [61]. This product can be more simply approximated as a gaussian angular sensitivity that combines the point spread function (airy disk width at half-peak intensity plus any additional blurring by the lens of a point light-source) and the

rhabdom acceptance angle (a ratio of the rhabdom width and focal length of the lens) [59]. This approximation is given in **Fig. 1.5**.

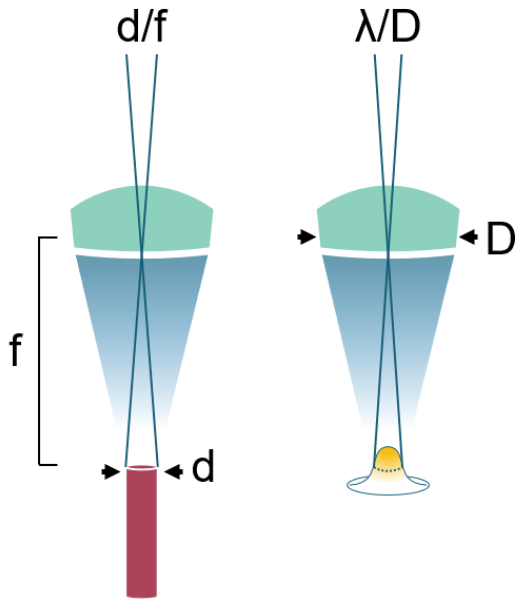

$$\Delta\rho \approx \sqrt{(\lambda/D)^2 + (d/f)^2}$$

Fig. 1.5 The ommatidial acceptance angle can be approximated by a combination of both the rhabdomic acceptance angle **(left)** and the point-spread function **(right)** of the airy disk generated by the lens. $\Delta\rho$ is the ommatidial acceptance angle, λ is the wavelength of focussed light, D is the lens diameter, d is the rhabdom diameter, and f is the focal length. This figure has been redrawn from Land 1997 [61].

Seeing prey at greater distances has advantages and is a common ability of predators. Visually guided predators generally have exceptionally good visual resolution for their size and eye-type. This is reflected in their investment within physiology. Within the birds, raptors (including owls) have eyes between 1.4 – 2.2× the mass which would be expected should they follow the scaling relationships of other birds [63]. Small visual angles of receptors increase the radius surrounding the predator in which prey will be perceived and thus the total number of prey that will be detected. For instance the American kestrel has a maximum strike distance on small mammal targets of 275m due to its high visual acuity [64]. Meanwhile, the killer fly *Coenosia attenuata* has been demonstrated to have a peak visual resolution three- to four-fold finer than comparable prey items such as fruit flies (Drosophila melanogaster) (~2.5° vs ~8° per ommatidium) [37]. The visual resolution of a compound

eye is limited by its size, as already discussed, with the most acute compound eyes, those of the large predatory dragonfly *Aeshna palmata* having inter-ommatidial angles of ~0.24°, again facilitating predatory behaviours [49].

One of the critical limits on the spatial resolution of the eye is in the effect that the small lens size has on the light passing through it. This is limit becomes apparent when the lens width approaches the wavelength of the light. This takes the form of an Airy disk (**Fig. 1.1**), which is a bright central spot surrounded by concentric rings of diminishing brightness, termed the Airy pattern. The airy disk represents the limit of the angular resolution and its angular width is given by **Eqn. 1.1**.

$$\theta = \frac{2\lambda}{D} \tag{1.1}$$

Where θ is the angular width of the airy disk, λ is the wavelength of light being focussed and D is the diameter of the lens. The 50% intensity bounds of the airy disk are half this value and thus given by λ/D [65]. The Rayleigh criterion gives an alternative measure for the airy-disc separation requirements of a visual system, set by the angular radius to the first minimum of the airy pattern given by 1.22 λ/D. The Rayleigh criterion allows for modulation of a sinusoidal grating by considering the requirements of separating point sources of light, accounting for a non-uniform grating across the eye, with the intensity peaks of point sources being separated by the radius of the airy pattern to the first minimum [66]. The 50% intensity bound given by λ/D will be used as in Horridge [67] due to its described similarity to the measurement of field widths of photoreceptors (angle-dependent sensitivity to incoming light), and because λ/D corresponds to a theoretical cut-off without grating modulation. However, it is worth noting that simply because a compound eye can focus light with a small airy disk, this only corresponds to the visual resolution if the acceptance angles of the photoreceptors themselves are the same size as the airy disk. If they are larger than the airy disk, the angular resolution is consequently poorer than would be predicted based on the disk alone.

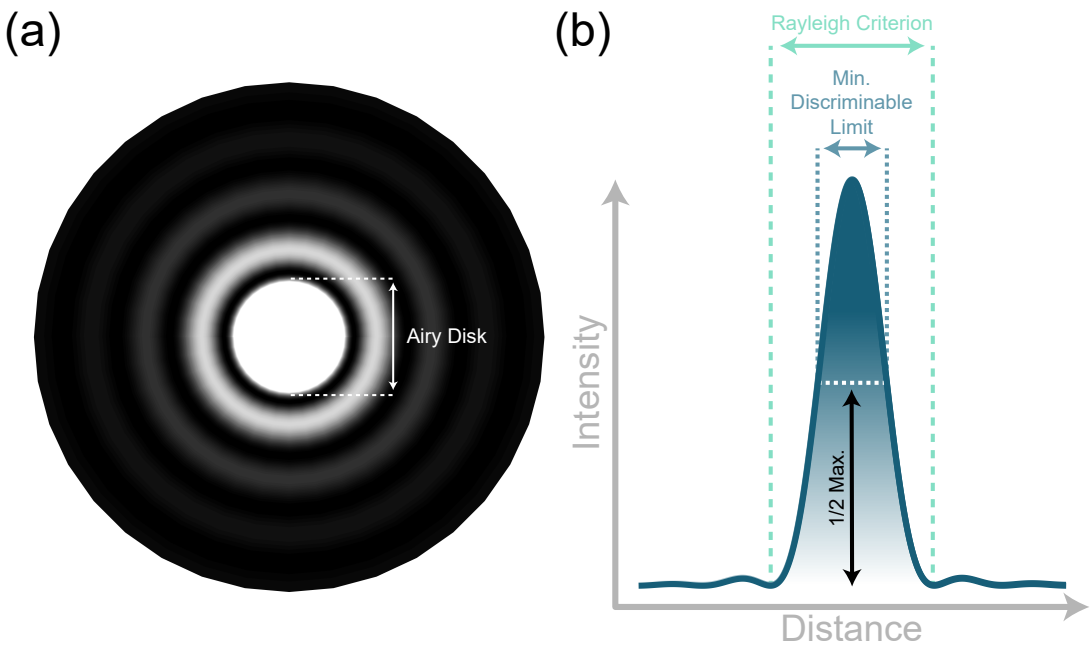

Fig. 1.6 **(Left)**A simulation of a point light-source focussed by an aperture forms a typical airy pattern. The central disk is termed the airy-disk. **(Right)** The contour of half-peak intensity frequently used for the minimal discriminable limit between two point-sources on an image. Alternatively, the Rayleigh criterion uses the width to the first minima of the shadow as the separable distance between two point-sources.

The neural superposition within fly eyes gives a secondary measure of the inter-ommatidial angle. This is because the peripheral photoreceptors of neighbouring ommatidia are summated, and thus their optical angle relative to the central axis of the photoreceptor corresponds to the inter-ommatidial angle, and therefore to the limit of the visual resolution.

Higher visual acuity in predators clearly does not serve only the function of object detection. Visual resolution also contributes to target assessment, such as the pictorial identification of targets and their context [68, 69]. Higher resolution also complements the speed of motion of the target. Higher spatial resolutions can measure angular speeds of visual features across the retina more accurately and with a shorter response latency. These angular speed measurements may facilitate target selection (chapter 2), target interception (chapter 3), and the measurement of one's own motion through optic flow [27, 70]. Visual resolution across different species of birds correlates positively with their average flight speeds [63]. Additionally, the specificity of the required steering manoeuvres used by peregrine falcons when stooping high above prey, rely on measurements only possible from extreme visual resolution like that of the raptor's fovea [71].

Eyes with high acuity rarely have an even distribution of the resolution throughout the eye. A familiar embodiment is the foveae of some vertebrate camera eyes. The term fovea stems from the latin word 'foves' meaning pit, due to its shape on the retina [72]. Acuity is of such importance to raptorial birds that the vast majority have two foveae, one centrally located in each eye and one temporally located. The temporal fovea images the area of binocular convergence over the beak [73] (exceptions include owls, black vultures (*Coragyps atratus*) and Andean condors (*Vultur gryphus*), which all have a single fovea per eye [74]). In such camera type eye, the resolution can be enhanced by increasing the packing density of the photoreceptors at the back of the eye, or by increasing the focal length. In contrast, the compound eye cannot pack more lenses into a fixed curvature without reaching the diffraction limitation of the lenses [60]. Nevertheless, many insects have higher acuity over regions of the eye, principally by varying the optical curvature of the eye [75].

The interommatidial angles vary over the compound eyes of many arthropods, effectively creating higher and lower resolution regions. In some species, the increase in resolution of small eye regions, critical for their behavioural requirements, are so extreme they are analogous to vertebrate "foveae". Within arthropods these are frequently not termed foveae due to the lack of the defining pit, and separately that the distributions of higher resolution take all manner of bands and shapes, dissimilar to a vertebrate fovea [67]. Instead they are termed acute-zones, to match the broadness of the terminology to the variability of the resolution gradients observed. However, this terminology is not consistent within the literature, and for this thesis we will consider them interchangeable.

Acute zones have been described in several species of insect. Mantids have forwards facing acute regions of each eye that they direct towards objects of interest in the surroundings [75, 62], although the term fovea is also used to describe the horseshoe-shaped band that encircles the region with the highest visual acuity [62]. Acute vision across a central region is also found in the male hoverflies of the species *Syrrita pipiens*, in which a forward-facing acute-zone with two- to three-fold higher acuity than elsewhere in the eye [32]. Dragonflies reserve their highest visual acuity for a central acute region on the dorsal side of their eyes, in which prey is centred during flight as the dragonfly approaches from below[49, 76]. Even in the small killer fly *Coenosia attenuata*, their improved visual acuity over *Drosophila melanogaster* is only found in the anterior, forward facing section of the eye. Elsewhere towards the posterior, the acuity gradually reduces by four-fold [37].

1.3 Determining the Visual Acuity of *Holcocephala fusca*

Upon close inspection, the eye of *Holcocephala fusca* is plainly not a homogenous hexagonal lattice (**see Fig. 1.7**). The lens diameter in both eyes increases toward a forward-facing anterior region. Work completed by Gonzalez-Bellido [77], from z-stacking 2-photon auto-fluorescent images, demonstrated that the corneal lenses in large *Holcocephala* specimens reach up to 78 μm in diameter, larger than in even relatively large dragonflies such as the green darner *Anax junius* (up to 62 μm [49]). This large lens size gives a minimum possible half-width of the airy disk when focussing mid-range ultra-violet light (i.e. 350 nm in wavelength), of 0.26° , representing the diffraction limit on the eye. Given that no receptor sensitivity data has been obtained thus far, the UV sensitivity is only an estimation based on *Holcocephala's* upward looking, sky facing posture. Should the peak sensitivity of the key photopigments be towards the green (i.e. 490 nm) as in other flies such *Drosophila melanogaster* [78], then this resolution limit is higher, at 0.36° . The 0.26° value is close to the best resolution of any compound eye (0.24° [49]), however this information on its own is insufficient to index the static spatial resolution of the eye, only the firm limitation to this resolution.

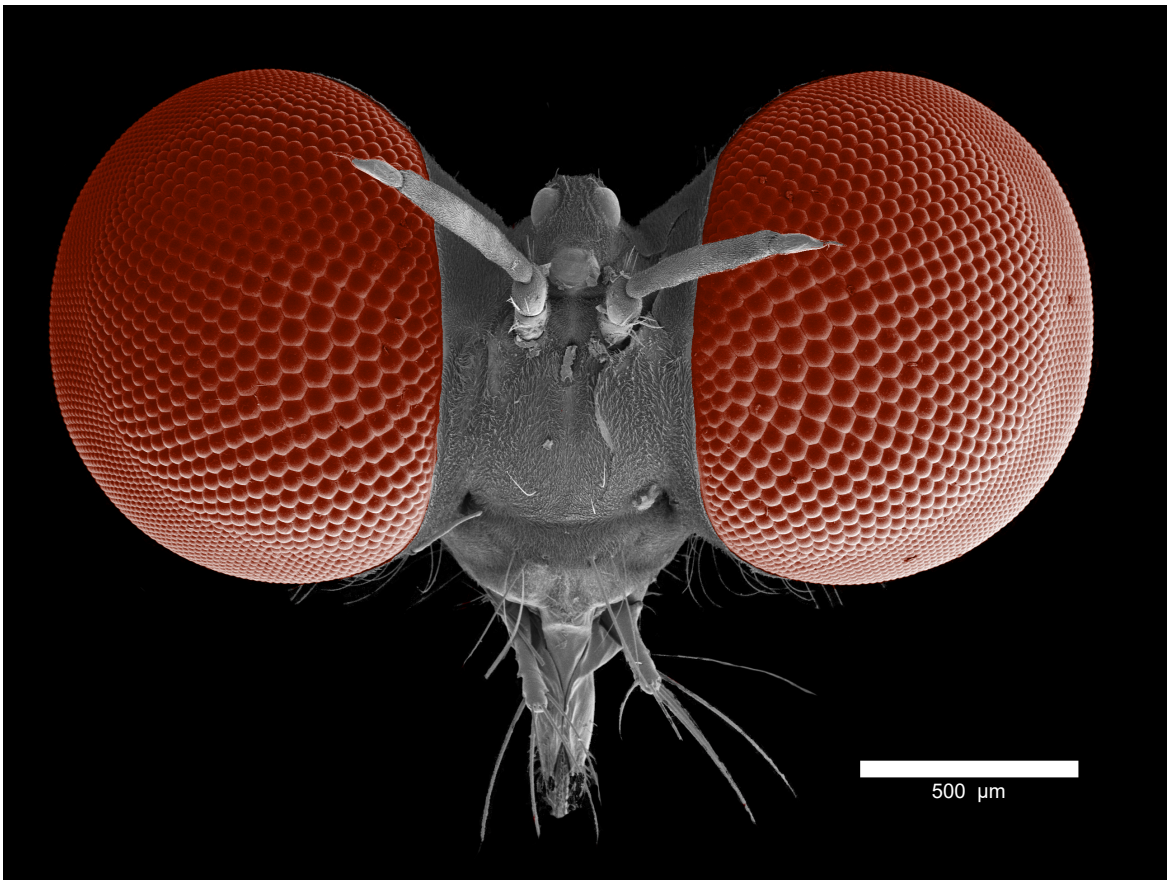

Fig. 1.7 *Holcocephala fusca* imaged under a scanning electron microscope, demonstrating the variation in the size of corneal lenses across the eyes.

Gonzalez-Bellido has also pioneered a new method for measuring the inter-ommatidial angles from the auto-fluorescent 2-photon z-stacks by tagging the joints of the lens perimeters and tagging the photoreceptors at the bottom of the ommatidia. Once centroids are applied to the lenses, a visual axis of the ommatidia can then be determined by the vector connecting the central R7 photoreceptor and the centroid of the lens. This yielded minimum values of the inter-ommatidial angles at $0.40^\circ \pm$ SE 0.19° [77].

To confirm the novel method, using more conventional and tested methods, we measured both the focal length of the largest lenses of the eye and the spacing of the receptors at the bottom of ommatidia within the acute-zone. We used this methodology rather than pseudopupil measurements elsewhere described, as the separating screening pigments of the eye were too dark to reliably contrast the pseudopupil against them and determine its angular width [75]. Based on the assumption that the lenses have their focal point at the tips of the photoreceptors, and that the signals of the spatially separated photoreceptors are neurally summated with neighbouring ommatidia, the calculated angle between the

visual axes of the photoreceptors should agree with the inter-ommatidial angles. While an optimal neural-superposition eye would have exact agreement between the axes of the individual photoreceptors and the central axes of the neighbouring ommatidia, this would require the rhabdomeres to interlace or touch. Thus, to prevent cross-talk and maintain separation, the optical axes of studied fly rhabdomeres are ~15-20% further apart than the inter-ommatidial angle [58, 79]. We also made the assumption that the acceptance angle for each photo-receptor near-equated the interommatidial angles, as found in *Coenosia* [37].

Experimental Aim:

We measured the the spatial dimensions of the ommatidia of *Holcocephala* in order to validate estimations of it's visual resolution determined by a novel, autofluorescence technique.

1.3.1 Focal-Length

The focal length of the central ommatidium was calculated using the hanging-drop technique, based on the method first described by Homman in 1924 [80]. In this methodology, the corneal lenses of the fly eye were separated out from a recently-deceased *Holcocephala* and then cleaned of the internal workings of the eye (cones, pigments etc. removed) using a paintbrush. The internal surface of the cornea was filled with Ringer's solution, an isotonic blend of salts (to prevent osmotic changes deforming the lenses), and then suspended below a glass slide. This slide could then be placed on a conventional light microscope, with the condenser removed, such that viewing through the eyepiece, one could see repeated images of the light source in each of the lens facets (**see Fig. 1.8**). Below this was placed a grating of known size (Edmund Optics 3"×3" Negative, 1951 USAF target). Images could then be taken through the microscope. The focal length could then be calculated based on Eqn. 1.2.

$$f = s\frac{\lambda_i}{\lambda_o} \tag{1.2}$$

Where f is the focal length of the lens, s is the distance between the grating to the lens, λ_i is the wavelength of the grating on the image and λ_o is the wavelength of the actual grating.

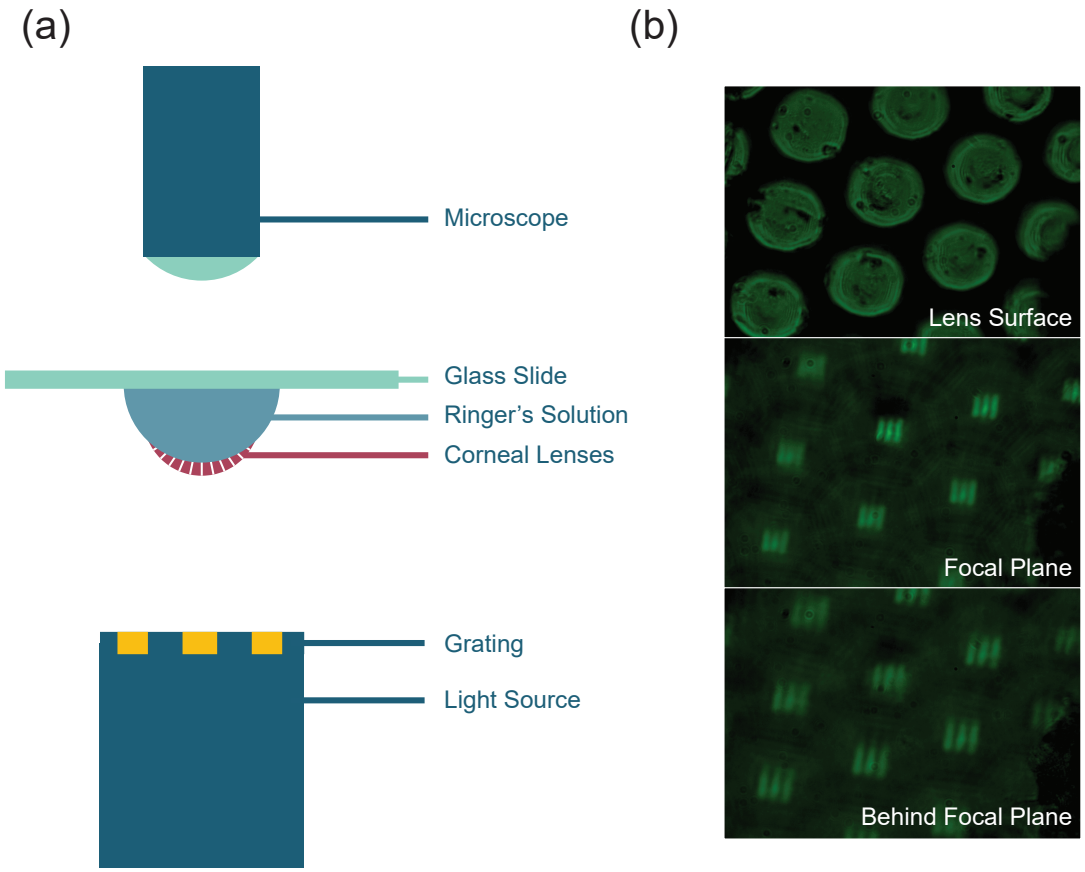

Fig. 1.8 **(a)** The focal length of corneal lenses can be determined by suspending them on a drop of ringer's solution, that hangs from a glass slide beneath a microscope. This is in turn above a light source with a grating of known wavelength. **(b)** Example images taken through the corneal lenses of *Holcocephala*. Focussing from the lens surface (top image) through the focal plane (middle image) and behind (bottom image).

To assess when the grating was at the focal plane, and thus in the sharpest focus, a custom written MATLAB script was used (Courtesy of the Buschbeck Lab, University of Cincinnati). The images were taken across a range in which the best focus of the lenses could qualitatively be seen to occur, at 5 μm intervals. The images were then compiled into a z-stack and a focal, central facet selected. The stack of this facet was then run through the script which determined the relative intensity of the bars of the grating image, with the greatest grating contrast corresponding to the focal plane of the lens (**see Fig. 1.8b**).

The longest focal length of the *Holcocephala* eye was found to be 190 $\pm$ SE 4 μm (n = 5).

Cross-talk between the rhabdomeres of the photoreceptors would effectively reduce the visual resolution, as light from one axis would stimulate neighbouring rhabdomeres. This stimulation of neighbours would reduce the accuracy to which the axis of the light could be determined. Crosstalk can be generated optically. Optical crosstalk is where light entering a rhabdom at a low angle of incidence fails to be totally internally reflected, and enters neighbouring rhabdoms. One property that affects optical crosstalk is the F-number, the ratio of the focal length to the aperture size, as given in **Eqn. 1.3**.

$$F = \frac{f}{D_l} \tag{1.3}$$

Where f is the focal length of the lens and D_l is the diameter of the lens. Low F-numbers create greater sensitivity, as incident light is gathered and concentrated by a larger lens. However, they also decrease the minimum incident angle of the light arriving at the tip of the rhabdomere. While in the fly eye there are screening pigments bounding the edges of the ommatidium that prevent optical crosstalk, the spatially separated rhabdomeres within an ommatidium are not always screened. Ideally, to maintain angular resolution, light should travel down the rhabdoms reflecting internally, in the manner of a waveguide or optical fibre [81, 82]. Should light escape, then it could potentially enter neighbouring rhabdoms and create cross-talk. The internal reflection of the light is governed by the difference in refractive index between the rhabdomere and the inter-rhabdomeric space. In the blowfly *Calliphora erythrocephala*, the ratio of the refractive indices of the two media has been described as low (rhabdom to inter-rhabdomeric space: 1.018, measured by monochromatic interference microscopy) [83, 84]. This low refractive index ratio lowers the maximum incident angle required for light to be internally reflected and from this is near F = 2 [78].

From the measurement of the maximum lens size (78 μm) and our longest measurement of the focal length (190 μm), we find that the central region of the *Holcocephala* eye has an F-number of F = 2.4. This is high enough that the light entering the rhabdoms should be totally internally reflected [78]. This value is also higher than those recorded for other flies including *Drosophila* (F = 1.25 [78]), Musca (F = 1.9 [85]), and the male blowflies of *Calliphora* and *Chrysomya* (F = 2.0 [86]). However, this is lower than the peak values found in localised regions of the male blowfly eye (F = 3.0 [87]). This high value for lenses of such large size is generated by an extremely long focal length that exceeds the lengths reached by larger animals such as the *Chrysomya* blowflies (maximum focal length of ~150 μm [86]).

1.3.2 Receptor Spacing

The spacing between the receptors is the second characteristic that define the visual axes of the individual photoreceptors. We imaged ultra-thin sections of resin-embedded *Holcocephala* photoreceptors (previously prepared by Gonzalez-Bellido) under a transmission electron microscope (TEM) (**see Fig. 1.9**). The spacing of the photoreceptors was then analysed in Fiji image analysis software (see [88]). The outline of each rhabdomere was traced by hand and then fitted with an ellipse, so that the centroids of the fitted ellipses could be determined and their physical separations measured. From these measurements, the minimal rhabdomeric spacing was 1.15 $\mu m \pm$ SE 0.16 μm.

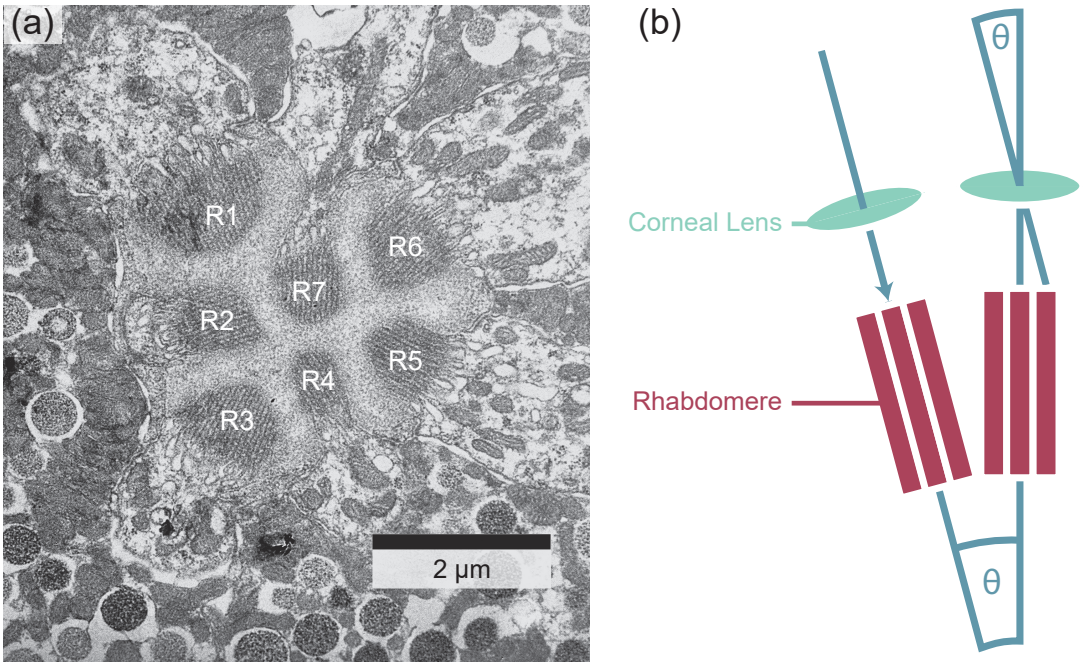

Fig. 1.9 **(a)** The rhabdomeres of *Holcocephala* photoreceptors imaged under TEM. Cells R1-6 surround the central R7 photoreceptor in a trapezoid arrangement. **(b)** In a neural-superposition eye, the visual axes of neighbouring ommatidia are separated by the same angle (θ) as the visual axes of the rhabdoms of the photoreceptors within a single ommatidium.

1.3.3 Angular Resolution of the Eye of *Holcocephala fusca*

The spacing of the rhabdoms (1.15 μm) and the focal length (190 μm) of the central facets of the eye of *Holcocephala* give a difference in visual axis of 0.35°. However, applying Pick's conversion based on the ~20% greater difference in rhabdomeric visual axes [58], we get the

value of 0.28° as the inter-ommatidial angle and thus the estimated angular resolution of the acute-zone of *Holcocephala fusca*. This is within the 0.40° ± SE 0.19° of the initial estimate based on 3D reconstruction from 2-photon auto-fluorescent images [77]. This is also within the range of the diffraction limit set by the airy disk of the lens diameter, provided that the wavelength of the light being observed is near the UV-blue region of the spectrum. This suggests that *Holcocephala* are close to the diffraction limit of their lenses at the centre of the eye.

0.28° is an extremely acute visual resolution for any compound eye, twice that of much larger organisms such as mantises [75, 89], a tenfold improvement over another miniature dipteran predator (*Coenosia attenuata*) [37, 78], and a twentyfold improvement over one of their prey species, *Drosophila melanogaster* [37, 78]. The visual acuity of *Holcocephala fusca* is only comparable with large dragonflies, which have a body lengths in excess of an order of magnitude larger [90]. Dragonflies feed using aerial interception of small targets, similarly approaching them from underneath, resulting in the targets being contrasted against the sky above [34]. It thus might be hypothesised that this style of feeding generates the selective pressure for extreme visual acuity (for a compound eye).

1.3.4 The Eye Parameter

An alternative measure used for considering the adaptation of eyes to fit the ambient light conditions of their environment is given by the "eye parameter". The eye parameter is inter-ommatidial angle (in radians), multiplied by the diameter of the lens (in notation $D\Delta\phi$). This eye parameter is useful when considering the sensitivity of the eye and the ability of the eye to overcome inherent photon noise at all intensities [75, 59]. The optimal value of $D\Delta\phi$ for an eye is not only given by the mean luminance (light per solid angle of visual space) of the environment (or object) which the eye is adapted to see, but also the angular speed of the objects within the visual field, and the luminance contrast of said objects.

For an eye that features a hexagonal lattice, the eye parameter of diffraction limited lenses is given by $\lambda/\sqrt{3}$ [59], and taking the assumption that there is a common intensity peak for insects at $\lambda = 0.5\ \mu m$, the eye parameter of diffraction limited lenses ($D\Delta\phi$) is 0.3 μm (or 0.25 for a square lattice where the limit is set by $\lambda/2$ [59]). This may not hold true for the eyes of *Holcocephala* in which $\lambda < 0.4\ \mu m$ may be more appropriate, as in the dorsal portion of dragonfly eyes [67]. This would instead set a hard limit closer to $D\Delta\phi = 0.2\ \mu m$. This diffraction limited region ($D\Delta\phi = 0.2 - 0.5\ \mu m$) is only suitable for those insects operating in bright diurnal conditions, high luminance contrasts and low object angular speeds. Outside

of these conditions, it is expected that the eye parameter would exceed these values, with higher values giving greater sensitivity and suitability for low light or high object angular speeds.

Existing work on the eyes of blowflies (*Calliphora*) shows that they have a relatively high (given they are primarily diurnally active) eye parameter of 1.3 μm, attributed to their extremely rapid flight manoeuvres that create high angular speeds of objects across the retina [59, 91]. The lowest eye parameters yet found are in the forward-facing acute zone of sand wasps (of the genus *Bembix*), which reduce down to $D\Delta\phi = 0.3\ \mu m$, close to the true diffraction limit [65]. *Bembix* sand wasps hunt flies like *Lucilia* in bright conditions, and will hover while scanning the surroundings or tracking targets [92], thus this could explain why their eyes are pushed up against the diffraction limit.

The acute region of the eyes of *Holcocephala* have facet sizes in the range of 70-78 μm and an interommatidial angle of ~0.28-0.35°. Together these give a range of the eye parameter $D\Delta\phi$ between $0.34 - 0.48\ \mu m$. This is the range that would be expected for an insect operating under bright diurnal conditions, low angular speeds, and high luminance contrast of the target. This matches well with the behavioural conditions of *Holcocephala*, hunting from below with targets back-lit against the sky, leading to high target contrast. As will be discussed in chapter 3, *Holcocephala* attacks targets at a comparatively long range, and resultantly targets have low angular speeds across the retina. This low angular speed of the target also matches the visual physiology and low eye parameter [65]. These values are in keeping with the most acute compound eyes, such as those of the diurnal dragonflies of *Hemicordulia* ($D\Delta\phi \approx 0.3\ \mu m$) and smaller than those of more diurnal-crepuscular generalists such as *Orthetrum* ($D\Delta\phi \approx 0.6\ \mu m$) [65].

1.4 Behavioural Object Detection Thresholds

1.4.1 Angular Size Threshold

The clearest advantage to improved visual resolution is the ability to detect objects at a greater range. Range and object detection are linked as objects of equal absolute size will appear smaller in the visual field at greater range **(Fig. 1.10)**. The subtended angle of an object is a product of its true size and its distance, as given by **Eqn. 1.4**.

$$\theta = 2 \times ArcTan(\frac{d}{2r}) \tag{1.4}$$

Where θ is the subtended size, d is the diameter of the object, and r is the range between the target and the fly. As previously discussed, objects can be detected that subtend a size smaller than the solid angle of a photoreceptor, due to the change in the intensity the object effects across the whole pixel **(Fig. 1.10)**.

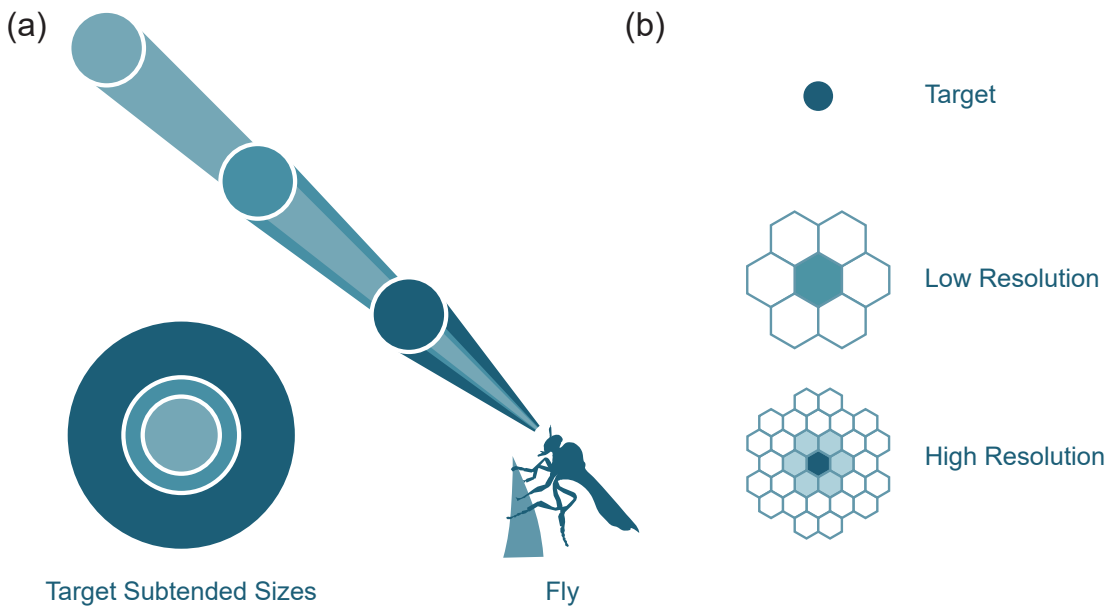

Fig. 1.10 **(a)** The angular size of an object varies non-linearly with its distance from the observer. Three objects of equal size, with equal spacing between them, appear at different angular sizes. **(b)** The sampling of a small target by two hexagonal lattices, one with twice the interommatidial angle of the other. While both lattices can detect the target by the dip in brightness, the higher resolution lattice has greater positional certainty. The low-resolution lattice has facets greater in size than the target image, yet the target can still be detected by the drop-in illuminance.

For a target to be detectable, its effected change in the signal of the observing photoreceptor/ommatidial unit must differ beyond a threshold from those of the neighbouring units observing the background. This can occur even when an object's subtended size is smaller than the field-of-view of a single pixel, if the resultant contrast change due to the object is significant across the summed solid angle of the ommatidial field-of-view. A familiar implementation of this contrast-based detection is in the manner that a human eye can perceive

nearby stars. During the night, the contrast of many stars are high relative to the surrounding sky, even though the largest angular size of any star is three orders of magnitude smaller than the imaging resolution (pixel size) of the human eye [93].

The contrast between object and background need not be as stark as that between bright stars and the night sky. Object detection based on contrast is not as simple as a binary "see or can't see" at a neuronal or psychometric level, instead responses increase non-linearly with increasing contrast. Contrast thresholds are here determined as when the neuronal or psychometric response of an animal is significantly different from the spontaneous background noise (e.g. neuron firing rate). Humans, assessed psychometrically, can detect gratings in which the modulation in luminance is as little as < 0.5 % [94]. Insects are also capable of near equally extreme feats of sensitivity. Hawkmoths, bumblebees, and hoverflies have all been demonstrated to detect a comparable < 1 % modulation grating (albeit at different angular velocities and spatial frequencies according to their visual ecologies [95]). Small target motion detectors (STMDs), in the lobula of hoverflies and dragonflies, respond to the movement of small regions of contrast through the visual field. These cells again demonstrate a comparably small detection threshold of ~1 % luminance modulation, for small targets moving across cluttered backgrounds [96].

Concerning aerial predation from below, as found in Holcocephala, the target is back-lit by the sky above. Thus, a target is represented by a localised dip in brightness, corresponding to the subtended size of the target image. The contrast-determined detectability holds true for a localised dip in brightness (as with silhouettes) as it does for a localised increase in brightness [93]. Thus, the deciding factors are the contrast of the object against the background, its visual size, and the intrinsic photon noise as light arrives in discrete photon-packets [59].

1.4.2 Motion Detection

A secondary consideration is the effect of hyperacuity. Motion hyperacuity, as defined by Nakayama [97], is the ability of a retina to detect a finer grain of target motion than the visual axes of its receptors would suggest. By correlating the changes in brightness across neighbouring ommatidia as the target image passes by, the motion of the target can be interpolated. In an aerial predation setting, targets will be moving overhead, and thus transitioning across the photoreceptors of the eye, successively dipping their brightness irrespective of whether they fully obscure the acceptance angle of the photoreceptors. Hyperacuity need not stem from movement of the target. Recent work has shown that the visual response of Drosophila to moving small objects is greatly beyond what their interommatidial angles would suggest

[98]. It is proposed that this is due to rapid photomechanical photoreceptor contractions [99] and the encoding activities of the photoreceptors is concentrated in time to rapid bursts of activity that together help reduce the effects of the motion blur of a target.

Detection of target by their motion is dependant on the fundamental means by which motion is detected. The means by which motion is encoded is based on the elementary motion detector (EMD). In insects, the circuit that has long been determined to be the EMD is the Reichardt-Hassentein detector [100, 101] (**Fig. 1.11a**. In this detector, the individual response of a sensor is delayed and multiplied with it's neighbour, the (positively signed) product of which is added to the (negatively signed) product of a mirrored circuit in which the second sensor's signal is delayed. This mirroring and summing of the circuits prevents a flicker on response from generating a motion signal. The spatial frequency of the detector is given by the separation in angular space of the two sensors (in this case interommatidial angle), and the temporal frequency given by the time delaying element (τ). Increasing τ tunes the response towards slower moving edges while decreasing τ has the inverse effect.

Targets are specific in motion as they have both a fore- and aft-boundary. The EMD detects motion in the change of pixel value, so a dark target on a bright background would be represented by two boundaries. One is the step from on to off and is the first to pass a sensor in the direction of travel, the second is the on response as the target as crossed that region of visual space. From this, the ESTMD model has been suggested in dragonflies [102, 103] (**Fig. 1.11b**) that would correlate a time-delayed off signal with an on signal, and thus unite an object for size-selectivity in the detection pathway [103]. Together these elementary detectors can be combined (with either leading the other) to form a directionally-selective, target-size-selective EMD-ESTMD or ESTMD-EMD.

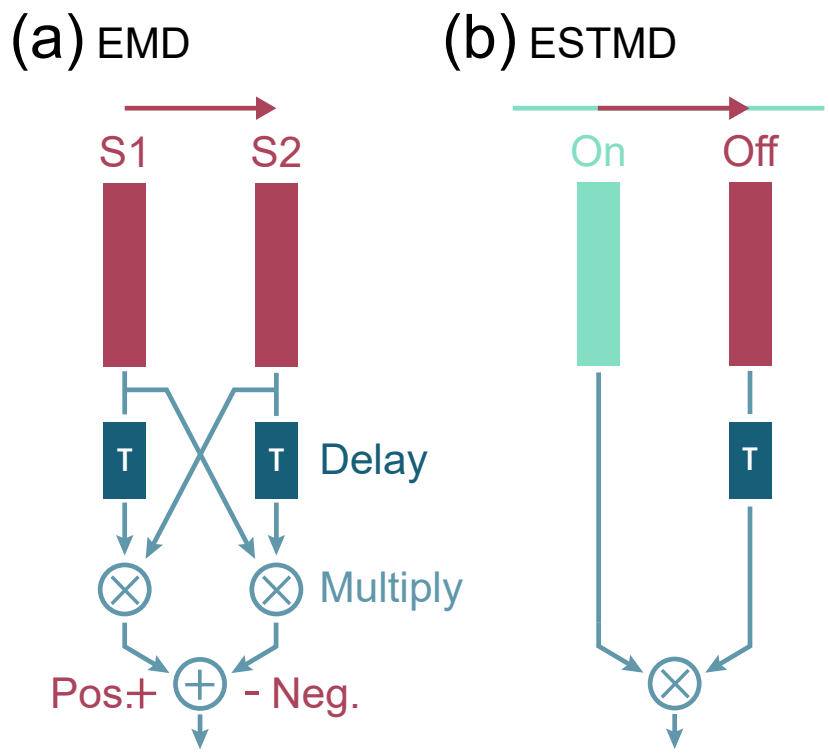

Fig. 1.11 **(a)** The Reichardt-Hassentein detector or elementary motion detector (EMD) in which two sensors (S1 & S2) have their signals both delayed, crossed, and multiplied with eachother. The delay is by a constant τ that tunes temporal dynamic range. The responses of the mirrored circuits are summed, but with opposing signs to give directional selectivity. **(b)** The ESTMD that correlates a time-delayed (τ) off signal from a target silhouette with the corresponding on signal as it passes over to generate a size tuning based on τ.

The importance of understanding this model of target detection is that the specific τ being used by either system will alter the detectability of the targets through temporal tuning. The velocity tunings of STMDs, potentially a product of EMD-ESTMDs, have been detailed for dragonflies [102, 104, 105], and converge around a maximum sensitivity to targets in the region of 60 - 100 $^{\circ}.s^{-1}$. We might then reasonably expect the behavioural tuning of holcocephala to peak in a similar range, and for extremely slow-moving targets to not be registered.

Experimental Aim:

Based on the assumption that *Holcocephala*, like other species, is unlikely to be limited to simply its optical angular resolution, we set out to behaviourally test the limits of *Holcocephala's* ability to detect targets.

1.4.3 Reconstructing *Holcocephala's* Behaviour in Field Conditions

All behavioural work with *Holcocephala fusca* was conducted in the field, at a site where the flies were naturally highly abundant (York County, PA, U.S.A.). The field site was a corridor of low understory following the path of a small stream and bordered by deciduous forest on both sides **(Fig. 1.12)**. The corridor ran North North East and fell within a slight valley. This, combined with the flanking forest, resulted in the sun only directly falling on the perches of *Holcocephala* during a narrow period during the middle of the day (approximately from 12:30 – 2:30 PM), weather dependent. Most behavioural responses were thus recorded when both fly and target were in shade, but with the target back-lit against the open sky above.

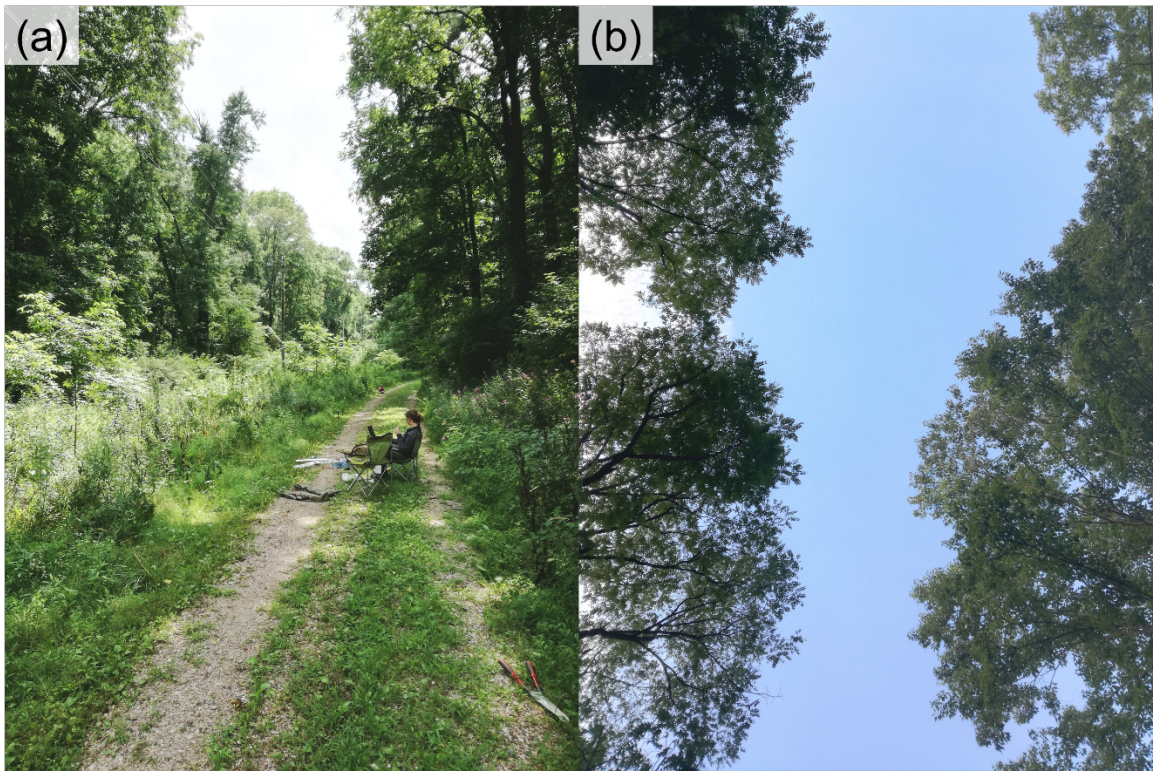

Fig. 1.12 **(a)** A photograph of the field site used for filming *Holcoephala fusca*, displaying the narrow corridor formed between two sections of forest. **(b)** An image taken vertically upwards from the field site gives an impression of the typical shape of the clear-sky tract *Holcocephala* look up towards.

Targets were small silvered beads of three different sizes (1.3 mm, 2.9 mm and 3.9 mm, **Fig. 1.13**) looped onto fishing line (Berkley Fishing, Trilene 2lb Breaking Strength). This fishing line was then fed around a Perspex U-frame, where it could be pulled by a stepper motor with controlled speed. Targets of all three sizes were presented in descending order of size for motivational control of target choice experiments, for more information, see Chapter 2: Target Selection.

To assess the behavioural thresholds of *Holcocephala* and compare these to its estimated visual resolution, we tested the distances at which *Holcocephala* would respond (i.e. take-off after) to dummy targets of varying size. It is worth noting that the target response of *Holcocephala* is not the sole product of its visual acuity, but also of an attack decision framework that assesses target suitability (to be explored in Chapter 2). For one, the peak visual acuity corresponds to an extremely small field of view at the centre of the eye. *Holcocephala* head-flick to targets in the manner of dragonflies, presumably to centre the target in the field of view of this high resolution region [43]. For this to happen, the target

must have been detected by another region of the eye, with its associated poorer visual resolution. While head-flicking may be a useful behavioural signature for the detection of a target by *Holcocephala*, the smallest targets were assumed to only be visible to the narrow acute region of the eye. Thus, the amplitude of any resultant turning action would be extremely small and could not reliably be detected; preventing us from using head-flicking as a signal of target detection. Constraints of working in a field environment also mean that there are frequent other targets airborne at any time, thus without a take-off response directed towards the presented dummy target, it is not evident whether the head-flick was to the intended stimulus.

Trials were recorded with a pair of high-speed video cameras (Photron Fastcam SA2) at 1000 frames per second. The binocular disparity of objects that fell within both fields of view could then be used to generate a 3-dimensional reconstruction of the trial. Camera calibration was provided by moving a known-sized (8.5 cm) chequerboard square within the fields-of-view of both cameras. Calibrations images were then fed to a custom written photogrammetric script in MATLAB 2014b, developed by Trevor J. Wardill. Both fly and target were manually tracked through the video frames of both cameras and their positions in space triangulated.

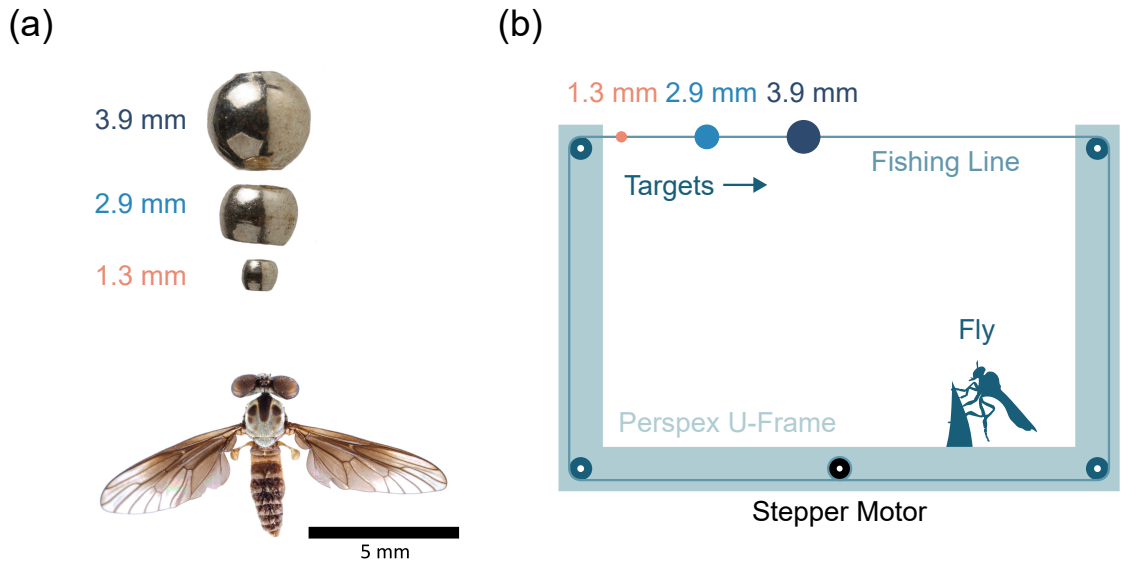

Fig. 1.13 **(a)** A dried specimen of *Holcocephala fusca* with the three silvered dummy target beads used to elicit chases, shown to scale. **(b)** U-frame apparatus used to present targets travelling in a linear fashion to *Holcocephala* (note that the real frame was transparent perspex). Apparatus is not drawn to scale.

1.4.4 Smallest Angular Size Response

Over the course of 3 field seasons on consecutive years, 455 trajectories were compiled and reconstructed in 3 dimensions. *Holcocephala* visually responded to targets at a large range of different angular sizes and corresponding target distances. The largest subtended size of a target, to which the fly took off, was 2.80°, a 3.9 mm diameter target at a distance of 80 mm. The smallest subtended size of any of the targets was 0.10°, a 1.3 mm target at a distance of 779 mm (**Fig. 1.14**). We take the smallest subtended target that elicited a flight to represent the limits of the recorded object detection threshold. Prior to take off, the rate of rotation of the line-of-sight to this farthest target was $9.0°s^{-1}$. The median angular size of targets approached by Holcocephala was 0.32° (n = 455). The median distance of response to targets was 268 mm (n = 455).

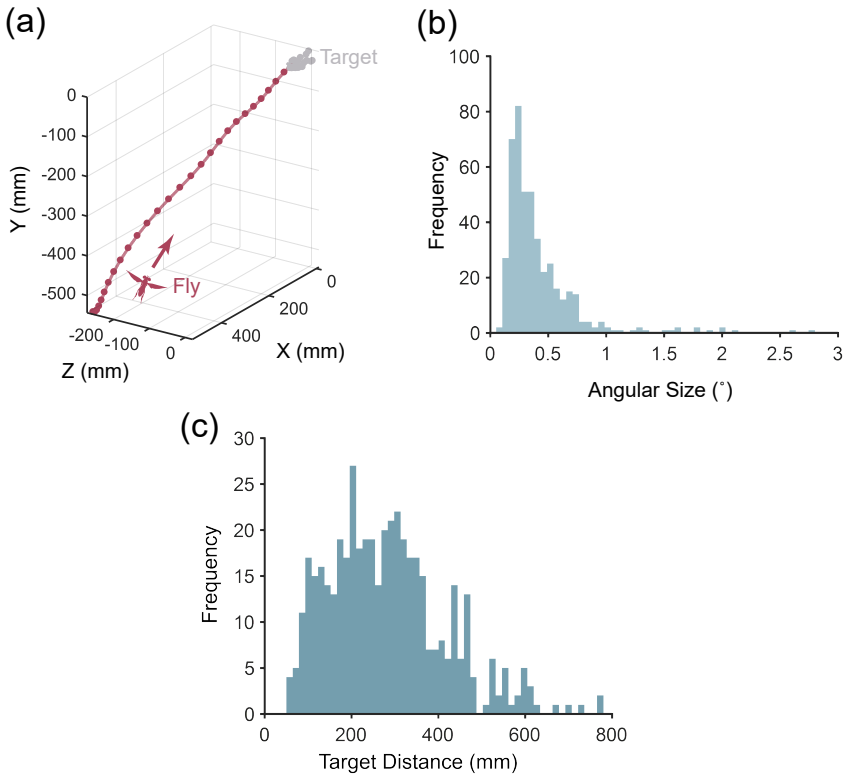

Fig. 1.14 **(a)** The longest observed interception by *Holcocephala* (red) towards a dummy target (grey). Target and fly positions are marked at 50ms intervals throughout the flight (time interval arbitrarily chosen). Coordinates originate at target starting position. **(b)** A histogram of the angular sizes of the targets that *Holcocephala* responded to. Targets of all three sizes (1.3 mm, 2.9 mm, 3.9 mm) are represented. **(c)** A histogram of the distances at which targets (of all three sizes) elicited a take-off.

1.4.5 Discussion

Holcocephala displays an ability to behaviourally respond to targets that subtend considerably smaller (near to three-fold smaller) visual angles than the smallest estimations of their inter-ommatidial angles. Thus, the inter-ommatidial resolution does not act as a hard limit to the visual perception of targets by *Holcocephala*. However, the estimated peak visual resolution (~0.28°) matches closely the median angular size of attacked targets (0.32°). The distribution of the attacked subtended sizes of targets closely matches that of the existing work from two species of dragonflies, which both feature positively skewed distributions of the angular size of targets that elicited a take-off responses, with very similar medians (0.28° for *Libellula luctuosa* and 0.36° for *Sympetrum vicinum*) [38]. The positive skew of the angular size of targets attacked is likely a necessary consequence of the non-linear relation of subtended size to target distance. A normal distribution of target distances at take-off correspond to a positive-skewed distribution of angular sizes. Furthermore, it is unsuitable to read into the response probabilities and distributions of the data at this stage. The presented distributions are for the summated data across multiple experimental procedures, not a systematic presentation testing of stimulus response purely based on angular size. For further details on target selection, see chapter 2.

The proposed mechanisms for hyperacuity [98, 106] rely on the interpolation of information gathered form movement of the target relative to the photoreceptors. This can stem from micro-saccadic movements of the retina [98] or from the movement of the target [93, 97]. In the most extreme response to a visual target, the rate of rotation in the line-of-sight (LOS) was relatively low (9.0 $^{\circ}s^{-1}$). This slow rate of angular travel is considerably lower than the peak sensitivities of STMDS in dragonflies. There is not yet the STMD data for *Holcocephala* to say whether its temporal tuning frequencies are similar to that of dragonflies. What can be said is that the ability to detect slow moving targets has also been shown in dragonflies [107]. This either shows that EMD-ESTMD is considerably lenient with its tuning function, or potentially that the high variability in the angular resolution of the eye accounts for some of the tuning discrepancy. The time taken to cross from sensor to sensor is dependent on the angular resolution of the sensors, thus in the central acute zone there would be a consequent slowing of the temporal freqency (given the same EMD delay constant τ). Taking the smallest estimate for the inter-ommatidial angle (0.28°), the mean time to cross between adjacent visual axes of photoreceptors within the acute zone would be ~30 ms (equivalent to the entire length of their behavioural response latency when intercepting the target, see chapter 3). This suggests a required τ of at least 30 ms, not out of keeping with those that are estimated for other fly species such as *Drosophila sp.* and *Calliphora sp.* [108].

1.5 Low Light Conditions

The close similarity of the interommatidial angle in *Holcocephala* to the diffraction limits of the lenses is what would be expected of a diurnal predator operating under bright conditions [50, 109, 78]. Neural superposition confers the ability to increase the sensitivity of high-resolution compound eyes [50, 58], and should thus increase the capability of *Holcocephala* to hunt into the evening as light levels begin to drop. *Holcocephala* is also aided by its upward-facing position, using the sky as a back-light, and thus is not reliant on light reflected by the surrounding scene, only on that scattered from the sky above. However, it is first worth considering how other insects compensate for the natural, large-scale, variation of light intensities over the course of a day.

Both dragonflies and blowflies can adjust the voltage response curves of their photosensitive pigments in order to adjust for fluctuations in light levels [110]. While in ants that are active in diurnal and crepuscular conditions (e.g. species of *Camponotus* or *Myrmecia*), there are retinomotoric deformations that change their light sensitivities [111, 112]. These include pupillary mechanisms to constrict the light passing to the rhabdomeres or length changes to the crystalline cone and rhabdomeres [111]. While the specific focal lengths of the lenses are not calculated, the shortening of the crystalline cones would lower the F-number (f/D) towards greater comparative sensitivity. What is not clear from this work is whether the lenses are deformed to alter their focal plane accordingly. Moving the receptors out of the focal plane loses spatial acuity through blurring, without accruing greater sensitivity [65], and thus would not clearly advantage the eyes low-light adaption.

Some dragonflies are capable of hunting into twilight, presumably adjusting their visual sensitivities accordingly (e.g. members of *Anax*, *Hemicordulia*, and *Aeshna*) although, there are not currently studies outlining how this adjustment might affect their behaviour. Some genera of dragonfly, such as *Zyxomma*, *Parazyxomma*, and *Tholymus*, are crepuscular specialists, hunting when mosquitoes abound in the late-afternoon/evening. While there are no extant flight trajectories or detailed recordings for the hunting of these groups, the vision of *Zyxomma* has been described in detail [65]. While the specific interommatidial angles are not listed, the eye parameter ($D\Delta\phi$) is given as a relatively high 1.0-1.5. Which, given the large facet size of 75μm, gives an interommatidial angle of ~0.76°. This is surprisingly large, given the relatively huge size of the lens facets. It might then be reasonably supposed that the high value of the eye-parameter is an adaptation for increased sensitivity specifically for low-light behaviour, at a cost to the spatial acuity of the eye.

Major light-adaption can occur through the migration of the absorbent screening pigments that shield ommatidia from optical cross-talk with their neighbours. This is present widely across arthropod taxa, with nocturnal species displaying the greatest capacity for light-adaption [113–117]. While nocturnal moths have multiple pigment migration mechanisms that not only have an immediate pupillary effect on the light entering the rhabdomeres, but also allow incident rays from neighbouring ommatidia to cross into rhabdomeres, increasing sensitivity at the cost of resolution at low light intensities [114]. Mantises and locusts both undergo swelling of the rhabdomere tips and a near doubling of the acceptance angle of their photoreceptors during their dark-adapted state, again increasing their sensitivity but decreasing their visual resolution [116]. This sensitivity variation allows both groups to remain active at night, although with marked behavioural differences such as broad-scale movement and migration rather than specific target or prey localisation. Within flies (i.e. *Calliphora*), pigment migration local to the rhabdomere, affecting the internal reflection such that there is increased side-mediated scattering when light levels are higher, reducing the light reaching the photosensitive pigments [115, 115] without consequently effecting the visual resolution.

If *Holcocephala* can adapt its eyes and hunt outside of bright, diurnal conditions, then there is a question over whether it is able to do so with the same degree of behavioural target discrimination. Increasing the optical sensitivity of the eye, by the means described above, frequently comes at the cost to angular resolution. However, the neural superposition eye of flies should yield greater sensitivity without costing angular resolution [50].

Experimental Aim:

We here tested whether *Holcocephala* was able to detect and intercept targets under crepuscular conditions, and whether lower light levels reduced their effective visual resolution.

1.5.1 Low-Light Filming

In order to film *Holcocephala* late into the evening, a powerful infrared light (RayTec Vario 2), was used which could be detected by the high-speed cameras. The wavelength of the light (850 nm) was invisible to the human eye and assumed to not to influence nor be visible to *Holcocephala*. Targets were presented on the Perspex U-frame as already described above. Targets were run through the pulley wheels by the stepper motor at reducing distances from the target until a behavioural response was elicited. Ambient light levels were determined

by the use of a lux meter (Sauter SO 200K). 2 light level measurements were made near to the focal perch of the video recording. One measurement was taken vertically upwards towards the sky, but out of direct sunlight (shade provided by overhanging trees). The second measurement was taken facing towards the ground below, of the light reflected upwards.

During twilight/ low-light conditions, targets were presented through a specialised methodology. Only a 1.3 mm target was affixed to the fishing line, wound around the pulleys of the Perspex U-frame. The apparatus was then held at a long distance from the fly and run through at a slow speed (0.32 ms^{-1}). If this failed to elicit a behavioural response from the animal, the apparatus was moved closer by ~5cm (decrements were approximated, due to the limitations imposed by working with hand-held equipment). If the fly took after the target, the recording was downloaded and the process started afresh.

1.5.2 Low-Light Behaviour Results

Holcocephala hunted long into the evening, with the latest recorded behaviour (20:24, 9^th August) falling after sunset (20:12). The median light levels (of all recorded flights) in which *Holcocephala* intercepted presented targets were; upward facing 6.38 klx and downward facing 0.82 klx (n = 240) (**Fig. 1.15**). The total range for both upward and downward facing light levels in which *Holcocephala* hunted dummy targets exceeded four orders of magnitude (maximum to minimum ratio of 5.7×10^4 for upward facing and 1.4×10^4 for downward facing).

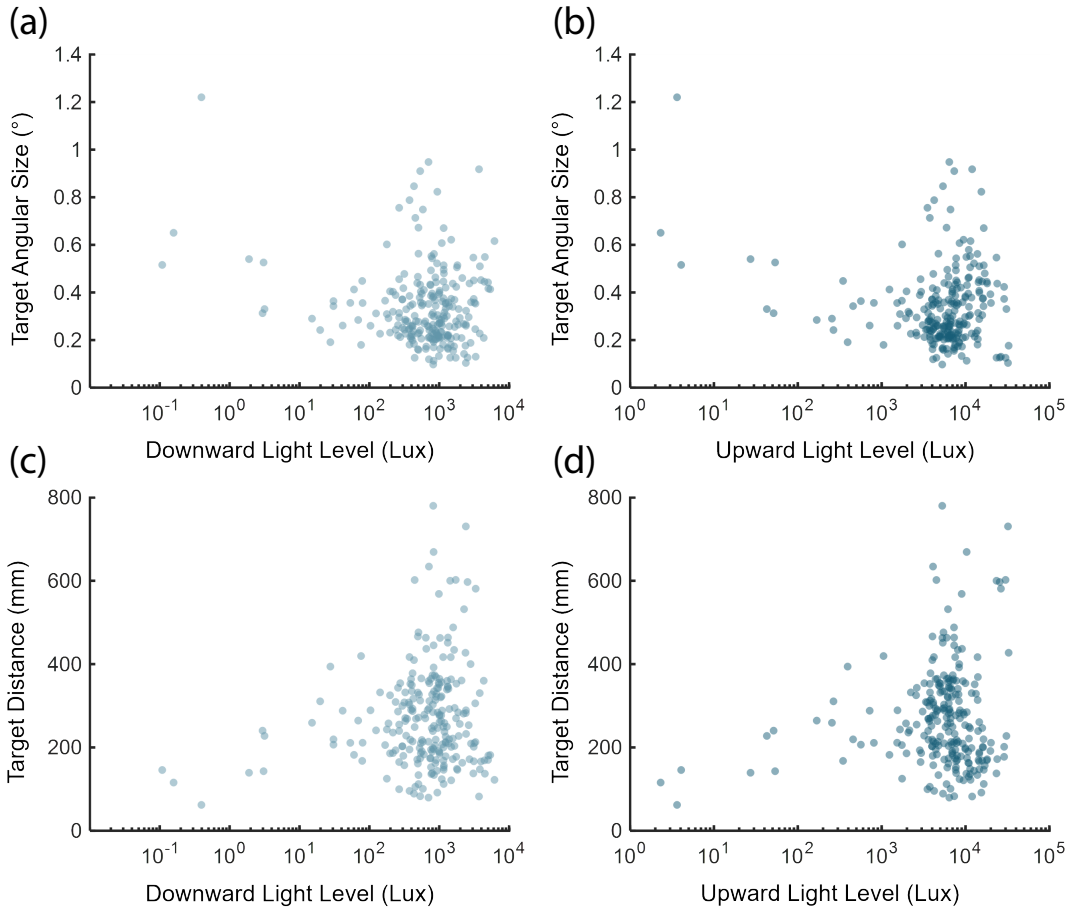

Fig. 1.15 The subtended size of targets **(a & b)** and their distances **(c & d)** is scattered against the ambient light levels of the recording. Light levels are either facing downwards, reading the reflected light from the ground **(a & c)** or directed upwards towards to the sky **(b & d)**.

There were limitations in the ability to collect low-light recordings of *Holcocephala* under wild conditions. The transfer time of recorded data from the high-speed cameras to data storage took approximately 20 minutes per recording, meanwhile light levels fall extremely rapidly during the twilight period. Of the 240 video recordings that had light levels associated, 19 had upward facing light levels of $< 10^3$ lx. This was applied as the limit of the low-light category, containing only flights using the low-light methodology of gradually decreasing the range between *Holcocephala* and the presented targets.

Within the Category of low-light behaviours, the distance at which a 1.3 mm target was attacked significantly varied non-linearly with the light intensity (Non-linear RMSE = 71, Mean-line RMSE = 88, **Fig. 1.16**). Thus, the angular size of targets that were approached increased as light levels fell. We have abstained from fitting a model to the data, given the uncertainty of the light units (lux) to a non-linear model of angular size response.

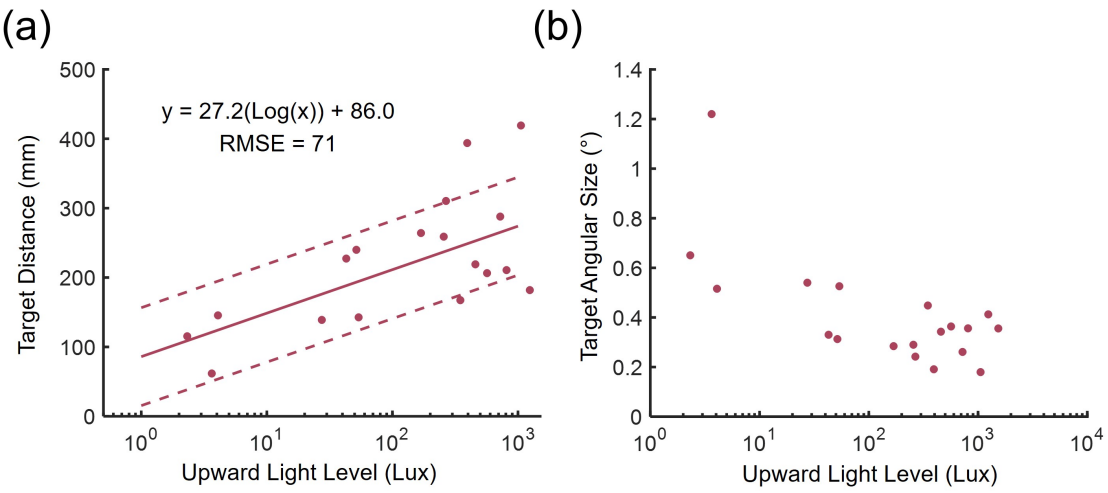

Fig. 1.16 **(a)** the distance at which a 1.3 mm target was attacked by *Holcocephala* across the natural light levels of closing twilight. Light levels are from upward-facing measurements as this has greatest significance for *Holcocephala*, which hunts from beneath its target and back-lights it against the sky. **(b)** The angular size of the targets against the upward-facing ambient light level.

1.5.3 Discussion

Low-light intensities compromise the ability of *Holcocephala* to detect targets from great distances. The results from *Holcocephala* are inconclusive as to whether there are dark-adaptive mechanisms within the eyes of *Holcocephala* that compromise the static optical resolution of the fly eye. The effects of the increased angular size of responded targets can be explained through a reduction in the signal-to-noise ratio of the eyes, which is dependent on the contrast created by the obscuring target. The signal-to-noise ratio is dependent on the light level back-lighting the target (due in large part the light intensity dependence of photon-noise [23, 59]).

The peak resolution of *Holcocephala's* eyes is represented only across a narrow region at the centre of the vision. Thus, for foveation to occur, the detection of many of *Holcocephala's* targets is by receptors with an interommatidial angle >0.3°. Given that range of subtended angular sizes at moderate low-light levels (~0.2 – 0.5°) would be in the hyperacuity range of detectability for the more peripheral (non-acute region) ommatidia, it would seem likely that the angular size increase of the pursued targets is a result of the lowered target-background contrast, rather than major remodelling of the eye through pupillary migration.

1.6 Target Detection Against Clutter

Holcocephala selects perches under the open sky [41, 42]. It has already been discussed that this back-lights the target giving great visual contrast of the target. By placing itself under the target and the clear sky, *Holcocephala* also avoids a variable object contrast to the background. There are no conflicting objects to confuse the image as seen by the fly, and thus the target is more salient. Many dragonflies also approach vertically towards their targets, isolating them from clutter [34], yet they must overcome the presence of background clutter during conspecific interactions [118], having poorer target detection against close background clutter with a similar spatial frequency to the target.

Many animals do not hunt with the target isolated from the background. This is the case for most raptors which stoop from above onto both aerial [71] and terrestrial [69] prey items. Cursorial predators must also separate the target from visual clutter along the horizon during chases [119]. Killerflies (*Coenosia attenuata*) discriminate and hunt against background clutter, in and amongst the foliage where gaps to the sky above are infrequent [33, 48]. Hoverflies that intercept conspecifics (e.g. *Eristalis tenax*) must discriminate targets that can emanate from any direction while they are hovering [65]. This discrimination has been studied down to a neuronal level, with background clutter removing the signal from some small-target detecting neurons, while others remain stimulated, displaying extreme contrast sensitivity [96].

For *Holcocephala*, the question remains as to whether their choice of perch reflects a complete inability to hunt against a cluttered background, or whether this choice reflects a preference for an easier hunting situation. This distinction is also important because hunting from below has additional benefits, such as preventing the target from perceiving the incoming predator by camouflaging itself against the cluttered background [31].

Experimental Aim:

Holcocephala generally hunts in bright conditions under the open sky. We tested to see whether they could or would still hunt dummy targets against a cluttered background.

1.6.1 Experimental Background Clutter Setup

Clutter was created though LaserJet printing patterns onto acetate sheets (Q-Connect KF00533 Laser Copier Film). Clutter patterns belonged to two distinct classes. The first is a “cloud”

pattern chosen in keeping with the visual frequency of natural scenes (**Fig. 1.17a**). This was created using 2-dimensional Perlin Noise, a function that visually mimics pseudo-random patterns of natural scenes [120]. 3 different levels of clutter intensity were generated by shifting the distribution of pixel values. This resulted in the minimum and maximum pixel values remaining consistent between the cloud intensity levels, but the distributions skewed towards darker or lighter intensities (**Fig. 1.17b**). The second noise type was a binary pixel noise. In this, pixels of either 0.25 cm^2 or 1 cm2 were used to create hard-edged clutter bounds. This clutter was used to mimic overhead tree cover in which the view of the sky above is patchy.

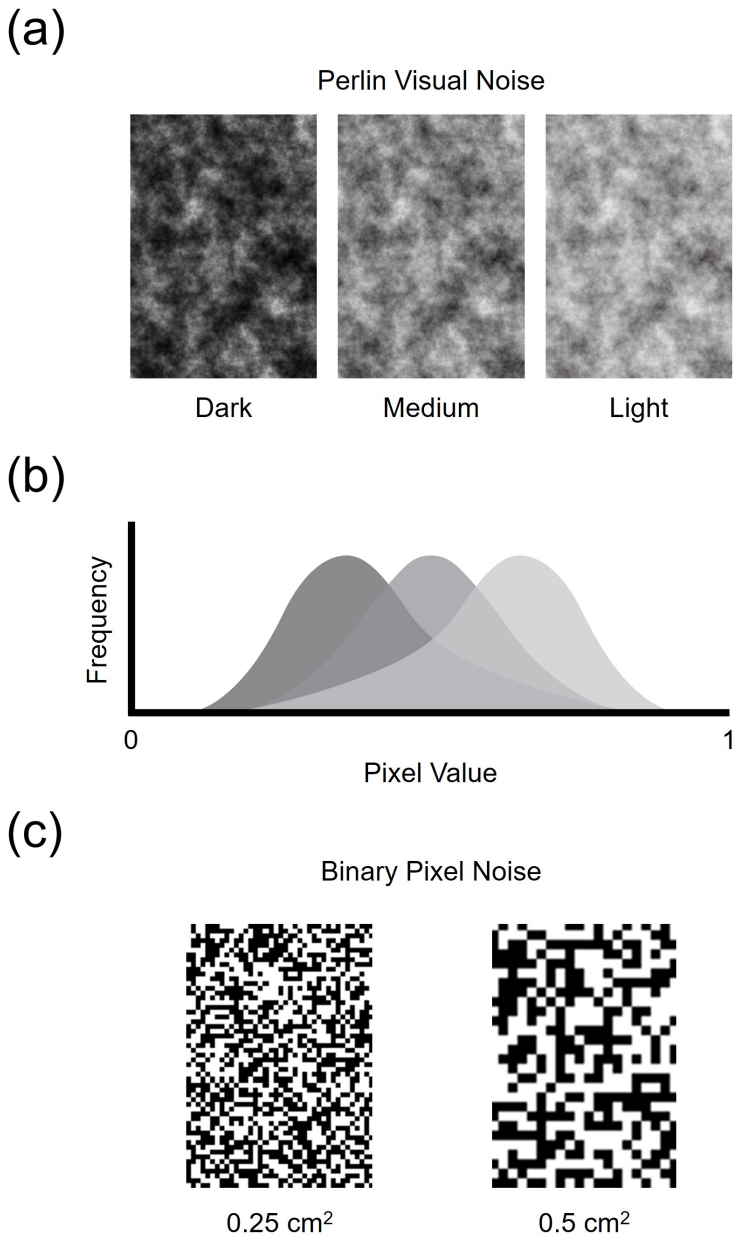

Fig. 1.17 **(a)** The three intensities of "cloud" clutter used to increase the noise of the target signal. **(b)** The skew and shift of the pixel value distributions (1 = clear, 0 = black) for each of the three cloud levels, represented by the opacity of the distributions. **(c)** The two sizes of binary pixel noise. These featured a random distribution of small (0.25 cm^2) or large (1 cm^2) square pixels that were randomly assigned values of either 1 (clear) or 0 (black).

Clutter presentation was by means of a rotatable tray that could be attached to the U-frame of the linear target-presenter. The clutter tray could rotate freely on its attachment axis, such that its plane was parallel with that of the ground. The tray could take 4 sheets of printed

clutter side-by-side (long edges touching as in **Fig. 1.19**, photographs in **Fig. 1.18**). The tray could be slid up or down the arms of the target-presenter, altering whether targets were presented in front or behind of the target. For the trajectories detailed here (other than those with clear or all-black acetate, to be discussed), the clutter is above the target such that the fly can contact the target without hitting the acetate. The clutter and target path were separated by 8 cm. All presented targets were silvered beads, 1.3 mm in diameter and the presentation speed was consistently 0.32 ms^{-2}.

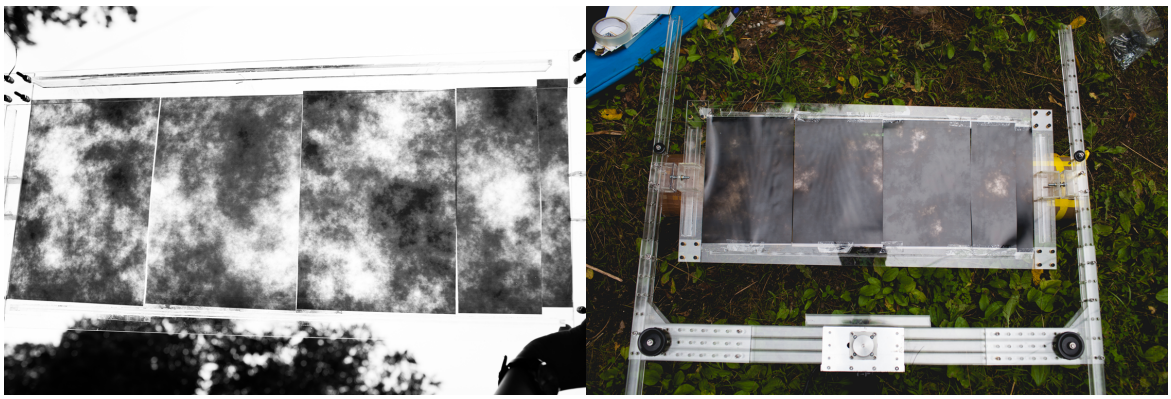

Fig. 1.18 The clutter tray, suspended on the linear target presenter, is photographed from below (*left*) and from the side (*right*). Note that the right picture shows the tray at 90° to its rotation when held above the flies.

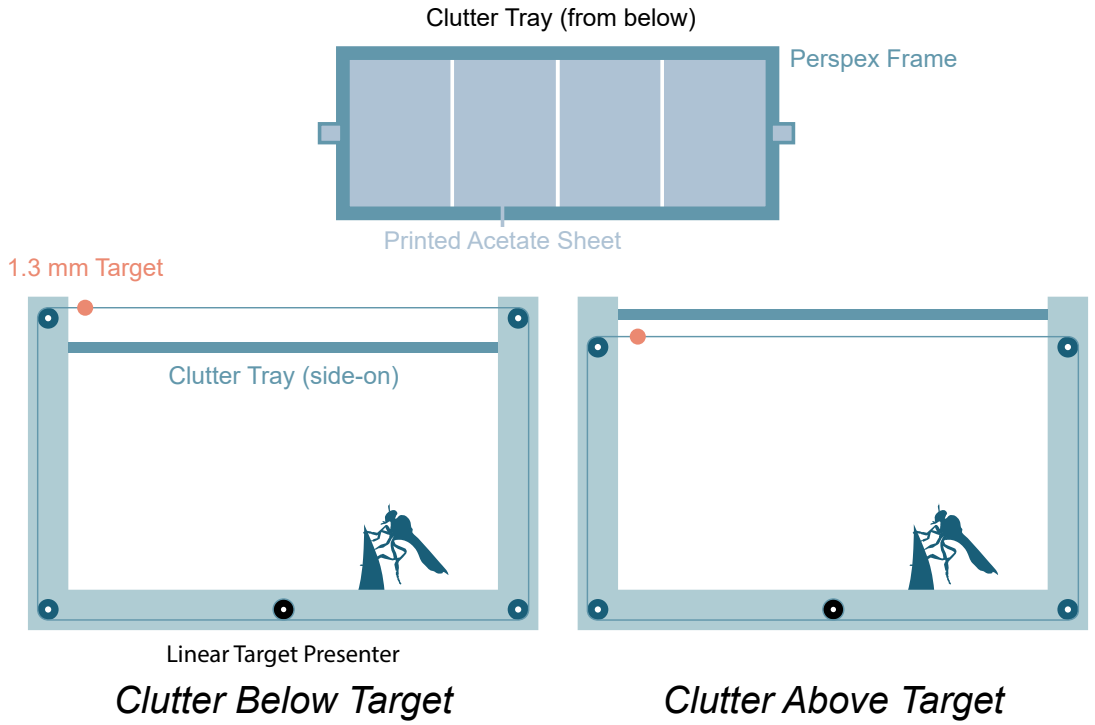

Fig. 1.19 Diagram of the clutter presentation methodology. The clutter tray, complete with printed acetate sheets, can be slid up and down the arms of the linear target presenter. While here the clutter tray is shown below the target, this was only the case for clear and all-black acetate presentations. All others had the clutter tray positioned on top of the target path.

The limitations of field-based experiments meant that the background illuminant of the sky could not be controlled for, meaning that exact contrast measurements could not be determined for the target against the clear or cluttered background. The acetate sheeting did not appear detectable or at least salient to the flies. This was determined by placing the clutter tray below the line of target travel and using clear sheets of acetate instead of clutter, the flies would take-off to intercept a 1.3 mm target, only aborting the flight after they physically collided with the acetate sheet (**Fig. 1.20**). The same manner of testing was used for all-black printed acetate sheets. Flies, however, could not be persuaded to remain perched when an all-black clutter tray was used. Subsequent experiments using black bars of printed acetate demonstrated that flies could not track targets through acetate printed all-black (see Chapter 6: Obstacle Avoidance).

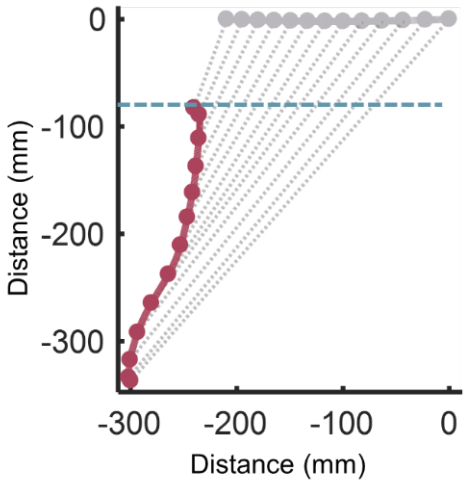

Fig. 1.20 *Holcocephala* rises to meet an oncoming target that is behind acetate sheets (blue line). The fly crashes into the sheet and thence returned to its perch.

Clutter presentation was frequently accompanied by a particular behaviour of flies. As the clutter tray was moved into place, over the region of sky approximately matching that directed towards by the body axis of the flies, flies would pirouette on their perches. Pirouetting behaviour would invariably then direct the body axis towards a region of the sky that was not covered by the clutter tray. Clutter presentation was also commonly accompanied by flies taking off and re-perching elsewhere, however the frequency of this behaviour was not measured.

1.6.2 Catch Frequencies

Holcocephala was able to take off and intercept targets that were shown in front of a cluttered background. *Holcocephala* did not show a systematic trend of deteriorating ability to catch targets for increased clutter intensity. The catch frequencies (successful catches as a proportion of take-offs) for the three intensities of clutter were: for light cloud 63% (19/30), for medium cloud 100% (7/7), and for dark cloud 68% (13/19). The flies were also equally able to intercept targets against binary pixel noise. The catch frequencies were: 50% for 0.25 cm^2 squares (5/10), and for 1 cm^2 50% (10/20).

1.6.3 Discussion

The results from this experiment clearly demonstrate that *Holcocephala* can detect and catch targets against a cluttered background. The equivalence of catch frequencies across multiple forms of noisy clutter show their tracking system is adaptable to variable contrast of the target against the background. This remains true for both "cloudy" patterns in which contrast variation is smoothly gradated, and for pixel clutter in which contrast variations are sharply defined.

These catch frequencies suggest that *Holcocephala's* perch selection is not based on an absolute limitation of what background targets can be pursued against. Within these clutter-presentation experiments, *Holcocephala* did not show systematic deterioration of its ability to catch targets against increasing visual clutter. However, the number of repeats were relatively low. The targets all travelled in a straight line and with constant speed, making their path predictable. While we have not yet presented evidence for the interception algorithms used by the flies (see Chapter 3), dragonflies have recently been shown to incorporate a prediction of the target flightpath into internal models that direct head-turning and target foveation [76]. This predictive fixation, in the manner of that described for predictive modulated neuronal gain in dragonflies [121], would act as a matched filter for a linear target trajectory (or its spherical projection onto an egocentric reference frame), potentially compensating for a cluttered background. If this were the case in *Holcocephala*, then cluttered backgrounds would have greater significance on the catch capabilities of flies hunting erratically moving targets, that vary both speed and direction of flight. Testing flies with targets that move variably against cluttered backgrounds would illuminate if this was a limiting factor, provided a control could be found for the inherent variability in catchability of targets that manoeuvre in different patterns and at different distances to the predator [35, 122, 123].

Another consideration is in the detectability of targets, rather than their catchability. The above experiment did not systematically test for the detection threshold for targets against different backgrounds, only the frequency of catching once the fly had opted to take-off after the target. We have already seen that the range at which small targets are perceptible is limited by low light levels, the same potential is inherent against clutter, which reduces the contrast of targets.

Secondary considerations of ecology and insect behaviour must also be considered. *Holcocephala's* site selection criteria may also be determined by the abundance of prey. Aerial prey is unlikely to be equally distributed through different levels of canopy occlusion of the sky. Forest boundaries frequently have high abundances of flowering plants while

water may attract numerous species of small insects including gnats/ mosquitoes. It is also worth considering that we make an assumption that *Holcocephala* is not distributed within the canopy or high on woody plants, yet were they present, they would not have been easily observable from the ground. Other publications have however noted that *Holcocephala* is found only on low-lying vegetation [41, 42].

1.7 Conclusion

Holcocephala fusca have exceptionally fine visual resolution, not only for their small size, but when compared to all other compound eyes. The estimates for their peak spatial resolution (~0.28°) approach the very best measures for compound eyes, in the largest aerial predatory insects, dragonflies (i.e. Aeshna palmata ~0.24°). Holcocephala achieves this visual resolution across a narrow acute region at the forward centre of each eye. The few ommatidia within this region have exceedingly large corneal lenses (up to 78 μm) which reduce the diffraction limit of optical resolution. These ommatidia also have long focal lengths (~190 μm) directed onto small and tightly bundled photoreceptor tips (1.15 μm inter-rhabdomic spacing) that, nevertheless, sample distinct regions of the visual scene for subsequent neural summation with corresponding neighbours. This neural superposition design (as yet uniquely demonstrated in Diptera [50]) increases sensitivity without compromising spatial resolution.

This fine optical resolution does not represent the behavioural threshold of the flies towards dummy targets. Flies consistently demonstrated the ability to detect targets that subtended smaller angles than interommatidial angles of the most acute regions of the eye (smallest subtended angle of 0.10° for a caught target). This allowed the fly to intercept a 1.3 mm target first observed up to 78 cm or 130 body lengths away.

The flies' eyes represent the hallmarks of a near diffraction limited compound eye, functionally adapted to high target contrast and low rates of rotation (eye parameter of ~0.35 μm). Despite this, *Holcocephala* demonstrated an ability to hunt in light levels that varied across 4 orders of magnitude, hunting into twilight hours after the sun has set. This low-light hunting ability comes at a cost to their target detection system, with the minimal angular size of targets that flies responded to increasing as light levels fell. Whether this is the result of optical adaptation or a consequence of reduced signal to noise ratios is not yet clear.

Holcocepahala is generally found perched upward facing towards clear regions of sky. This perch choice gives the greatest visual signal-to-noise as targets are silhouetted against the open sky. This choice of perch is not representative of the firm behavioural limits

of the fly. *Holcocephala* is capable of hunting against noisy backgrounds that have both diffuse perlin noise variation and hard-edged binary pixel clutter. Varying the skewness of the intensity of the diffuse clutter and the size of pixel clutter did not degrade the catch probability of the targets, suggesting that once a target is being visually tracked, the fly is capable of compensating for large variations in target-background contrast. Low-light levels reduced the hunting range of the flies. While hunting range was not systematically tested or demonstrated for noisy, cluttered backgrounds, theoretically the same should apply (increasing noise decreases target detection range). It is therefore suggested that perch choice may reflect either ecological prey distributions or maximisation of the initial detectability of prey and the range over which it can be seen.

Chapter 2

Target Selection

Abstract

This chapter concerns the remarkable ability of *Holcocephala* to distinguish the suitability of targets based on their true size. *Holcocephala* shows a preference for smaller prey items, selectively hunting the smallest (1.3 mm) dummy target with much greater probability than either of two isometrically scaled counterparts (2.9 mm & 3.9 mm). We controlled for object size cues such as angular size and angular speed (controllers of hunting probability in the killer fly) but found that *Holcocephala* still opted to attack the smallest target at a greater frequency than the other two. We controlled for further potential cues such as target looming and even held the targets in near static positions. In both cases, we were unable to break *Holcocephala's* ability to pick out the smaller, more suitable target. This work suggests that *Holcocephala* may implement an absolute means for detecting target range and absolute size, at least for a ~20 cm range.

2.1 Size and Predation

For survival, predators must outweigh the energetic costs involved in attacking other animals with the payoff provided by catching a proportion of them. One way to improve the return per effort is to select the best targets. When fast responses are obligatory, a range of simple strategies such as matched filters or heuristic rules free the animal from time consuming integration of information. For example, dragonflies and killer flies attack fleeting prey, and their attack decision can be predicted by a combination of angular size and angular speed of

prey in their visual field [33, 107]. In contrast, animals that cannot correct the attack once launched, or those unlikely to have a second chance of attacking, are primed for accuracy. Thus, they invest into mechanisms for gathering highly reliable information. For example, to calculate the absolute distance to their target, jumping spiders use their four-tiered retinas to observe distance-dependant aberrations [124], chameleons use the accommodation required of their lens to focus the target image [125], and mantids use the image disparity between their two compound eyes [126].

Myriads of parameters may affect prey selectivity, including predator body size [127, 128], sensory ability [129], and energetic investment per attack [130], as well as prey type [39], density [131] and activity [132]. Therefore, when aiming to understand what adaptive mechanisms underlying predatory decision making, it is useful to investigate animals behaving at the extremes. In miniature visual predation, this is exemplified by *Holcocephala fusca*. As discussed in the preceding chapter, *Holcocephala fusca* is a North American robber fly (Asilidae) only 6 mm long. In its predatory posture, *Holcocephala* sits on a perch diagonally (see Choice and Biology of Research Species), looking towards the clear sky and taking-off after smaller arthropods that fly overhead [41, 77]. As seen in chapter 1, the spatial visual acuity of *Holcocephala* is on a par with those of aeshnid dragonflies, as the best in any known compound eye [77]. Because visual acuity and eye diameter are correlated (see Box 2, from [133]), this is a particularly extreme adaptation for a small predator with small eyes (~0.75mm). This unusually high visual investment allows *Holcocephala* to detect and attack prey that are 130x times the distance of its own body length [33]. As will be examined in chapter 3, *Holcocephala* intercepts its prey, using control algorithms analogous to those used to guide modern missiles [134]. After contact is made mid-flight, *Holcocephala* must grapple with the prey and carry it back to the perch.

Larger prey items have greater energetic rewards, but are also likely harder to subdue, and are likely able to travel faster, limiting which predators will be able to consume them [135]. Predator size has been shown to be reflected in the size selectivity of different dragonfly species [38], with larger species having a preference for larger targets. *Holcocephala* continue this trend, being observed to consume only a narrow range of small prey sizes (1 to 3 mm [41]). While size selectivity may appear strongly enforced, prey species is not. *Holcocephala* show an extreme breadth in their diets, intercepting many different orders of insect, as well as ballooning spiders [41]. Despite this, there are numerous “unsuitable” targets that regularly fly overhead, including birds and larger insects (e.g. large Lepidoptera, Coleoptera, Hymenoptera etc.). Previous work on prey selectivity in *Holcocephala* has focused on the study of prey items brought back to the perch [41, 42]. Thus, it is unclear whether the selectivity is pre-take-off, or whether it reflects a success of interception relationship where

larger targets are unsuccessfully attacked. However, unsuccessfully attacking large targets could pose significant risks and costs; it is in the interests of the robber flies to not waste this time and energy.

To determine whether a potential prey is within such a size range, *Holcocephala* could gather relative visual cues and employ heuristic rules, as dragonflies and killer flies do [33, 107]. This approach is effective because it meets time pressures for the task, avoids loading a miniature neural system with further computation, and still provides the animal with the opportunity to abort the attack, should more reliable cues become available. However, every time the attacked target turns out to be unsuitable, an energy cost is incurred without any pay-off. Since prey density and diversity is high in the riparian habitat of *Holcocephala*, the costs of such errors could be high, especially so for a predator with a long detection range. *Holcocephala* could therefore increase its fitness dramatically by choosing targets based on actual prey size, but for this, absolute distance would need to be known.

2.2 Visual Size Assessment

There are numerous cues available to an observer that allow it to assess the size of an unknown object within its visual field. Primarily, an observer must combine the visual angle subtended by an object with an index of the distance to the object to gain an accurate impression of size. In isolation, the subtended size of an object gives no information as to its true size. An object could, for instance, be twice the size and double the distance away without changing its apparent subtended size to an observer.

2.2.1 Parallax

Absolute information on target distance can be found from parallax. Parallax is the rule that the composition of a visual scene changes depending on the vantage point of the observer, and that these changes are a product of the proximity of the elements making up the scene. For a fixed distance between two vantage points, the angular change in the placement of a target image is greater the closer it is. The compared vantage points can be sampled either at distinct times or cotemporally.

To sample a visual scene at two timepoints represents a principle named motion parallax [136]. This can be done with a single eye but requires knowledge of one's own self motion [137]. The distance between the two vantage points being compared is critical to the distance

calculation, and can either be integrated from sensory information or innately known through the performance of stereotyped translation of assumed magnitude [138, 139]. Motion of the target is also of critical importance. Should the target be stationary, then no compensation need be made, however any translation on the target's part will alter its change in visual angle and thus alter the distance calculation unless factored in. While this calculation is here being represented as a two-timepoint comparison, it works equally as a comparison between two time-series, rate of rotation of the line-of-sight to the target and the rate of one's own self translation.

Motion parallax is conducted by locusts and other orthopterans prior to a jump to assess the proximity of nearby objects. In the desert locust (*Shistocera gregaria*) a peering behaviour, in which the animal rapidly translates its head side-to-side, precedes a jump [140] and alters the jump velocity in accordance with the calculated distance to the target [138]. Another similar case is the body swaying that generates motion parallax which mantis nymphs use to judge jumps from exposed positions onto nearby objects [139]. Motion parallax in relation to predation of a moving target has been suggested as one potential explanation for how tiger beetles adjust the gain of their pure-pursuit steering controller at critical distances from the target [137]. As the tiger beetle runs, its head bobs from side-to-side and by comparing the image position of a target at either extremity of the head-bob, the tiger beetles have the possibility of assessing the distance to the target. This still requires they account for the relative velocity of their target, with no current suggestion of how they might do this. One potential way to assess target motion would be in the contextual cues of the target on the ground, comparing the motion of the target to visual features it is near. This is untested, but nevertheless would not work for *Holcocephala*, where targets are silhouetted above the predator and isolated from nearby contextual cues. Tiger beetles may also use a visual elevation mechanism, but based on their height from the flat plane of the ground and the visual angle of the target from the horizon [137]. *Holcocephala* cannot make assumptions about the plan on which the target rests, thus this method is not applicable. Motion parallax has been suggested to facilitate prey size selectivity of dragonflies [38, 43], but subsequently discounted based on reconstructions of head movements showing they have near no translator component [107].

Problems of knowing motion, either the target's or one's own, are not present if multiple (2 minimum) vantage points can be assessed cotemporally (**Fig. 2.1**). This requires the observer to have at least two eyes, whose fields of view at least partially overlap despite having a physical separation between them. The observer must also solve the correspondence problem, that being identifying elements of the visual scene as the same between both eyes. Triangulating distance from two eyes is termed range-finding stereopsis [141]. Distance

judgement through stereopsis is well established in vertebrates, from humans [142] to cats [143] and falcons [144]. Examples of stereopsis from arthropods are far fewer. The effective range of stereopsis is a product of both the interocular distance and the spatial resolution of the region of binocular overlap. Arthropods tend to both be smaller (and thus have reduced interocular distances) and have poorer visual resolution than camera-eyed vertebrates. Nevertheless mantids use stereopsis as a cue to initiate striking at a target that has come into range [126]. Stomatopod mantis shrimps have a unique visual physiology, including the ability to judge absolute distance using either of their two eyes singularly. They achieve this as each eye is effectively trinocular, with three regions of ommatidia having overlapping fields of view in each eye [145]. Dragonflies have also been suggested to be using stereopsis to influence their target selection [38] by using their high-resolution acute regions that have a significant binocular overlap [65], however this has not been conclusively demonstrated.

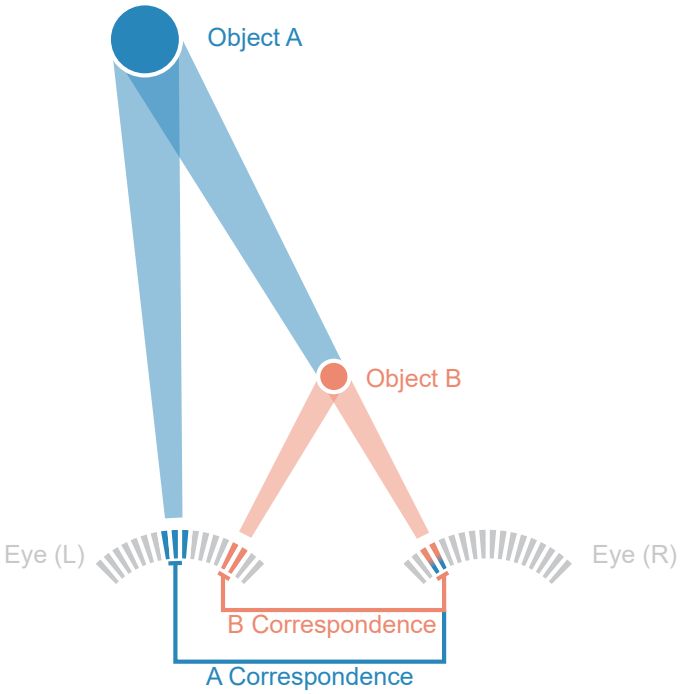

Fig. 2.1 Two objects (A & B) would be visually identical from the perspective of the right eye. However, with a second eye the distance and size of both targets can be calculated, providing the correspondence of each object between the two vantage points can be determined. While the eyes are represented as performing stereopsis, sampling at the same time, this principle applies if a single eye was moved between both locations, as in motion parallax, provided the distance travelled is known and the object remains static.

2.2.2 Heuristic Cues

Instead of absolute cues, of target distance, insect aerial predators have been found to be using heuristic rules that filter potential targets based on the limited cue space that targets in the real world are to occupy. First described in killer flies [33] and more recently in dragonflies [107], a loose-fitting angular speed / subtended size ratio (with units of $[\text{TIME}]^{-1}$) describes the take-off probability of the predator in response to dummy targets. Body lengths per unit time across the visual field can filter out unsuitable targets based on the characteristic speeds flying animals of different sizes are likely to take. As described in Olberg 2000 [38], larger animals likely fly faster than smaller ones. For instance insects typically fly 2 – 4 times slower than birds[146, 147, 20] in part due to the higher drag acquired when flying at low Reynolds numbers (dimensionless quantity that describes the ratio of viscous to inertial forces at different velocities and spatial scales [148]). However, the variation in size and speed are not linearly proportional, resulting in an animal that is small and flying close to the observer likely having a higher size/speed ratio than one that is larger and flying further away. We might expect *Holcocephala* to use a similar ratio to that of the killer fly *Coenosia attenuata*, that loosely fits a ratio of 0.3 ms^{-1} [33].

Targets travelling on a linear path at a fixed speed past an observer will increase in apparent angular speed until the zenith, overhead, and will then decrease again. The same is true of their angular size. The magnitude of the rise and fall in subtended size and angular speed is particular to and covariant with the ratio of the two. Thus, there is the potential that predators could be selecting target size not based purely on an angular speed / subtended size ratio, but on a threshold rate of change in angular size or speed that is indicative of a smaller target. In the case of a biological system, absolute information about target size and distance may not be required, it may only require that a system is good 'enough'. Rough, heuristic rules for gauging target size may not be true or optimal for all possible stimuli (i.e. extremely fast, large flying objects), but may be sufficient given that only a naturally limited range of potential targets are encountered in the real world.

The conditions imposed on an aerial predator like *Holcocephala*, launching upwards from a perch towards a target silhouetted and moving against the open sky greatly restrict the use of other potential distance cues. One such would be a target's context within a visual scene, but when against the open sky, the target is not set within a context it can be compared to. They are also likely unable to use pictorial cues or recognition as they behaviourally respond to dummy targets that bare very limited resemblance to true prey items [77]. A predator could also classify the size of flying animals based on their wingbeat frequency, as smaller insects generally have higher wingbeat frequencies than larger ones [149, 150].

Predatory insects tend to have fast vision with a high flicker fusion frequency [37], and thus are potentially capable of detecting this variation. The use of this cue has not yet been demonstrated for an insect predator. However it is clear that for most tested insect predators, this cue is not a required feature as marked by their attacking small targets that do not have an inherent flicker to them, whether dummy targets [33, 76, 77] or small ballooning spiders floating on gossamer silk threads [41].

In this section of work, we have investigated whether *Holcocephala* uses heuristic cues to determine suitable targets. We use target choice field experiments, in which visual cues were tightly controlled. The results from these experiments suggest that the predatory choice by *Holcocephala* arises through a calculation of absolute distance to potential targets and hence prey size, within a ~20 cm range. Beyond this ~20 cm range, *Holcocephala* behaviour can be explained by the use of monocular visual cues, such as angular prey size and velocity.

2.2.3 Methodology

To test the size discrimination of *Holcocephala*, individuals were presented with dummy targets of three distinct sizes. Targets were silvered beads with diameters of 1.3, 2.9 and 3.9 mm (**Fig. 2.2**). These sizes were chosen based on exploratory testing and on the size ranges of the prey items *Holcocephala* was observed intercepting. Presented targets that were knotted onto fishing line. Predatory flights were filmed with a pair of high-speed cameras (Photron fastcam SA2) with overlapping fields of view and running at 1000 fps, resulting in a 1ms time resolution in all presented data. The flights were then reconstructed using an 8.6 cm calibration square displayed to both cameras simultaneously, such that the position disparity between the fly and target in both cameras could be converted into positions in 3D space. Both target and fly were tracked by hand in the high-speed videos, and the raw data smoothed to remove jitter generated during the tracking process. Smoothing took inspiration from [151], and used a penalisation of jerk (time derivative of acceleration) in the path integral as a means of regularising a generative model of object position. The exact weight given to the penalisation was assessed using ordinary cross-validation in which each data point is in-turn removed and a weighting estimate is made for the rest of the data. The resulting data point has its prediction error calculated and these errors are summed. The least sum of error was taken to be the most reliable weighting.

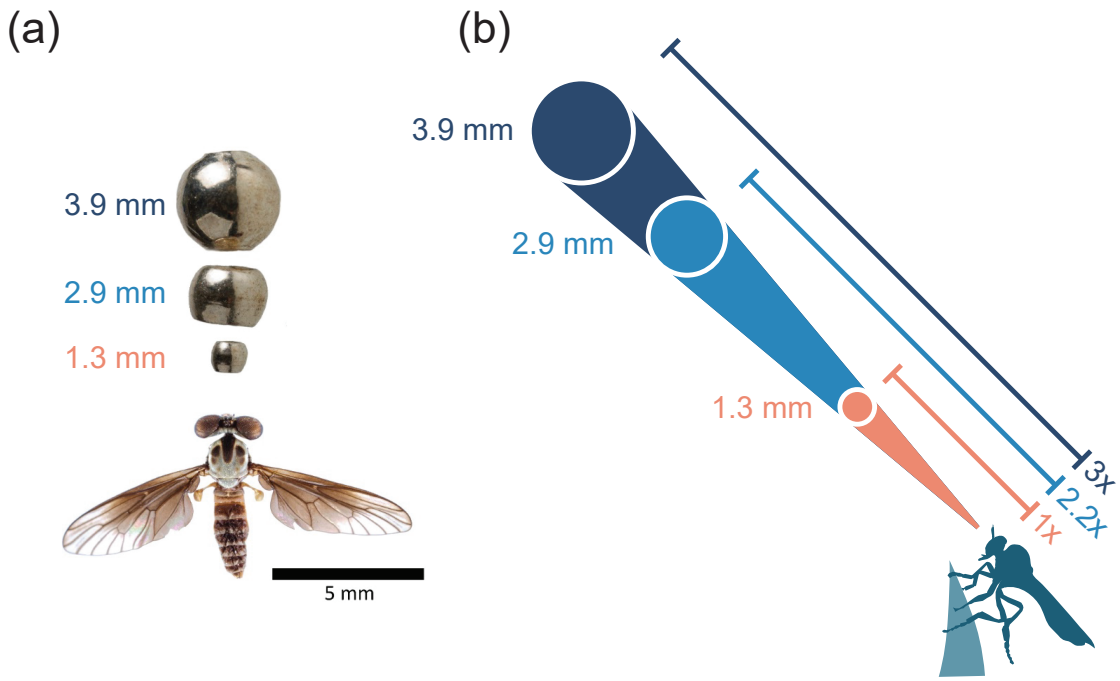

Fig. 2.2 A dried *Holcocephala* specimen is photographed next to the three sizes of silvered targets used for target choice experiments.

Linear Target-Trajectories

In the first experiment, we moved targets linearly, and sequentially. Beads of three sizes were threaded onto fishing line in order of decreasing size (3.9, 2.9 and 1.3 mm). The three beads were presented in each trial by moving the fishing line around 4 wheels on a U-shaped frame, with a stepper motor (23HS-108 MK.2) whose speed could be accurately controlled through a computer interface (ST5-Q-NN DC input stepper drive Q controller) (**Fig. 2.3**). The U-Shape frame was aligned such that the fishing line passed through the visual field of a fly sitting at the top of a perch. As the motor wheel rotated, the targets were presented in a linear fashion. This arrangement controlled for response detection and motivation. This was based on the assumption that if *Holcocephala* did not take off after the large target, but attacked the smallest one, the initial refusal was based on a choice, and not a lack of object detection or hunting motivation. This was an important control, as motivational states influence the take-off probabilities in other predatory flies [33]. The trials where no response was elicited for any of the targets were not saved for further analysis.

Beads were presented across a broad range of different distances to test the effect and role of prey angular size and velocity: Target linear speeds (0.1 – 1.0 ms^{-1}) were selected so

that the ratio of the angular size to the angular velocity would overlap between the targets of different absolute sizes. If the fly took after one of the targets, the recording of the trial was saved. Due to time constraints of transferring data from the cameras to storage, only the section of the video involving the pursued target was saved and digitised.

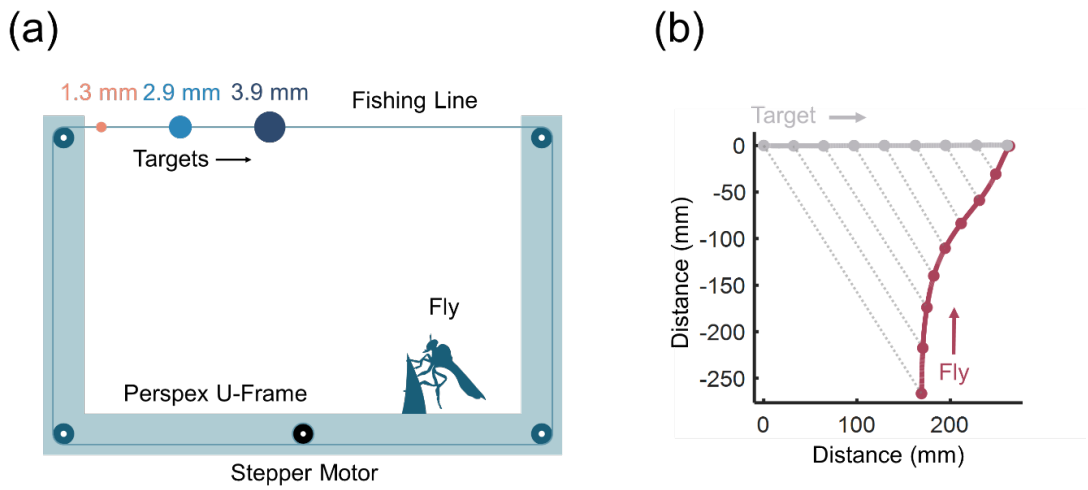

Fig. 2.3 **(a)** Presentation of targets travelling in a linear trajectory. Targets are pulled through pulleys around a Perspex U-frame by a speed-controlled stepper motor. Targets are presented, knotted onto a fishing line, in decreasing size. **(b)** An example trace of *Holcocephala* intercepting a linearly travelling target.

Round Target-Trajectories

In the previous experiment, two cues may have influenced the results: looming and priming. Targets travelling in a straight line vary predictably in angular size and speed as they pass an observer. This is because the range between an observer and an object on a linear path necessarily varies, at first decreasing and then increasing as the target passes its closest approach (its zenith). A predator can apply a filter in order to select for targets whose angular size, angular speed, or both changes rapidly. To remove the distance cue provided fluctuation of angular size or speed, in the round-trajectory experiments targets were made to travel in an arcing orbit around an individual fly. We achieved this by attaching the fishing line with a single target of one of the three sizes (1.3, 2.9 & 3.9 mm) across a small foamboard U-frame. We attached the small U-frame to a rotating arm, operated by a pulley connected to a stepper motor (**Fig. 2.4**). To vary the distance and thus angular size of the target, we moved the U-frame up and down the rotating arm. By moving in an arc, the target neither approached nor receded from the fly and did not vary in angular velocity.

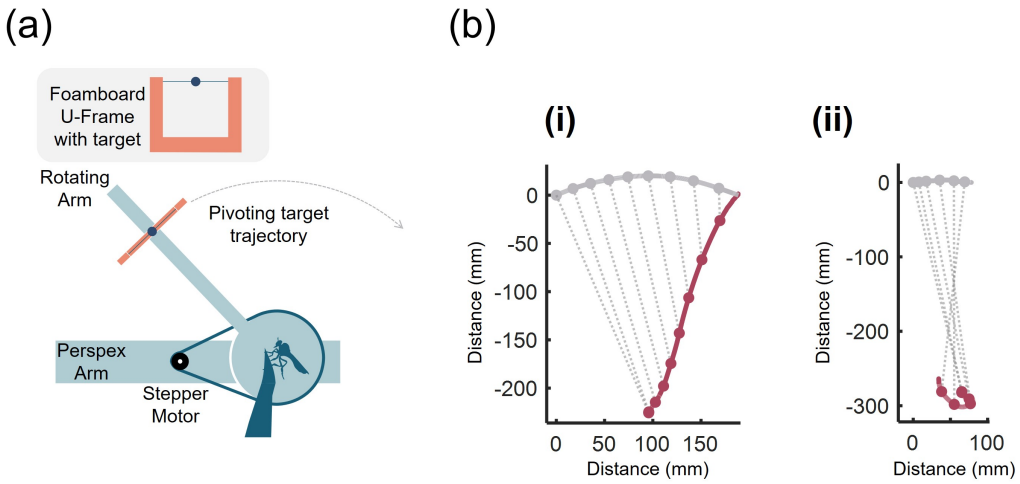

Fig. 2.4 **(a)** Presentation of targets travelling in arcing trajectories. Individual targets are suspended on a foamboard U-frame, affixed to a rotating Perspex arm. The Perspex arm is in turn driven by a pulley connected to stepper motor. **(b)** Two alternative flight behaviours to arcing targets. (i) *Holcocephala* intercepts an arcing target successfully. (ii) *Holcocephala* takes off but retreats from the target, not attempting to intercept it.

Mirror Trials

The final test of the size-discrimination capabilities of *Holcocephala* was to reduce the prey motion to a minimum. We achieved this using a mirror to cover the target (suspended on a U-frame), as it was placed into the field of view of the experimental fly (**Fig. 2.5**). The U-frame could be slid up and down an arm to vary distance from the fly. We angled the mirror such that it would reflect the sky behind the fly as the target was put into place. Once in place, we removed the mirror, revealing the target to the fly. If the fly took off for the target, we noted this as an attack and recorded. If the fly did not take off after ~5 seconds, the mirror was placed in its original location, in front of the target, and then removed again. In this manner, the target was revealed at most 3 times, in the same spot. We revealed the target multiple times to account for possible effects of distraction by other (live) targets at the same time the bead was revealed. If the fly did not take off after the 3rd presentation of the bead, the video of the final presentation was saved for analysis.

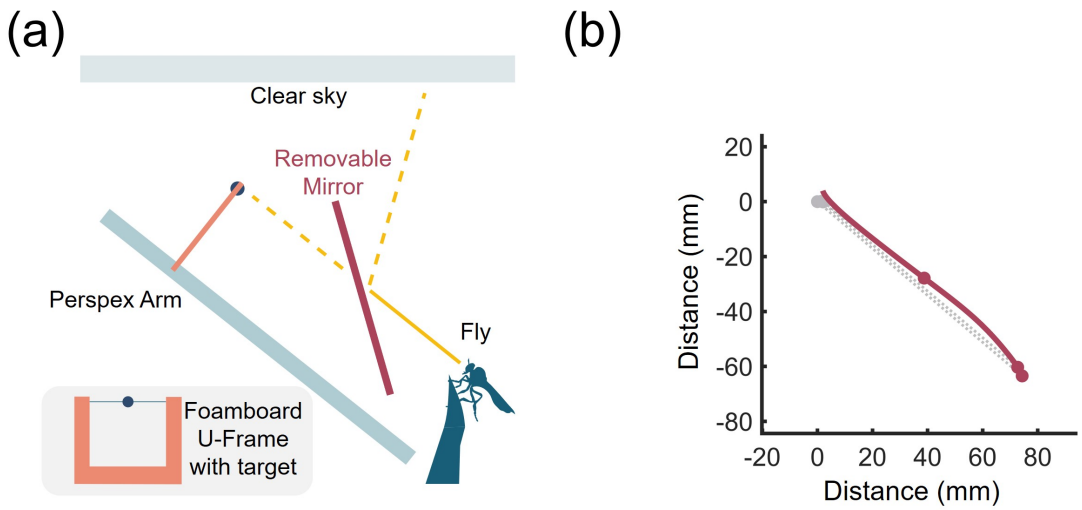

Fig. 2.5 **(a)** Presentation of targets from behind a mirror. Targets suspended on a U-frame affixed to a static Perspex arm are revealed by pulling away a vertical mirror, to remove potential target movement cues. **(b)** *Holcocephala* intercepts a near-stationary target revealed from behind a mirror.

Behavioural Classification

The initial behavioural classification for any trial in any of the three experiments was binary. This binary categorisation was based on whether the fly took-off or remained on the perch and ignored the target. Within the take-off trials, flights could be separated between those where the predator caught the target (**Fig. 2.6a**) and those where the predator quit before making contact with the target (**Fig. 2.6b**). Within some of the quit trials, the predators exhibited a shadowing behaviour, similar to the behaviour elsewhere called 'tracking' [32, 152]. During shadowing, at some point during the flight aimed for interception, the fly stopped closing the range between itself and the target and began to maintain a near-fixed range (**Fig. 2.6c**). These are worthy of note as dissimilar to other quits, which did not feature a shadowing phase. The exact motivations behind a quit cannot be determined, but they can be correlated with type of target presented, and interaction i.e. predator losing track of the target or switching to an avoidance tactic based on a visual feature (e.g. looming rate).

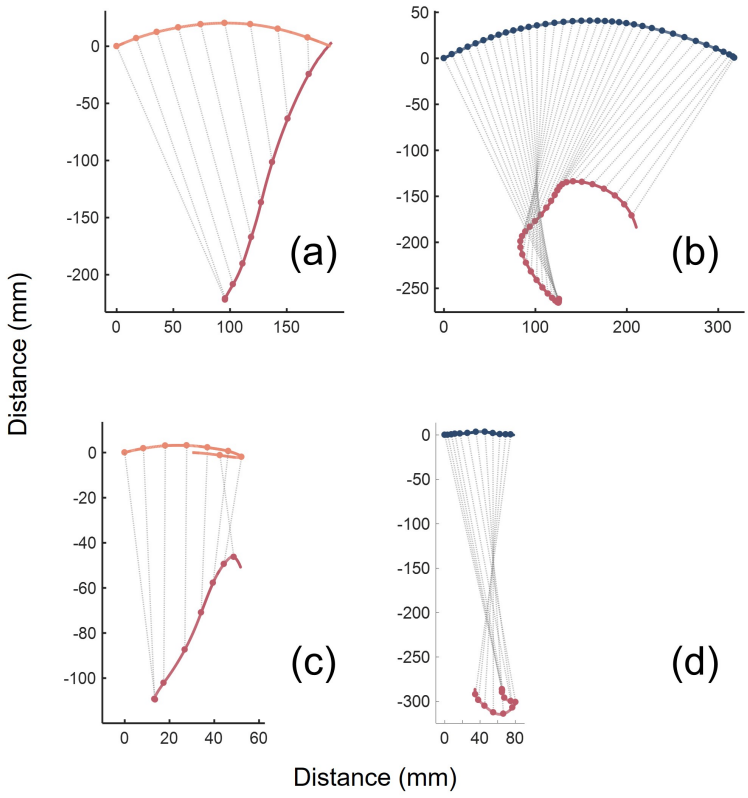

Fig. 2.6 **(a)** *Holcocephala* (in red and below) takes off vertically to successfully intercept a dummy 1.3 mm target (in orange) that travelled in an arcing path. **(b)** *Holcocephala* quits the interception of a 1.3 mm target as the target doubles back on itself at the end of its track. **(c)** *Holcocephala* quits an interception towards a 3.9 mm target (in orange). **(d)** *Holcocephala* undergoes a "retreating" behaviour, taking-off, but with a course that avoids rather than intercepts the target. Points along trajectories represent 50ms intervals, at which dotted lines-of-sight are drawn between the predator and the target.

2.3 Results

2.3.1 Linear Target-Trajectories

We first asked if the probability of take-off by *Holcocephala* is correlated with two cues that can be gathered monocularly: angular size and angular velocity of the target. We did so to test if manipulation of these parameters can fool *Holcocephala* into attacking beads that are outside of its normal prey range, as this is the case for Killer flies [33]. The impact of hunger and hunting motivation of each tested fly was controlled for by presenting the three size targets consecutively in decreasing order; if the fly took off after the 3^{rd} (1.3 mm,

smallest, and most suitable target) then we assumed that the fly was motivated to hunt but had opted not to attack the first 2 targets (all travelling at the same constant velocity, **Fig. 2.3**). As a control for potential priming biases, 11 trials were conducted in which the 1.3 mm target was presented first, followed by the other two targets in increasing size. In all 11 instances, the first (1.3 mm) target was intercepted, demonstrating that the flies did not simply ignore the first targets and respond to the third based on attention priming. These results are not included in the following target-choice test results, which all use the three targets in decreasing size.

A total of 90 responses were recorded (**Fig. 2.7**); 70 take-offs to the 1.3 mm target, 10 take-offs to the 2.9 mm target, and 10 take-offs to the 3.9 mm target. In each flight, the fly either caught the target or quit the interception, returning to its perch. The attack reached the target in 67 flights (74 %). Flight abandonment rates were 9 % (6/70 flights) for the 1.3 mm target, 70 % (7/10 flights) for the 2.9 mm targets and 100 % (10/10 flights) for the 3.9 mm targets.

None of the monocular cues recorded (i.e. angular size, angular velocity or the ratio between the two) can clearly account for *Holcocephala's* target choices (**Fig 2.7a-c**). Moreover, successful target captures occurred in response to a large range of angular sizes (0.12° to 1.05°, **Fig. 2.7a**), angular velocities (0.32 $^{\circ}s^{-1}$ to 0.01 $^{\circ}s^{-1}$, **Fig. 2.7b**), and angular speed/size ratio (0.05 ms^{-1} to 0.69 ms^{-1}, **Fig. 2.7c**). In addition, across the amassed trials, 80% of the ignored 3.9 mm and 2.9 mm beads were within the window of angular size in which *Holcocephala* successfully attacked and intercepted the 1.3 mm target. Likewise, 89% of the ignored 2.9 and 3.9 beads were within the window of angular speed/size ratio for which the take offs were directed towards the 1.3 mm target. These data indicate that target choice is either driven by a monocular cue not measured, such as looming, or by the actual bead size. It is noteworthy that a high proportion of responses to the two larger beads resulted in quits. This indicates that in the majority of the responses to the large beads, the predator had been fooled into choosing those targets as suitable prey. Even the top speed of targets (1 $m.s^{-1}$), we recorded captures of the target, displaying that *Holcocephala* was capable to intercept targets at this speed. Further analysis (i.e. binary logistic regression) was not carried out in this data set due to the lack of the 1.3 mm ignored beads trials and possible priming biases.

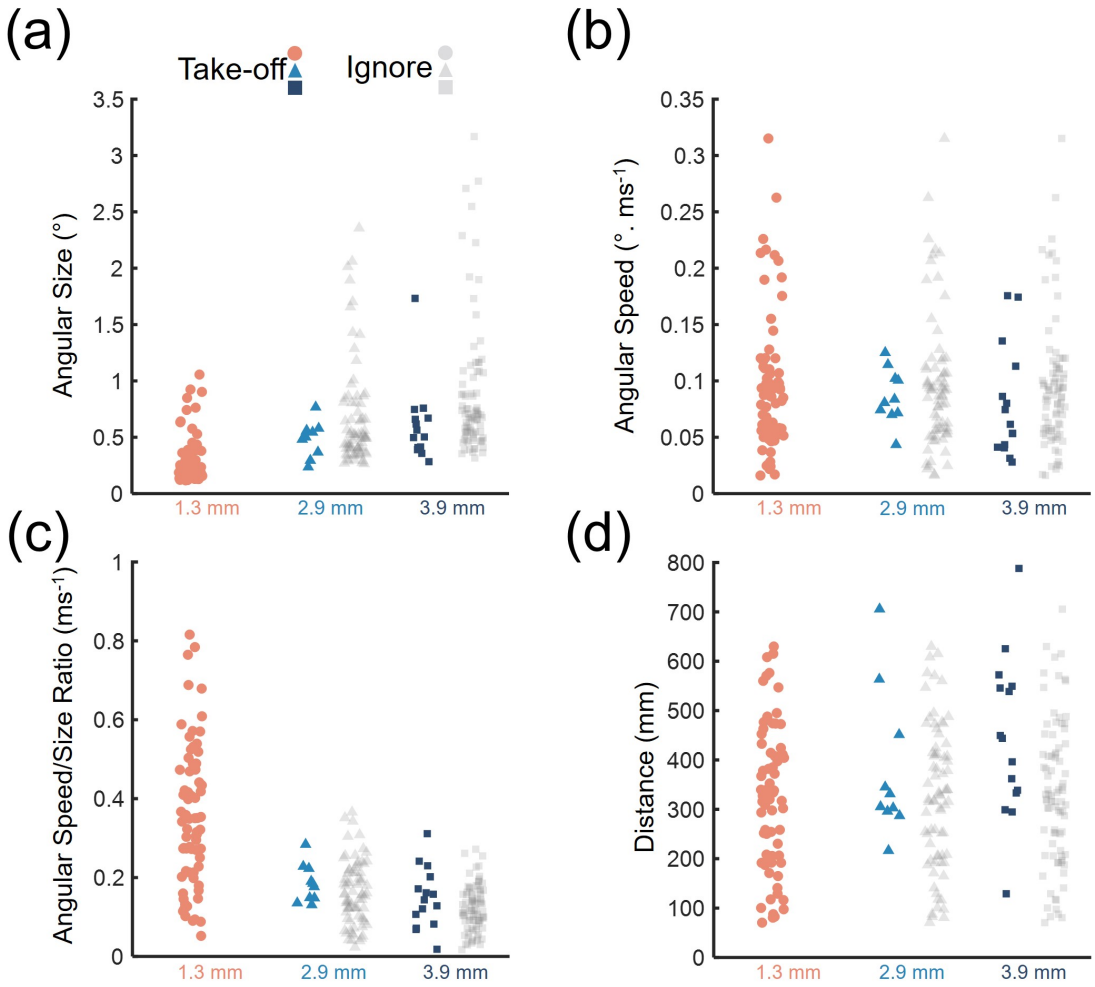

Fig. 2.7 The properties and behavioural responses to targets that travelled in a straight-line past *Holcocephala*. Take-off responses are displayed in their corresponding colours, while ignored targets are translucent grey. **(a)** The angular sizes (in degrees) of presented targets, sorted by size and behavioural response. **(b)** The angular speed (in degrees per millisecond) of presented targets, sorted by target size and behavioural response. **(c)** The angular size/ angular speed ratio (in units of per millisecond) of presented targets. **(d)** The distance (in millimetres) from the fly to presented targets.

2.3.2 Arcing Target-Trajectories

We improved the previous experiment by: (i.) presenting the targets independently to control for possible priming biases, (ii.) recording the positive and negative responses to all three target sizes, and (iii.) removing any looming cues by presenting the target on an arcing path.

We recorded 120 flights of Holcocephala taking off in response to dummy targets travelling in an arcing path (**Fig. 2.4**). These included 77 take-offs to the 1.3 mm target, 28 flights to the 2.9 mm target and 15 flights to the 3.9 mm target. The total number of ignored targets was 114. Of these, 11 were to the 1.3 mm target, 56 were to the 2.9 mm target and 47 to the 3.9 mm target.

When reviewing the digital recordings, we noticed that not all take-offs appeared intended as attacks because after take-off, the predators sometimes increased the distance to the target, and thus retreated by flying away from it (**Fig. 2.6d**). To quantify this behaviour, we used the angle formed between two vectors. Namely, the vector joining prey to predator (called Line-of-sight, LOS), and the vector of the fly velocity at the start of the trajectory (**Fig. 2.8**). An angle below 90° will close range on the target, and above will increase the range. Of the take-offs in this experiment, 5% (4/77) of responses to 1.3 mm targets, 71% (20/28) of responses to 2.9 mm targets, and 53% (8/15) of responses to 3.9 mm targets initially increased the fly's range (**Fig. 2.11a**). Thus, the majority of the responses to the two larger beads involved the predator increasing the distance between the target and themselves, indicating that such flies were retreating from the bead, and had not been fooled into attacking it. Statistical testing (binomial logistic regression) shows that the only monocular variable that has a significant effect on *Holcocephala's* target choice was angular size (Table 1, angular size $p = 0.04$), while size/speed ratio was of near significance ($p = 0.07$). Moreover, the only variable that had a highly significant effect on the choice of prey was the absolute (real) size of the target ($p < 0.001$).

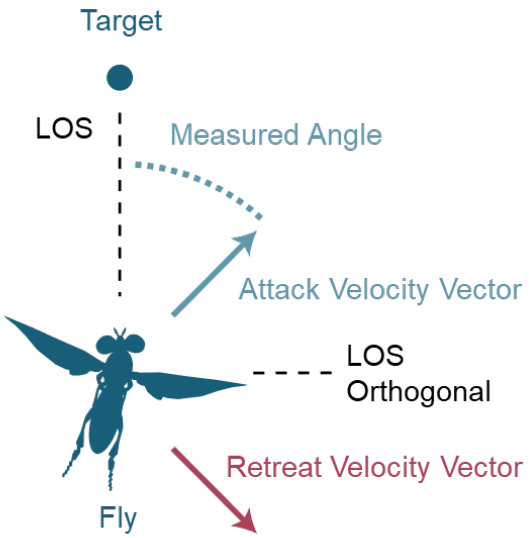

Fig. 2.8 Retreat behaviour was classified based on the fly's heading relative to the LOS. If the angle formed was acute, it was classed as an attack, if obtuse, a retreat.

A smaller bead presented at the same distance will subtend a smaller size than a larger one. This correlation could have confounded the regression results. Therefore, we applied cut-offs, which established a range of angular size and ratios (i.e. acting as a band pass filter for the trials). Such cut off allowed us to test probability of an attack to the same range of angular sizes and angular speed/size ratios across the three beads. The cut-offs for the angular size were set by the greatest tested angular size (0.77°) of the 1.3 mm target, and the smallest tested angular size (0.31°) of the 2.9 mm target (**Fig. 2.9a**, white background range). The thresholds for the angular speed/ angular size ratio were set by the maximum (0.10 ms^{-1}) and minimum (0.01 ms^{-1}) tested for the 3.9 mm bead (**Fig. 2.9c**, white background range). Within this set, the attack probabilities differed between the three bead sizes tested, with 63% (15/24) for the 1.3 mm, 10% (4/40) for the 2.9 mm, 12% (4/33) for the 3.9 mm target (**Fig. 2.11b i**). Inversely, the 'retreat probability' i.e. those flights in which the predator responded but increased range on the target were 13% (3/24) for the 1.3 mm, 18% (7/40) for the 2.9 mm, 18% (6/33) for the 3.9 mm target **(Fig. 2.11b ii)**. Thus, the distribution of the possible behavioural outcomes (attack, retreat, and ignore) differed between the three bead sizes (X^2=27.1, p<0.001). Moreover, binomial logistic regression shows that the monocular variables do not play a significant role in the *Holcocephala* choice when presented with potential targets (Angular speed p = 0.82, angular size p = 0.72, ratio p = 0.68) and that the only significant variable is actual bead size (p < 0.001).

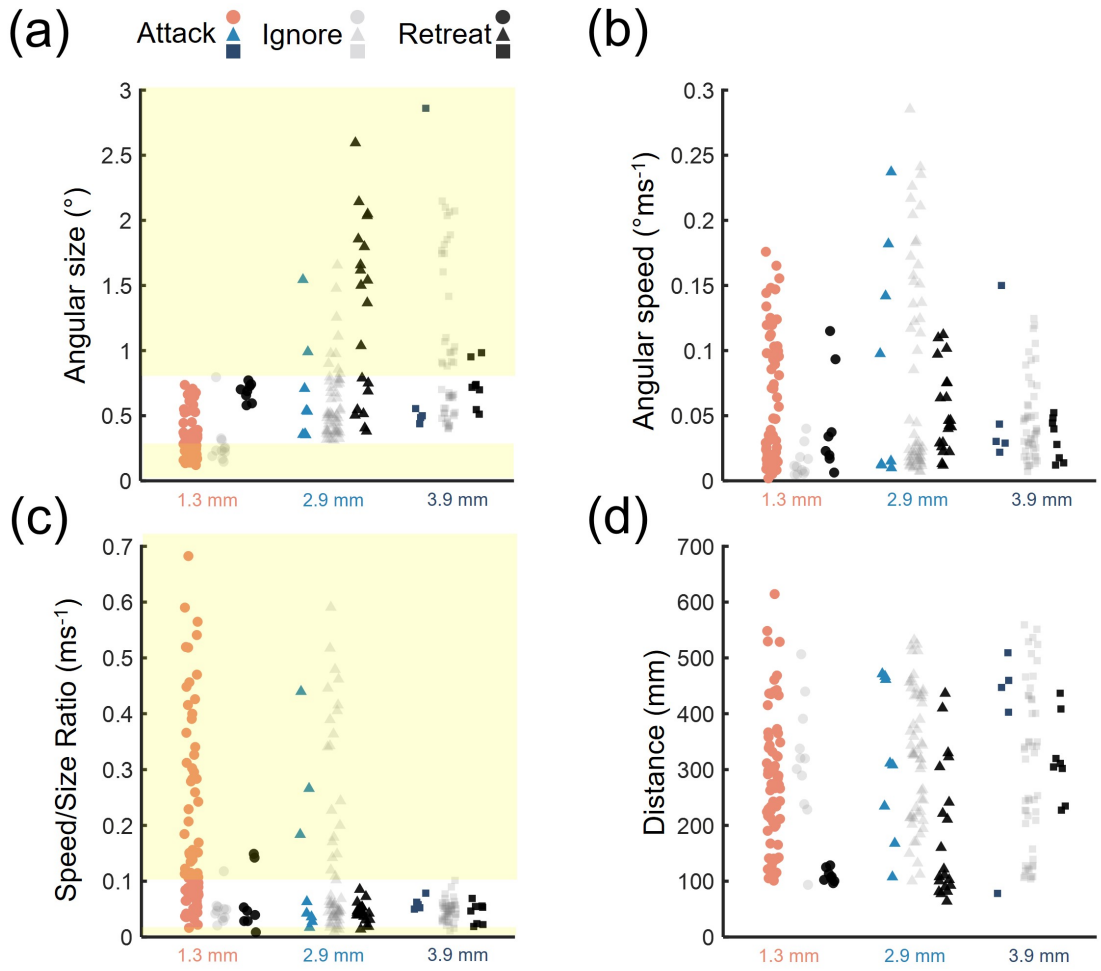

Fig. 2.9 The properties and behavioural responses to targets that travelled in an arcing trajectory past *Holcocephala*. Take-off responses are displayed in their corresponding colours, ignored targets are translucent grey, and targets retreated from are in black. Targets excluded from the matched stimulus set are displayed on the yellow background. **(a)** The angular sizes (in degrees) of presented targets, sorted by size and behavioural response. Angular size match window displayed at 0.4° - 1.0° **(b)** The angular speed (in degrees per millisecond) of presented targets, sorted by target size and behavioural response. **(c)** The angular size/ angular speed ratio (in units of per millisecond) of presented targets. Size/speed ratio match displayed at 0.01 – 0.10 ms^{-1}. **(d)** The distance (in millimetres) from the fly to presented targets.

In this experiment, 63% (55/88) of the total number of flies that attacked the arcing targets were successful in contacting the bead. The flies never contacted the largest of the beads (100%; 7/7 attacks aborted to the 3.9 mm target). The majority of the attacks towards the 2.9 mm bead were also aborted (75%; 6/8 flights). In contrast, only 32% (23/73) of the

responses to the 1.3 mm target resulted in aborted flights. Moreover, we noticed that some of the quitting behaviour coincided with high target accelerations that took place when the target reached the end of the arcing path and reversed its direction (**Fig. 2.10**). Such quits, induced by target path reversals, were all from 1.3 mm bead trials (n = 10 for all), which reduced the unexplained quits of the 1.3 mm target down to 18% (13/73). Similar accelerations were not found during aborted flights to the 2.9 mm or 3.9 mm targets.

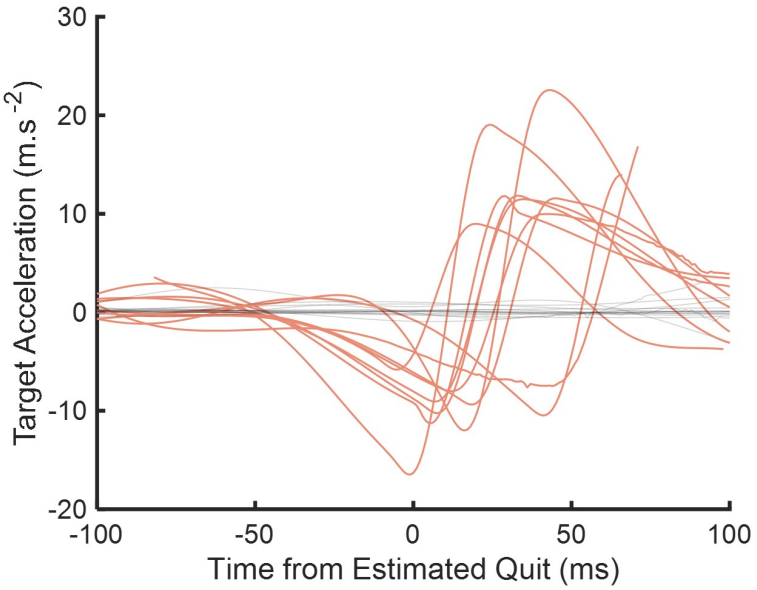

Fig. 2.10 Target acceleration is plotted across the estimated quit point of the fly. Flights identified as acceleration induced are drawn in orange.

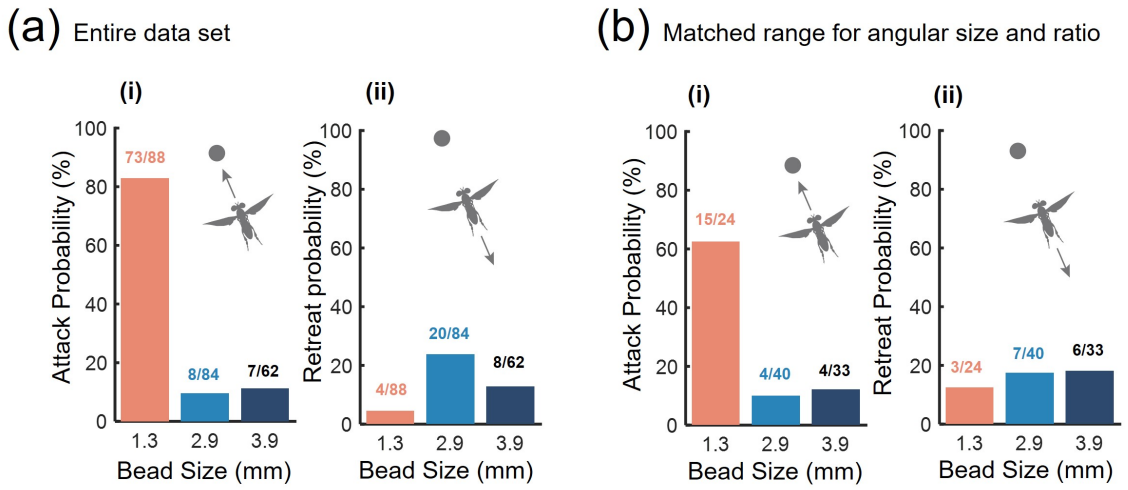

Fig. 2.11 **(a)** The probability of response for all targets presented on an arcing path including: **(i)** the attack probability & **(ii)** the retreat probability of the three target sizes. **(b)** The probability of responses to targets occupying a matched range of angular size (0.4° - 1.0°) and angular speed (0.01 – 0.10 ms^{-1}). Behavioural responses to the three target sizes are either **(i)** attacks & **(ii)** retreats.

Thus, in this experiment, were the monocular views were controlled for, the only significant variable resulting in an attack choice was the actual size of the bead. In addition to receiving significantly fewer attacks, the two larger beads, had the highest proportion of aborted flights.

2.3.3 Mirror-revealed targets

To further probe the importance of angular size cue in *Holcocephala's* target choice, we presented the flies with targets that had no net displacement and minimal velocity. This allowed us to test if flies relied on angular size in the absence of consistent velocity information. Bead presentations for each bead size were independent of each other. A total of 41 presentations were performed: *Holcocephala* took off after the 1.3 mm target in 60% (12/20) of instances, but never towards to the 2.9 mm (0/9) or towards the 3.9 mm (0/12) beads (**Fig. 2.12**). Thus, across all beads, there was a drop in the attack probability when compared to arcing targets (1.3 mm 83% to 60%, 2.9 mm 10% to 0%, 3.9 mm 11% to 0%). However, the distribution of the attacks to the 1.3 mm bead was not random. All the 1.3 mm targets presented between 0.40° to 0.90° were attacked (100%, 12/12). None of the 1.3 mm beads with angular sizes below 0.40° (0/8) were attacked. A similar pattern was also present in the arcing targets experiment, where the animals ignored a higher number of 1.3 mm targets when they were

below 0.40° angular size (5%, 1/19 ignored of targets > 0.4° vs 16%, 10/61 ignored of targets < 0.4°). For a 1.3 mm bead to be 0.4 degrees or smaller, it has to be presented at a distance of 187 mm or more. Therefore, the reduction in attack probability could reflect: (i.) a lack of detection at a given distance, (ii.) a lack of ability to estimate the actual distance to the target, or (iii.) a refusal to invest into catching a target located at such distance.

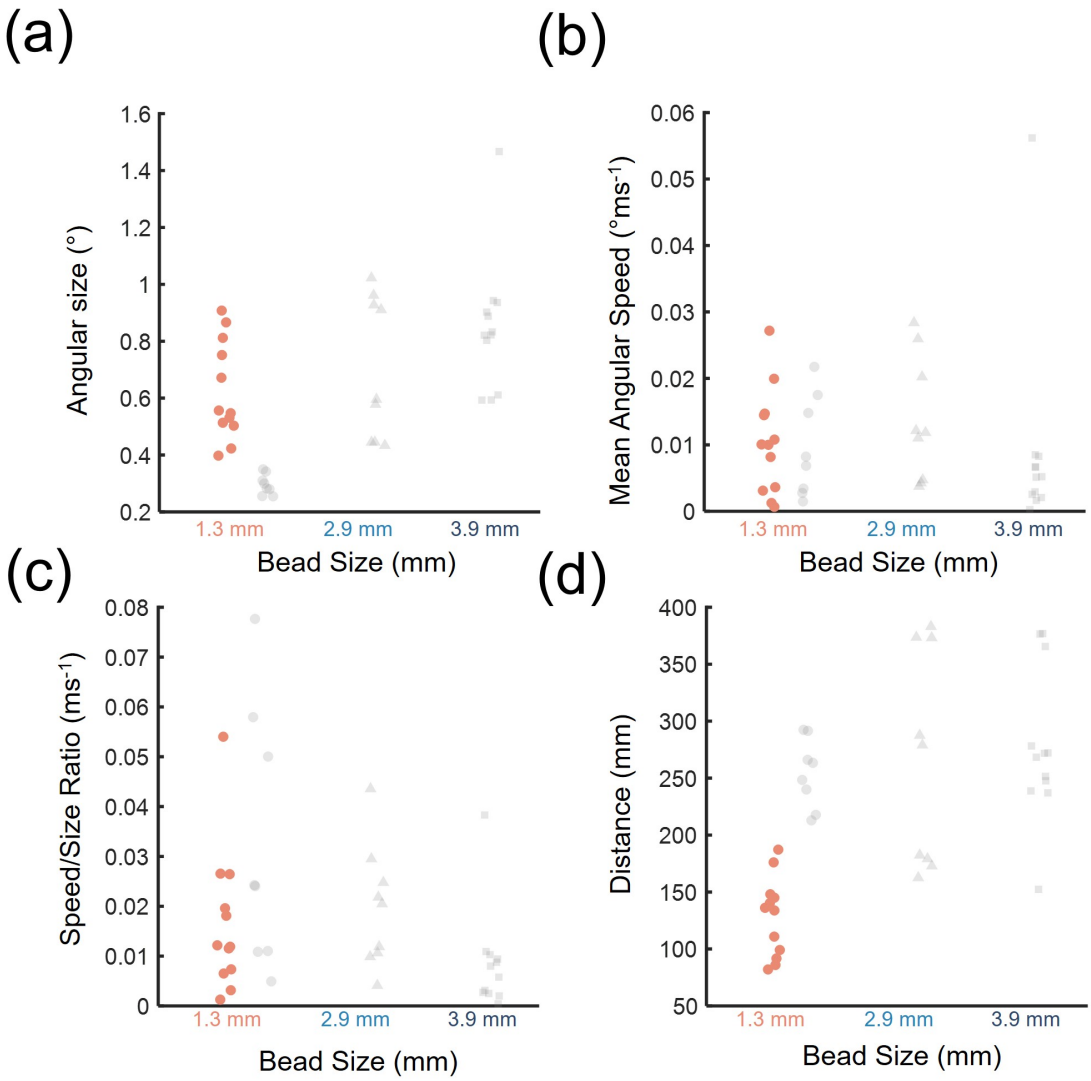

Fig. 2.12 **(a)** the distance and angular sizes of the targets presented by being revealed from behind a mirror. Attacked targets are shown in full colour, whilst ignored targets are half-coloured. **(b)** The angular speeds of the mirror-revealed targets are displayed separated by true target size. **(c)** the angular size/speed ratios of mirror revealed targets by distance. **(d)** the mean angular speed of targets by distance is overlaid by a model of fixed "jitter" of targets. This model does not give better fit than a linear model where angular speed is invariant with distance.

To match the angular size of the different beads, they necessarily needed to be presented at different distances (**Fig. 2.12d**). This may have resulted in an indirect monocular cue, because a small jitter in the hand held apparatus would have transferred as target motion. The angular velocity of such target movement would be correlated with distance (i.e. the same hand movement would produce higher angular velocities for targets that were presented closer to the fly). However, we found that despite the variation in distance to targets, the mean angular speeds of the targets were not significantly different between the three groupings (ANOVA, F = 0.42, P = 0.67) (**Fig. 2.13**). Because the variation in the jitter between trials outweighs any systematic variation in angular speed due to the distance to the target, animals could not have used angular velocity in this experiment to estimate the distance to the target.

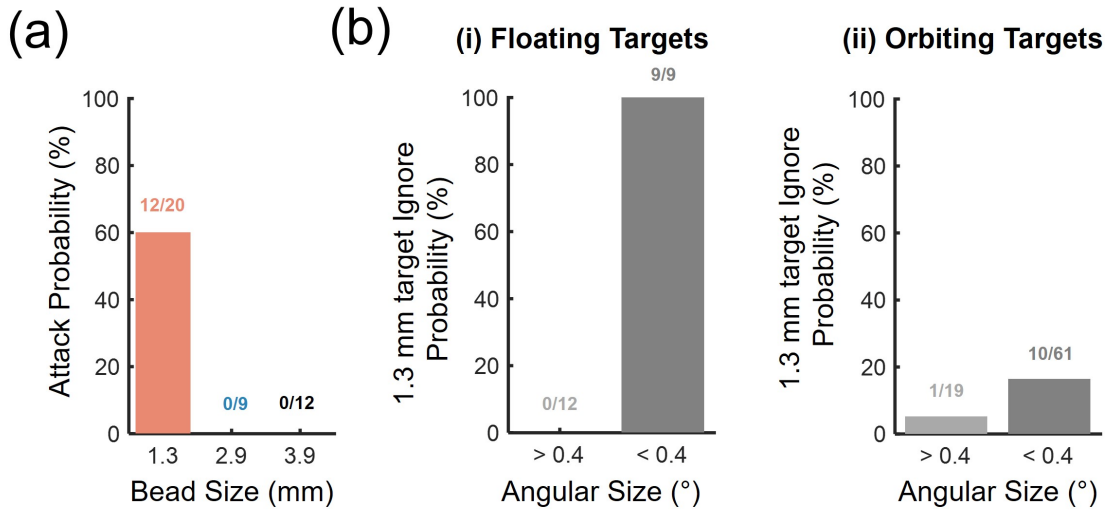

Fig. 2.13 **(a)** The attack probability of *Holcocephala* to targets revealed from behind a mirror. **(b)** The ignore probabilities for 1.3 mm targets are compared across a 0.4° cut-off for **(i)** floating, mirror-revealed targets and **(ii)** arcing, orbiting targets travelling in a circular path.

Thus, this experiment was consistent with the previous two. It further confirmed that when monocular cues (angular size, looming and velocity) are tightly controlled in different ways, *Holcocephala* stills displays a highly significant preference towards the smallest bead ($X^2 = 17.8$, $p < 0.001$).

2.4 Discussion

Despite controlling for the obvious potential cues that *Holcocephala* could be using, the flies still showed differential responses to targets based on their absolute size. From all

experiments here described, it is clear that *Holcocephala* does not have privileged window of angular size/speed ratio that is required for targets to elicit a response, as shown in killer flies [33] and dragonflies [107]. *Holcocephala* will respond to targets with exceedingly low ratios (with a minimum for mirror-revealed targets at 0.001 widths.ms^{-1}, and maximum responded to but not caught for linear targets at 0.816 widths.ms^{-1}). Secondly, when the angular speed/size ratios were matched for arcing target-trajectories it would be expected that *Holcocephala* would take off indiscriminately after targets. Despite the matching relative stimuli, *Holcocephala's* strong preference for the smallest absolute size of target remains; they are not indiscriminate.

Mirror-revealed targets had extremely low angular speeds, suggesting that this is not an essential character for discrimination of target size. The overlapping angular size of the targets of different true sizes does not allow for this to explain the size-selectivity of *Holcocephala* either. The size preference response of *Holcocephala* to targets on arcing trajectories also suggests that target size is not discriminated based on characteristic change in their angular size or angular speed. Target identification or recognition through pictorial cues is ruled out as the targets did not resemble real prey items and are scaled versions of each other.

Motion parallax is an unlikely cue for the distinction of different target sizes as while the flies do head-flick to targets, as in dragonflies these are primarily rotational motions and not translate [107]. Even if there were translation during head-flicking, without an internal model for the target's motion, the retinal displacement alone of the target during these motions would not give accurate information on the distance to the target [137].

So far, the plethora of negative results has demonstrated many ways in which *Holcocephala* is not deducing the size of targets. There is, however, one clue to a potential explanation of how they are managing this feat. For mirror-revealed targets, there was a sharp cut-off in the distance and angular size that flies would respond to, with them attacking all presented 1.3 mm targets up to 187 mm (0.40° across in the visual field) and attacking none after this point. This could represent a cut off in the detectable size of a target that is not appreciably moving to the observing fly but could also represent a true distance-determined limit. The physical separation (~1.3 mm) between the acute regions of each eye does allow for at least the possibility of parallax distance estimation via stereopsis. As discussed in chapter one, the interommatidial angle of *Holcocephala* is ~0.28° [77]. While the inter-ocular distance is small, this high visual resolution means that the visual regions covered by two parallel ommatidia converge at 27cm, representing the theoretical limit for stereopsis. Below this range, a target's image will have disparity between the two eyes. In reality, it

would be unsurprising that the hard limit to stereopsis range is higher than the behaviourally demonstrated discrimination. Disparity of targets increases with their proximity [141–143], and thus the discrimination threshold could be anywhere below the limit of 27cm (e.g. our behavioural limit of static targets at ~19 cm).

Unlike mantids, the attack range of *Holcocephala* stretches far beyond their predicted stereopsis limit. Should stereopsis be a factor within the rules applied for size discrimination, its influence may stray beyond the 27 cm limit. A target at the maximum size of interest to *Holcocephala* will have a set angular size at the threshold distance limit for stereopsis. The flies could operate a rule that if a target is larger than this in angular size, it must also have a non-parallel convergence between the two eyes. Applying a high-pass angular speed/size ratio filter to targets that are sufficiently small in angular size would then approximately distinguish larger targets that were flying much farther away from small targets flying outside of the stereopsis threshold, as within nature, animal size and flight-speed are not linearly-proportional [146, 147, 20]. However, given that *Holcocephala* will attack targets with extremely low angular speeds and at relatively high angular sizes, we have demonstrated that a high-pass or band-pass angular size/speed filter will not explain the data alone.

The conclusive test for stereopsis would be to experimentally alter the convergence point of the lines-of-sight to a target, making it "appear" closer to the animal (e.g. using prismatic lenses in the manner of Rossel [126]). Should decreasing the distance between the fly and convergence point elicit a response to an otherwise ignored target, then this would signal that the flies are using stereopsis as found in mantids. The small size of the flies does not make them readily amenable to the affixing of lenses to their bodies. These experiments are also curtailed as *Holcocephala* are extremely reluctant to perch within laboratory conditions (i.e. not under open sky) or when affixed to a tether (e.g. single thread glued to the abdomen). Instead, future work may be more fruitful studying larger species of robber flies (e.g. of the genus *Laphria*) that can carry the weight of affixed micro-lenses, albeit that their target selection systems may be utterly different from *Holcocephala*.

Holcocephala occasionally abandon attacks towards a target and quit their course for interception. In doing so, they display that the target selection is an ongoing process even whilst in the air. Quitting was disproportionately found to affect larger targets, suggesting that the initial take-off response had been revised by the fly as they had "realised" that the target was inappropriate for them to catch. It is not clear what information results in quitting behaviour. Some of the quits were as a result of a severe acceleration of the circular target reversing on itself, which could either be due to flies losing track of the target, or that the severe acceleration causes them to "choose" not to intercept the target. Dragonflies have

shown to have predictive internal models for the linear paths of targets, allowing them to reduce the tracking latency of their heads as they pass underneath the target [76]. If such were present in *Holcocephala*, then they could use the rotation of the line-of-sight as they pass under the target to gauge its distance. *Holcocephala* would need accurate knowledge of their own self-motion, in what is effectively aerial motion-parallax. Internal models for tracking a target, which is translating relative to the observer, necessitate knowledge of the target distance, and thus would need to be supplemented with initial distance assumptions to start any motion-parallax system. Motion parallax whilst airborne without internal knowledge of target motion will not give reliable distance information [137]. The looming (angular size increase) of the target is a product of target size and the closing velocity between the target and fly (termed Vc). Vc is the time derivative of the distance between the target and the fly and without this information, the looming rate does not give accurate information about the size of the target [153], thus this is unlikely the root cause of quitting. Stereopsis could potentially explain quitting behaviour. The visual disparity of an object in the visual field will increase with proximity between the target and the fly. Thus, a target that was initially pursued in error will become more apparently incorrect as the fly approaches. However, within the series of experiments performed, it is not possible to state categorically whether stereopsis is being used by *Holcocephala fusca*, only that its presence would help to explain the results and the target choice discrimination of the flies.

2.5 Conclusion

The ability of *Holcocephala fusca* to select a target based on its actual size exceeds that which should be expected from the potential heuristic cues available in the targets that have been presented in the above three sets of experiments. By presenting targets of different sizes that either match or have an absence of cues such as the angular speed/size ratio, we have shown that *Holcocephala* does not follow the simple rules expressed in other predatory insects. The exact criteria that *Holcocephala* use to differentiate the size of targets has not yet been clearly deciphered. One potential remaining cue is in using their high-resolution acute regions in both eyes to conduct stereopsis and triangulate the distance to the target, but this is yet to be conclusively shown experimentally. Future work is required to experimentally alter the line-of-sight convergence of the target (e.g. through prisms) and find whether this can persuade the flies to respond to inappropriately large targets.

Chapter 3

Target Interception

Abstract

Within this chapter, the exact means by which the two predatory fly species, *Holcocephala fusca* and *Coenosia attenuata*, navigate their way to moving targets is tested. Both flies use a system that can be modelled as an analog of proportional navigation (Pro-Nav), which is implemented in modern missile guidance and control. Through this discovery, we can model the navigational gain (N) of each system, with *Holcocephala* using an energetically conservative N $\approx$ 3 and *Coenosia* using a lower N $\approx$ 1.5 that is more stable given it's higher stimulus. The modeled delays on both systems were extremely short, with 28 ms for *Holcocephala* and 18 ms for *Coenosia*. Pro-nav operating with this short delay allows both flies to navigate to the optimal (straight line) path to a moving target without ever making a formal calculation of relative speed, distance or target size.

The greater part of this chapter has been published in the following article: "Fabian, S. T., Sumner, M. E., Wardill, T. J., Rossoni, S., & Gonzalez-Bellido, P. T. (2018). Interception by two predatory fly species is explained by a proportional navigation feedback controller. Journal of The Royal Society Interface, 15(147), 20180466."

3.1 Getting to the Target

Once the target has been detected and deemed suitable for attack, the animal faces perhaps its greatest challenge. It must get to the target. As soon as the predator takes to the air, it not only needs to maintain its own flight stability, but also maintain tracking of the target within the

visual field. While for many predators the energy expended searching for prey exceeds that used in chases [130], predatory chases and manoeuvres may still have a significant energetic cost [154, 155]. The predator will gain most from the interaction if it minimises the linked parameters of flight-speed, flight-time and flight-distance. These are not equally weighted, as the energy used on a flight is proportional to the distance covered and to the time taken, yet the resistant drag is proportional to the speed squared. There are considerations other than energetic that concern trajectory shape and flight speed. Extended flight-times may pose risks for the predator itself and may give time for evasive manoeuvres by the prey [35, 71]. Approaching the target too fast has costs in itself, that of reduced catch probabilities, in similar fashion to the cognitive speed/accuracy trade-off [156]. The faster the closing rate to the target, the smaller the window of time in which the target is within grappling range of the predator, requiring faster predator reactions. Secondly the kinetic forces involved in the collision are greater, potentially increasing the chances of prey slipping through the grasp of the pursuer.

Predators can either pursue or intercept the target (**Fig. 3.1**). These two methods are entirely distinct. Pure pursuit gets a predator to its target by directing it along a straight-line path to the target's current location, taking no account of target motion. Interception biases the predator heading towards a future point of contact with the target and thus necessarily accounts for the motion of the target. The details of the relevant algorithms will be detailed later within this chapter, but the principal differences are worth noting here. Pursuing a moving target from anything other than directly behind generally results in a tail chase and a curved flight-path that takes longer than necessary to reach the target. Interception, on the other hand, will reduce the speed, time, and distance requirements of catching the target. However, most of the insects so far studied for behavioural algorithms engage in pursuit behaviour straight towards the target [157–160]. These examples are not of predators, but of conspecific pursuit. The only insects so far studied for their aerial interception are dragonflies [76, 161, 162], killer flies [33], and hover flies [163], without a control law being demonstrated so far (Hover flies have been shown to use an open-loop estimation to initiate their trajectories, but it is not shown how they update this further into the flight).

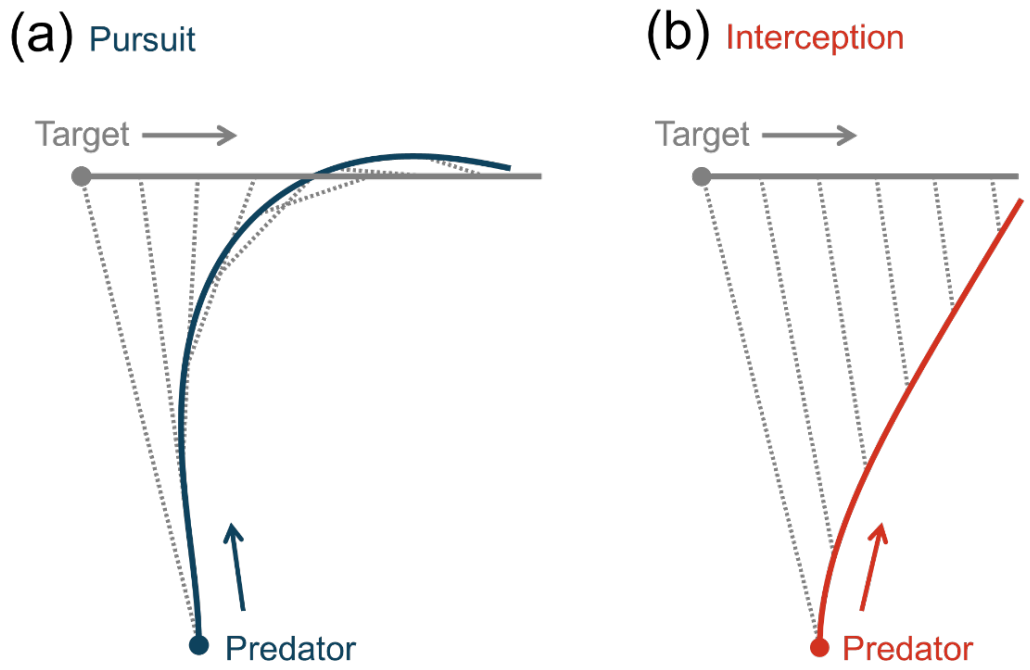

Fig. 3.1 Two alternative steering controllers catch a moving target. **(a)** A pure pursuit controller enters a tail chase behind the moving target. **(b)** An interception controller (proportional navigation) steers onto a direct collision course with the target. In both simulations, initial predator position and heading are the same, as are the speeds of the predators and targets respectively. Metric speeds and control system constants are set arbitrarily for demonstrative purposes.

The interaction between the predator and prey is governed by three factors; initial geometry, prey behaviour (i.e. speed and acceleration), and predator behaviour. The predator only has direct control over the latter and partial control over the initial conditions (they can choose when and where to attack). It is thus unlikely that any two engagements will be identical. Predators therefore need reactive, closed-loop strategies that are applicable to a broad swathe of different engagement conditions and prey behaviours. The pursuer has two distinct means of controlling the trajectory it takes to hit the target. These are speed and heading (alternatively called flightpath angle [164]). Speed has a minimum cut-off. For a pursuit system that enters a tail-chase, the speed simply needs to be greater than that of the target. For interception, there is a minimum speed at which the predator can travel to hit the target, but this is not necessarily greater than the speed of the target, as interceptors may take shorter routes to the interception point.

Steering is needed to maximise the proportion of the linear speed that is put into closing distance between the predator and prey. Steering for pursuit is consistent between interactions and is not dependent on the speed of either pursuer or prey, the pursuer must simply direct its velocity along the line of sight to the target. Steering for interception is inherently a much more difficult problem. It is not a simple task to steer towards the future meeting point; the location is conceptual and thus not marked by physical cues. Even if the navigation to such a point in space were a soluble problem for the predator, it is highly variable as prey and predator accelerate. The information required to make a precise calculation of a future rendezvous may not be accessible to a small insect predator. The location of the meeting point between the predator and prey is set by the relative speeds of both parties, as well as the exact heading of the prey. Knowledge of the exact target velocity is unlikely to be available to the predator, let alone an exact measure of its own speed. Remarkably, this method of steering through absolute calculation has been documented as the means by which male hoverflies initiate interception of female conspecifics, based on the fact that hoverflies can make innate assumptions about the flight-speeds and sizes of their quarry and their own characteristic acceleration [163]. How hoverflies update their steering during the interception flight is still a mystery. Nevertheless, generalist predators cannot make such specific assumptions about their targets, and so the same system is unlikely to be in play. Guided missile design is a branch of research that has vastly more literature on the control of navigation towards a moving target (e.g. [165, 166]). This work provides extremely useful tools for understanding the flight behaviour of predatory insects. In missile design, thrust and control surfaces tend to be separated. Thrust is created by either a solid-fuel booster or a liquid-fuel engine and generates linear acceleration parallel to the longitudinal axis of the missile body. Steering is facilitated by lift-based control surfaces as in aeroplanes, in the form of movable fins distributed across the body. It is important to consider these aspects of missile design for the subsequent chapters, and their contrast to insect flight, physiology, and intention. While geometric rules and guidance laws may be consistent, assertions of optimality or implementability cannot be assumed to hold true between human engineering and biologically evolved systems. The problem of intercepting a target has been considered in human engineered guidance for millenia. The concept originates in the avoidance of ship collision at sea (or its creation in the case of piracy or military engagement). One rule with uncertain but ancient linneage is that of constant bearing, decreasing range [165, 166]. This rule simply represents geometry, that two individuals maintaining a constant bearing from one to the other against a global reference (e.g. from magnetic north), and getting closer to one another are on a collision course. This rule does not require either party to know their speeds or headings, only the angular rotation of the line-of-sight to the other

individual and whether this rotates over time. In guidance literature, we now term this as parallel navigation (**Fig. 3.2**), so called as when drawn on a map, the lines connecting the positions of the two interactors remain parallel as they translate towards the collision point. This does not apply only to planar engagments affixed to the surface of the land or sea, but also to those in the air. Even in 3 spatial dimensions, engagements between a predator and a prey are planar, the plane being that which intersects the points of predator, prey, and is parallel to the velocity of the prey. The engagement geometry can be fairly compressed into this plane, from here termed the engagement plane, and any movement from this plane by the predator represents a wasting of effort (provided we assume the predator is simply trying to hit the target on the shortest possible path). Parallel navigation is a statement of geometry, not an algorithm nor a methodology for collision. It describes a condition to be sought, but does not state what corrective measures should be taken in order to achieve it. Thus, when parallel navigation's use or lack thereof is stated as describing the interception behaviour of an animal, what is really meant is its fullfillment. Within this thesis, it is hoped that the fullfillment of parallel navigation is demonstrated to be a relatively meaningless statement when concerning the underlying mechanisms of target interception. Nevertheless, it does have use in the identification of intercepting behaviour, as not all interceptors may fulfill 'good' parallel navigation, but all those partaking in parallel navigation are intercepting their targets, as opposed to pursuing them.

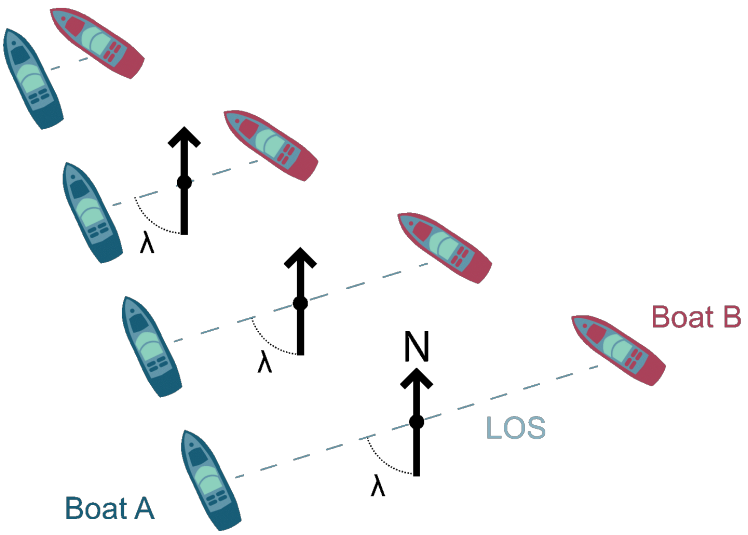

Fig. 3.2 The geometric rule of parallel navigation is demonstrated by two boats approaching one another. As they approach, the line-of-sight (**LOS**) between them shortens but does not rotate relative to the global axis (represented by North). This results in the bearing angle (λ) staying constant throughout the course.

So far, a handful of animal groups have been marked as fullfilling parallel navigation, although frequently given separate terminology (e.g. constant bearing strategy or constant absolute target direction). Big brown bats (*Eptesicus fuscus*) [167] and northern goshawks (*Accipiter gentilis*) [69] have both been demonstrated to be satisfying parallel navigation when intercepting erratic targets. Meanwhile humans also satisfy this rule when engaging a linearly travelling target [70]. Bridled leatherjacket fish (*Acanthaluteres spilomelanurus*) generally pursue falling food items, however they are recorded as maintaining a parallel navigation trajectory, should their and the targets motion happen to fall into such a condition [168]. Dogs also fulfill parallel navigation when intercepting frisbees, although this connection is not explicitly stated within the publication [169].

Perhaps the most contested example is that of dragonflies. Olberg details the interception behaviour of dragonflies [34] and secondarily asserted that the basis of their interception was an algorithm that fullfilled parallel navigation [170], finally suggesting a potential mechanism in a review paper [162]. Olberg makes clear that while to him, dragonflies are fulfilling parallel navigation, his suggested mechanism is only a parsimonious way to achieve this and evidence is not supplied to conclusively demonstrate it is the method of interception. Olberg's suggested mechanism is proportional navigation, and will be revisited in the next

section. These conclusions are thrown in doubt by Mischiati et al. [76], when they concluded that they 'rule out parallel navigation as the steering strategy' in dragonflies. According to their measure of parallel navigation, range vector correlation, the trajectories do not fullfill the geometric rule satisfactorily. Their suggestion is based on the fact that 'at constant speed prey do not manoeuvre' and that deviations from parallel navigation 'must have arisen from non-parallel-navigation manoeuvring by the dragonfly'. This is true, but it is worth considering that these manoeuvres may represent biomechanical or flight constraints, a point made by Dickinson in his primer to the paper [161].

3.1.1 Pure Pursuit

The model of getting to a target in insects is most commonly that of pure pursuit. As has already been mentioned pure pursuit is about aligning the axis of a pursuer's motion with the line-of-sight (LOS) to the target. The means by which this is achieved is proportional control. Proportional control requires that the response (i.e. magnitude of turning towards the LOS) is in direct proportion to the stimulus (the error angle between the LOS and the pursuer heading). This model has been found to explain the flight trajectories of conspecific chases in blowflies [160], houseflies [159], long legged flies [158], honeybee drones [157], cursorial prey pursuit of tiger beetles [171], and the steering of bats tailing conspecifics in order to steal meals from them [172]. The model takes the form of Eqn. 3.1.

$$\dot{\gamma} = k\delta \tag{3.1}$$

In which $\dot{\gamma}$ is the turning response of the animal, δ is the error angle between the heading of the animal and the LOS to the target, and k is constant of proportionality with the units s^{-1} (**Fig. 3.3**). While this gain is generally considered to be a fixed quantity, additional terms can be added that are in effect gain modifiers as in the case of tiger beetles. In tiger beetles there is a multiplicative gain modifier that alters turning magnitude in proportion to the range to the target [137]. The time units of the proportionality constant (s^{-1}) suggest an innate optimum with the control time constant (28 ms, half the time for the beetle to take a stride). The optimal gain for the system is given by Eqn. 3.2 [173].

$$k = 1/\tau e \tag{3.2}$$

Where τ is the delay of the system. Given the beetle's delay of 28 ms, the optimum value obtained for the control gain is 13.1 s^{-1} which the beetles nearly match in fitted data with a control gain of 12.7s^{-1} [171]. The constants obtained for airborne species are considerably higher, when available. Honeybees do not have their control system and corresponding gains clearly outlined, other than that they align their axes along the LOS to the target [157]. For houseflies (*Fannia canicularis*) the constant k is given as 20 s^{-1} [159]. There is an additional feature of the control system described within houseflies. When the error value lies below 35°, the second order motion of the target becomes important, i.e. angular velocity of the LOS. This is then proportional to the fly's turning by dimensionless constant of 0.7, converting LOS angular velocity into pursuer heading angular velocity. The constant falling below 1 means that this system never acts as a proportional navigational controller or deviated pursuit controller (to be discussed later), instead it simply dampens the control system, as in the derivative term in an engineering PD controller. This principle is apparent if the motion of the LOS is thought of having an internal 'momentum'. The LOS may make a small error angle compared to the current heading, yet if it arrived there with a high angular velocity it is likely to continue across the centre of the visual field, while first order control makes little corrective adjustment. Incorporating the velocity allows the pursuer to begin correcting for future error and ultimately reduce the sum of error over the flight.

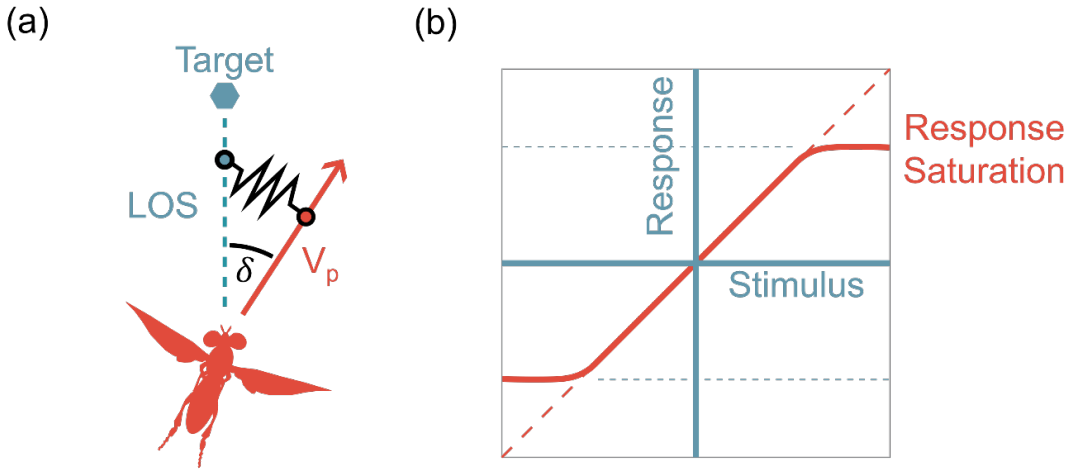

Fig. 3.3 **(a)** In pure pursuit, a pursuer can be represented as having a metaphorical "spring" between the line of sight to the target (LOS) and its current velocity heading (V_p). The greater the angle between the two vectors, the greater the force of attraction pulling the velocity heading back towards the LOS (i.e. the turning response of the fly towards the LOS). **(b)** The principle of proportional control is outlined by the linear relationship between a stimulus and a response. To be a "controller", the response should act to diminish the stimulus. While the response would ideally be indefinitely linear, in application, there is typically a response saturation, at which point the controller cannot further respond despite the magnitude of the stimulus.

3.1.2 Deviated Pursuit

A deviated pursuit controller can shorten the pursuer trajectory by using the same control system as pure pursuit but fixing the intended error angle (δ) at a positive value (instead of zero) [18]. Instead of the pursuer attempting to null the angle between its velocity and the LOS, it instead holds it at a fixed value (**Fig. 3.4**). The proportional mechanism is identical, only differing in that the error angle is that between the pursuer heading and an axis of fixed offset from the LOS. Typically, this bias would be ahead of the targets position, in the direction of the target velocity. This reduces the path distance to the target, whilst not requiring any form of global reference frame that would be required in other interception algorithms (see human constant bearing model, or proportional navigation).

This strategy is suitable for animals that can estimate absolute target size, or have this knowledge available innately, and thus can calculate the optimal error angle (the angle that would allow them to take a straight-line path to a non-manoeuvring target) based on the angular size and speed of the target. This is the case for male hoverflies chasing females [16],

but it would seem unsuitable for generalist aerial predators when size assumptions will not match all potential prey items (although see [14], [48], and chapter 2 concerning heuristic target size assessment).

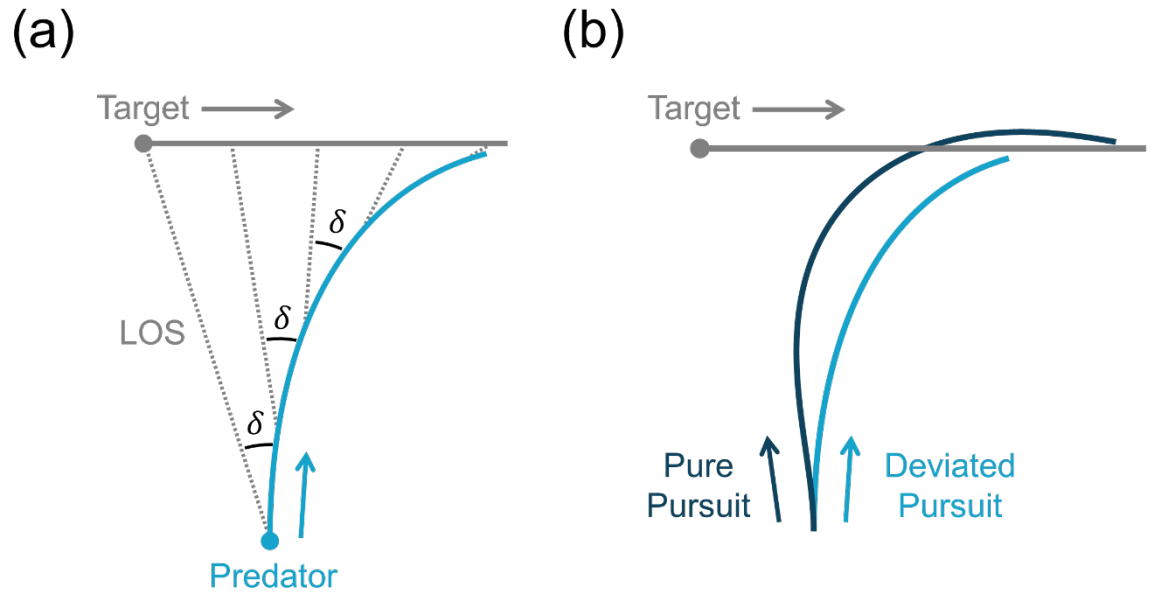

Fig. 3.4 **(a)** In deviated pursuit the error angle (δ), between the line-of-sight (**LOS**) and the predator heading, is held constant throughout the flight. **(b)** Deviated pursuit takes a shorter path to the target than does pure pursuit.

3.2 The Human Model of Target Interception

The model put forward by Fajen & Warren [174] to explain the data collected on humans walking to intercept a moving target [70] is called the constant bearing model, and uses angular acceleration of interceptor heading as the behavioural output and angular velocity of the line-of-sight to the target (LOS) as the input. This model is demonstrated in 3.3.

$$\ddot{\gamma} = -b\dot{\gamma} + k\dot{\lambda}(d+c) \tag{3.3}$$

Where $\ddot{\gamma}$ is the angular acceleration of the interceptor heading, and $\dot{\gamma}$ its angular velocity. $\dot{\gamma}$ is the rotation rate of the LOS and d the distance separating the interceptor and target. b & k are constants of proportionality for the angular velocities of interceptor and LOS respectively

while c is a constant limiting the minimising effect of proximity between interceptor and target. For the purposes of dissection, the above equation can be rewritten in a more intuitive form of Eqn. 3.4.

$$\text{interceptor angular acceleration} \propto (\text{LOS Rotation} \cdot \text{Target Distance}) - \text{Dampening} \quad (3.4)$$

The model is based on two attractors within the parameter space: (a) the error angle between the heading of the interceptor and the LOS should create a zero-miss projection ahead (if both interceptor and target continue their trajectories, they will hit each other), and (b) the heading of the interceptor should not rotate once condition (a) is met. (a) is approached by the LOS rotation term and the reason that is approaches this condition will be detailed later, as it is identical to the basis of proportional navigation. The unique feature of this model is the inclusion of the dampening term and the representation of response by angular acceleration. Without dampening, this model continues its angular velocity of a corrective manoeuvre even though it has reached a collision course with the target. The inclusion of the dampening suggests that the interceptor need measure its own angular velocity and slow itself in proportion. This is feasible for humans using the local optic flow cues to counteract their rotation, yet this step is unnecessary if instead the response variable is the interceptor's angular velocity, rather than its angular acceleration. This is the basis of proportional navigation, and represents a more parsimonious algorithm for interception, to be discussed later.

The distance term is based on the empirical finding that humans moderate their turning acceleration near-exponentially in proportion to their proximity to obstacles, increasing their turns when closer to the object [175, 176]. The turning moderation is inverted. This moderation of gain is advantageous given the natural evolution of LOS rotation during a trajectory and as the interceptor nears its target. Rotation in the LOS represents that the two interactors are not matched in the transverse velocity component of the plane (the interceptor and target have unequal velocity components normal to the LOS). An imbalance of transverse speed influences the LOS rate proportional to the arctangent of 1/distance . Thus, the stimulus for rotation naturally increases as the range between target and interceptor decreases. Applying the distance term in the proposed model accentuates the LOS rate of distant objects and steering the interceptor onto a more optimal path earlier in the trajectory. This same concept of distance modulation is applied within missile design, both for taking more optimal paths, and in stabilising the final approach on the target where LOS rates may be extremely high [177, 178].

As discussed by Fajen and Warren, the constant bearing model is not actually an attempt to define the underlying control law. Instead they use the term "behavioural dynamics" [175, 174]. Control laws reflect the input, translation, and output of a system. Behavioural dynamics provide models from an external perspective, that may roughly map the movement of the agent, but do not necessarily accurately map the processing and information the agent is using internally. As will be seen with proportional navigation, a simpler control law can effect similar results whilst requiring fewer inputs.

3.2.1 Constant Absolute Target Direction

Recently, a new methodology of interception has been proposed in the aerial interception of moving aerial targets by bats [167]. This was again described as being the underlying basis of the attack of moving targets by goshawks [69]. The model proposed takes its form from the geometry (**Fig. 3.5a**) of the engagement, as of Eqn. 3.5.

$$\lambda = \gamma + \delta \tag{3.5}$$

And thus Eqn. 3.6 follows.

$$\dot{\lambda} = \dot{\gamma} + \dot{\delta} \tag{3.6}$$

From these equations, they derive a constant bearing strategy, where $\delta = 0$ and thus generate Eqn. 3.7.

$$\dot{\gamma} = \dot{\lambda} \tag{3.7}$$

Which is equivalent to a formulation of proportional navigation with a navigational constant of N = 1 (see next section for details on proportional navigation).

This concept is then extended to form an interception algorithm based on the principle of parallel navigation. They state that in parallel navigation, and on a collision course, $\dot{\gamma} = 0$. From there achieve the statement that to maintain this condition Eqn. 3.8.

$$\dot{\gamma} = -\dot{\delta} \tag{3.8}$$

However, this algorithm will not be pursued further as it does not consider an alternative geometry in which the reference line falls between the interceptor velocity vector and the LOS (**Fig. 3.5b**). The alternative case is given by Eqn. 3.9.

$$\lambda = \delta - \gamma \tag{3.9}$$

This demonstrates that the Eqn. 3.5, whilst occasionally true, is not true by definition and thus the following statements do not hold true in all cases.

There is a more fundamental problem with the formulation as well, in considering the attraction of the model to an interception course. An interception algorithm should drive the interceptor's heading towards an "optimum" heading which will collide with the target's future position. In the primary assumption of CATD, the LOS is not rotating ($\dot{\gamma} = 0$), which means that the predator is already on a collision course with the target, thus no steering is necessary. Where a steering algorithm should come into play is when $\dot{\gamma} \neq 0$ (the LOS is rotating) as this only occurs when there is an error between the V_p and the optimum heading. The proposed steering algorithm in CATD patently does not correct the interceptor heading onto the optimum course. If we consider a 1° increase in δ would lead to a 1° decrease in γ. When the LOS is rotating away from the V_p, the pursuer steers away from the LOS, and vice versa. This is the exact inverse of what would direct the predator towards a collision course and thus this is not an interception algorithm.

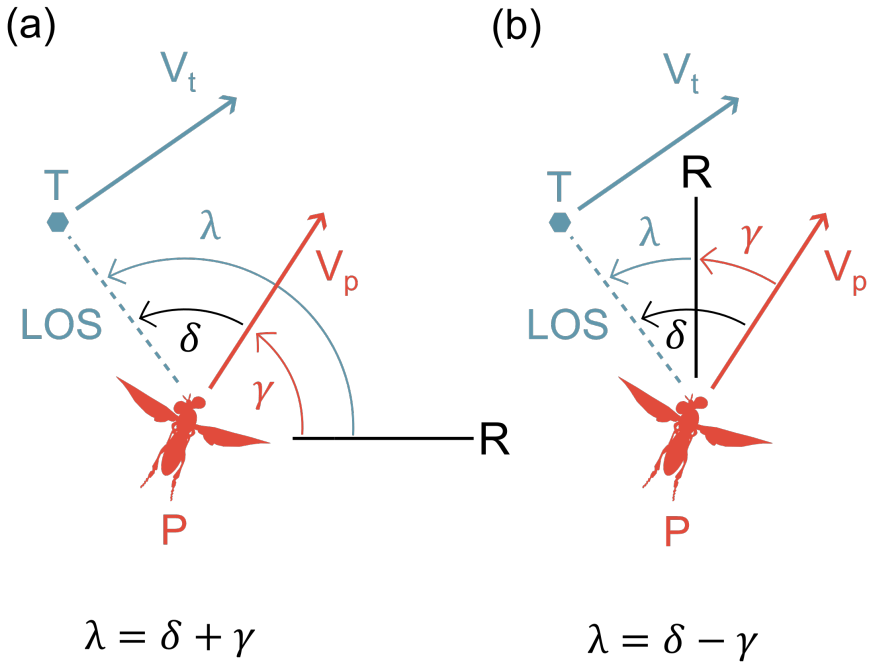

Fig. 3.5 Constant Absolute Target Direction (CATD) uses a standard framework of critical angles and vectors formed by the target (**T**) and the predator (**P**). However, it is commonly noted and based on the principle that the target bearing angle (λ) (formed between the reference vector (**R**) and the line-of-sight to the target (**LOS**) is a consistent sum of the heading angle (γ) (formed between the interceptor heading and the LOS) and the error angle (δ) (formed between the interceptor heading and R). As demonstrated by the differences between **(a)** and **(b)**, λ is not always a sum of γ and δ.

3.2.2 Proportional Navigation

The guidance law suggested by Olberg [162] to underpin dragonfly interception is one taken from extensive literature on modern homing missiles, proportional navigation (pro-nav). This guidance law has also recently been demonstrated to underlie the final attack phase of peregrine falcons homing in on their prey [179]. Proportional navigation has the angular velocity of the interceptor's heading as its means of controlling flight trajectory, rather than the angular acceleration. Angular velocity (turning) is created by applying force orthogonal to the current heading, and thus makes sense as the frame in which the control of an animal can be represented. Pure pro-nav in its most essential form is given by Eqn. 3.10.

$$\dot{\gamma} = N\dot{\lambda} \tag{3.10}$$

Where $\dot{\gamma}$ is the interceptor's angular velocity (turning response), $\dot{\lambda}$ is the LOS rotation rate, and N is the navigation constant, which is dimensionless and has no units (**Fig. 3.6**). N is generally between 3 - 5 within human technologies [166], while in the peregrine falcons the mean N was ~2.6, with considerable variation between different flights and individuals(first and third quartiles of constant fittings at N = 1.5 & N = 3.2) [179]. This system takes the rotation of the LOS (in a global, non-egocentric, reference frame) and applies a magnified proportional rotation to the heading of the pursuer. A term to moderate gain in response to target distance can be added as well to compensate the high LOS rates found when in close proximity to the target, similar to that already seen for the human constant-bearing model [178]. This guidance system underpins the vast majority of modern missiles [166, 180, 165] and has done since the lark missile first intercepted a target using pro-nav in 1950 [181]. The reason for its widespread use and extensive literature, is its relative simplicity in reducing the miss-distance of an interceptor with minimal information about the target.

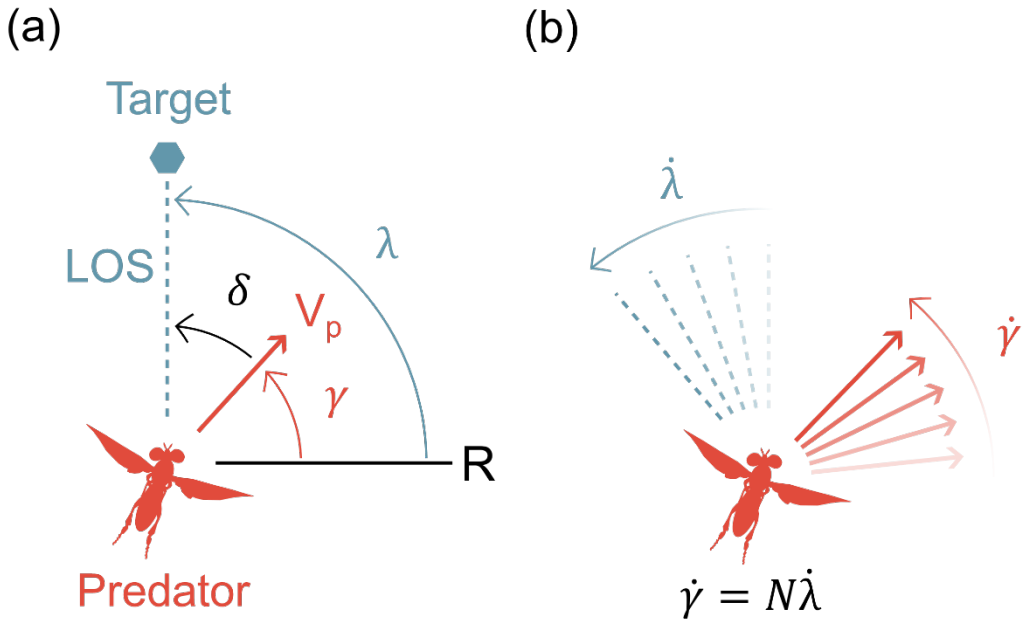

Fig. 3.6 **(a)** The angles involved in representing the proportional navigation controller involve the three critical vectors of predator velocity ($\mathbf{V}_p$), the Line-of-Sight to the target (**LOS**) and a reference vector (**R**). These may be referred to as the heading angle (γ), the target bearing angle (λ), and the error angle (δ) (error used here to align with pure pursuit terminology). **(b)** the principle of proportional navigation is represented as the rotation in the LOS ($\dot{\lambda}$) is magnified by the navigation constant (**N**) and applied to the pursuer velocity vector's rotation ($\dot{\gamma}$).

In its pure form (as opposed to the true or generalised formulations) proportional navigation works by swapping speed between two components of the engagement plane (**Fig. 3.7**). The components are set in the frame of the LOS, one parallel along its length and the other orthogonal (at a right-angle) along the engagement plane. The interceptor has a fixed amount of speed to mete out between these two components. Parallel LOS are generated by objects that have the same orthogonal components of their speed. If the LOS are parallel, then the interceptor's remaining speed should be put into closing range on the target, directed into the parallel component. If the difference of the target's and interceptor's parallel components is positive, then parallel navigation is achieved, and the interceptor is on the shortest path it can take to the target (assuming a non-manoeuvring target). However, the magnitude of the orthogonal vector of the target is not available to the interceptor and so must be approximated, which is where the pro-nav controller is used. If the orthogonal vectors are non-matched, there will be rotation in the LOS. If this rotation is towards the heading of the interceptor, the interceptor's orthogonal velocity is too slow, and if away, it is too fast.

If the same rotation in the LOS is applied to the heading (i.e. N = 1), then the amount of interceptor orthogonal velocity remains the same, as does its error angle between heading and LOS (δ). However, if the rotation is magnified by a fixed navigation constant (N > 1), then speed is exchanged between the two components. If the interceptor is being outpaced by the target, speed is taken (through heading rotation) from the parallel component and added to the orthogonal component. Should the interceptor be outpacing the target, then speed is taken from the orthogonal component and added to the radial. The polarity of the exchange is given by matching the axis of rotation of heading to that of the LOS.

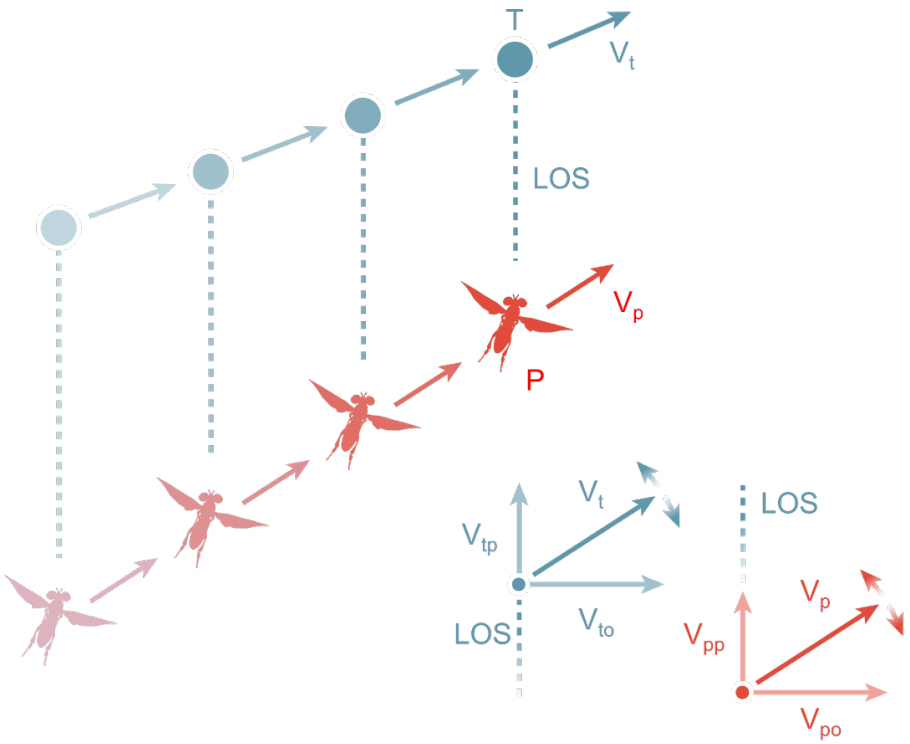

Fig. 3.7 A predator (**P**) rises to meet a target (**T**), connected by the line-of-sight (**LOS**) between them. Both P and T have velocities ($\mathbf{V}_p$ and $\mathbf{V}_t$ respectively) that have components relative to the LOS. For each, one of these components is parallel to the LOS (V_{tp} or V_{pp}) while another is orthogonal to the LOS (V_{to} or V_{po}). Rotating a velocity vector whilst maintaining its length (steering with constant speed) necessarily swaps speed between the two components. In order that a predator maintain parallel navigation and close range on the target, V_{po} must equal V_{to} while V_{pp} must exceed V_{tp}. LOS rotation is symptomatic of an inequality of V_{pp} and V_{to}. Should the rotation of the LOS be towards V_p then V_{to} exceeds V_{po}, and if away, the inverse is true.

In this way the pro-nav algorithm finds its way to a parallel navigation without requiring knowledge of the target's transverse component. The reason that this will be used over the human constant bearing model is that it is the most biologically relevant for the control system internal to an organism using it. While it creates near identical kinematics to a suitable weighted human constant bearing model (excluding the proximity term), it does not require the dampening effect as when there is no rotation in the LOS, there is no rotation to the interceptor heading. The reduced input requirements make it a more parsimonious control law, and more likely describes implementable internal control systems than more simply describing the behaviour from an external perspective.

Summary Table of Guidance Laws:

Control Law	Input	Output	Advantage	Drawback
Pursuit	Retinal target position relative to the centre (egocentric)	Direct heading to the current target position	Extremely simple & robust	Takes a longer than necessary path to a moving target
Deviated Pursuit	Retinal Target Position relative to a preordained lead position (egocentric)	Lead heading leads the target by a fixed deviation	Shorter trajectory than pure pursuit but nearly as simple	Heading is not optimised and still doesn't take the shortest possible route
Human Constant Bearing	Target Distance, LOS Rotation (exocentric), Current Heading Velocity (exocentric)	Rotational Acceleration of the interceptor heading	Accurately models the behavioural dynamics of a human intercepting a moving target	Incorporates physical and behavioural inputs and thus unlikely to represent fundamental guidance law
Constant Absolute Target Direction	LOS Rotation (exocentric)	Turning away interceptor heading from LOS Rotation	N/A	Does not effecively induce interception
Proportional Navigation	LOS Rotation (exocentric)	Amplified turning of the interceptor heading in proportion to LOS Rotation	Robust navigation to a moving target without calculating a future meeting point	Requires measurement of the external reference frame
Absolute Calculation	Target Heading, Target Speed, Interceptor Heading, Interceptor Speed (all exocentric)	Optimal route to a linearly travelling target that does not change speed	Shortest route to the future meeting point with the target	Requires information unavailable to a visual predator & requires extensive computation

3.3 Interception in *Holcocephala fusca* and *Coenosia attenuata*

Through interception, a chaser can reach the target faster than if using pursuit, but in principle interception is a more difficult strategy. Miniature dipteran flies such as *Holcocephala* and *Coenosia* have limited neural capacity when compared to other intercepting animals such as falcons [179] or mammals [182]. This raises the question of whether these much smaller animals implement the same systems as large vertebrates [179], or even large insects such as dragonflies [162]. In addition to a feedback controller, dragonflies are believed to use a predictive mechanism to reduce lag in head-tracking the target, i.e. using internal models of both their own bodies and prey flightpaths, something that could be used to aid steering an interception course [76].

Small predatory flies tackle what is essentially the same predatory task as that of dragonflies, but their behaviour has not yet been tested against any models for guidance. In this chapter, we investigate if a simple control law like those detailed above can explain the aerial hunts of the North American robber fly (**Fig. 3.8a**) (*Holcocephala fusca*, ~6 mm body size) and the Mediterranean killer fly (**Fig. 3.8c**) (*Coenosia attenuata*, ~4 mm body size) towards objects moving with either constant or erratic velocities (example behaviours in **Fig. 3.8b** for *Holcocephala* and **Fig. 3.8d** for *Coenosia*). As a recap, both of these miniature dipteran species are sit-and-wait generalist predators [41, 183] that catch their prey in mid-air. However, the two species differ in visual acuity (*Holcocephala* have an acute region with peak resolution 10× better that of *Coenosia* [37, 77]) and environment (i.e. *Holcocephala* hunts against clear sky, while *Coenosia* can hunt against and between foliage). We have analysed their predatory flights and tested if these can be predicted with any of the three most probable simple controllers detailed above; (i) pure pursuit, (ii) deviated pursuit or (iii) proportional navigation. These control laws were selected as CATD has been demonstrated to be flawed, while the human bearing model of interception is extremely similar to proportional navigation, but less parsimonious (in requiring dampening proportional to the pursuer's angular velocity, which pro-nav does not).

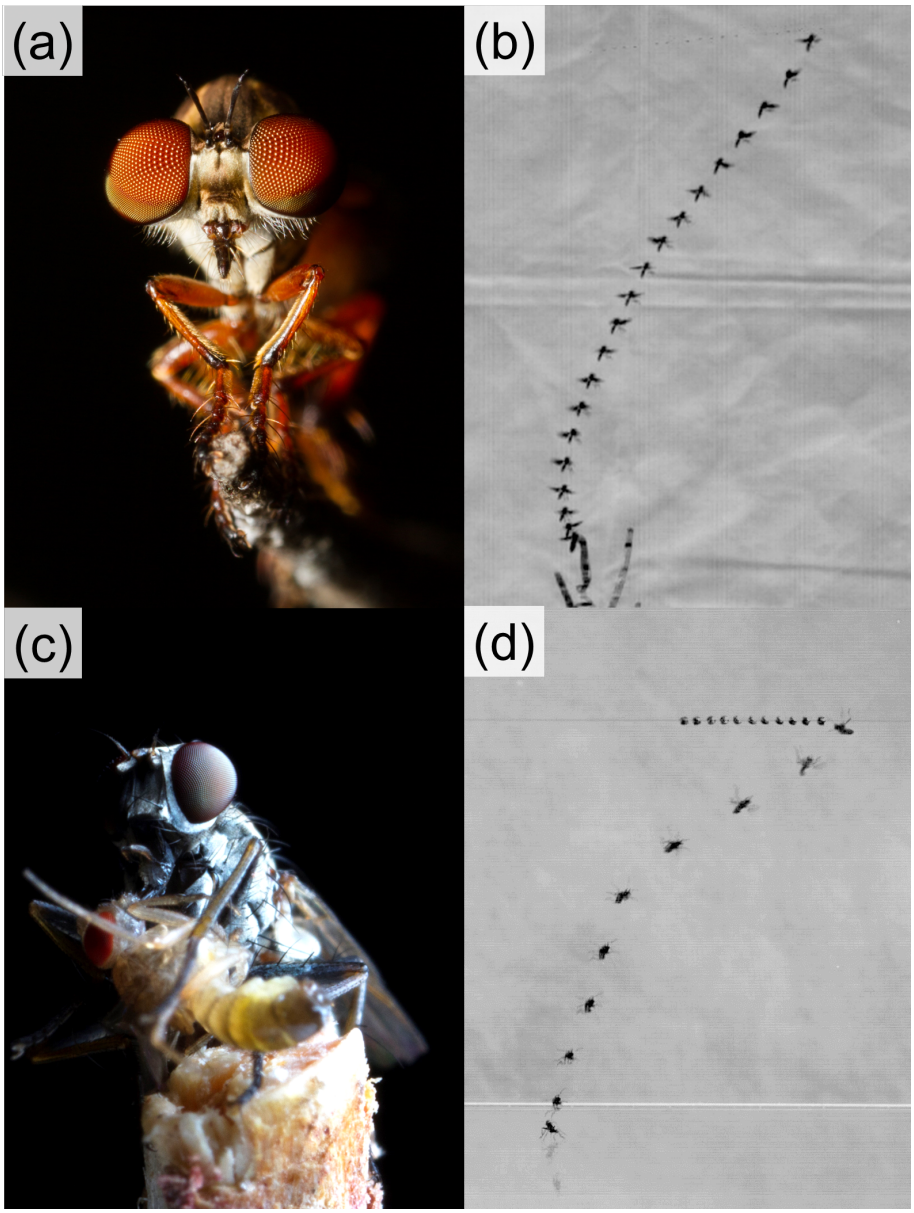

Fig. 3.8 **(a)** *Holcocephala fusca* perched. **(b)** An overlay image of *Holcocephala* intercepting a dummy target. **(c)** *Coenosia attenuata* with a fruit fly previously caught mid-flight. **(d)** An overlay image of *Coenosia* intercepting a dummy target.

Here, we have analysed and modelled the attacks of *Holcocephala* and *Coenosia* flights. The results are consistent with the use of a proportional navigation controller, with gain and delay adjusted to suit the adaptations of each species and the environments in which they operate.

3.4 Experimental Methods

3.4.1 Animals and Experiments

Holcocephala fusca used in experiments were from wild population and left in situ, experimental apparatus being arranged around their chosen perches. *Coenosia attenuata* were obtained either from lab-reared stocks of a captive population held within the University of Cambridge for experiments involving dummy targets, or from wild population and left in situ in the greenhouse when intercepting “natural” targets. Dummy target experiments conducted with *Coenosia* were in laboratory conditions and under artificial lighting (6.7 KLx upward, 1.2 KLx reflected).

Behavioural data was acquired with a pair of time-synchronised Photron Fastcam SA2’s with overlapping fields of view so that 3-dimensional placement of pursuer and target could be attained. Cameras were calibrated with known-sized checker boards which were moved by hand in the field of view of both cameras. The checkerboard was "wobbled" sinusoidally, varying its aspect relative to the cameras, as it was moved towards and away. In this fashion, it was contrived to occupy the 3 dimensional space that the recorded behaviour had taken place in. All flights were captured at 1000 frames per second and the placement of pursuer and target in both frames tracked. Temporal resolution of 1 ms is retained throughout all analysis. Raw positional data was smoothed to account for erroneous small perturbations generated through tracking that could lead to false measurement of line-of-sight (LOS) rotation. Further details given in supplementary information of [77] and for details on trajectory smoothing, see 2.2.3 and [151].

3.4.2 Visual Stimulus

To elicit predatory behaviour, flies were presented with dummy targets. As in chapter 1 & 2, these targets took the form of silvered beads of variable diameters (1.3, 2.9 and 3.9 mm) on fishing line. To get the targets to pass in a straight line and at set speeds, the fishing line was passed around a U-frame with wheels at all four corners and a central stepper motor that controlled bead movement (see [77]). To move targets erratically for *Holcocephala*, and thus generate unpredictable changes in the line-of-sight rotation rate, a single 1.3 mm target was hung from a length of fishing line tied to a 30 cm long thin wooden stick. These targets could then be moved by an operator in front of the flies and produce variable, non-linear trajectories where both the bearing and speed of the target varied greatly. To move targets

erratically for *Coenosia*, fruit flies (*Drosophila melanogaster*) were released from a vial near a perched *Coenosia*.

Linear *Holcocephala* targets were tested across a speed range of 0.03 – 1.05 ms^{-1}, a mean speed variation within flights of 0.12 ms^{-1} ± SE 0.01 ms^{-1} (n = 109) and a mean target heading deviation from initial conditions of 18.8° ± SE 3.0° (n = 109) within flights. For *Coenosia*, linear targets had a speed between 0.10 – 0.79 ms^{-1}, a mean speed variation of 0.01 ms^{-1} ± SE 0.00 ms^{-1} (n = 59) within flights and a mean target heading deviation of 0.9° ± SE 0.1° (n = 59) within flights. Holcocephala erratic targets travelled between 0.07 – 0.73 ms^{-1}, had a mean variation in speed of 0.42 ms^{-1} ± SE 0.05 ms^{-1} (n = 17) within flights and heading deviation of 62.4° ± SE 7.9° (n = 17) within flights. Coenosia erratic targets had a speed between 0.54 – 1.23 ms^{-1}, an average variation in speed of 0.26 ms^{-1} ± SE 0.10 ms^{-1} (n = 8) within flights and a mean heading deviation of 35.4° ± SE 8.5° (n = 8) within flights.

3.4.3 Data Analysis

All analysis of captured data was conducted in MATLAB 2016b with custom written scripts. Only flights where contact with the target was made were included in the analysis. This is because in the attacks that were abandoned before the target was caught (Coenosia 43% and Holcocephala 36%), it was not clear at which point the flight motivation switched from interception to avoidance. The early part of the pursuer's trajectory, at the beginning of the hunt, was not included in the analysis as this reflected take-off dynamics (e.g. high accelerations). Hence, when models were being tested and applied, the start point was taken at 20% of the way through the flight course. Likewise, analysis was stopped 1 cm before the pursuer hit the target, as within a body-length of the target, the flies' wings frequently caught the fishing line of the target. Individuals could not be tagged due to limitations related to field-based research and animal size. Hence, some flights may be from the same individuals. For *Holcocephala*, the flight data are from female and male flies, although the sex of the subject was not noted for each flight. For *Coenosia*, the flight data are from females. Male *Coenosia* were not used in this study as they are far less abundant in the colony than females and frequently take-off even when targets are not being presented.

To test for parallel navigation, range vector correlation is used as a measure of LOS parallelism, a measure that ties in with existing work (i.e. [76, 77]) (**Fig. 3.9**). The correlation value is given by (i) the angle difference between successive LOS vectors and (ii) the difference of their magnitudes. A value of 1 indicates that LOS are parallel and getting

longer (i.e. the target is increasing range from pursuer), a value of 0 means that distance to the target is maintained but LOS are rotating and a value of -1 indicates that LOS are parallel and the range to the target is decreasing (i.e. perfect parallel navigation). Flight time was normalised to a percentage of flight complete so that all flights could be overlaid.

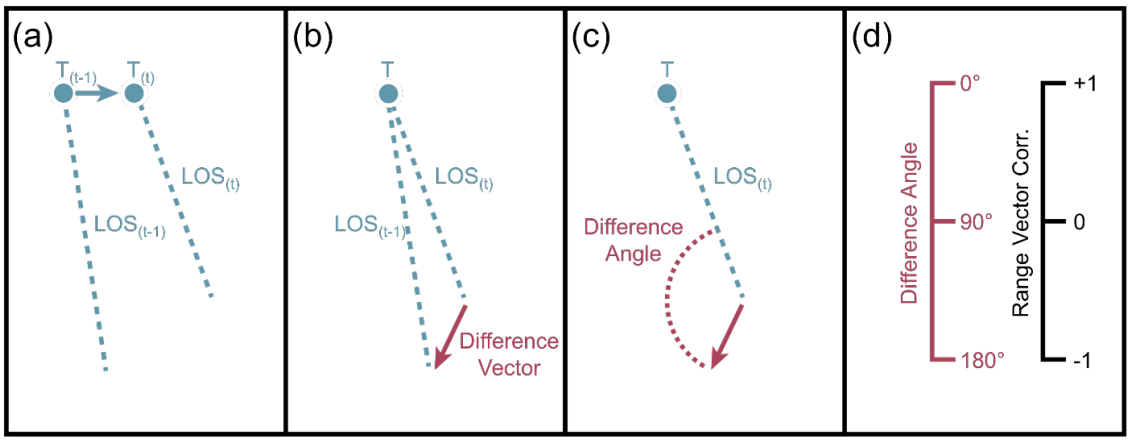

Fig. 3.9 The process by which range vector correlation (an index of parallelism of successive LOS) is measured. **(a)** the LOS for a trajectory is taken and then **(b)** time-differentiated to find the difference vectors. **(c)** the angle between the LOS and the difference vector gives the difference angle. **(d)** This angle is then converted into a range vector correlation value where -1 corresponds to parallel navigation, 0 corresponds to rotating LOS with no shortening, and +1 corresponds to parallel LOS that are elongating over time. This final conversion is done to be in keeping with existing literature.

Optimum heading analysis was conducted by taking the properties of fly speed and the three components of motion of the target and solving a pair of simultaneous equations. These equations distribute fly speed into the three components, such that it will meet the target in X, Y and Z at the same time, signalling connection with the target. The formulation of these simultaneous equations is given in Eqn. 3.11 and Eqn. 3.12.

$$S = \sqrt{{V_{px}}^2 + {V_{py}}^2 + {V_{pz}}^2} \tag{3.11}$$

$$\frac{r_x - (\tau \times V_{tx})}{V_x} = \frac{r_y - (\tau \times V_{ty})}{V_y} = \frac{r_z - (\tau \times V_{tz})}{V_z} \tag{3.12}$$

Where S is pursuer speed. V_{px}, V_{py}, & V_{pz} are pursuer velocity components in 3 dimensions, of unknown magnitude. r_x , r_y, & r_z are the range vectors between target and pursuer. V_{tx}, V_{ty} & V_{tz} are target velocity components of known magnitude. τ is an unknown time-to-contact.

Analysis was conducted in the full 3-dimensions recorded, except for investigation into correlation between the rotation of LOS and pursuer velocity. In this case, flights were flattened to the 2-dimensional engagement plane. Flattening to 2-Dimensions allows a polarity to be given to the rotation of both LOS and pursuer heading. This plane was defined by three points, the starting positions of fly and the two points of greatest displacement of target. This gave the least amount of information loss about the flight course when the 3rd dimension was removed (**Fig. 3.10**).

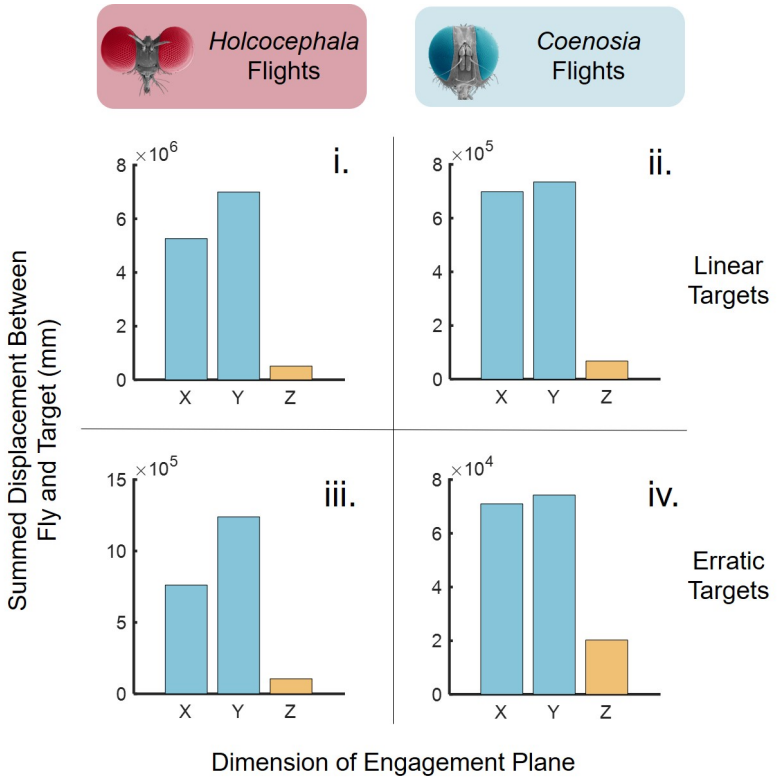

Fig. 3.10 Data were rotated onto the (XY) engagement plane, defined by the starting position of the fly and the two points of greatest displacement of the target. The plane has axes X & Y while distance orthogonal to the plane is in axis Z. The summed displacements between fly and target in each dimension are given for *Holcocephala* linear **(i.)** & erratic **(iii.)** targets and *Coenosia* linear **(ii.)** & erratic **(iv.)** targets. The Z dimension is removed when correlating the rotation in pursuer heading with rotation in the LOS.

3.4.4 Control Laws and Flight Simulations

We simulated three models on recorded successful flights: pure pursuit, deviated pursuit, and proportional navigation. These models are described in the introduction. To run the simulation, the forward speed of the predator during the actual flight was fed into the simulation. A fixed time delay, acquired from correlations in the entire data set of each species, was also fed into the model. The temporal resolution of the models was equal to that of the flight (1 ms), which is well below the predicted reaction time of these flies (between 10 and 30 ms). These simulations then output the rotation in heading according either to (i) error between LOS and fly heading (Pure Pursuit) or (ii) rotation of LOS (pro-nav and N = 1 proxy for fixed angle of deviated pursuit). The simulations started at the same position and with the same heading as the fly at the beginning of the navigation phase of the flight, but after this point the LOS rate and error angle were measured with regards to the model alone, and not taken from the true flight.

The measure of fit between simulations and true trajectories was an angular error between the heading of the model and the heading of the true fly trajectory at all time points. To independently test which gain (navigational constant) provided the best fit, we sequentially fitted gains across a range (from 1 to 10, incrementing by 0.1). We define the best fitting gain as the one that resulted in the lowest mean error across the navigation phase of the flight. We used this method (instead of a distance measure between fly and model at all time points), because it provides a metric for how well the simulation matched the shape of actual pursuer trajectory, even if the position at which it did so differed from the real position of the fly. Time delays used in model fitting were taken from best fitting correlations of LOS rotation and pursuer velocity rotation (28 ms for *Holcocephala* and 18 ms for *Coenosia*). Pro-nav models are depicted with an arbitrary ± 30 % of fitted gain to demonstrate the sensitivity of flightpath to the chosen gain. Pure Pursuit models are depicted with a 10× gain range from 10 s^{-1} to 100 s^{-1} to demonstrate a wide range of gains do not improve model fit. This range was chosen to encompass the gains described in the aerial pursuit of other insects [158, 159].

We also tested for the advantage of using a pro-nav controller (tuned to either of the two fly species), versus a pure pursuit controller by carrying out flight simulations. Advantage was quantified as the percentage difference in time-to-contact between a pure pursuit and pro-nav. The difference was tested at different target speeds but with the same starting positions and headings. For the pure pursuit simulation, we used the mean starting positions for each species (acquired from the data) and set the trajectory starting from the pursuer's origin. For the pursuit course simulation, when flight-time exceeded that of the true flightpath, and the fly had not reached the target, target velocity and fly speed were extrapolated from

the last available values. Similarly, a separate pro-nav model was also set off from the origin to test whether it had a similar advantage, over the pure pursuit model, as the true flights. The navigational constants for the pro-nav controllers (N = 3 for *Holcocephala* and N = 1.5 for *Coenosia*) in the simulations were taken from the best fitting correlative data in this study. The pursuit model took the constant value (k = 20 s^{-1}) from recorded work for the housefly *Fannia canicularis* [159].

3.4.5 Tests for Optimal Take-off Distance

We tested whether the timing of the predatory fly at take-off was time-optimal (i.e. whether it allowed the animal to intercept prey in the shortest possible time). For this analysis targets were simulated travelling left to right. Target movement was presented across a range of increasing altitude, spanning both approaching and receding distances. Targets were presented above a pursuer that sets off vertically from the origin. The pursuer is steered by a pro-nav model with its navigation constant matched with that particular to each species (for *Holcocephala* N = 3, delay = 28 ms, for *Coenosia* N = 1.5, delay = 18 ms). The speeds for target and pursuer used in the simulations were taken from the means from the recorded flight data for each species. Time-to-contact was measured and normalised for each target altitude. This allowed us to find the time/location along the target's horizontal flightpath where the fly should take-off to produce minimal time-to-contact. To compare the timing of the simulated (optimal) predatory take-off vs the timing of the real take-off, a common reference frame was necessary. To obtain it, the recorded flights were rotated until the linear target trajectories were aligned to the horizontal axis. We then noted the position of the target as the pursuer took off.

3.5 Results

3.5.1 Flight Parameters

Flights of both fly species were reconstructed in 3D (**Fig. 3.11a**). Both *Holcocephala* and *Coenosia* use similar mean average flight speeds (0.71 ± SE 0.02 $m.s^{-1}$ (n = 109) and 0.69 ± SE 0.02 $m.s^{-1}$(n = 59)) and accelerations (mean peak 7.3 $m.s^{-2}$ for *Holcocephala* and 9.3 $m.s^{-2}$ for *Coenosia*) to intercept targets, even though their mean wingbeat frequencies differ substantially (*Holcocephala* = 130 ± STD 10 Hz (n = 10); *Coenosia* = 306 ± STD 19 Hz (n = 10)). *Holcocephala* pursues targets at much greater range than *Coenosia* (81-788 mm

for *Holcocephala*; 23-212 mm for *Coenosia*). To test for parallel navigation, range vector correlation (an indicator of LOS parallelism), was calculated for both species. *Holcocephala* (**Fig. 3.11b** i) shows near-parallel navigation (parallel navigation = correlation value -1), with a strong correlation appearing early in the flight (correlation 20% into the flight = -0.8). Coenosia (**Fig. 3.11b** ii) also trended towards parallel navigation as the flight progressed, but at a slower rate (correlation at 20%, 50% and 90% of the flight = -0.57, -0.58 and -0.80, respectively). The mean error from optimum heading was 14.1° ± STD 7.4° for *Holcocephala* (**Fig. 3.11b** iii) and 25.0° ± STD 11.2° (**Fig. 3.11b** iv) for *Coenosia*. Together, the data indicate that *Holcocephala* has a more optimal controller, or that it may implement turning commands more accurately. Alternatively, the closer range of *Coenosia* flights could simply result in lower performance. Next, we investigated if the pursuer heading rotations within flights are supporting of a pure pursuit, a deviated pursuit or a pro-nav controller. As highlighted by [179], models that predict turning behaviour would be most informative when tested against turning targets. For this reason, both fly species were tested with linear and with erratically moving targets (with changing speed and direction).

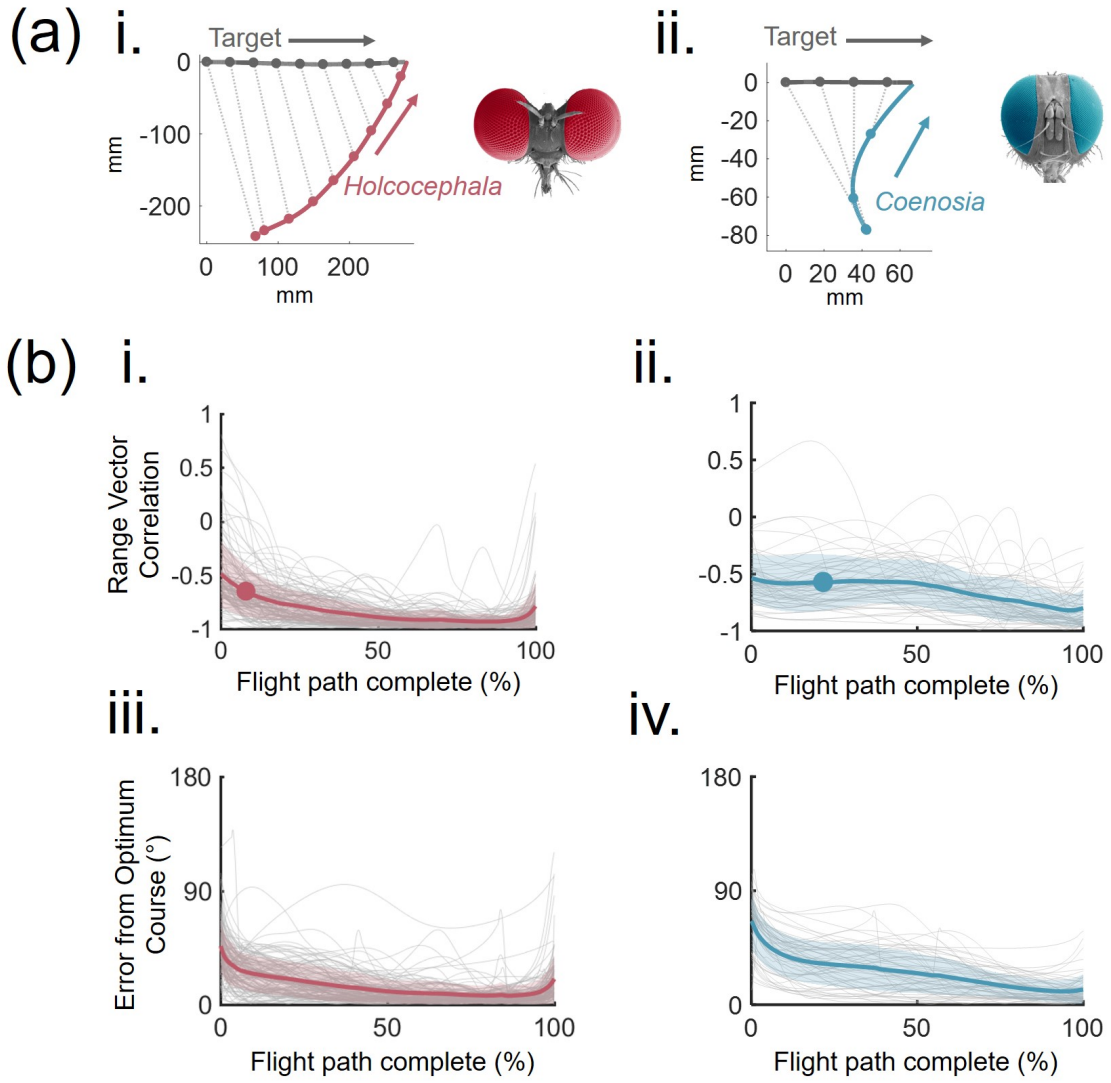

d

Fig. 3.11 **(a)** Example trajectories (compressed in 2-dimensions) of *Holcocephala* **(i)** and *Coenosia* **(ii)** are plotted intercepting linear targets, from perch to catch. Lines of sight are plotted at 50 ms intervals throughout the flight, time resolution of flight is 1 ms. **(b)** From all captured flights, an index of line of sight parallelism, range vector correlation (where -1 = parallel navigation), is plotted along the time-normalised flight length for *Holcocephala* **(i)** and *Coenosia* **(ii)**. Mean points where an optimum course becomes available through acceleration are marked by plotted circles. The angular error between pursuer heading and the optimum course, once one becomes available, is plotted for *Holcocephala* **(iii)** and *Coenosia* **(iv)**.

3.5.2 Pure Pursuit Test and Simulations

A strong positive correlation between pursuer heading angular error from the LOS and rotation rate of the pursuer heading would be expected for a pure pursuit navigation system. However, we did not find such correlation with either linear or erratic targets and for both *Holcocephala* and *Coenosia* (**Fig. 3.3.12a**). The best fitting linear regression models for both flies had little explanatory value (for Coenosia, with linear targets k = 10.2, R^2 = 0.02 and with erratic targets k = 8.4, R^2 = 0.04. For Holcocephala, with linear targets k = -2.3, R^2 = 0.04 and with erratic targets k = 2.4, R^2 = 0.01). For the linear targets, the fit of time constants continually increased to the maximum tested at 50 ms for both species, whereas with the erratic targets this value was 22 ms for *Holcocephala* and 15 ms for *Coenosia* (**Fig. 3.12b**). Regardless, the flight simulations with a pure pursuit controller model don't match the trajectories taken by either species of predator (**Fig. 3.12c**). In the experiments both fly species steer ahead of the target's position, but in the pursuit simulation the pursuer undershoots the target trajectory and must enter a tail-chase towards the target, only catching it once its linear speed exceeds that of the target. We ran the same simulation with a wide range of constant values (10 s^{-1} to 100 s^{-1}), but this did not improve the fit of the model (**Fig. 3.12c**). Thus, a pure pursuit controller is not supported by the data.

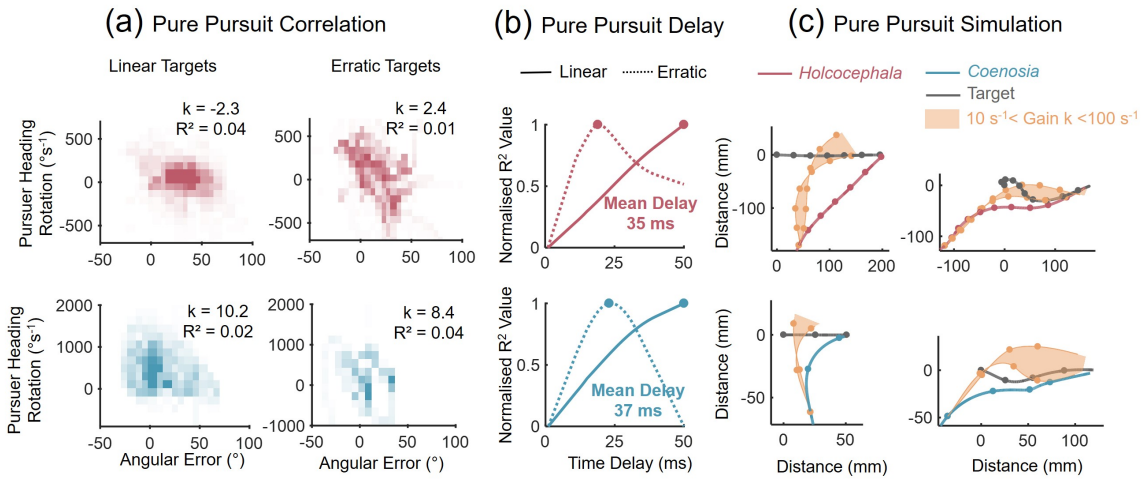

Fig. 3.12 **(a)** Purser heading rotation is plotted against the error between pursuer heading and the LOS in both *Holcocephala* (red) and *Coenosia* (blue), shown for linear (left) and erratic (right) targets. Histograms of points are displayed with occupancy representing frequency count within a block. Data is displayed at the time-delay that gave the highest coefficients of determination for a linear model. The best fitting model gain (k) and resulting coefficient of determination are depicted by each panel. **(b)** Coefficients of determination, normalised from lowest to highest, are plotted against the respective applied time delay between stimulus and recorded response, with peaks marked by points. **(c)** Pure pursuit flight simulations (compressed in 2- dimensions) are plotted across a wide range of constant values (trajectory variation represented within the shaded area) and at best fitting delays, using flight speed and target position taken from recorded data. Points mark 50 ms intervals.

3.5.3 Pro-nav Test and Simulations

For interception of targets moving at a constant velocity, we found a correlation between rotation rate of the pursuer heading and rotation rate of LOS, for both *Holcocephala* and *Coenosia*. For *Holcocephala*, the correlation was stronger for the erratic targets (For linear, N = 2.56; R^2 = 0.28, n = 109 flights. For erratic, N = 3.04, R^2 = 0.59, n = 17 flights **Fig. 3.13a**). For *Coenosia*, the strength of the correlation was similar for linear and for erratic targets (N = 1.4; R^2 = 0.65, n = 59 flights vs N = 1.2; R^2 = 0.57, n = 8 flights, respectively, **Fig. 3.13a**). This correlation is the hallmark of a proportional navigation control system. These results were obtained with a best-fit temporal delay for linear-erratic targets of 29-27 ms for *Holcocephala* 19-17 ms for *Coenosia* (**Fig. 3.13b**). Even though the targets were presented with similar velocities to both species (see Methods section 2.2.3), for linear targets the mean rotation of the LOS in *Holcocephala* was an order of magnitude less than that of the *Coenosia* (33.4 $°s^{-1}$ ± SE 0.3 $°s^{-1}$ as opposed to 333.8 $°s^{-1}$ ± SE 3.1 $°s^{-1}$). The mean

rotation of the LOS in *Holcocephala* for the erratic flights was also less than that of *Coenosia* (60.9 $°s^{-1}$ ± SE 1.0 $°s^{-1}$ as opposed to 228.2 $°s^{-1}$ ± SE 8.7 $°s^{-1}$). For any relative movement of prey normal to the LOS from the reference frame of the predator, the resulting rotation of the LOS is proportional to the arctangent of 1/range between target and pursuer. Thus, the higher rotation rates in Killer flies likely arise from the shorter target range on take-off.

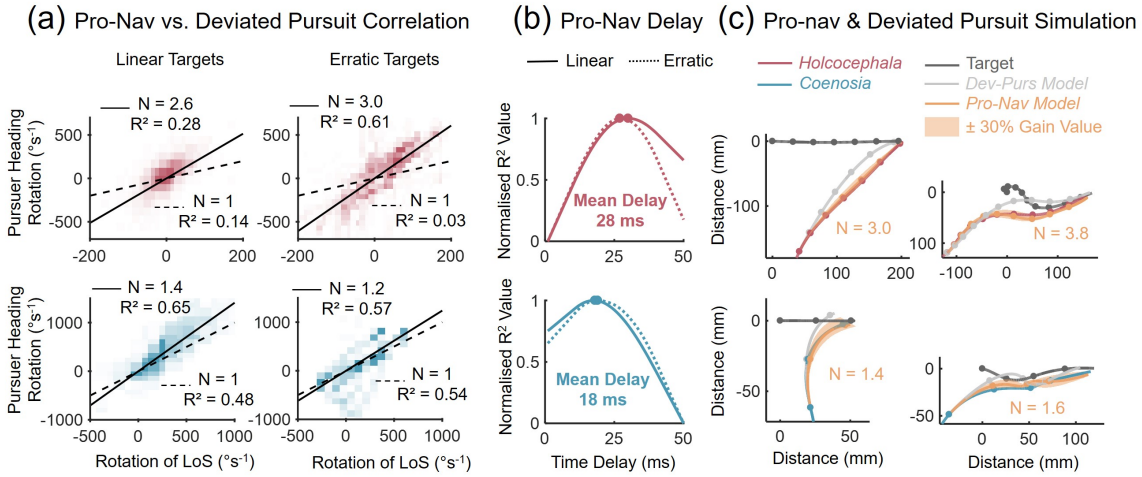

Fig. 3.13 **(a)** Purser heading rotation is plotted against the rotation of the LOS for both *Holcocephala* (red) and *Coenosia* (blue), shown for linear (left) and erratic (right) targets. Histograms of points are displayed with occupancy representing frequency count within a block. Data is displayed at the time-delay that gave the highest coefficients of determination for a linear model. The best fitting pro-nav gain constant and resulting coefficient of determination are depicted top left each panel. Deviated pursuit (Dev-purs) behaviour, where N = 1, is also tested for and the model gain and coefficient of determination displayed bottom-right of each panel. **(b)** Coefficients of determination, normalised from lowest to highest, are plotted against the respective applied time delay between stimulus and recorded response, with peaks marked by points. **(c)** Pro-nav flight simulations (compressed in 2-dimensions) are plotted at individually fitted navigation constant values and best-fitting time delays, next to N = 1 Dev-purs simulations, using flight speed and target position taken from recorded data. Points mark 50 ms intervals.

The pro-nav steering model results in well fitted simulated flight trajectories, for both species when intercepting both linear and erratic targets (**Fig. 3.13c**), despite not taking account of any potential biomechanical limitations nor environmental perturbations. When the model was tested with sequential fitting of constants incrementing from N = 1 to 10, similar peak gain fittings to the correlative measure were found for the navigational constant of both species. For linear targets, the mean best fitting gains were N = 3.4 ± SE 0.1 (n = 109) for *Holcocephala* and N = 1.6 ± SE 0.1 (n = 59) for *Coenosia*. For erratic targets they

were N = 3.9 ± SE 0.1 (n = 17) for *Holcocephala* and N = 1.4 ± SE 0.2 (n = 8) for *Coenosia* (**Fig. 3.14**).

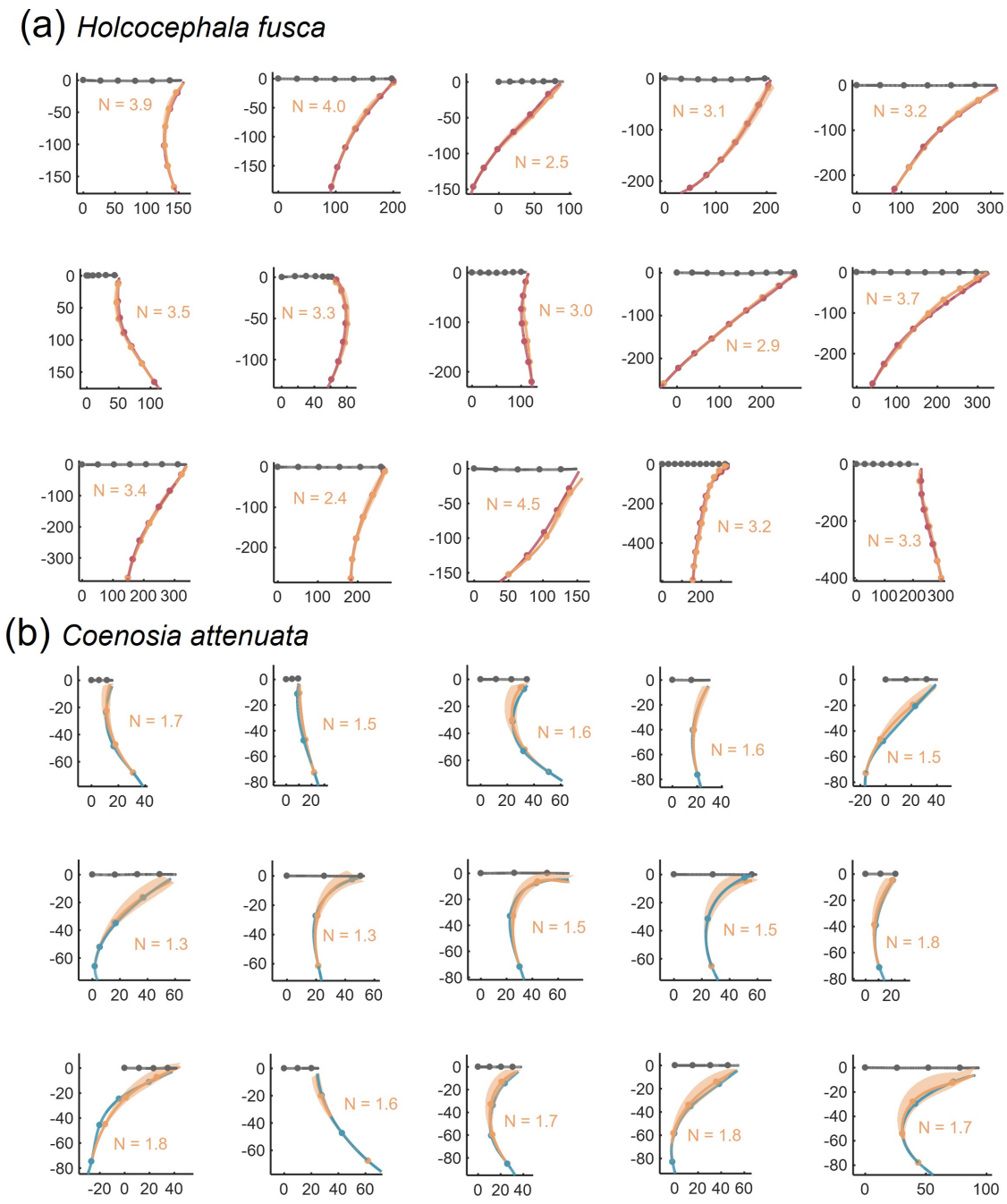

Fig. 3.14 Example curve fits are displayed with their corresponding navigation constants, for both (a) *Holcocephala* and (b) *Coenosia*.

For linear target intercepts by *Holcocephala*, the simulation showed a mean distance from the true flightpath of 5.8 mm ± SE 0.5 mm and angular error of 7.4° ± SE 0.6°. For linear target intercepts by *Coenosia*, the mean distance between the simulation and the true flightpath was 3.86 mm ± SE 0.5 mm and mean angular error 7.0° ± SE 0.6°. For erratic targets intercepts by *Holcocephala*, the simulation had a mean 8.47 mm ± SE 1.79 mm distance and 9.7° ± SE 1.46° error from the true course. For *Coenosia* intercepts of erratic targets, the simulation had a mean 8.3 mm ± SE 2.5 mm distance and 9.0° ± SE 1.8° of error from recorded flight paths. The sensitivity of the gain fitting is depicted in **Fig. 3.15**.

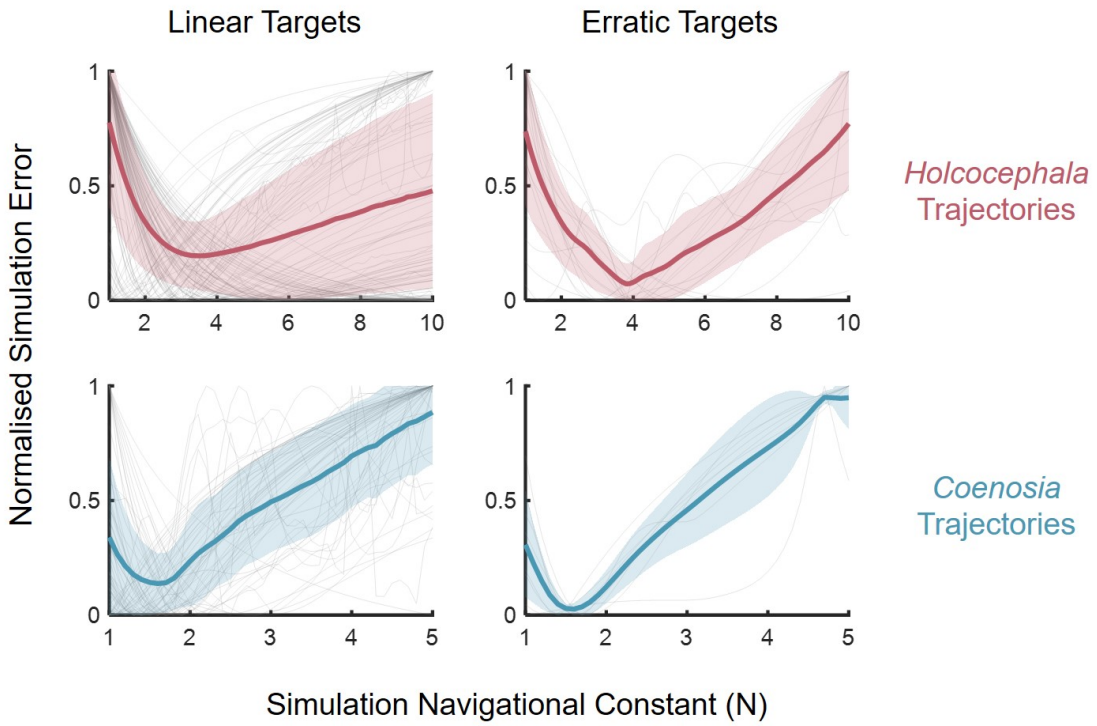

Fig. 3.15 The simulation error (for calculation, see methods), individually normalised for each flight, is plotted against the navigational constant (N) used in the simulation, for each of the experimental conditions (*Coenosia* or *Holcocephala*, linear or erratic targets). Mean and standard error for each panel are represented by the coloured lines and shaded areas respectively. The sensitivity of fitting N to trajectories by the alignment of simulation velocity with true fly velocity is indexed by the steepness of the slope of the mean line.

3.5.4 Deviated Pursuit Test

A third possibility is that the two predatory species employ a deviated pursuit controller, which aims to maintain a fixed error angle between pursuer heading and LOS. To maintain a

fixed error angle, a rotation in line of sight must be exactly matched by a rotation in pursuer heading (1:1). Thus, one may suspect a deviated pursuit controller may be in place if the best fit gain constant for a pro-nav controller yields N $\approx$ 1. However, a deviated pursuit controller correlation (N = 1) performed poorly when fitted to *Holcocephala* flights towards linear (deviated pursuit R^2 = 0.14) and erratic (deviated pursuit R^2 = 0.03) targets (**Fig. 3.13a**) and is therefore unlikely to be the underlying system. For *Coenosia*, the deviated pursuit correlation was also lower for deviated pursuit than for pro-nav, towards both linear (R^2 = 0.48) and erratic (R^2 = 0.54) targets (**Fig. 3.13a**), but this difference is not striking, and thus, insufficient on its own to ignore deviated pursuit as the controller for *Coenosia*. A secondary measure of a deviated pursuit controller is not whether it successfully maintains a fixed angle, but whether it turns in proportion to the error from that fixed angle. For this we would expect a linear correlation between the pursuer heading error from the LOS and rotation rate of the pursuer heading to be a positive linear correlation, but with a positive, non-zero intercept. As seen for both *Holcocephala* and *Coenosia* there are no such trends in the data (see pure pursuit test), and on this basis a deviated pursuit controller is unlikely to be driving predatory flights in these species.

3.5.5 Effect of Neural Delay and Proportional Gain on Performance of Flight Simulation

To individually test the effects of differing gain and time delay between the two species, we took four trajectories from each species and ran pro-nav simulations, with the best fit gain and time delay interchanged. Simulating a *Holcocephala* flight with the delay and gain observed in *Coenosia* (d = 18 ms and N = 1.5; **Fig. 3.16a** i), results in a longer route to the target. Most of this effect arises from the lower gain (**Fig. 3.16a ii**), with the shorter delay having little effect (**Fig. 3.16a iii**). Simulating a *Coenosia* flight with *Holcocephala* delay and gain (d = 28 ms and N = 3; **Fig. 3.16b iv**) also results in a longer path to the target. In this case, both, longer time delays (**Fig. 3.16b ii**) and higher gain (**Fig. 3.16b iii**) result in additional over-compensating turns by the pursuer and much longer routes to the target.

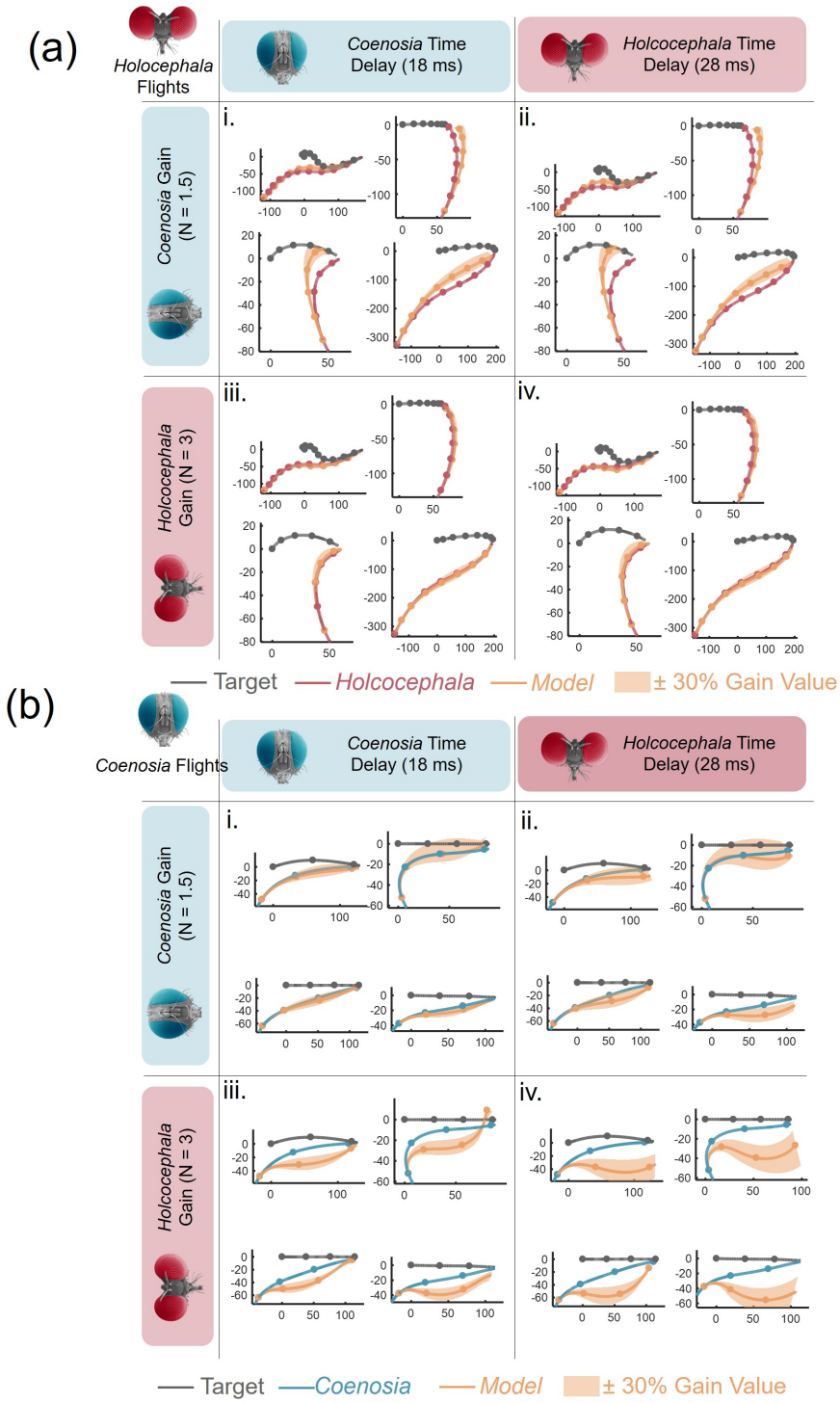

Fig. 3.16 Best fitting gain and temporal delays are interchanged between both fly species and applied to models overlaid on the four example flightpaths (compressed in 2-dimensions). This demonstrates the independent effects of time delay and navigation constant variation on *Holcocephala* **(a)** and *Coenosia* **(b)**, under their differing flight parameters such as take-off distance. Points mark 50 ms time intervals.

The effect of the navigation constant on resulting flightpath is dependent on the ratio of pursuer speed to the closing rate between pursuer and target (V_p/V_c ratio). Both *Holcocephala* and *Coenosia* have V_p/V_c ratios of near 1 (For linear targets 0.99 ± SE 0.02 and 1.08 ± SE 0.13 respectively and for erratic targets 1.01 ± SE 0.06 and 1.34 ± SE 0.60). Thus, the effective navigational constant N' approximates N [166], the importance of this similarity is described in the discussion.

3.5.6 Efficiency of Pro-Nav vs Pure Pursuit Controller on Real Flight Conditions

To quantify the relative efficiencies of investing in proportional navigation over pure pursuit, the relative time-to-target advantage was calculated for both species (**Fig. 3.17a**). For this, we used the data from interception of linear targets i.e. by feeding in the starting positions and velocities of both target and predator, then letting the pure pursuit model steer the predator through the simulation flight until contact with target (*Holcocephala* n = 109, *Coenosia* n = 59 flights). We then calculated the flight time difference between the pure pursuit simulation and the real flight. The greater the speed of the target relative to the pursuer, the greater the time advantage of the fly trajectories over a pursuit controller (**Fig. 3.17a i-iii**). Time-to-contact differences of actual flights vs the pure pursuit model are matched by the time advantages of a theoretical pro-nav controller (with gain matched to the flies, respectively), demonstrating that the change in controller is responsible for time-to-contact savings.

Time-to-contact is also affected by the initial attack angle on take-off (angle between initial LOS and target flight-path). Our flight simulations demonstrate that there is an attack angle which uses minimal time-to-contact for the controller tunings and mean flight-speeds (**Fig. 3.17b**). This value is 39° for *Holcocephala* (**Fig. 3.17b i**) and 35° for *Coenosia* (**Fig. 3.17b ii**). Both species of fly took off after targets near to this optimum attack angle, with mean attack angles of 32.8°± SE 1.7° for *Holcocephala* and 37.0°± SE 1.9° for *Coenosia*.

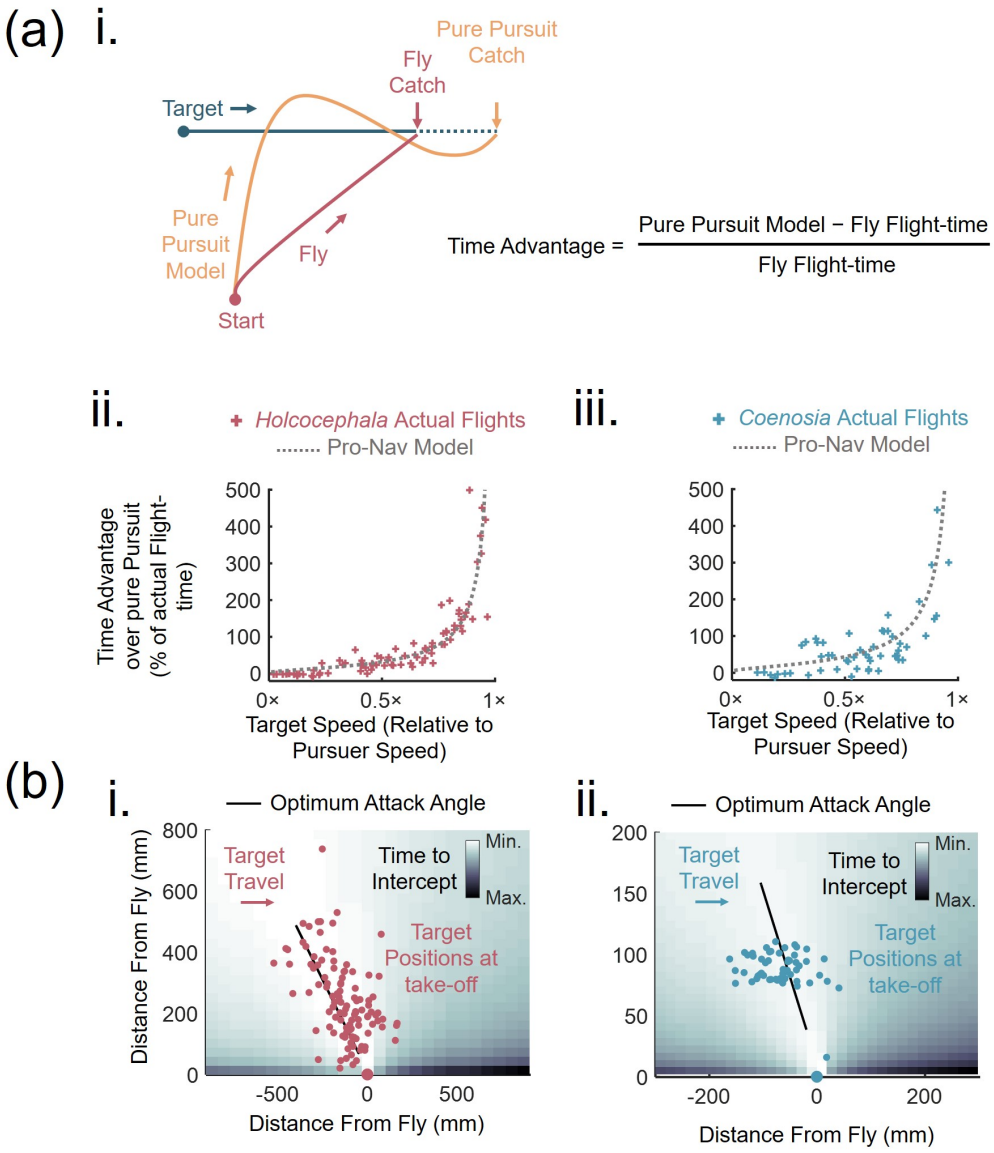

Fig. 3.17 **(a) (i.)** Diagrammatic representation of time advantage for flight courses taken by flies compared with a pure pursuit model. Calculated time advantages as a percentage of actual flight-time plotted against the relative speed of the target for **(ii.)** *Holcocephala* (n = 109) and **(iii.)** *Coenosia* (n = 59). The mean theoretical advantage of a pro-nav model, given the same conditions as the fly is overlaid (dotted line). **(b)** Target positions (relative to pursuer) at the time of fly take-off are plotted for **(i.)** *Holcocephala* (n = 109) and **(ii.)** *Coenosia* (n = 59). Underneath is a map of relative time-to-contact for different hypothetical target starting positions according to fitted proportional navigation models, travelling at the mean speed of each fly respectively, and starting vertically from the origin. Target headings are aligned to travel left to right across the page.

3.6 Discussion

The two species in this study see with differing spatial resolutions, but they set out to solve the same challenge, to catch other aerial arthropods. We raised the question whether they have evolved the same means of navigating to their target. *Holcocephala fusca* and *Coenosia attenuata* are unlike other studied insect navigational systems [158, 159, 163, 157, 171, 184] with the potential exception of dragonflies [162]. This is because they intercept targets without needing knowledge of target properties, implementing pro-nav that turns them towards a near time-optimal course to the target. Given the correlation between the rotation of pursuer heading and line-of-sight, and the agreement of modelled flightpaths with fly trajectories, we find the most parsimonious explanation of interception behaviour in both species to be proportional navigation. We firmly rule out pure pursuit navigation, as found in many other studied insect systems, because there is neither correlative evidence nor agreement with model simulation. We also rule out deviated pursuit navigation (which would yield identical behaviour to pro-nav with a constant fixed at N = 1), as this explains the correlative data less well than a pro-nav controller and deviated pursuit simulations do not match flight trajectories. Harder to rule out are alternative models that employ rotation of line-of-sight (LOS) as a measured cue (such as the constant bearing model put forward in humans [174]) and result in flightpaths with similar curves to those obtained from a pro-nav controlled simulation. However, due to its simplicity, pro-nav stands out as still the most parsimonious controller that can explain interception flights as the constant bearing model affects angular acceleration rather than angular velocity and incorporates a damping term. Proportional navigation engenders near identical results with fewer input variables and is simpler to implement, and thus we suggest much more likely.

Correlative and simulation fitting methods produced consistent results; *Holcocephala* appear to use a control gain of $N \approx 3$ to steer their flightpath. This value matches the lower end of the envelope of gain constants used in human mechanisations of pro-nav, such as in guided missiles ($3 \leq N \leq 5$) [166]. Additionally, the terminal attack phase of the Peregrine falcon, *Falco perigrinus*, is modelled well by proportional navigation with mean gain of N = 2.6 [179], which is similar to the gain found in *Holcocephala*. The efficacy of the navigation constant is also dependent on target motion, and to describe this, the effective navigation constant (N') is used, as given in Eqn. 3.13.

$$N' = N\frac{V_p}{V_c} \tag{3.13}$$

V_p being the predator speed and V_c the closing speed between pursuer and target. For intercepting a non-manoeuvring target, the control optimum N' is 3, ensuring zero-miss with minimal cost of control (integral square of lateral accelerations) (for detailed work-through see next section or [166, 123]). For near-stationary targets the V_p/V_c ratio is 1 but for intercepting moving targets, as with the two flies in this investigation, N' may potentially vary from N. We found that for both flies N' $\approx$ N and thus *Holcocephala* uses near the optimum control gain of N' = 3. *Coenosia* use a low gain of near N = 1.5. This is below the optimal control level and below the range used in missiles [166]. This could represent limitations given by the high LOS rates they experience through close target proximity and the necessary neural lag between stimulus and reaction. We demonstrate in **Fig. 3.16** that given the proximity to target at which *Coenosia* hunt, employing an optimal control gain or longer time delay would frequently cause overcompensation in the turning response, and thus longer paths to the target. *Coenosia* maintains a course further from optimal than *Holcocephala* does. By only studying flight traces and range vector correlation, it would be easy to conclude that that they are not attempting to fulfill parallel navigation, as previously reported for dragonflies [76]. However, simply because killer flies do not successfully maintain near parallel LOS, it does not mean that they do not use pro-nav, as demonstrated by the model's accurate description of their behaviour.

We suggest that the difference in gain intimately reflects the differences in physiology and predation tactics of the two species. The higher acuity of *Holcocephala* vision enables them to spot suitable targets at greater range [77], and thus encounter lower LOS rates and use the optimal control gain to steer into targets. The lower acuity vision of *Coenosia* [37] results in close proximity attacks that create high rotations in LOS and necessitate a short time delay and lower gain. Most significantly, this study can be compared with the only other described use of proportional navigation in an animal, that of the peregrine falcons [179]. It is remarkable that peregrines, operating at much greater speeds and with radically different flight morphology use the same system as miniature predatory flies, and with a very similar near-optimal gain tuning to that of *Holcocephala*. This demonstrates that proportional navigation could well underlie interception behaviours across further animal taxa (e.g. [69, 162, 167]). Moreover, the comparison between *Holcocephala* and *Coenosia* needs to be augmented by further species that are physiologically dissimilar and hunt in differing habitats. Such studies would give evidence to explanations for the distinct control gains or present diverse specialisations of the control system to reflect the variation between differing groups' tasks, physiology or geometry of interaction.

An alternative explanation of the lowered gain of *Coenosia* involves the parasitic attitude loop. This effect should be familiar to biologists in principle, although not by this name.

To rotate its heading, the fly must rotate its body. This rotation potentially affects the measurement of LOS rate of the target and could create instabilities in tracking. These can be prevented by reducing the navigation constant [165]. It is unlikely that the parasitic attitude loop is responsible for the gain differences found in this study, as flies (like other animals), are most likely capable of accounting for rotations of their own bodies to stabilise vision [22, 76, 185]. This accounting can either be conducted predictively [76, 186] or reactively [24, 30] to separate self-induced rotation of the pursuer body from actual rotation of the LOS relative to the exocentric reference frame.

Correlative evidence for pro-nav in *Holcocephala* was weakest for interceptions of linearly travelling targets. These flights had relatively low LOS rates, meaning any noise in tracked positions of target and fly will more easily mask the effects of the control system, thus resulting in a lower sensitivity to constant fitting. When LOS rates were increased by using erratically travelling targets, the correlation of LOS rate and pursuer turning rate of *Holcocephala* showed stronger evidence for a pro-nav controller. The anatomy of *Holcocephala* suggests some potential clues to their implementation of pro-nav. Their highly specialised fovea seems likely to track the target, resulting in rotation of the head relative to the body as in the gimbal seeker of a missile. By maintaining target fixation and using either visual or inertial cues for rotation of the head, the fly can measure rotations in the LOS relative to the exocentric reference frame and thus conduct pro-nav. The use of pro-nav does not exclude the possibility that internal models are used to maintain gaze fixation on the target, reducing tracking lag as found in dragonflies [76] (likely through a corollary discharge), only that the rotation of fixated gaze is fed into the pro-nav controller.

Thus, we raise the question, not why both *Holcocephala* and *Coenosia* utilise a proportional navigational controller to attack targets, but why other described species of fly use a pursuit controller. Proportional navigation is likely to have a higher cost of implementation than a pursuit controller, or a narrower applicability. Most of the work hitherto completed on dipteran aerial tracking used the approach to conspecific targets (e.g [158, 159, 157]). This is a fundamentally different problem than the one faced by a predator. While predators are subject to strong selective pressure to successfully grapple with targets, social engagements involving pursuit may not be selected for success of aerial interception, instead simply following a potential mate or chasing away a rival may count as a "success" without need for actual contact. In cases of conspecific interception, innate knowledge of the target allows for biasing of any potential control system given that assumptions can be made about rough flight speeds and target sizes. Just such biasing underpins initiation of aerial interception of female hoverflies by males [163]. We have discounted sexual motivations in flights for both species; female *Coenosia* chase all conspecifics with cannibalistic purpose (males need

to out manoeuvre females to initiate mating) and male *Holcocephala* search for stationary (perched) females before attempting to copulate. It is therefore unlikely that the recorded behaviour towards moving dummy targets was other than predatory in function.

The relative simplicity of aligning axis of motion directly along the LOS to the target may have lower physiological and computational requirements than the variable coupling of thrust axis and LOS required for proportional navigation. To investigate further, knowledge of the head-body relationship during flight would be required, which is challenging for the two species studied in this work due to their small size. Robber flies (Asilidae) are a large family of flies, containing genera with much greater body size than *Holcocephala* (i.e. *Microstylum* or *Laphria*). These groups would make head-body relationships a more tractable question, should they also use pro-nav to intercept targets. This is our current line of work, assisted by electrophysiological work into the relationship between target stimuli and the motor commands transported to steering muscles down the descending neurons. However, robber flies are a large family of flies with extremely diverse hunting methods. Many are not sit-and-wait predators like *Holcocephala*, instead actively foraging for prey [187]. The results of this study with *Holcocephala fusca* should not be taken to transfer across to other species of robber fly. Just as the different hunting habits of *Coenosia* and *Holcocephala* have resulted in different gains on their control systems, the difference in other robber fly hunting styles may mean their target-navigation systems are entirely different.

Both predatory fly species here studied, *Coenosia attenuata* and *Holcocephala fusca*, take-off while targets are in the time optimum catch window. This does not necessarily suggest that flies wait for targets to reach this window, but that they might simply apply a filter to their target selection preferences or align their body orientation for this purpose. For instance, *Holcocephala* most often sit with their body at 30-50° in elevation, potentially aligning their visual axis along the optimum take-off window. If most targets are likely to be flying roughly parallel to the ground, a fly then need only give preference to targets coming towards it, with the time-optimum point for take-off coinciding with the target moving into the centre of its visual field. Additional work is needed to elucidate the exact cues that trigger the predatory behaviour at a particular time for both species, which would demonstrate how these animals take-off while targets are in the optimum catch window.

3.7 Conclusion

By studying the behaviour of the small flies *Holcocephala fusca* and *Coenosia attenuata*, we demonstrate that intercepting prey by flying a near time-optimal course need not be

underpinned by forward prediction of target path. Instead, the behaviour of both species is explained by proportional navigation, the basis of predatory behaviour in peregrine falcons and underpinning guidance in modern missiles. *Holcocephala* uses a higher, optimal gain of near N $\approx$ 3 to steer into targets over long ranges, similar to findings in falcons. In contrast, *Coenosia* uses a lower gain of near N $\approx$ 1.5, potentially overcoming high rotations in line-of-sight created by their proximity to targets at take-off. Both species have short time delays on their control systems, *Holcocephala* at 28 ms and *Coenosia* at 18 ms. The simplicity of implementation and energetic savings of proportional navigation mean that there is a wide applicability and suggest it may underpin predatory interception in other organisms. Studying such biological implementations may improve our general understanding as the organisms studied may demonstrate energetic saving tactics and such innovations could lead to improved human produced proportional navigation controlled systems.

The most fundamental question that results from the work above on the implementation of proportional navigation, is how flies are able to measure the rotation of the LOS and translate this into a steering manoeuvre. For pro-nav, the LOS rate must be indexed as relative to the external world, not relative to some local aspect of the fly's own anatomy. Suggestions from the flies' physiology already suggest potential clues as to how this is achieved.

Chapter 4

The Problem of Miss and Gain

Abstract

This chapter concerns a more in-depth analysis of gain tuning within a proportional navigation framework. Gain variation can dramatically alter the behavioural kinematics of an interceptor, and thus is the key to the optimality tuning of pro-nav. Stability analysi of pro-nav is more complex than in more conventional proportional control systems due to the highly variable effectiveness of the control effort, dependant on the immediate physical geometry of the system. Secondly, the conventional linearisation of the navigation problem is considered, and the optimality of a navigational constant of 3 is substantiated. Thirdly, gain optimality is then tested through simulations under fly-like conditions which do not necessarily match the assumptions of linearisation. Despite the difference from the idealised linear framework, the simulations suggest that the same optima hold true, namely that N = 3 generates the minimal miss distance with the minimal required control effort. Finally, an explanation is given on why speed is not an equivalent steering measure, despite its crucial importance to solving the interception problem.

4.1 Stability Analysis

Discussion of the optimal tuning of control and of stability is already prevalent in the literature on both pursuit and interception within animals. While the form of the delay-differential equation for pursuit lends itself directly to standard stability analysis [171, 173], applying these to interception can lead to confusion and erroneous statements.

In pursuit:

$$\dot{\gamma} = k\delta \tag{4.1}$$

And as described in the pursuit introduction section [173], the optimum control with a minimum of the integral of error at:

$$k = 1/\tau e \tag{4.2}$$

And this has led to an extension into interception control systems by the same paper that devised CATD [167]. In this description of the animal behaviour the interception model acts as follows:

$$\dot{\gamma} = k\delta_{opt} \tag{4.3}$$

Where δ_{opt} is the error angle formed between the current interceptor heading and the optimum heading. In this control system, the gain has units $[\text{TIME}]^{-1}$ and thus the same optimality of gain law can be applied as to pursuit [137]. However, there is an error in taking this control system as applying to the underlying biology. Simply because an animal can steer onto a collision course with a target, it does not mean that it is represented by the delay differential equation above. The pursuit guidance law uses inputs that are direct and biologically salient, the LOS to a target and the axis of heading (whether true velocity or assumed from body axis). This delay differential interception guidance law requires an organism to input the optimum heading, without suggestion of how this would be derived from the information available. This would then need to be neuronally represented such that the angle between the optimum course and the current heading could be completed.

Instead, if we took the control law of proportional navigation, which does push the heading of the interceptor towards a collision course, we would find that the behaviour is not modelled by this delay differential equation. The stimulus for control in pro-nav is LOS rotation, which indexes δ_{opt} but also includes the effects of the distance between the interceptor and the target. This means that k is not a true constant.

Proportional navigation is typically excluded from the typical stability analysis that can be applied to other controllers (e.g. PD controllers) [166, 180]. The navigation constant

N is dimensionless, and thus its stability for any given time delay is not readily accessible. Instead the stability of any set gain for a given delay is determined by the geometry of the engagement and is not scale independent. However, it is worth noting that there are general guidelines applied in mechanised forms of pro-nav, which rely on the predicted decay of the zero-miss distance under "typical" conditions. These state that the time-delay on the control system should be below $1/8^{th}$ the length of the entire flight [166].

4.2 Linearization and Optimisation of Proportional Navigation

It has already been noted that the effectiveness and stability of the navigational constant is dependent on the initial geometry. However, excluding the cases in which a time delay is poorly-matched (i.e. too long) for the trajectory, there is an optimal constant at N = 3, shared by modern applications of proportional navigation and *Holcocephala fusca*. Analysis of the optimal navigational constant is most intuitively done using near-collision-course assumptions (NCCs). At NCC and set in a reference frame where the target T is at the origin and the predator P is at (x,y), the LOS necessarily near equates to the x-axis and the engagement is entirely planar (geometry given in **Fig. 4.1**) [166, 123].

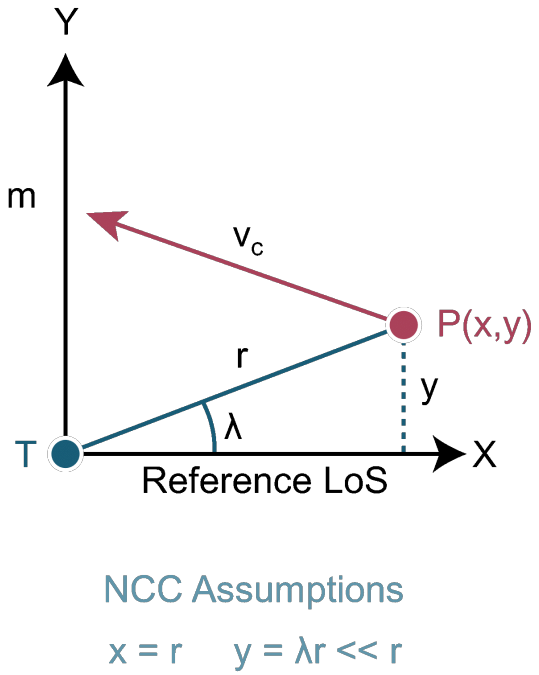

Fig. 4.1 The engagement geometry is depicted, with the coordinate system centred around a target (**T**) that remains at the origin and is approached by the displaced predator (**P**) along the closing velocity ($\mathbf{v}_c$). This generates a zero-effort-miss distance (**m**) by which the predator will miss the target without future corrective manoeuvres on the part of the predator nor acceleration from the target. This figure is redrawn from Shneydor 1998 [166].

Also implicit within the NCC is that the trajectory near fulfils parallel navigation. By this assumption the speed of both parties is constant and the time-of-flight (t_f) is dependent on the range and its time derivative as in:

$$t_f = -\frac{r_0}{\dot{r}} \tag{4.4}$$

Where r_0 is the initial range vector (r) (equivalent to LOS) at the beginning of the flight. This statement simply puts that the closing velocity (v_c) between the target and the predator is constant throughout the flight such that:

$$r(\tau) = v_c \tau \tag{4.5}$$

Where the range from the target (r) at a time-to-go until contact (τ) is equal to that time to go multiplied by v_c.

An index of performance for different constants of the pro-nav system under their planar, linearized assumptions, can then be formulated as below:

$$J = \frac{1}{2}C_1 y^2(t_f) + \frac{1}{2}C_2 \int_{t_0}^{t_f} {a_p}^2(t)dt \tag{4.6}$$

C_1 and C_2 are independent "weighting" constants that represent the importance given to either of the two component factors. J represents the cost index, which should be minimised through optimisation of the two terms. The first term is represented by the y displacement which is effectively the zero-effort miss distance based on a planar engagement geometry and under the given NCC assumptions that the v_c and r near equal the x axis (see **fig. 4.1**). The second term considers the control effort required in the summed square of the lateral accelerations (a_p) that are required of the predator in order to complete the trajectory. The ration of C_1 to C_2 defines the preference between the minimisation of miss distance and the minimisation of the control effort expended.

If the miss distance is to be minimised at any cost (absolute hit required) then $C_1 \to \infty$ and any miss has an absolute cost. The solution to the cost function is given by Bryson [188] and repeated by Shneydor [166] as below:

$$a_p(t) = \frac{3\tau}{\frac{3}{C_1} + \tau^3}[y(t) + \dot{y}(t)\tau] \tag{4.7}$$

Where τ is the time-to-go before collision. as $C_1 \to \infty$ then $\frac{3\tau}{\frac{3}{C_1}+\tau^3}$ simplifies to $\frac{3}{\tau^2}$. This leads via the NCC assumption to the form:

$$a_p(t) = 3v_c\dot{\lambda}(t) \tag{4.8}$$

This is the same formulation as proportional navigation with a navigational constant of 3 (for complete steps and formulation see [123, 166, 188]).

The conclusion derived from this is that the optimal navigational constant under NCC assumptions is 3, which assures a connection with the target, but with minimal sum of lateral accelerations.

4.3 Demonstration by Application

A more application derived way to view the optimization of the navigational constant is through the simulation of pro-nav engagements but varying the gain under lag-free conditions. Simulation has the advantages of not requiring the linearizing assumptions that have hitherto been applied. From these simulations, both the resultant miss distance and control effort (i.e. summed squared lateral accelerations) can be measured directly, and the topography of the results mapped, for factors affecting the engagement (i.e. including temporal lag).

The zero-effort miss-distance is the first parameter to be minimised. Miss distance can be described in planar terms by future projection of the velocities of the predator and of the target (**Fig. 4.2**). Overshooting is described by the predator crossing the targets trajectory before the target has passed the intersection, whilst undershooting is the inverse in which a target has already passed the trajectory intersection point.

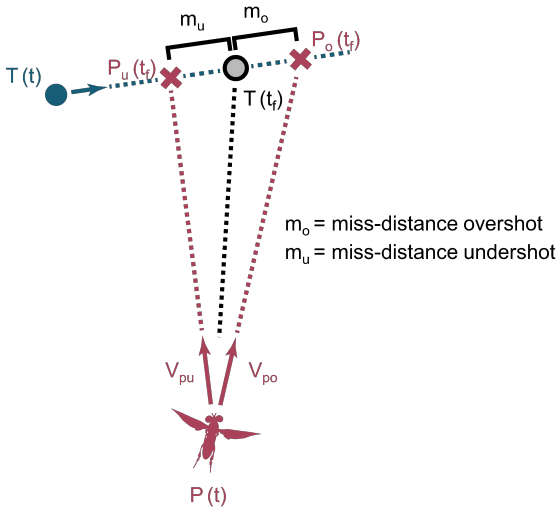

Fig. 4.2 The zero-effort miss-distance of a point along a trajectories path is shown for two alternative velocities (V_{pu} and V_{po}) of a predator (**P**) intercepting a target (**T**). The predator trajectory reaches the trajectory of the target at the time-of-flight (t_f), at two alternative positions. Pu is the position of the predator as it undershoots the target, Po where it overshoots. The distance between these two positions and the position of the target ($T(t_f)$) gives either an undershooting miss-distance (given positive + sign) or an overshooting miss-distance (given negative – sign).

The second parameter to be minimised is the summed square of the lateral accelerations. These are directly available from the simulation and calculable from the required rotation of the velocity of the predator and the speed at which its travelling. For the purposes of the presented simulations, speed was kept constant throughout the flight, for both the target and the predator. As with other simulations, the predator originates from the bottom of the figure to intercept a target that travels left to right above it.

4.4 *Holcocephala* Gain Tuning Simulations

As section 3.5, for simulations of the gain tuning optimality within *Holcocephala*, the speed of the simulated target and fly were matched to the means of the real flight trajectories (predator speed = 0.71 m.s^{-1}, target speed = 0.49 m.s^{-1}), and for the simulation purposes the predator was initiated at 200 mm distance and travelling exactly orthogonal to the target. The results of these simulations are displayed in **Fig. 4.3**.

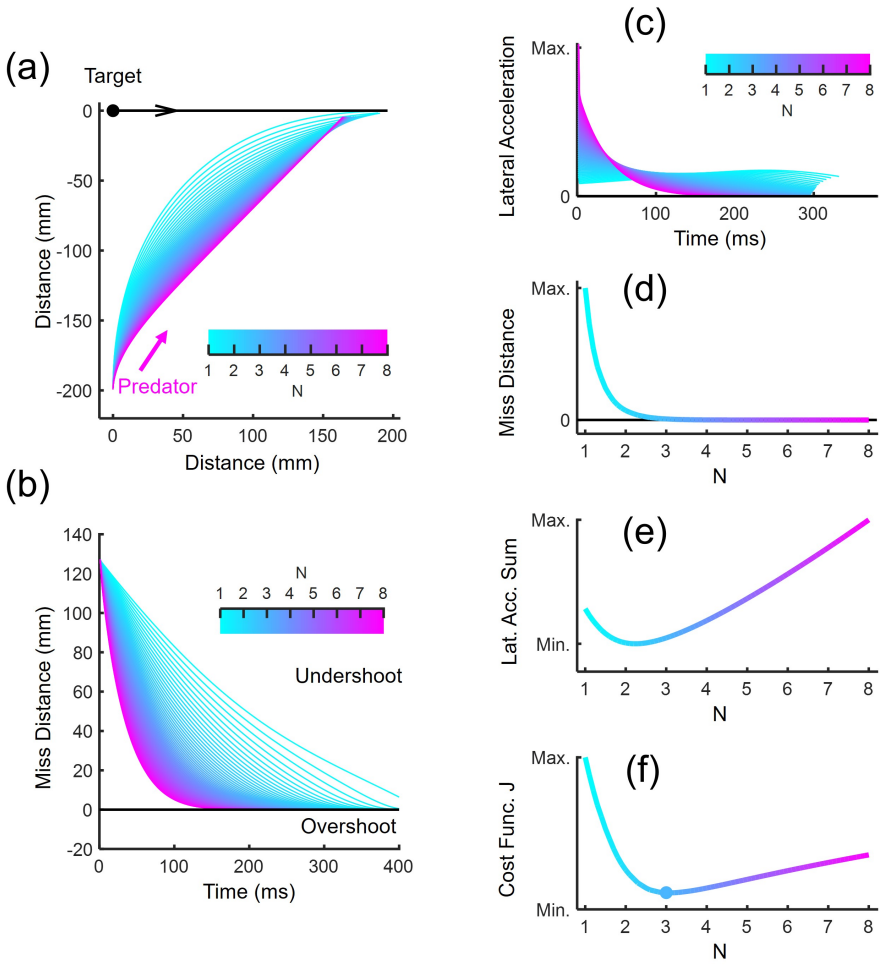

Fig. 4.3 **(a)** Simulations of Holcocephala intercepting a target without temporal lag are overlaid, with their colour corresponding to the simulation navigational constant. **(b)** the resultant miss-distance throughout the flights, colour coordinated with the corresponding simulated gain. Undershooting corresponds to a positive score, overshooting a negative score. **(c)** Lateral accelerations of simulations are overlaid, with their colour corresponding to the simulated gain. **(d)** Final miss-distance of the simulation as it reaches the target trajectory, plotted against the simulated navigation constant. **(e)** The sum of the squared lateral accelerations plotted against the navigation constant. **(f)** The cost function product J, incorporating summed squared lateral accelerations and final miss distance, (constant weightings tuned arbitrarily to highlight plot shape) plotted against the simulation navigation constant. A point is plotted at the minimum of the cost function, at N = 3.

From **Fig. 4.3**, it can be seen that the higher navigational constants quickly approach a straight-line course to the target intercept, while the lower constants more slowly arc into a tail-chasing trajectory. **Fig. 4.3b** shows that the higher navigational constants reduce the miss-distance to 0 more quickly than lower ones. **Fig. 4.3c** shows that the higher

navigational constants concentrate the lateral accelerations earlier in the trajectory, whilst lower navigational constants ultimately require lower peak lateral accelerations, but with a more even and tail-ended distribution of lateral accelerations. The predator has a final miss distance on the target at lower constant levels until N = 3 after which there is no miss distance (**Fig. 4.3d**). The sum of the squared lateral accelerations is however higher at higher navigational constants, due to their much greater initial peak magnitude, while they also rise at the lower N trajectories which take longer to reach the target (**fig. 4.3e**). The combination of the falling miss distance and rising summed squared accelerations with a higher navigational constant results in N = 3 having the lowest combined cost (**Fig. 4.3f**).

Once temporal lag (28 ms, as found in *Holcocephala*) is added to the predator's steering responses, the further cost of higher navigation constants becomes clear (**Fig. 4.4**). As the fly's gain is increased to high values (N > 6), the trajectory does not settle into a straight-line trajectory as seen in **Fig. 4.3a**, instead the trajectory oscillates around fixed line, albeit with effective dampening reducing their amplitude over time (**Fig 4.4a**). This is more clearly seen from the miss distance across the trajectory (**Fig. 4.4b**). All the trajectories begin equally undershooting the target's future position, but only at the higher gains does the predator overcorrect, straying into overshooting the meeting position of the target.

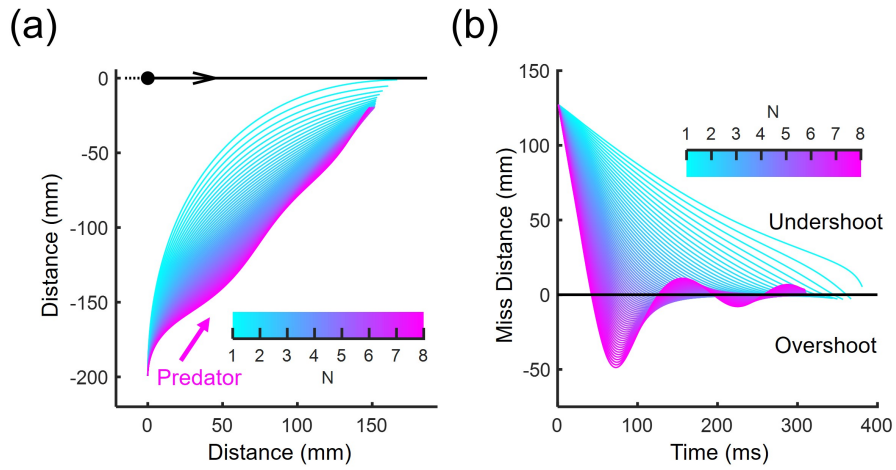

Fig. 4.4 **(a)** Overlaid simulated trajectories of a predator taking-off vertically to intercept a target travelling (left to right on the page) directly above it. Steering responses of the predator lag behind the stimulus by 28 ms. Speed of both predator and prey were fixed to the mean speeds within *Holcocephala* flights (0.71 & 0.49 $m.s^{-1}$ respectively). Trajectory colour corresponds to the navigational constant used for the simulation. **(b)** The zero-effort miss-distance throughout the time-delayed flights. Line colour corresponds to the navigational constant used for the simulation. Arbitrarily, positive miss distance is assigned to the undershooting of the target trajectory by the predator, while negative values correspond to overshooting the trajectory.

Overcompensation where a heading lagging (positive miss-distance) the optimum course strays into leading it (negative miss-distance) is a product of time delay between stimulus and the response of the predator. The generation of overcompensation by time-delays is visualised in **Fig. 4.5**. **Fig. 4.5b** shows that under mean *Holcocephala* speeds, the there is only minor overcompensation (maximum 3 mm) even at a 30 ms time constant and N = 3, when the initial distance between the predator and target is 150 mm. However, as in **Fig. 4.5d**, when this starting distance is 80 mm, the maximum overcompensation at 30 ms delay (19 mm) is much greater, even though the starting miss distance is considerably lower than at 150 mm (initial miss distance of 55 mm vs. 104 mm).

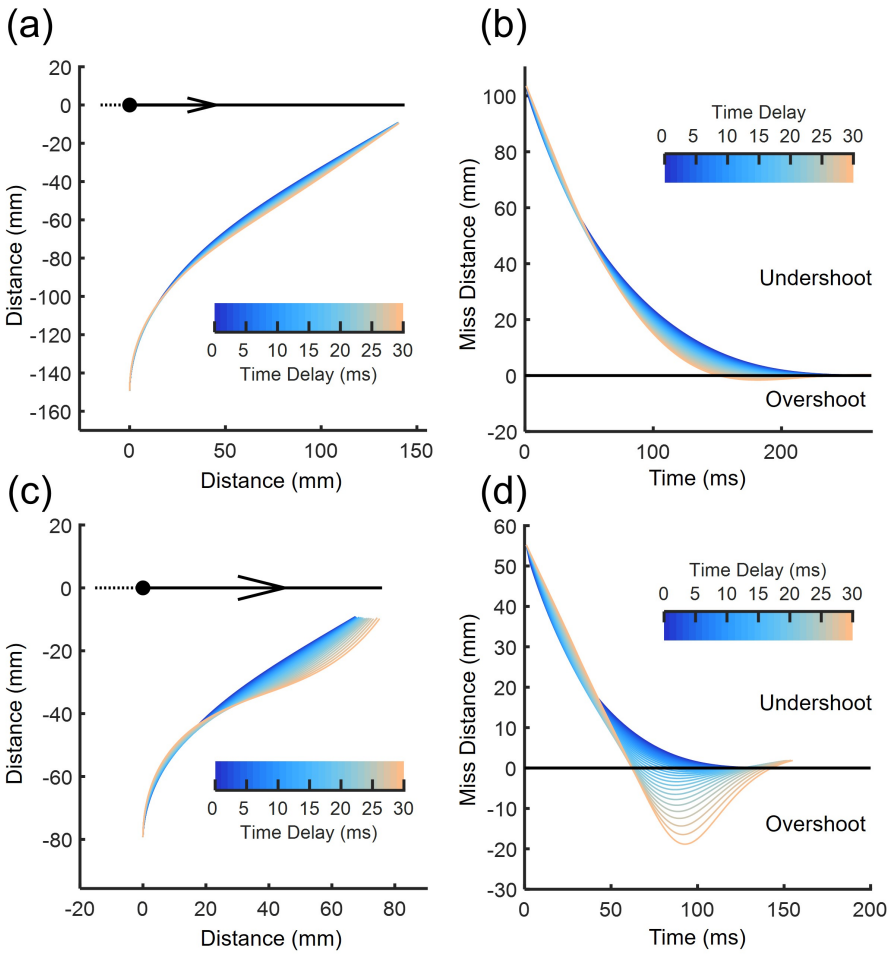

Fig. 4.5 **(a)** Overlaid simulated trajectories of a predator beginning 150 mm away from the target, using proportional navigation (N = 3) to intercept with constant speed (target = 0.49 m.s^{-1}, predator = 0.71 m.s^{-1}). The trajectories are colour coordinated to the time delay constant between the rotation of LOS and the steering response of the fly. **(b)** The resultant zero-effort miss distances, coloured by time delay, for a predator beginning 150 mm from the target. **(c)** Overlaid simulated trajectories of a predator beginning 80 mm away from the target (N = 3, target = 0.49 m.s^{-1}, predator = 0.71 m.s^{-1}). **(d)** The resultant zero-effort miss distances, coloured by time delay, for a predator beginning 150 mm from the target.

The stability of any combination of navigation constant and time delay constant is dependent on numerous parameters. One such is the initial error of the predator heading from the straight-line course that would take it to the target. This error-angle will result in the rotation of the line-of-sight and create a stimulus for predator correction. This stimulus is not symmetrical (i.e. 10° of error either lagging or leading the target, relative to the optimum lead, do not have equal effects on the trajectory and resultant miss-distance). This is visually represented in **Fig. 4.6** for a 28 ms time delay. The asymmetry is created due to lagging the

optimum course directing the velocity closer towards the targets current position, shortening the range faster than in leading the optimum course and generating greater LOS rates. This higher stimulus for rotation generates an overcompensation that is not represented in the over-leading trajectories.

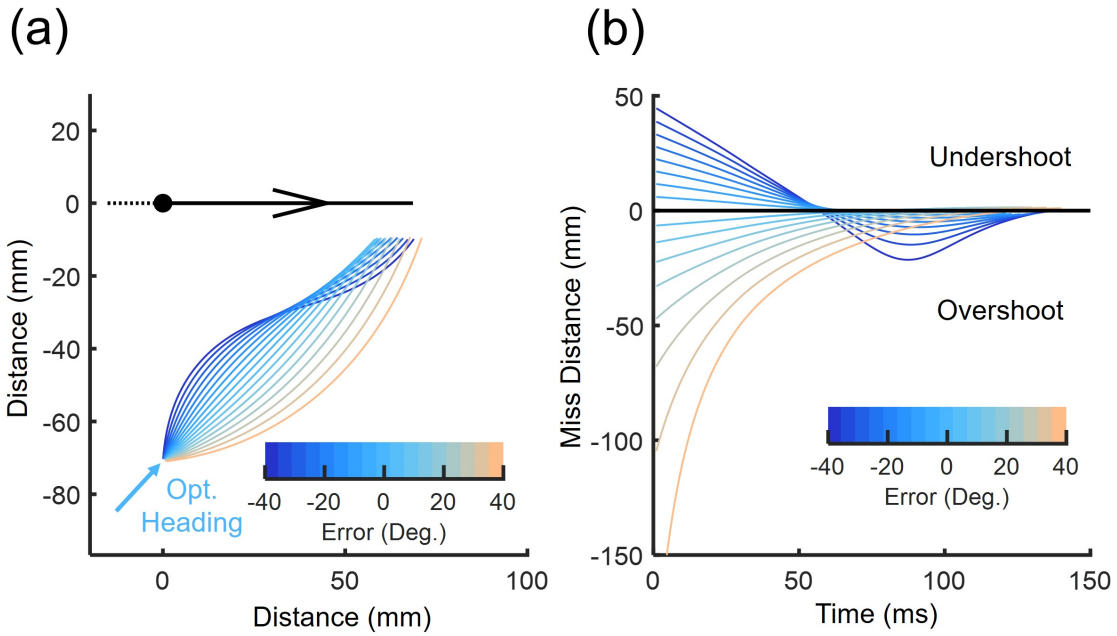

Fig. 4.6 **(a)** Trajectories of simulations with varying initial errors from the optimum (i.e. straight-line) heading that would take them into conjunction with the target. Colours are coordinated with the degree of error. For all simulations, time delay is 28 ms, N = 3, and speeds were target = 0.49 m.s^{-1}, predator = 0.71 m.s^{-1}. **(b)** The zero-effort miss-distance across trajectories that initiate with varying levels of lag or lead error over the optimum course.

The error from the optimum course can also be represented with a fixed initial velocity vector provided there is variation in the initial position of the predator. As in **Fig. 4.7**, a predator that launches vertically at varying positional leads from the target (i.e. the predator is displaced by different distances along the axis parallel to that of the target's velocity) will have necessarily varying trajectories and miss-distance profiles. The optimum start is defined as the position under which a vertical launch will require no steering commands in order to intercept the target given the fixed speed of target and pursuer. Despite the symmetry of the initial miss distances (as in **Fig. 4.7b**), the initial closer proximity of the negative distances from the optimum result in greater steering commands and a faster reduction in the miss-distance. On the other extreme, the high lead distances and longer range between target and predator create do not generate enough stimulus for the predator to correct the

initial miss distance before reaching the target path, resulting in a final miss-distance with the target.

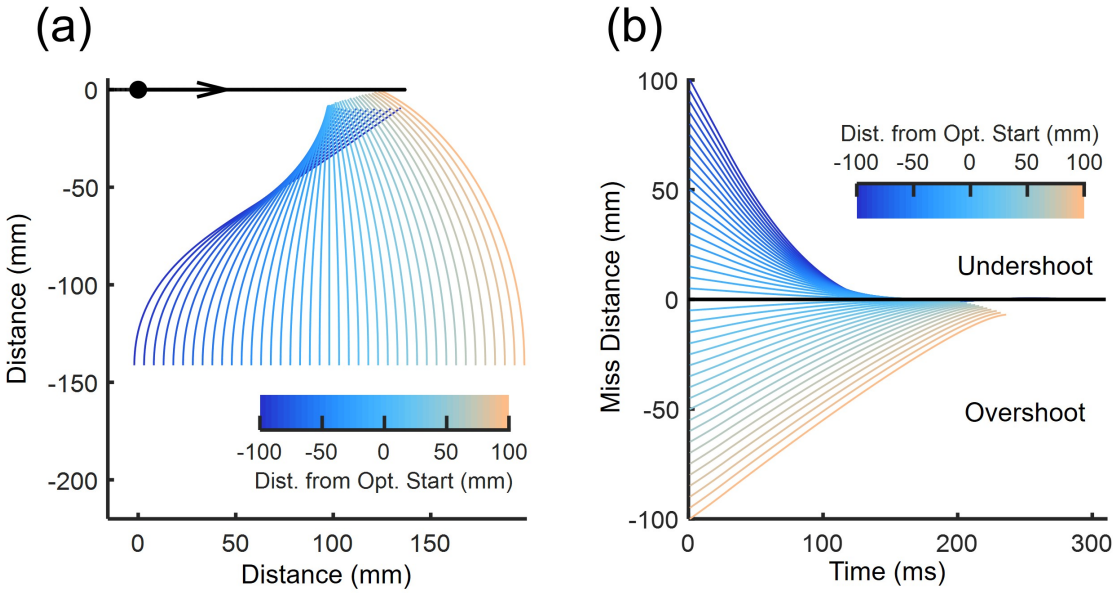

Fig. 4.7 **(a)** Trajectories for simulated predators launching vertically to intercept a target travelling left-to-right above them. Simulations are begun with varying lead on the target along the x-axis, which is parallel to the target velocity. Trajectories are coloured relative to their starting x-distance from the optimum course (i.e. no steering would be required to hit the target). For all simulations, time delay is 28 ms, N = 3, and speeds were target = 0.49 m.s^{-1}, predator = 0.71 m.s^{-1}. **(b)** The zero-effort miss-distance profiles of trajectories that initiate with varying lead distances from the target, coloured relative to their initial distance from the optimum course.

These considerations alone make up only a portion of the potential variation that initial geometry and spatial and temporal scales can render in the trajectories of an interceptor using proportional navigation. Further considerations include removing further assumptions that have hitherto been imposed. For instance factoring in the acceleration of the predator or more importantly the accelerations of the target. Target acceleration creates perturbation in the system, changing the optimum course, and generating stimulation for steering corrections by the predator.

Miss distance is a useful metric for considering a "first-pass" engagement for a predator of limited mobility. However, it is worth considering that the engagement is not truly necessarily "completed" when the predator crosses the target trajectory path. Especially if the angle between V_p and V_t is acute, then the corrections are ongoing even after the predator has crossed the path. Pro-nav does not require that the predator is close to the optimum heading

of the target, thus missing on the first-pass will have a non-absolute cost, these trajectories may be salvageable and still result a target interception. This is further explored in the falcon-diving behaviour of the killer fly (Chapter 5).

4.5 Interceptor Speed

The relative flight speed of predator and prey are determinants of the optimal collision course and the solution of the interception problem of getting to a moving target. Given that steering controls the bearing of the predator and we have extensively discussed how this is under closed-loop control, it is not immediately obvious why speed, as a factor, is not an equivalent controllable measure for engendering collision with targets.

Speed could be thought to control collision in planar terms, so long as the velocity of the predator leads the LOS by $< 90^{\circ}$. In this case, the projected forward heading vectors must cross at some future time, and the predator could speed up or slow down in proportion to the LOS rate to reach that crossover contemporaneously with the target. This however does not work in three dimensions, non-parallel lines do not necessarily meet in 3D space (as they do in 2D). Thus, speed would only be an effective tool in planar engagements, and cannot correct for two axes of error from the optimal course.

Speed control is necessary to ensure that the navigational system has enough speed to hit the target, and in controlling the time taken and the resultant catch velocity. A slower flight speed will cause a scenario closer to a tail chase as the angle between the target and required predator velocities become more acute. This effect may influence the catchability of the target, and thus slowing before the catch would be a suitable means to contrive greater catch success. Excessive speed can also be a hindrance, the primary subject of the following chapter.

Chapter 5

Understanding Behaviour Through Proportional Navigation

Abstract

This chapter analyses a curious behaviour of the killer fly (*Coenosia attenuata*), in which the fly drops from the ceiling of its enclosure towards its quarry, only to miss and continue down, occasionally crashing headfirst into the ground. Using proportional navigation, it is shown that there exists a no-catch zone for a each particular size and speed of the target, in conjunction with the fly's acceleration. When falling from the ceiling, the fly is actively powering itself down, resulting in a much greater acceleration than that of a fly launching from either wall or floor. This added acceleration, results in a faster approach to the target and greater required turning accelerations to follow proportional navigation. These accelerations exceed that produced by the fly tenfold. When a pro-nav model was fitted that had its turning acceleration limited to that of the flies' maxima, it closely agreed with the courses taken by the flies. Instead of a applying a functional explanation to this behaviour, the most parsimonious reasoning suggests that flies simply fail to take account of their inverted position, which may not be a common natural positioning.

5.1 Falcon-Diving in the Killer Fly (*Coenosia attenuata*)

A predatory dive, called a stoop is common among many bird species, especially raptors [189]. During these stoops, birds will fold in their wings, fall, and attain close to their terminal

velocities in near vertical drops [71, 190]. The function of these drops has been recently shown to increase the probability of hitting the target, through an increase in airspeed that consequently generates much higher aerodynamic forces [71]. Thus, while at high speeds, turns by the predator may have a greater radius of arc, the greater range and smaller relative speed of the target compensate to increase catch success. The accuracy of steering and control becomes of paramount importance under these conditions as angular error increases miss-distance with range from the target.

During work on a separate project, a colleague noted that the interception behaviour of killer flies had a seemingly peculiar facet when they began their flights upside down from the ceiling of their enclosure. Killer flies will regularly take after targets from this position in captivity, but their behaviour falls broadly into one of two alternative qualitative classifications. We named these two alternatives either "smooth-dives" or "falcon-dives" based on the latter's apparent similarity to the to the stooping of raptors (**Fig. 5.1**). We took the quantifiable difference between the two behaviours from the pitching of the fly as it descended. If the fly had pitched up vertically, with the body axis beyond parallel with the bead's path before the fly had crossed beneath the path of the target, then the flight was classified as a smooth-dive. If the fly crossed the level of the bead's flightpath whilst still pitched downwards and towards the floor, then this was classed as a falcon-dive. These classes are relatively arbitrarily chosen to roughly separate the variation in flight trajectories. Falcon and smooth diving are not suggested to be reflected in a binary categorical switch in behaviour, but as extremes at either end of a spectrum. We intended to outline this behavioural variation and how it is generated by the internal control laws of the fly.

These dives by *Coenosia* serve as an extreme counterpoint and comparative tool in which to look at stooping between animals that use the same control system (peregrine falcons also use pro-nav, but with highly variable gain of ~2.6 [179]) but at radically different spatio-temporal scales. The two systems are operating at vastly different speeds (killer flies < 1.5 $m.s^{-1}$, peregrines > 30 $m.s^{-1}$), and steer with radically different morphologies. Peregrines stoop from great heights onto their targets (sometimes >1 km [71, 3]), gaining tremendous airspeed, yet the killer flies were diving within an enclosed surround, 8cm above their targets (see methods), thus the space and nature of the engagement of killer flies is not set within a natural framework. This is important when considering the implications for the optimality of the killer fly system and whether the represented behaviour one that would commonly affect the fitness of *Coenosia* and thus be a major agent for selection and adaptation.

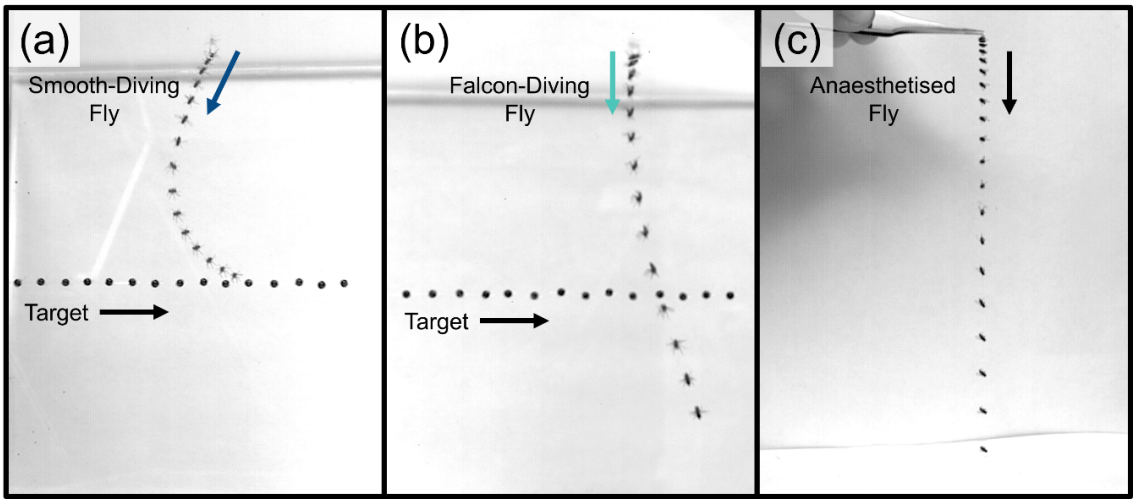

Fig. 5.1 **(a)** A smooth-diving killer fly drops from the ceiling of its enclosure but curves its trajectory before reaching the line of the target, slowing its descent. **(b)** A killer fly falcon-dives from the ceiling, maintaining a high vertical speed as it drops past the altitude of the target's flightpath. **(c)** A CO_2 anaesthetised killer fly is dropped from a pair of forceps to gain an estimate of the fly's acceleration due to gravity while in air. Images comprise overlays of frames from high-speed videos. Frames are at 10 ms intervals.

While the data had been collected, digitised, and qualitatively described, what we were missing was a functional explanation or model for why the killer flies appeared to vary their behaviour and whether they gained the same advantages as falcons in diving onto targets. The data set of smoothed trajectories was investigated whether an explanation of the behavioural differences was implicit in the initial conditions of engagements and its combination with the control system, proportional navigation (see Chapter 3). The alternative was that these stooping dives represented the implementation of some separate control system and thus a different behaviour entirely. There is some suggestion from existing literature that pro-nav interception flights descending beneath the target (i.e. missing on the first pass) are a product of low navigational constants [71], however the analysis did not penetrate further. We have however seen that pro-nav with a constant $N < 2$ does not null the miss distance (section 4).

Fig. 5.2 illustrates examples of the two behaviours. The smooth diving flights are typified by a flightpath that quickly deviates from the vertical and rotates to near horizontal by the time the fly is at the same altitude as the target. Falcon dives, on the other hand, remain near the vertical and cross the target altitude still heading steeply downwards, seemingly without much turning to bring themselves onto a collision course with the target.

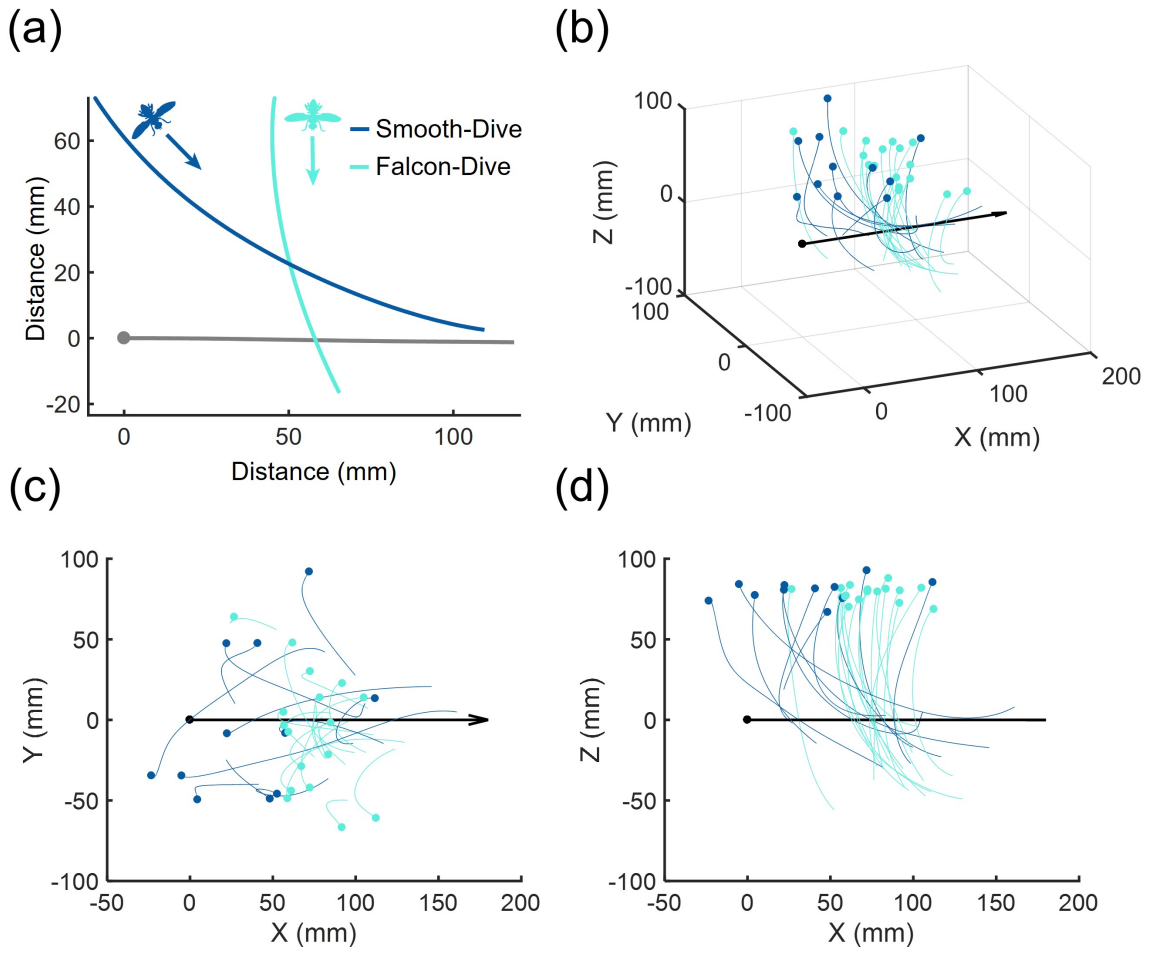

Fig. 5.2 **(a)** Two real flight trajectories are overlaid such that the bead begins from the origin in both attacks (travelling left to right). Both flights begin on the ceiling of the enclosure. **(b, c, & d)** Flights falling from the ceiling are overlaid, such that the target is consistent between all of them, travelling from the origin and parallel with the x-axis. Flights are coloured according to the binary classification of falcon or smooth diving.

Experimental Aim:

The hypothesis to be tested in this chapter is whether the trajectories of *Coenosia* diving from the ceiling still follow the guidance law of proportional navigation, despite their missing the target. Secondarily, it is to investigate whether proportional navigation can be used as a framework for understanding exactly why the flies miss there targets.

5.2 Experimental Methods

5.2.1 Behavioural Setup

Coenosia were allowed to free settle within a cuboidal Perspex box. The dimensions of the box were 16 cm × 16 cm × 50 cm. The box was laid with is longest axis lying flat, and through its centre passed a fishing line controlled by a stepper motor, such that targets could be passed through the centre of the box, stimulating flies sitting either on the walls, floor, or ceiling of the container. During these behavioural trials, the target speed was kept constant at 0.77 m.s^{-1} while the target size was also kept constant at 2.14 mm. Raw behavioural data collection and fly tracking for these experiments was conducted by Rossoni.

5.2.2 Drag and Power Estimations

To find an estimate for the power requirements of the flight, and to test whether flies are driving themselves towards the floor, or simply falling, the deceleration due to drag needed to be estimated for the flies. To find the acceleration during free-fall, we anaesthetised flies under CO_2 and dropped from a small platform in front of two high-speed video cameras such that their path could be traced in the same manner as the flight trajectories. From this the fly airspeed and rate of acceleration could be compared to acceleration due to gravity (9.81 m.s^{-1}). This does not permit the estimation of quantities such as the coefficient of drag for the fly, but acts as a rough estimation based on the principle that drag is proportional relative to the squared velocity difference between the object and the fluid medium [191]. Thus, we shall refer to a drag constant, proportional to the square of speed, but it is important to note this is different to the drag coefficient of fluid dynamics. The calculation of the drag constant was based on the equation:

$$C_{drag} = \frac{G - a}{v^2} \tag{5.1}$$

Where C_{drag} is the drag constant, G is acceleration due to gravity (9.81 m.s^{-1}), a is the fly's acceleration, and v is the fly's velocity. Power calculations were restricted to the gravitational axis (i.e. velocity & acceleration in the equation is the vertical component of the fly's total velocity) to test for whether flies are actively powering themselves downward

during dives. Power was then calculated based on the acceleration of the fly. This was given that:

$$F = ma \tag{5.2}$$

Where F is force, m is fly mass, and a is the acceleration of the fly (minus acceleration due to $C_{drag} \times v^2$). From this force, power is calculated based on the equation:

$$P = Fv \tag{5.3}$$

Where P is power in watts.

The muscle-mass power requirements of the flight motor system required to meet the vertical acceleration are based on the weighing of CO_2 anaesthetised flies. From these the estimations of the flight muscle mass have to be made as there are not current physiological measurements of this for *Coenosia*. The marginal requirements of the flight muscle mass to total body mass ratio (FMR) is between 0.10 to 0.15, with flight muscle masses above this threshold serving to improve flight performance [192]. FMR in dragonflies may be as high as 0.60 (but with very large variation between individuals) [193], or in robber flies up to 0.45 [194], and was estimated to be ~0.3 in *Drosophila* [195]. For the power requirements of *Coenosia*, a reasonable estimate in keeping the fact that *Coenosia* tend to crash to the ground on obtaining prey may be an FMR of ~0.35, combined with the their likely aerial superiority over their prey species such as *Drosophila* [35]. This figure represents a best estimate but is highly likely to change on further physiological investigation. This does not affect the pattern of the vertical power requirements, nor their relation to one another. However, the uncertainty of flight muscle mass limits any conclusions drawn about the exact magnitude of the power requirements compared with other, more physiologically supported, studies of power requirements for other behaviours.

The muscle-mass-specific power (W/Kg) of the flight is calculated based on:

$$P_{mm} = \frac{P}{m \cdot FMR} \tag{5.4}$$

5.2.3 Proportional Navigation Simulation

Proportional navigation has been demonstrated to be the control system used by *Coenosia* to intercept targets (See Chapter 3). This steering controller uses the rotation of the Line-of-Sight (LOS) to the target, relative to the external environment, to engender magnified proportional rotations in the pursuer heading (See Schneydor 1998 [166]). The model takes the form of the differential equation:

$$\dot{\gamma} = N\dot{\lambda} \tag{5.5}$$

In which $\dot{\gamma}$ is the rotation of pursuer heading, $\dot{\lambda}$ is the rotation of the LOS and N is the navigational constant. To test whether the same navigational controller was being used during falcon-dive descents from the enclosure ceiling, the above model was fed the initial position and heading of the fly after take-off and subsequently only fed the relative linear acceleration of the fly so both fly and simulation have identical speed. After this point, LOS rotation is read only from the model, with no input from the fly, and the simulation steers in response. The navigation constant for simulations was fixed at N = 1.5 with an 18 ms lag between stimulus and response, in keeping with the findings of Chapter 3.

5.2.4 Geometry of Engagement

We tested for the effects of the initial conditions of engagements on resulting flightpaths, and whether this explains the switch to falcon-diving. Proportional navigation simulations were started dropping vertically from a ceiling 8cm above and parallel to a target travelling at 0.77 $m.s^{-1}$ from the origin, matching the conditions of the recorded real flights. The speed profile of the simulation was matched to the mean of the recorded flights (accelerating non-linearly from 0.22 to 1.20 $m.s^{-1}$) for the first 100 ms of flight, after which the peak speed was maintained either until contact or the end of the simulation at 1000 ms. Time-to-contact was measured for each of the simulations and colour coded onto a map of the starting positions. Contact was determined by the model being within a body-length of the target (4 mm).

5.3 Results

5.3.1 Proportional Navigation Fitting

Dives determined to fit the falcon-dive shape share extremely high peak LOS rates as the fly passes the target (mean 1016 ±SE 2670 $°s^{-1}$ versus 235 ±SE 712 $°s^{-1}$ (**Fig. 5.3a**) Wilcoxon rank sum test results: z = -2.96, p = 0.003). Pro-nav requires that the heading of the pursuer rotates at a magnified rate to that of the LOS, and thus high LOS rates of rotation require high rotations in the pursuer heading. Interception simulations using a proportional navigation controller did not fit the recorded flight data well, using much greater lateral accelerations than the flies (peak mean of 13.0 ±SE 1.2 ms^{-2} for *Coenosia* and 133.3 ±SE 37.5 $m.s^{-2}$ for pro-nav simulations **Fig. 5.3b**). These extremely high required lateral accelerations are not found in flies taking off from either the wall or the floor of the enclosure (**Fig. 5.4**).

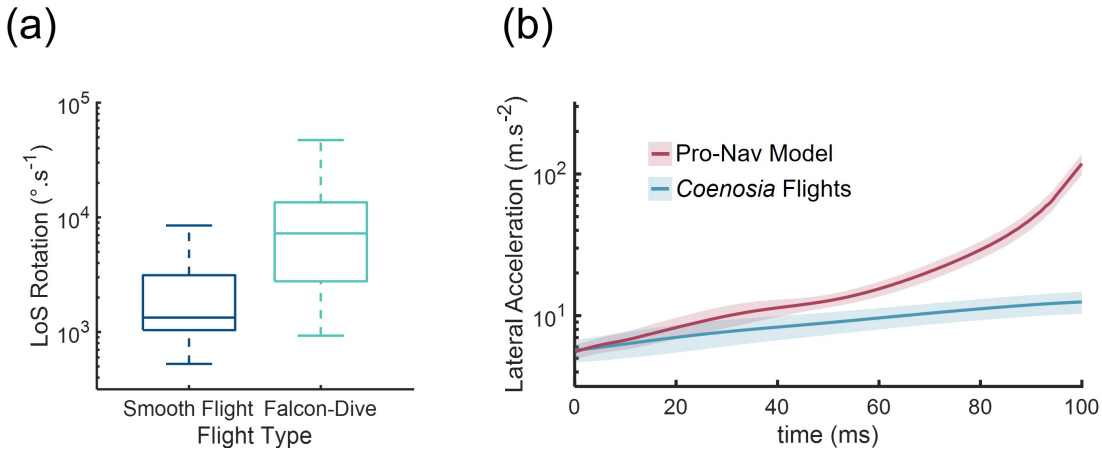

Fig. 5.3 **(a)** Rotation in the Line-of-Sight (LOS) for smooth (blue) and falcon-dive (green) type flights. **(b)** Mean lateral acceleration of true *Coenosia* flights (blue) against that of a pro-nav model tuned to N = 1.5, time delay = 18 ms. Shaded regions represent ±SE.

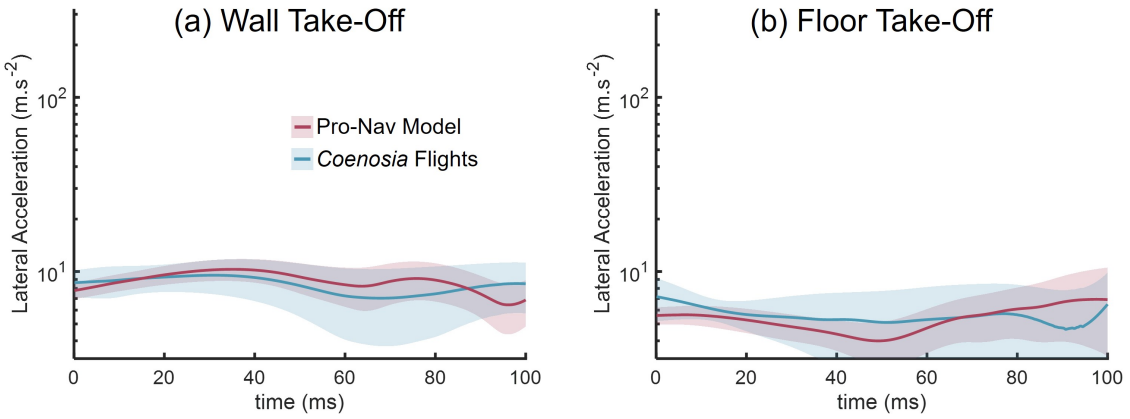

Fig. 5.4 Mean lateral acceleration of true *Coenosia* flights (blue) against that of a pro-nav model tuned to N = 1.5, time delay = 18 ms taking off from **(a)** the wall (n = 13) and **(b)** the floor (n = 9) of the enclosure. Shaded regions represent ±SE.

We took this maximum lateral acceleration of *Coenosia* and applied a limit to the model, such that the model only has the capacity to turn with a maximum lateral acceleration of 13.0 ms^{-2}. Applying the rotation limitation improved the fit of the model through the latter stages of the flight (**Fig. 5.5a**). This is qualitatively evident from flight traces displaying both free rotation and capped rotation simulations as the examples show in **Fig. 5.5b**.

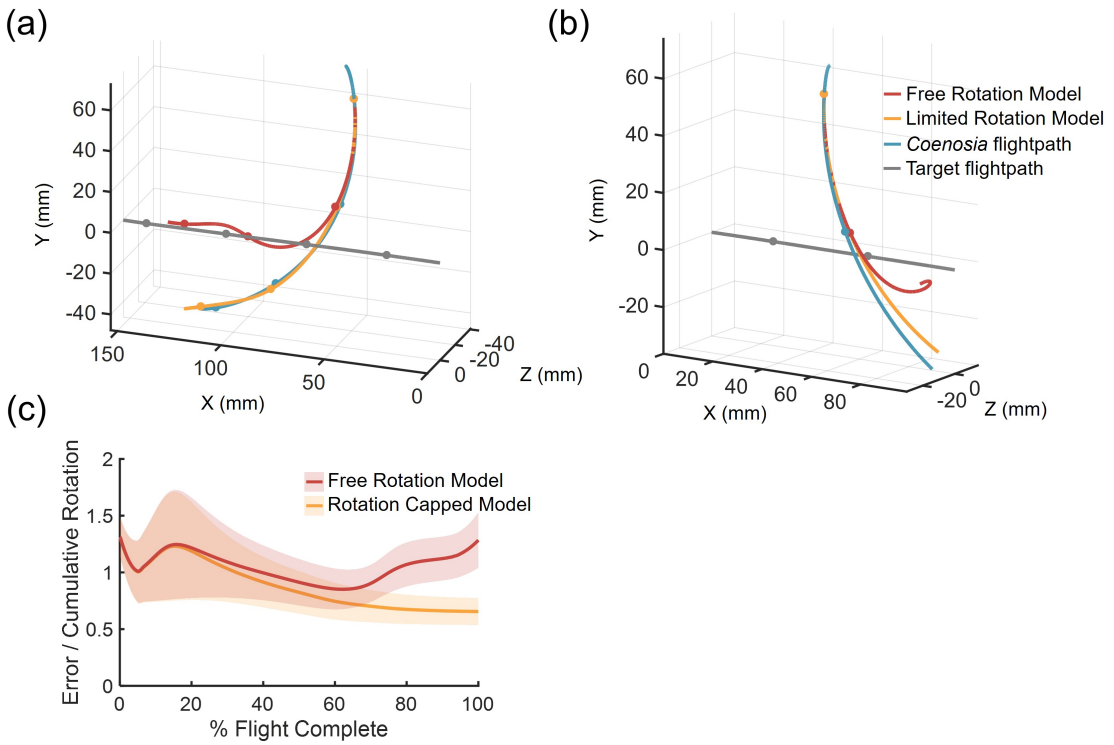

Fig. 5.5 **(a & b)** Example simulations of a pro-nav model with free (red) and limited (orange) ability to rotate its heading. **(c)** Mean simulation fit is compared between the free (red) and limited (orange) models across the time-normalised flightpaths. Shaded regions represent ±SE.

5.3.2 Drag and Power Requirements

The mean calculated drag constant from dropped anaesthetised flies was 2.38 m^{-1} ± SE 0.08 m^{-1} (n = 12). We weighed 45 anaesthetised female flies, which had a mean mass of 2.8 mg ±SE 0.1 mg. These means were subsequently incorporated into model simulations in order to calculate the power requirements of accelerations within the gravitational axis of flight.

5.3.3 Geometry of Engagement

Rotation-limited simulations of flies dropping from virtual ceiling, and steering towards a target travelling horizontally, illustrate a sharp cut off at which flies will be unable to hit the target on a first pass (**Fig. 5.7**). Flies beyond this cut off do not turn onto a collision course with the target until they have dropped lower than the trajectory of the target, at which point the target passes behind them. Freely rotating simulations turn a full loop and return

to a near-collision course with the target, or else enter an unstable flightpath taking them further from the target. Limited rotation simulations are unable to loop, continuing a course taking them further from the target (**Fig. 5.7b i**). Limiting the lateral acceleration of the flies reduces the maximum simulated vertical power output requirements of proportional navigation by 848% (from a maximum of 329 W.Kg^{-1} to 39 W.Kg^{-1}) (**Fig. 5.7a&b iii**). The vertical power requirements of the engagement are determined by the initial geometry (i.e. the distance of lead between target and pursuer at take-off). X-position of the fly relative to the target at take-off directly determines the vertical power requirements (**Fig. 5.7 ii & iii**). Taking the initial start positions of the recorded flightpaths, split by qualitative falcon or smooth label and then simulating their power requirements as purely an output of initial geometry and proportional navigation produces similar patterns of difference in the power requirements of falcon and smooth diving trajectories (**Fig. 5.6**).

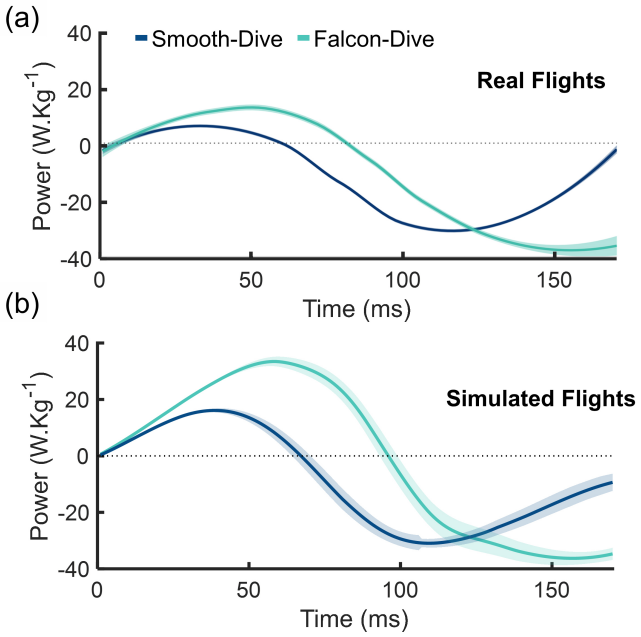

Fig. 5.6 The mean (± SE) power calculated for **(a)** real flights and **(b)** simulations that originate from the same location as real flights and adopt their smooth or falcon classification.

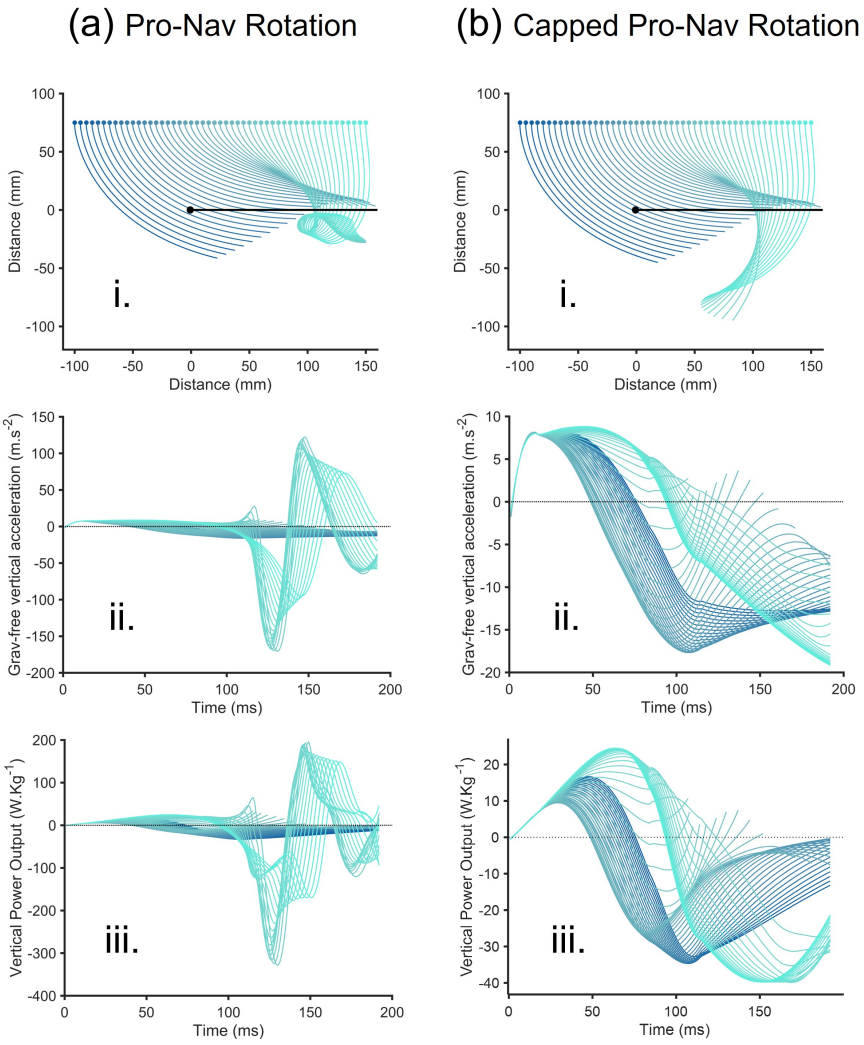

Fig. 5.7 Simulations of multiple starting points (5 mm separated, coloured from tailing the target in blue to ahead of it in green), both for uncapped **(a)** and maximum-capped **(b)** proportional navigational models (N = 1.5, delay = 18 ms). **(i.)** flight traces of the simulations towards a target starting at the origin and travelling rightwards. **(ii.)** The fly-powered (i.e. minus gravity) vertical acceleration of the fly, coloured accordingly to the start position in (i.). **(iii.)** The estimated power output of the flies into vertical acceleration during the flights, including estimated drag resistance.

While we have a mechanical cause for the behaviour, we raise the secondary question of why *Coenosia* are opting to take off after targets in and around the falcon-dive cut off when it is feasible for them to take off later after targets and avoid this complication. Flies dropping from the ceiling reach peak speed much sooner than those taking-off from either the walls or the floor (**Fig. 5.8**).

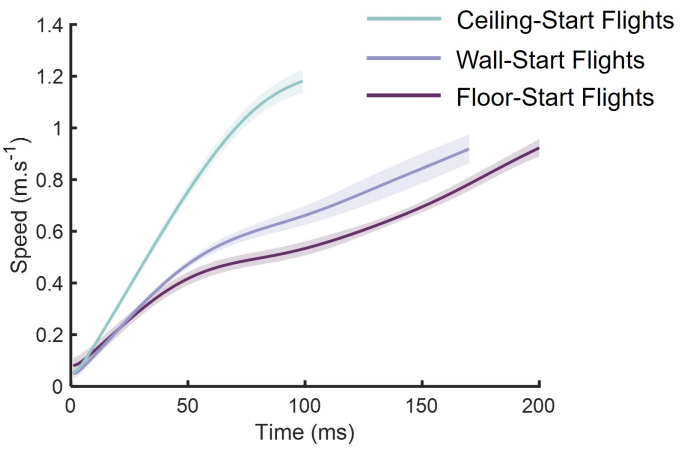

Fig. 5.8 Flight mean speed profiles for flies taking off from the ceiling (n = 28), the wall (n = 13) and the floor (n = 9). Shaded regions represent ±SE.

If all turning restrictions are removed from the model, the mean take-off locations for both falcon diving and smooth flights are proximally located to the position of minimum time-to-contact (**Fig. 5.9**). However, when turn limitation is applied, a no-catch region forms in which flies will falcon-dive past targets (**Fig. 5.9b**). This region cuts between the mean starting position of the smooth flights and those classed as falcon-dives. If the simulation uses the profiles of flies launching from the walls and ceilings in turn-limited simulations (**Fig. 5.9d & e**), the take-off points for both smooth and falcon-dive flights once again align with the minimum time-to-contact region.

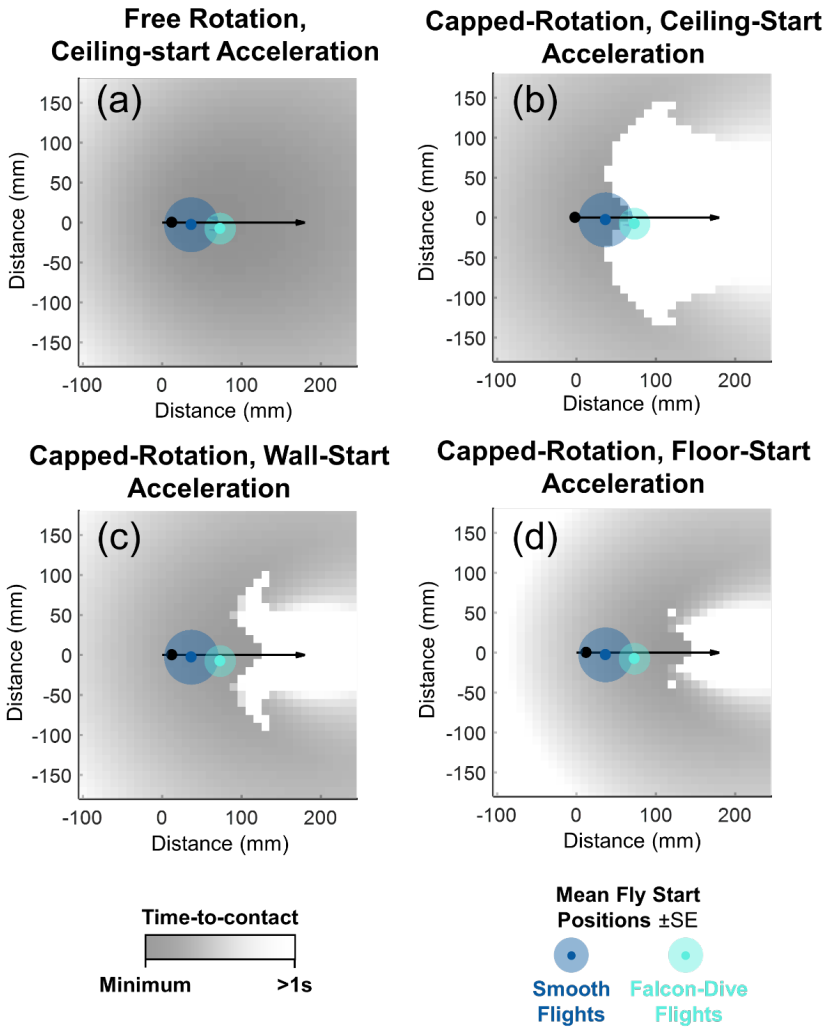

Fig. 5.9 Time to contact maps are displayed for: **(a)** free-rotation simulations using ceiling-start speed profiles. and limited-rotation simulations using **(b)** ceiling-start, **(d)** wall-start and **(e)** floor-start speed profiles. Mean starting positions for smooth (blue) and falcon-dive (green) flights are marked, shaded region denoting ±SE.

5.3.4 The Effect of the Navigational Constant

It is not enough to say that the guidance law, geometry, and gravity-assisted acceleration will lead to the effect of a falcon-dive past the target. The guidance law can be tuned and gain dependence of flight trajectory has already been discussed in the preceding chapter. As already described, higher navigation constants steer interception systems faster towards a collision course (toward fulfilling parallel navigation). Therefore, an obvious tactic would

be for *Coenosia* to simply used an elevated gain, steer earlier in the flight and avoid the bunching of control requirements towards when the target is at close range.

For a time-lag free control system and without turn-limitation, a higher gain of N = 5 eliminates the falcon-dive miss problem for many of the initially diving flights (**Fig. 5.10**). All the mapped positions led to collision with the target on the first past with at most marginal dipping (< 5 mm) below the target flightpath.

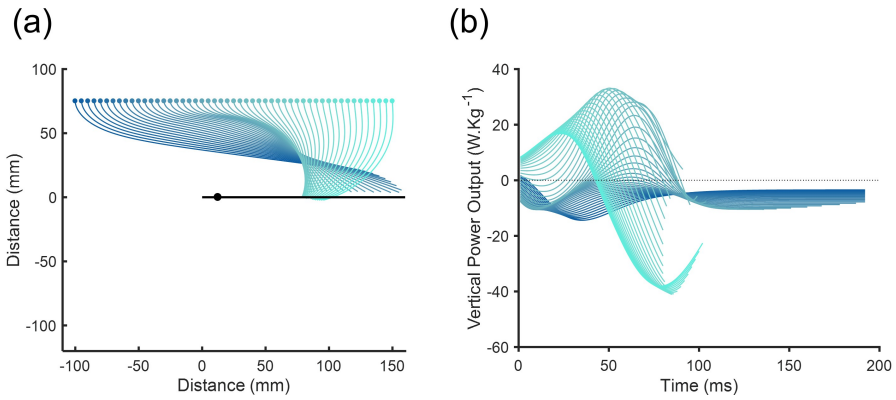

Fig. 5.10 **(a)** Flight trajectories of simulated killer flies launching vertically from the ceiling towards a target travelling left to right from the origin. Simulations do not have a time delay between stimulus and simulation response. The navigational constant is N = 5. **(b)** From the acceleration profiles of the simulations descending from the ceiling, the panel shows the power output requirements of the simulated flights within the vertical dimension.

However, this method of avoiding the falcon-dive problem is undermined when the simulation is given the appropriate time delay for *Coenosia* (18 ms, see Chapter 3). As described within other engagements, the higher gain of N = 5, combined with close target proximity results in unstable flight paths that overshoot the collision course for the target and fail to maintain it (**Fig. 5.11**).

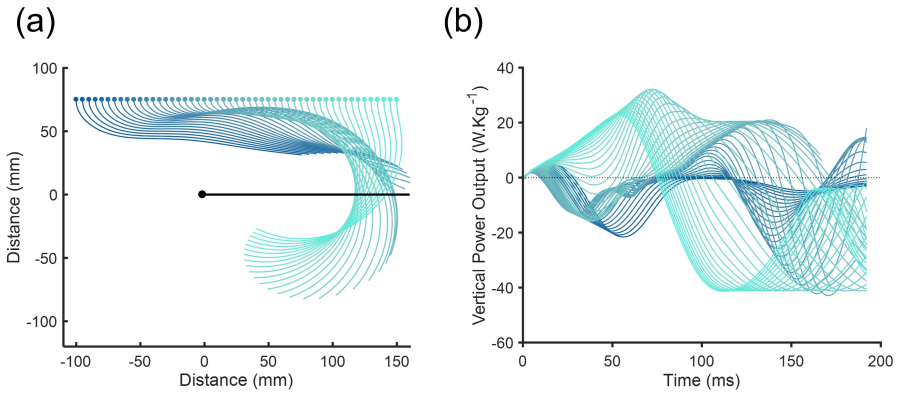

Fig. 5.11 **(a)** Flight trajectories of simulated killer flies launching vertically from the ceiling towards a target travelling left to right from the origin. Simulations have a time delay of 18 ms between stimulus and simulation response. The navigational constant is N = 5. **(b)** From the acceleration profiles of the simulations descending from the ceiling, the panel shows the power output requirements of the simulated flights within the vertical dimension.

5.4 Discussion

The curious behaviour of *Coenosia attenuata* when descending from a ceiling, in which some of the flight trajectories appear to slope in towards the target and others drop straight past it, can be explained in terms not of intent, but of limitation. The flight trajectories of *Coenosia* taking off from the ceiling demonstrate that stooping or diving can hinder rather than help the interception of prey items, exemplified by not a single killer fly managing to intercept the target during a falcon dive. Proportional navigation is still effective at describing the behaviour yet requires constraints in order to fit the data.

The constraint within the interception system is mediated by a maximum acceleration. While it holds true that at greater speeds, animals can use greater aerodynamic turning forces that square with speed [191], the centripetal force required to maintain a circular trajectory also scales with the square of speed. Thus, assuming the scaling of aerodynamic effects holds, an animal should be capable of maintaining a constant minimum turn radius [141]. This does not occur as there are tolerance limits on the amount of lateral acceleration a body can manufacture, which may explain the command saturation and maximum lateral acceleration observed in *Coenosia*.

The properties of speed and proximity of the target and fly scale together, with pro-nav engagements being typified by their initial geometry and the time-to-contact Thus, when comparing the stoops of peregrines and of *Coenosia*, it is worth noting that the time of

interception from the start-point is at least an order of magnitude greater for peregrines, based on their much greater range from the target, which outpaces their increased speed. This time is required for proportional navigation to manoeuvre the velocity of the predator onto a collision course with the target, thus short time-to-contacts with low navigational constants do not provide the time for a pro-nav controller to reach a collision course and so the target is missed.

This problem could be compensated by the raising of the navigational constant, more quickly directing the interceptor onto a collision course. However, this you require a much shorter time constant than the already short 18 ms found in *Coenosia*. Without shortening the time constant, a higher navigation constant will lead to overshooting the optimum course and failure to connect with the target.

While the behaviour can be linked to the stooping of raptors [189, 71, 179] and many analogies can be drawn between them, it is important to draw distinctions. Firstly, this behaviour is not being recorded within a natural environment nor is it known how natural this behaviour would be for killer flies. While they will readily settle on the ceiling of an enclosure in captivity, the frequency of this upside-down posture in wild conditions is unknown.

There is a secondary method of escaping the falcon-dive miss zone. This is to let the target pass underneath and take-off after they have reached the zenith of their path. This has the advantage of not requiring a modification of the control system or gain tuning to be effective, and yet flies take off extremely close to the falcon-dive cut-off. One potential reason for this is already hinted by the optimality of take-off positioning work in chapter 3. The minimum time-to-contact region is proximal to the placement at which a fly would take the shortest time to intercept the target. Should the acceleration profiles be closer to those flies launching from the wall or floor of the enclosure, then *Coenosia* would be taking off at the exact position that would result in minimal time to contact the target. This suggests that the falcon-dive miss effect is generated by the fly's inability to detect or compensate for the added acceleration that dropping from the ceiling engenders. This may likely be due to the relative rarity of flies hanging upside down within a natural context.

Both powered and passive dives are extant in insect flight studies, however almost all concern evasive manoeuvres to avoid predators, as in mantids [196, 29] and in moths [197, 198]. This limits their comparability to *Coenosia* in terms of functionality, the optimality criteria for evasion differing greatly from interception [122, 123, 197]. The vertical acceleration and muscle-power profiles demonstrate that *Coenosia* do not passively fall or dive, but push themselves downwards using their flight muscles. Given that their already high acceleration

appears to hinder them on the interception of targets, further powering themselves down would seem to be counterproductive. This may represent that *Coenosia* are not naturally selected to perform diving behaviour vertically onto targets, and that their flight motors are perpetually "stuck on" when in the air. The size of small insects results in their using "slow flight" in which there is little reliance on their forward momentum for force generation, instead relying on a vertical component of the thrust generated by flapping [4, 18].

It is also worth considering that the speed of the target effects the engagement. The combination of speed and proximity of the target, plus the acceleration of the fly combine to create zone of take-off without the possibility of catching. Prey travelling faster, or more slowly, may well not form the same zone. It would thus be a suitable next step to repeat the diving experiments, but with targets travelling at a slower, and faster speed.

Chapter 6

Integrating Obstacle Avoidance and Target Interception

Abstract

Holcocephala displays a surprising capability to navigate to moving targets while simultaneously avoiding salient static obstacles. This ability can be described by a conflict between two alternative control systems. One is pro-nav, pulling the fly heading towards a target-collision heading, and the other is a target avoidance model that is attempting to pull the fly's heading away from the obstacle. This interplay is governed primarily by the weighting gain given to the avoidance algorithm, which prioritises targets close to the current heading, or that are looming within the fly's vision. A limited field-of-view (assumed to center on the target) appears in operation as two instances the fly collided with the obstacle without apparent deviation or avoidance. This conflicting guidance measure of control reflects a new framework for considering navigation in complex situations involving moving targets and obstacles.

6.1 Path and Visual Obstruction

So far, the extent of the problem faced by an interceptor is mere 2-body, that of itself and the target. The problem solution is further simplified as both these bodies can be resolved down to points in space. However, this is not the case when obstacles either obstruct the LOS to the target or the path of the interceptor. LOS obstruction represents a switch from a closed

to open loop, and ultimately has one of three solutions: (a) abandon the interception, (b) hold position until the target reemerges, or (c) maintain the current course until the target is detected again. Obstacle avoidance is superficially a much more complex issue. An obstacle cannot be reduced to a point in space, as their exact size and shape is integral to how to avoid them. This either means that the 3-dimensional structure needs to be computed and stored within some mental map of the surroundings, or that there are rules in place that serve to index edge location and steer around an obstruction without complete information about it [199].

Typically, *Holcocephala* sit atop perches that are high relative to the surrounding foliage. Targets that fly overhead are unlikely to be obscured as *Holcocephala* also tends to perch out in open environments. It would thus seem likely that they have not been put under strong selection to avoid potential obstacles during predatory chases. It would be constructive to understanding the navigational control system of the species to investigate their behaviour when the target becomes obscured behind an obstacle that blocks the line-of-sight or the fly's future path. While collision avoidance in flight has been extensively studied, with work on locusts [200], fruit flies [201], and pigeons [202], these all fundamentally differ from the problem of collision avoidance for a predator. Within these studies, the problem is concerned with only the maintenance of flight and the avoidance of collision. In these simpler scenarios the avoidance algorithms can factor in the loom rates to derive steering commands to avoid obstacles. The existing work with pigeons determines that they use a proportional control system of aligning their heading to the direction of gaps in clutter, overlaid on an internal model of the 3-dimensional positions of the obstacles [202]. While the case of pigeons is complex, overlaying a control system on internal models of space and biasing the gap selection based on gap-size, the stimulus is still confined to the obstacles, in their frequency and requirement for flight deviation. A predator must contend with maintaining sight of the target whilst manoeuvring, and also balance the optimality of a short collision course with the need to avoid obstacles.

Obstacle avoidance when manoeuvring to a target destination has been considered for humans [175, 174]. In these experiments humans navigated a 12×12 m arena using a head-mounted display which rendered the visual stimuli of a virtual environment. Participants navigated to a designated goal location avoiding static virtual obstacles in their path. This differs from other studies (i.e. [200–202]), as both the goal and obstacle avoidance are attractors in the system. The results of this are described by what we shall term here a distance-dependant pursuit-avoidance behavioural dynamic. The term behavioural dynamics is applied here in keeping with Warren and Fajen's terminology. Behavioural dynamics

describe (through differential equations) the actions of a subject from an external perspective without necessarily representing the internal information processing happening within.

The pursuit element of the pursuit-avoidance dynamics describes the contemporary model of human navigation to targets, which is similar in behaviour pursuit control law discussed in chapter 3 for moving targets (as in Chapter 3, Fajen and Warren's behavioural dynamics use angular acceleration with dampening as the behavioural output rather than angular velocity). The turning response of the navigator is in response to the angle formed between the LOS to the target and the navigator's heading. Steering responses from obstacles follow an inverse trend, with greater turning responses stimulated by smaller heading-LOS angles. Distance plays a critical role in the steering responses. Navigation towards a single target may use distance irrelevant indicators such as LOS position. When multiple objects are present, their order in space matters. As concerns obstacles, proximity takes primacy; a navigator should steer away from closer obstacles at a higher rate than more distant ones. The behavioural dynamics of humans have been replicated within autonomous robots steering towards a goal and to avoid obstacles [203], demonstrating that they do form an implementable framework.

Distance ranking of targets is present in the model put forward in [175], where the steering aversion from obstacles is exponentially proportional to their proximity. This model maps human behaviour through cluttered fields well, and it is plausible that humans may create internal models of the surroundings to judge distance and respond appropriately. The manner of distance judgement is not tested, however. A factor noted in the discussion is that the exponential distance relationship behaves extremely similarly to the angular size variation of objects as they are approached (proportional to atan(1/distance)). This expansion-rate dependant distance measure is present in the time-to-contact measure, tau, formerly used in psychological models of collision prediction across many species and conditions [153, 204, 205]. This is no longer cited as an absolute measure of time to contact with targets [153], but its use in collision avoidance still stands. Obstacles expanding at greater rates in the visual field are those that require the greatest avoidance responses. This is of relevance when considering obstacle navigation in situations where only relative monocular cues may be available.

This human behavioural dynamical model of obstacle navigation takes the form of layered navigation, where the required steering commands of each obstacle and target are stacked together and summed to produce the immediate heading direction. The use of monocular cues and simple guidance controls means that the predatory flies within this study could use comparable systems to intercept moving objects in the presence of obstacles, but such

algorithms and layering remain untested within non-human animals, as does navigating obstacles to intercept moving targets.

6.2 Methodology

In order to obscure targets, the same apparatus was used as for the visual clutter experiments (see Chapter 1). A large Perspex tray was suspended from a Perspex U-frame, underneath the line of the target travel. Targets travelled in a linear fashion around the U-frame, directed through pulleys by the stepper motor already discussed in previous sections. Obstacles took the form of black acetate strips of two widths (2.5 cm and 5.0 cm) that could be stretched between the arms of the Perspex tray (**Fig. 6.1**). As the target passed above the fly, it would be obscured by the black acetate. Trajectories were filmed at 1000 fps with a pair of Photron fastcam SA2s and trajectories reconstructed as previously discussed. Obstacles were digitised by tracing the four corners of the acetate sheet, then from flight reconstructions it could be determined when the target was out of sight. Presentations had consistent target speed and direction; the target was coming towards the fly and travelling at 0.31 $m.s^{-1}$.

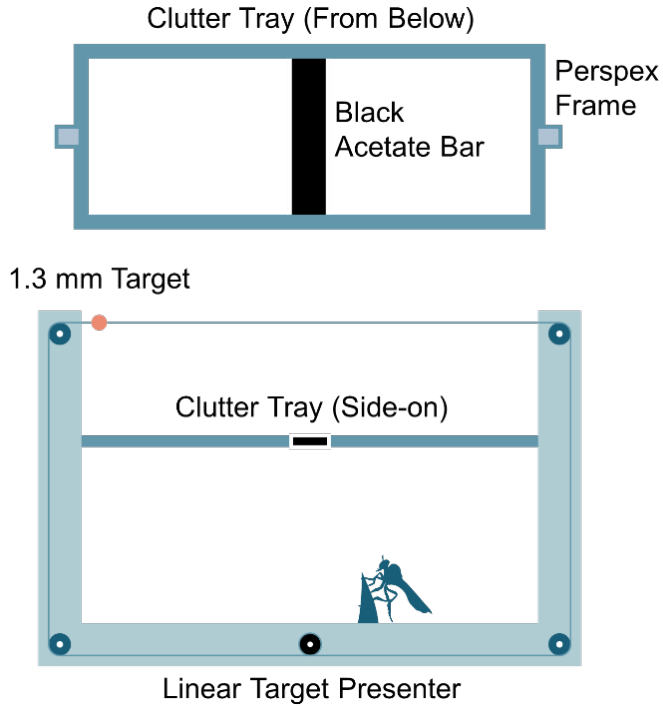

Fig. 6.1 Obstacle presentation is by means of conversion of the linear target presenter from chapters 1, 2, and 3. Black acetate bars were either thin (2.5 cm wide) or thick (5.0 cm wide).

6.3 Results

Target engagements in the presence of an obstacle were dependent on the initial bar placement and on the target position on fly take-off. This meant the point of obscurement of the target was highly variable between flights, as it was not possible to control the point at which the fly took-off after a presented target. Holcocephala took multiple options when attacking targets that became obscured. These included terminating flights at the point of obscurement, flying through to the other side and finally they flew to deviate their path and avoid the obstacle. Each of these response types is separated and detailed below:

6.3.1 Re-engagement Trajectories

Re-engagement trajectories (example in **Fig. 6.2**) are typified by an initial interception trajectory that deviates once the target is obscured but then returns to an (albeit new) interception course once the target is within the visual field once more. Pro-nav simulations display that the deviation in flight course is not in accordance with the standard control system, and that the fly is unable to maintain an interception course during the time in which a target is obscured, suggesting lack of an internal model of the absolute spatial position of the target or at least the lack of an ability to implement such a model for interception.

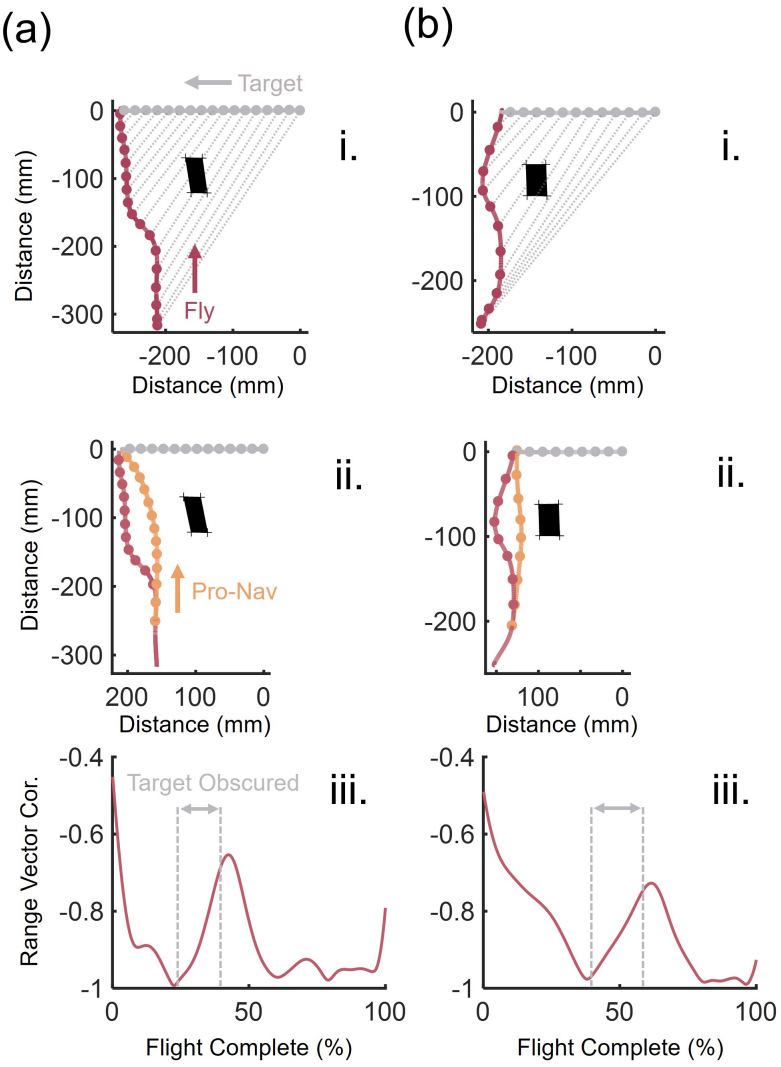

Fig. 6.2 Two examples **(a & b)** of re-engagement of Holcocephala to linear targets in which **(i.)** the fly (red) rises to meet a target (grey) travelling linearly above it. Lines-of-sight are plotted (grey and dotted) are 50 ms intervals. The obscuring black obstacle is marked and filled. **(ii.)** a proportional navigation simulation modelling the engagement should the line-of-sight not be obscured (N = 3, time delay = 28 ms). **(iii.)** Range vector correlations for both flights against their normalised length, with point of obscurement marked.

Re-engagement occurred in 6 thin bar (2.5 cm) flights out of a total of 7 in which the target was temporarily obscured by the target. Of the thick bar (5.0 cm), the interception was not re-engaged in any of 10 instances in which the target became obscured (see trajectory termination). Re-engagement trajectories are also characterised by a deviation from parallel navigation point where the target becomes obscured (rise in the range vector correlation of **Fig. 6.2 iii**).

Re-engaged targets were obscured for a significantly shorter time-period than terminated targets (Wilcoxon Rank-Sum, Z = 2.7, p = 0.007). Re-engaged targets were obscured for a mean 65 ms ±SE 2 ms (n = 6), while terminated trajectories were obscured for a mean 164 ms ±SE 23 ms (n = 11). The minimum time for trajectory re-engagement was 60 ms, and the maximum 72 ms (thick-bar). Obscurement times are plotted in **Fig. 6.3**.

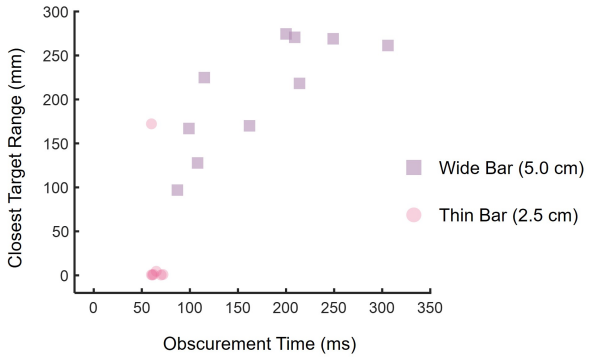

Fig. 6.3 The length of time that the target is obscured by either of the two bars is plotted against the closest range that the fly reached to the target (0 being direct contact after re-engagement). Point colour and shape corresponds to the width of bar presented as an obstacle.

6.3.2 Terminated Trajectories

Termination of trajectories in which the fly had lost sight of the target were qualitatively similar to the quitting behaviours observed in other experimental setups (see chapter 2). After the target became obscured, the fly deviated from an interception course, and began deceleration (**Fig. 6.4**). Unlike re-engagements, the fly returned to the perch rather than attempting a new interception course once the target came back into the visual field.

Trajectory termination occurred in 1/7 instances of target obscurement by the thin bar (2.5 cm) and 10/10 instances of target obscurement by the thick bar (5.0 cm). Once visual contact with the target had been lost, the flies decelerated and used a slower speed to return to the perch (**Fig. 6.4 iii**).

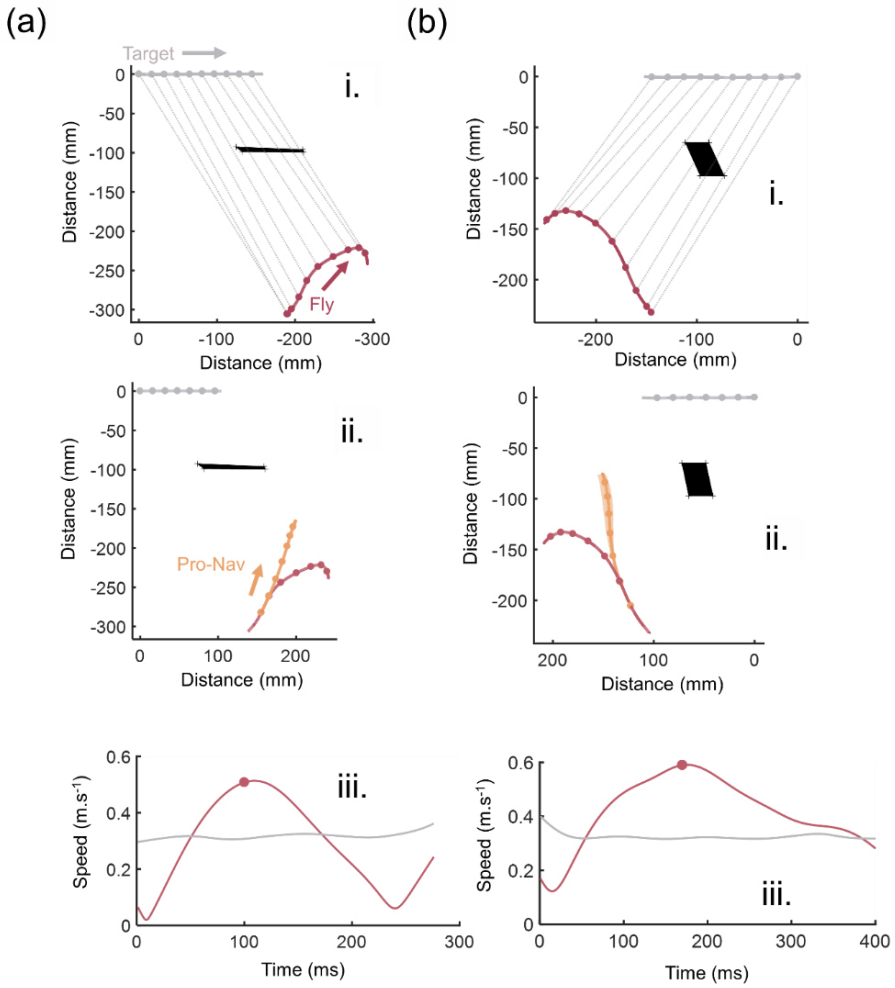

Fig. 6.4 **(a & b) (i.)** Holcocephala (red) rises to meet a target (grey) travelling linearly above it, until the target is obscured, and the fly quits the interception. Lines-of-sight are plotted (grey and dotted) are 50 ms intervals. The obscuring black obstacle is marked and filled. **(ii.)** a proportional navigation simulation modelling the engagement should the line-of-sight not be obscured (N = 3, time delay = 28 ms). **(iii.)** Time-series of the speed of flies (red) and their targets (grey) with target obscurement time marked by a point.

6.3.3 Obstacle Avoidance

On only 2 occasions (of 28 total recorded presentations) was there a visually obvious deviation in the flightpath of the fly due to the obstacle the prevented the target from being obscured (**Fig. 6.5**). In 3 instances the fly collided with obstacle, resulting in the fly returning to the perch. Obstacle avoidance was qualitatively evident from the flight traces in that, unlike other flights, the LOS rotate throughout the flight rather than remaining parallel. This

departure from parallel navigation is represented in the range vector correlations of the flights. Range vector correlations varied from their initially low value and increasing as LOS became less parallel (closer to 0) periodically throughout the flight. This deviation from parallel navigation is not explainable through pure proportional navigation, with some of the velocity rotations being in the opposite direction to rotation in the LOS and thus disagreeing with a proportional navigation framework.

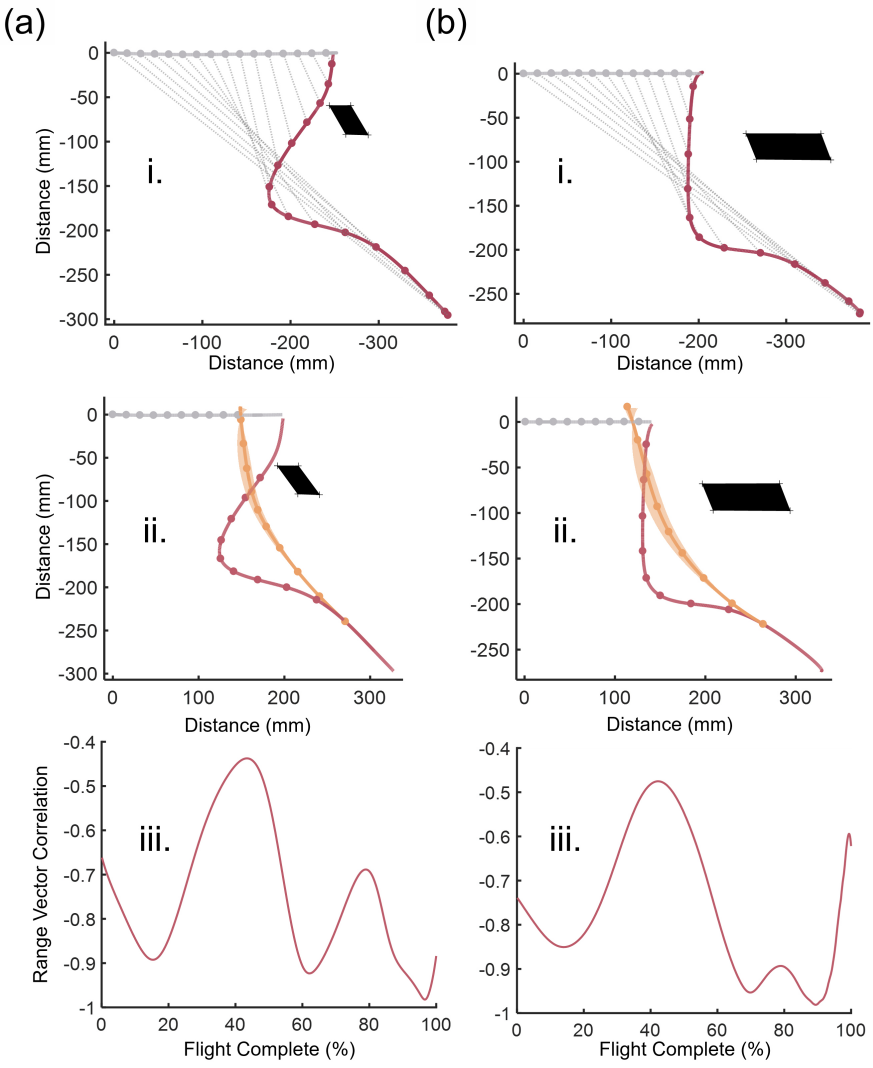

Fig. 6.5 The two examples of obstacle avoidance of both the thin (2.5 cm) obscuring bar **(a)** and the thick (5.0 cm) obscuring bar **(b)**. **(i.)** displays flight trajectories with lines-of-sight plotted at 50 ms (grey and dotted). **(ii.)** Pro-nav simulations of the obstacle avoidance trajectories (N = 3, time delay = 28 ms, shaded region represents $2.7 < N < 3.3$). **(iii.)** Range vector correlations of the flight trajectories in which obstacles were avoided.

6.3.4 Obstacle-Aversive Pro-nav

Humans appear to use a layered pursuit-avoidance strategy. Thus, we tested to see if a similarly layered navigational algorithm could be implemented in the obstacle avoidance behaviour of *Holcocephala*. Rather than a pursuit-avoidance algorithm, this would take the form of an obstacle-aversive pro-nav algorithm. The control law is as follows:

$$\dot{\gamma} = N\dot{\lambda} + \frac{c\dot{\phi}}{\omega} \tag{6.1}$$

Where, as in pro-nav, $\dot{\gamma}$ is predator heading rotation, N is a dimensionless navigational constant and $\dot{\lambda}$ is the rotation in the LOS to the target. The new term features the rate of change in the angular width of the obstacle (from the fly's perspective) $\dot{\phi}$, the angle between the LOS to the centre of the obstacle and the predator's heading ω, and c, a constant with units $^\circ$ (**Fig. 6.6**).

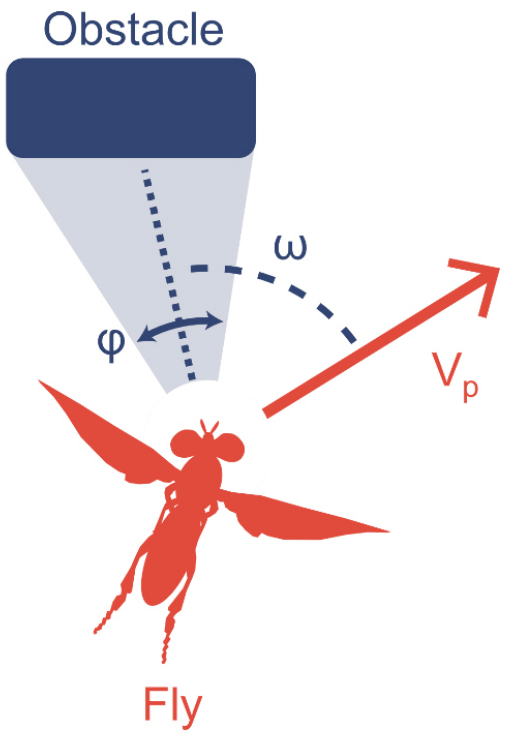

Fig. 6.6 An illustration of the geometry underlying the obstacle aversive element of the new model. ω is the angle between the LOS to the obstacle and the velocity of the predator (V_p). ϕ is the angular size of the target, from which the time derivative ($\dot{\phi}$) is input into the control law.

In this model, the interception term of pro-nav conflicts against the steering aversion from a single obstacle. As ω increases (the angle of the LOS to the obstacle to the predator's heading), the obstacle-related steering term decreases. This makes sense dynamically, as static objects visually close to the fly's axis of motion are more likely to obstruct its path than those further away in visual space. Those obstacles that have greater expansion rates are also given greater weighting to steering aversion, as this indexes their relative distance and weights closer obstacles higher, increasing their aversion priority. In the described algorithm, objects retreating from the target (when $\dot{\phi} < 0$) will attract the course of the predator, rather than repulsing it. This did not make sense from a biological context; it is not advantageous for stationary obstacles behind the observer ($\dot{\phi} < 0°\text{s}^{-1}$ when $\omega > 90°$) to generate steering deviations. Thus, the navigator was given a mode switch. If $\dot{\phi} > 0$, the navigator would be the obstacle-averse pro-nav detailed above. If $\dot{\phi} < 0$, the navigator would simply follow pure pro-nav.

While the obstacle-aversion and pro-nav elements of the model compete for the steering of the fly, they may operate under different delay constants. Thus for simulations, the delay-differential equations was given two time delay constants: One fixed at the time-delay of response to the target in pure pro-nav fitting (28 ms), whilst another was for the time-delay of the response to the obstacle-aversive element of the equation (looming and heading error of the obstacle), which was individually fitted to each trajectory.

6.3.5 Obstacle Aversive Simulations

Obstacle-aversive pro-nav explained much of the deviations that were not accounted for in the pure pro-nav model. It also served to highlight obstacle aversion in flights where the deviation from the pro-nav course was not as clear cut as the two examples shown in **Fig. 6.5**.

There were few cases (n = 4) in which *Holcocephala* flew in close proximity to the obstacle but did not lose sight of the target (**Fig. 6.7**). This sparsity of flights should temper conclusions about the constant and time-delay fittings as there are a great number of parameters to be fitted within the new model. Constants for the obstacle-aversion and time-delay were fitted by sequential fitting, selecting the best fitting constant that have the most similar curvature (as in Chapter 3). The constant c was fitted at 0.01 intervals between 0.01 and 0.50. Time delays were fitted at 10 ms intervals between 10 and 150 ms. There was broad consensus between the fitted flights on the fitted constant (mean = 8° ± SE 3°), and with the fitted time delay (mean = 100 ms ± SE 10 ms).

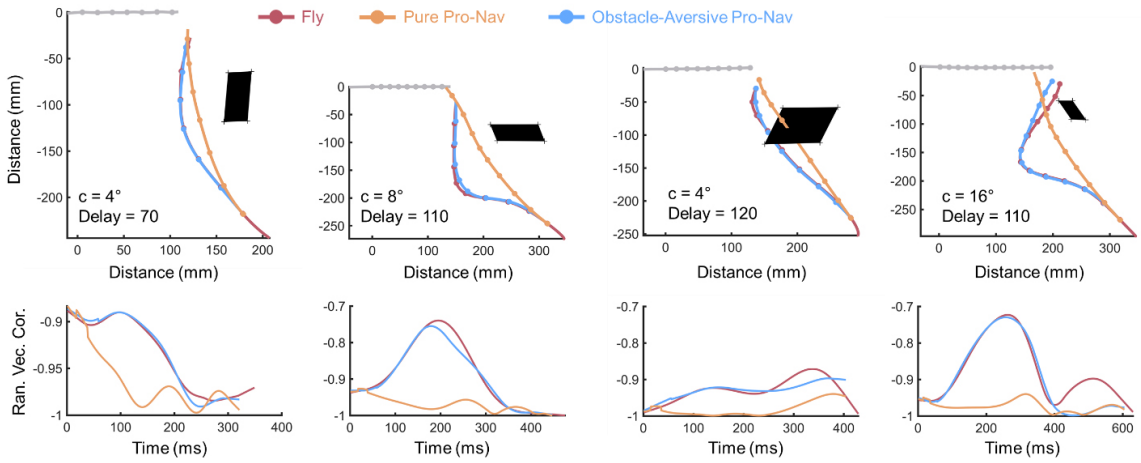

Fig. 6.7 Obstacle-aversive pro-nav is fitted to 4 trajectories. The pure pro-nav element of the algorithm is fixed at N = 3, Delay = 28 ms. The obstacle aversive element of the algorithm is individually fitted for each trajectory, both in constant c and time delay as displayed on each panel. Positions of both models and fly are highlighted at 50 ms intervals. Range vector correlations of the two models and the actual fly trajectories are displayed below each panel.

Confusing the obstacle avoidance algorithm are flights in which there appears to be little deviation from the obstacle, up until the point at which the fly collides or is at near collision with it (**Fig. 6.8**). This lack of deviation in heading on the part of the fly suggests that either the obstacle avoidance factor is not always active, or that it operates within a narrow field-of-view surrounding the LOS to the target.

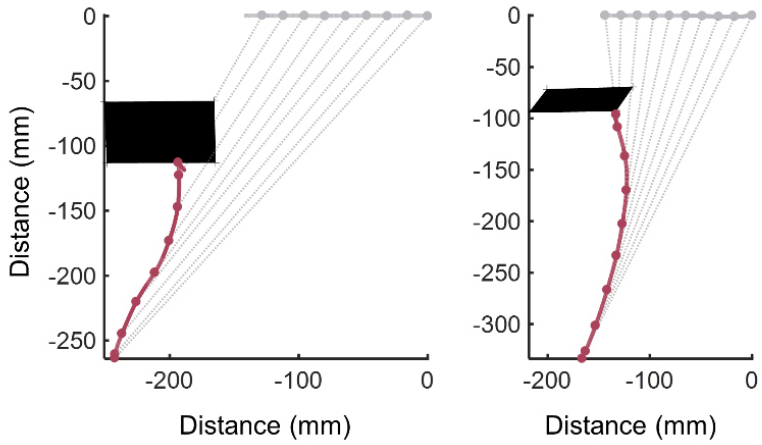

Fig. 6.8 Two trajectories are plotted in which Holcocephala collided with the largest (5 cm) obstacle without deviating to avoid it. Positions and LOS are plotted at 50 ms intervals.

A further modification to the model was made, such that while the target was being obscured by the obstacle, the pure pro-nav element of the algorithm was inactive. The deviations from the optimum heading seen in the re-engagement trajectories were always away from the obstacle, suggesting that the deviation was not random. Applying this new model that factored in the observability accounted for most of the deviation in the heading of the fly (**Fig. 6.9**).

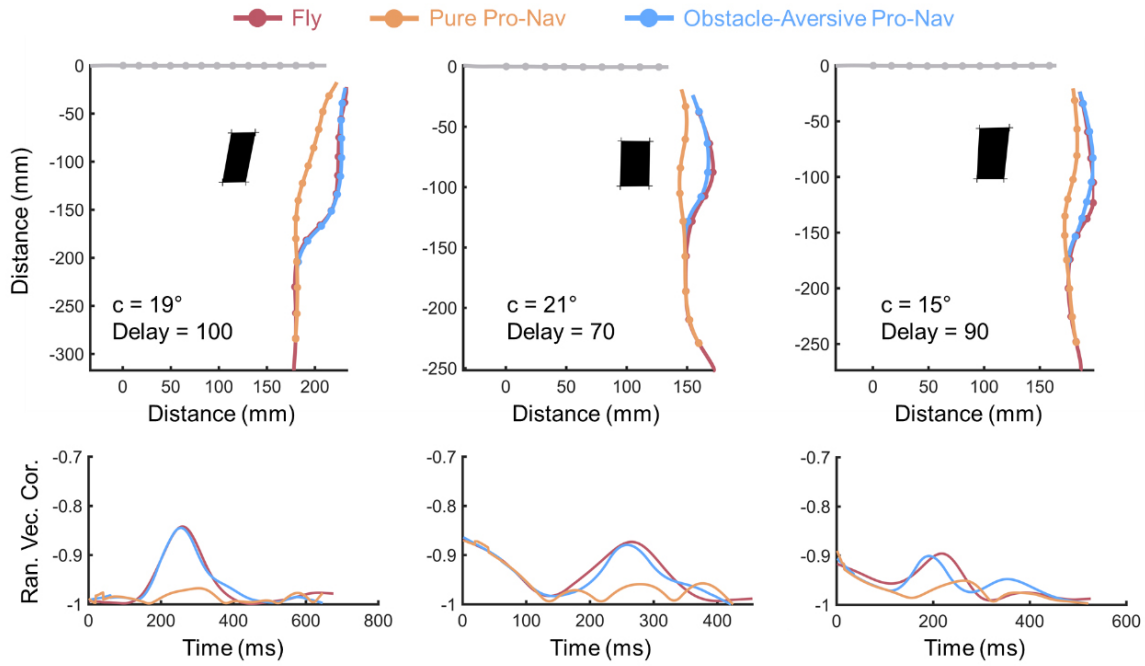

Fig. 6.9 Obstacle-aversive pro-nav is fitted to 3 trajectories in which the target is obscured from the fly. During the obscuring of the target (time-delayed by pure pro-nav 28 ms delay) only the steering control is based on the obstacle aversive element of the algorithm. The pure pro-nav element of the algorithm is fixed at N = 3, Delay = 28 ms. The obstacle aversive element of the algorithm is individually fitted for each trajectory, both in constant c and time delay as displayed on each panel. Positions of both models and fly are highlighted at 50 ms intervals. Range vector correlations of the two models and the actual fly trajectories are displayed below each panel.

6.3.6 Gain Variation and Obstacle Aversion

In keeping with the miss and gain simulations of Chapter 4, we ran simulations of hypothetical interceptions, varying the constant c (**Fig. 6.10**). In these simulations, N = 3, and pure pro-nav time-delay = 28 ms. The obstacle aversive time-delay was fixed at 100 ms. These simulations the linear speed of target and interceptor was kept constant, in keeping with

the means found in Chapter 3 (0.71 $m.s^{-1}$ for the interceptor, 0.49$m.s^{-1}$ for the target). Sensitivity of the predator's flight course to the chosen gain c can be seen by the evolution of colour coordinated trajectories as the gain varies.

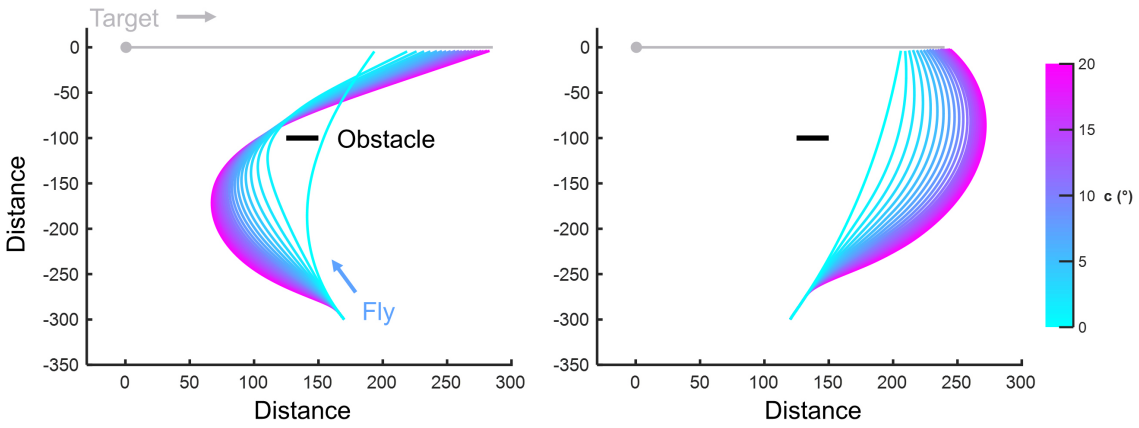

Fig. 6.10 Two sets of conditions are simulated in which an obstacle is avoided by the interceptor either passing in front (left) or behind (right) an obscuring target. Gain c variation is color-corresponded for each trajectory.

6.4 Discussion

The robber fly *Holcocephala fusca* is capable of intercepting targets in the presence of physical obstacles. This is despite *Holcocephala's* usual perching spots tending to prevent this from being necessary, within a natural setting. Even if *Holcocephala* do not normally engage targets in an environment where they would be required to simultaneously evade obstacles, it is unsurprising that they can aerially navigate around them. Aerial obstacle avoidance and navigation is necessary for *Holcocephala's* non-predatory behaviours, such as mate searching and navigating to new perches [41, 42].

Holcocephala does not require a permanent visual lock on the target throughout the trajectory in order to intercept the target. Targets that have been obscured can be re-engaged successfully, however there appears to be a restriction on this based on the length of time or space in which the fly was unable to see the target. Targets that disappeared for a longer amount of time (due to a larger obstacle) were abandoned. The length of time could represent a "patience" of the fly in maintaining an engagement without visual contact with the prey, or alternatively it could represent the cumulative deviation of the flight-path from the interception trajectory that results in the fly either abandoning the intercept, or failing

to spot the target once it is possible to do so once more. This latter interpretation is similar to the dichotomy of the abandonment of highly-accelerating targets seen in Chapter 2. One final interpretation would be that the size of the obstacle in itself affects whether the flies quit, yet how this is indexed (whether based on angular size or some integrated object size perception) is beyond the scope of these experiments to determine.

The more dramatic of the results is in the apparent deviation from pure proportional navigation which *Holcocephala* can perform. The new model, obstacle-aversive pro-nav, is essentially two control systems competing for one output. This less represents a switch from the standard control system, but the additional effect of a control system that is likely always present but not stimulated in the experiments of other chapters. *Holcocephala* does not spend its entire time hunting, and despite it being extremely sedentary for an asilid [187, 194], it must navigate between perches and interact with the three-dimensional context of its environment [41, 42]. The obstacle-aversive pro-nav algorithm behaves extremely similarly to the behavioural dynamics displayed within humans [174]. The principal difference from the human behavioural dynamics is that this uses pro-nav to drive the steering towards a moving goal, rather than a pursuit algorithm. The second difference is that this algorithm represents a potential control law rather than behavioural dynamics. As discussed in Chapter 3, behavioural dynamics are concerned with modelling how from an external perspective, and do not necessarily represent the internal information processing of the navigator [174, 175]. It is, however, worth noting that when navigating to a stationary target, both obstacle-aversive pro-nav and obstacle-aversive pursuit algorithms would display extremely similar behaviour. It would be extremely interesting to see the behavioural dynamics of navigation from [176] applied to moving targets as in [175], but in the presence of obstacles.

The new model described in this chapter, obstacle-aversive pro-nav, is a control law in that it generates a biologically relevant output using minimal, obtainable information about the target. The new inputs of obstacle angle from navigator heading and the looming rate of the target have both been described as stimuli in other biological systems. The angle of the LOS to an object from navigator heading is used within the pursuit frameworks of navigation within other insect species [157–160, 171]. Retinal expansion triggers avoidance behaviour in locusts [200] and in fruit flies [201], whilst at a finer level, it represents one of the core tenets of optic flow, the means by which most visual navigation of environments is achieved [206, 207, 22]. However, this obstacle avoidance is in contradiction to elements of the pursuit navigation of blowflies [160] where the peripheral visual field is supressed and optomotor cues ignored. These results demonstrate that *Holcocephala* do not suppress all cues from their peripheral vision, although it remains unclear as to whether this applies to other optomotor pathways.

The work on *Holcocephala* presented here conclusively demonstrates that the flies are not oblivious to their surroundings when intercepting a target. While in some cases they did collide with the obstacle, they were also capable of navigating a path around it which involved the parallel processing of the target and obstacle locations. This demonstrates on-line, closed loop responses to obstacles, which does not require absolute distance information, nor internal models of the physical environment. This work does, however, leave many questions outstanding. One such question is what other optomotor responses are running in the background of pro-nav engagements. We have discussed that *Holcocephala* could be using inertial or ocellar inputs to determine a global reference frame for rotation measurements. Obstacle avoidance suggests that the optic-flow processing of the compound eye is still functional while engaging a target. This could present another global reference frame calculation, in which the angular trajectory of a target across the visual field is combined with the optic flow across the eye. In Chapter 1, we saw that *Holcocephala* is capable of intercepting a target against a cluttered background. One conclusion from this is that the flies separate the target from salient visual features of the background, the first step that would be required for the subsequent inclusion of optic flow.

Final Conclusions

Vision

The vision of *Holcocephala fusca* is centred around a remarkably acute region where the spatial resolution (~0.28°) near matches the very best recorded for compound eyes. This has demonstrated that *Holcocephala's* small stature is not a barrier to it achieving extreme spatial resolution, albeit at a cost to the eye's field of view and with an extremely small region of increased resolution. We have discussed extensively how this will consequently affect the object detection thresholds and distances of *Holcocephala* when searching for its prey. However, there is an additional implication not yet described.

The discovery of proportional navigation as the fly's interception system highlights another important benefit of higher spatial resolution. The compound eye measures rotation as the object transitions through the fields of view of neighbouring pixels (pixels not necessarily corresponding to single photoreceptors due to neural superposition). The slower the rotation of the LOS, the longer it will take a target to transition from pixel to pixel. This effect can be countered by increasing spatial resolution of the eye, as the smaller the interommatidial angles, the faster the target transitions across the pixels. This pixel-pixel transition time is effectively a time-lag in the reception of LOS rotation and potentially a limiting factor to the "rotational resolution" of the eye. Via an increase in spatial resolution, a consistent EMD delay (τ) can generate different temporal tunings. The much higher STMD optimal angular speeds found in dragonflies are confusing when considering their demonstrated ability to detect and intercept targets at a much lower angular speed. This could be partially explained by the STMDs currently recorded all having much greater optima for the angular size of targets than those that dragonflies chase (<1°), potentially suggesting that the acute zones are not being incorporated within the STMDs currently recorded. The solution of this puzzle will likely develop further within the research done on dragonfly STMDs, but its

implications will have consequence for our understanding of *Holcocephala* and its ability to detect comparatively slow target motion.

In Chapter 3, we demonstrated that the LOS rates of *Holcocephala* are considerably lower than those of *Coenosia*, mainly due to the great range at which *Holcocephala* hunts its targets. These low LOS rates would consequently generate long time-delays, or steering inaccuracies unless matched by equivalent increases in the eye's spatial resolution. The acute zone of *Holcocephala* could thus be additionally interpreted as a means to increase the steering accuracy of long-range flights. It would be fascinating to see how LOS rates and angular resolution of eyes correlate across multiple species of predator, and how this is reflected in their hunting methodologies.

Fig. 6.11 The relationship of spatial resolution to the movement of the target across the eye is demonstrated between two eyes compound eyes, one with twice the resolution of the other. The higher resolution eye can measure half the LOS rate of the low resolution eye with an equal pixel-pixel transition delay.

Target Choice

The means by which *Holcocephala* assess the size and suitability of their targets remain has not yet been firmly demonstrated. Numerous options have been discounted, and it can be said that the flies are not likely applying the same heuristic rules that are used by killer flies and dragonflies. They appear not to require much movement of their target, but do not rely on angular size alone.

From the results detailed within this thesis, we can construct a hypothetical model for *Holcocephala's* prey selection that would fit the data so far gathered. The model is detailed in the figure below. This model is far from conclusively demonstrated. While testing stereopsis in *Holcocephala* proves extremely difficult, due to their small size and performance requirements, it would be interesting to test if large targets, tested further away than in this thesis, began to elicit responses as their angular size dropped below that of a 1.3 mm target at ~20 cm (i.e. ~0.4°). The current data features few large target presentations below this angular size.

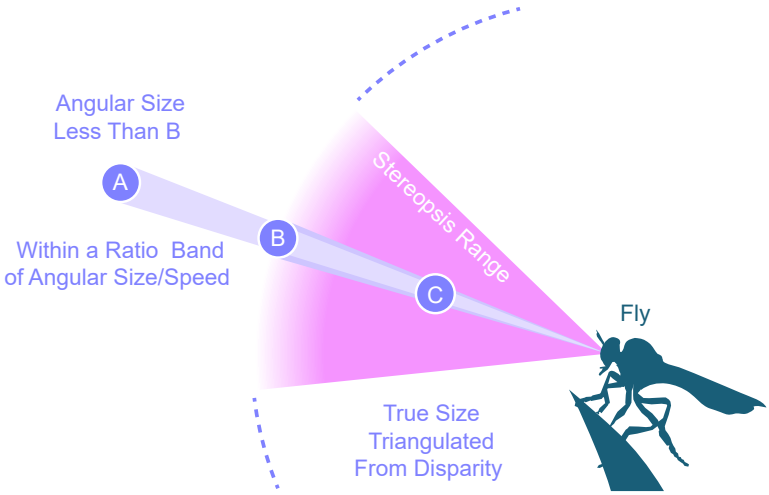

Fig. 6.12 The diagram demonstrates a potential system that could explain the prey-size selectivity of Holcocephala fusca. Three targets of equal size (and of suitable size for Holcocephala) are displayed: A, B, and C. C is within the stereopsis range, and thus its image disparity between the two compound eyes of the fly can be used to calculate its distance accurately. A is outside the stereopsis limit of the fly, and thus does not have disparity between the eyes. A is only attacked if its angular size is smaller than that of B, at the limit of the stereopsis range, and if it has a size/speed ratio within a privileged band.

Interception

The widest ranging of the conclusions to be drawn from the findings of this thesis is in the control of interception. From Chapter 3, we can conclude that interception within *Holcocephala fusca* and *Coenosia attenuata* is underpinned by a biological implementation of the control law proportional navigation. This is the first such description an interception (rather than pursuit) control law within insects . This work parallels that which has recently

been conducted in peregrine falcons , and the same models could potentially produce the behavioural dynamics seen in humans. The repeated hallmarks of parallel navigation reflect the systems simplicity in required input and computational requirements.

The gain tuning of proportional navigation varies between the two flies within this study. *Holcocephala* uses a higher, theoretically energetically optimal gain tuning of N = 3. This gain minimises the heading error throughout the flight whilst minimising the lateral accelerations and thus energy used in control. *Coenosia* uses a lower gain of N $\approx$ 1.5 and a control time-delay near 2/3 that of *Holcocephala* (18 ms vs 28 ms).This different gain tuning is potentially due to the extremely high stimulus that is created by their taking off so close to their targets (~3 - 15 cm rather than ~10 – 80 cm in *Holcocephala*). When this close proximity is combined with the high acceleration of diving from the ceiling, a no-catch zone is created, where the hunting success of flies is limited by their ability to generate lateral accelerations. This is in contrast to the diving behaviour of peregrine falcons, that use dives to not only gain high speed, but critically, gain range on the targets to improve catch success.

Holcocephala are capable of avoiding potential obstacles and intercepting targets against cluttered backgrounds, even though their normal perch choice does not require them to do so. Obstacle avoidance demonstrates that *Holcocephala* does not ignore wide-field optic flow stimuli during interception, in contrast to conspecific pursuit in blowflies.

Proportional navigation represents a new paradigm in which to consider the control of movement within animals. While it is especially effective for heading-off moving targets, the same system can intercept stationary targets. It is likely that pro-nav and similar derivatives will be demonstrated to be implemented in many more animal species. It is also likely that it will be supplemented by other fine-tuning controllers, like that found with obstacle-aversive pro-nav model. One such would be the biasing based on the angular acceleration of the LOS, which would increase the effectiveness of predator compensation for target acceleration.

The Biological Implementation of Proportional Navigation

The major question left from this work is the exact nature of the information acquisition and processing performed by flies when they use proportional navigation. The flies must use a global, inertial, reference frame for the rotation of the LOS, which is not available without combining information from different sensory fields. The behavioural work on display within this thesis represents a top-down approach to understanding the control system. However,

work from the bottom-up, neuron-first perspective may already have found decisive elements of how pro-nav and its global reference frame is achieved.

Small target motion detectors (STMDs) are cells found within the lobula of dragonflies and hoverflies [98,209]. These cells respond to the movement of small objects that move in the visual field. These cells are also capable of detecting targets moving against visual clutter. Interestingly, some of the ~20 classes of STMD still respond to a contrasting target when the movement of the background and the target are the same [96].

This small target motion is then passed on to large target-selective descending neurons (TSDNs) in dragonflies, which rate encode the speed and direction of target image motion across the retina. Eight pairs of TSDNs have been described in dragonflies [208], each with their own specificity in the motion of target they respond to. Extremely recently, the dipteran equivalent of these cells, dTSDNs, have been described both in hoverflies, and *Holcocephala* itself [209]. Of significant relevance to the findings of this thesis is that the dTSDNs are inhibited and silenced in both hoverflies and *Holcocephala* when the background motion of clutter matches that of the target. Given that STMDs are able to detect an object in clutter, this suggests the silencing of the dTSDNs is not a product of a lack of ability to detect the target, but an adaptive feature. To gain a global reference frame for LOS rotation, a fly could subtract wide-field motion (clutter movement) from the target retinal motion i.e. small-field motion. Performing this would exactly produce the cancellation of responses to targets moving exactly with the clutter, as in a global (i.e. clutter background) reference frame, the LOS has not rotated. From the work within this thesis, and that on the lobula and TSDNs of insects, the map below has been constructed to represent the potential implementation of proportional navigation within *Holcocephala*. This model is hypothetical, but feasible. There may be many more elements, and features such as the input of ocelli and halteres are highly speculative. Nevertheless, this should serve as one potential map for the information transfer and response of the pro-nav control system implemented within a biological framework, to be pruned and reshaped as more experimental work is conducted.

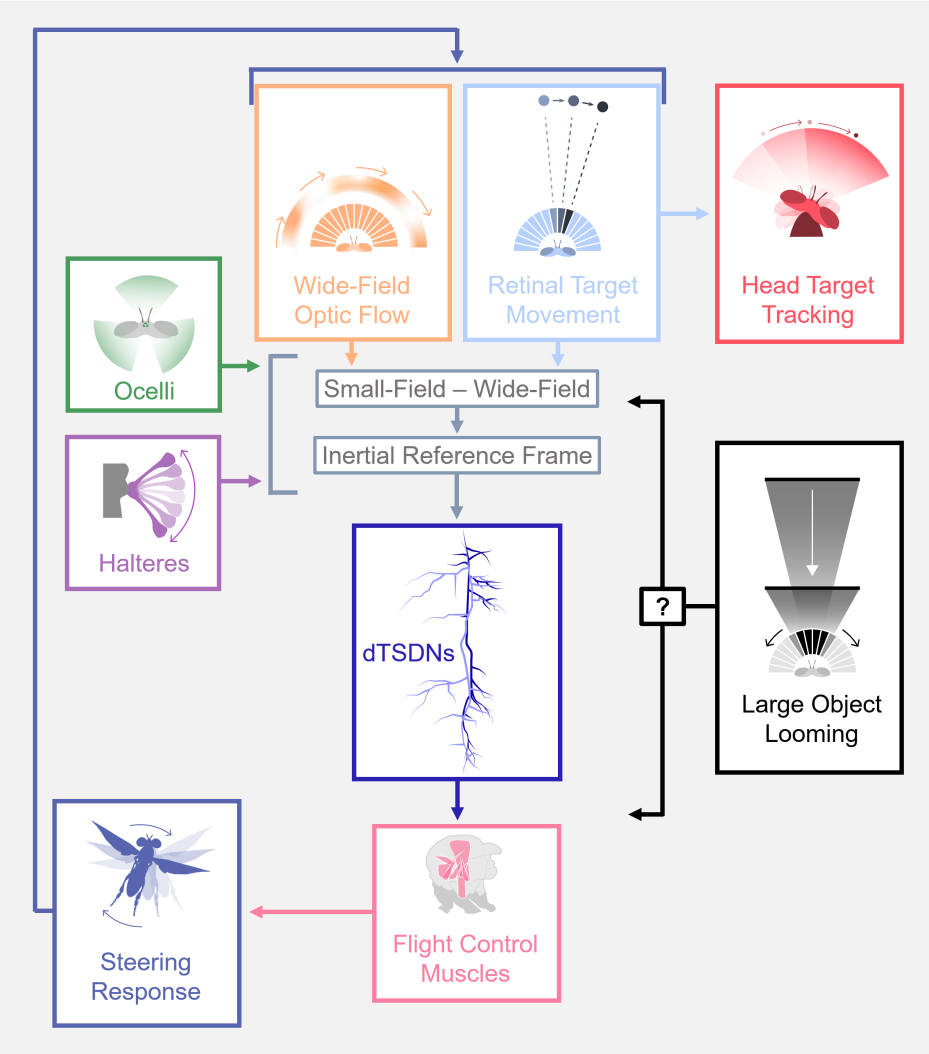

Fig. 6.13 Potential System Map for *Holcocephala's* implementation of Proportional Navigation

There is a further question of where the navigational constant N is represented within the system. The input and output do not have the same form; thus we are not looking for a specific constant of proportionality (i.e 3). Instead we are looking for proportionality between the LOS rate of the target and of each of the system responses. One example test would be to vary the speed (i.e. angular velocity) differential between the target and a cluttered background, whilst recording from dTSDNs. If the above model were true, then it would be expected for there to be a strongly correlated change in spike rate for LOS rate (presumably positively correlated). Other network possibilities are plausible but limited, given that there are only a small number of TSDN pairs. For instance, it would seem improbable that TSDNs have different LOS rate bandwidths (a band-pass filter on LOS rates to response) to potentially

work by combination, given that they also need to encode directionality within the same network.

Whatever the network of connections underpinning pro-nav, it is unlikely that proportionality will be simple and linear within the fly's system. The exact nature of how signal and responses move through network, and what that network looks like, is left to future research to build. The research within this thesis will, hopefully, act as a behavioural scaffolding for such building, outlining the shape of the neural and biomechanical structures animals use to intercept moving target

References

[1] T Fenchel. Marine Plankton Food Chains. *Annual Review of Ecology and Systematics*, 19(1):19–38, 2003.

[2] Phil F. Battley, Nils Warnock, T. Lee Tibbitts, Robert E. Gill, Theunis Piersma, Chris J. Hassell, David C. Douglas, Daniel M. Mulcahy, Brett D. Gartrell, Rob Schuckard, David S. Melville, and Adrian C. Riegen. Contrasting extreme long-distance migration patterns in bar-tailed godwits Limosa lapponica. *Journal of Avian Biology*, 43(1):21–32, 2012.

[3] Thomas Alerstam. Radar observations of the stoop of the Peregrine Falcon Falco peregrinus and the Goshawk Accipiter gentilis. *Ibis*, 129:267–273, 1987.

[4] David E Alexander. *Nature's flyers: birds, insects, and the biomechanics of flight*. JHU Press, 2004.

[5] Knut Schmidt-nielsen. Locomotion : Energy Cost of Swimming , Flying , and Running. *Science*, 177(4045):222–228, 1972.

[6] R. Dudley. Mechanisms and Implications of Animal Flight Maneuverability. *Integrative and Comparative Biology*, 42(1):135–140, 2002.

[7] Nigel E Stork. Insect diversity: facts, fiction and speculation. *Biological Journal of the Linnean Society*, 35(4):321–337, 12 1988.

[8] Nigel E. Stork, James McBroom, Claire Gely, and Andrew J. Hamilton. New approaches narrow global species estimates for beetles, insects, and terrestrial arthropods. *Proceedings of the National Academy of Sciences*, 112(24):7519–7523, 2015.

[9] Josef Rusek. Biodiversity of Collembola and their functional role in the ecosystem. *Biodiversity and Conservation*, 7(9):1207–1219, 1998.

[10] C. G. Johnson. *Migration and Dispersal of Insects by Flight*. Richard Clay (The Chaucer Press), Ltd.,, Bungay, Suffolk, 1969.

[11] Marcello La Greca. Origin and evolution of wings and flight in insects. *Bolletino di zoologia*, 47(sup1):65–82, 1980.

[12] Juan Manuel Grande, Juan José Negro, and María José Torres. The evolution of bird plumage colouration: A role for feather-degrading barcteria? *Ardeola*, 51(2):375–383, 2004.

[13] Gabriel S Weyman. A review of the possible causative factors and significance of ballooning in spiders. *Ethology Ecology & Evolution*, 5(3):279–291, 9 1993.

[14] J. A C Humphrey. Fluid mechanic constraints on spider ballooning. *Oecologia*, 73(3):469–477, 1987.

[15] Michael H. Dickinson and Karl Götz. Unsteady aerodynamic performance of model wings at low reynolds numbers. *J. exp. Biol.*, 174:45–64, 1993.

[16] Richard J. Bomphrey, Toshiyuki Nakata, Per Henningsson, and Huai-Ti Lin. Flight of the dragonflies and damselflies. *Philosophical Transactions of the Royal Society B: Biological Sciences*, 371(1704):20150389, 2016.

[17] Hao Liu, Sridhar Ravi, Dmitry Kolomenskiy, and Hiroto Tanaka. Biomechanics and biomimetics in insect-inspired flight systems. *Philosophical Transactions of the Royal Society B: Biological Sciences*, 371(1704):20150390, 2016.

[18] Michael H Dickinson, Fritz-Olaf Lehmann, and Sanjay P Sane. Wing Rotation and the Aerodynamics Basis of Insect Flight. *Science*, 284(1999):1954–1960, 1999.

[19] Charles P. Ellington, Coen Den Van Berg, Alexander P. Willmott, and Adrian L.R. Thomas. Leading-edge vortices in insect flight. *Nature*, 384(6610):626–630, 1996.

[20] Cp Ellington. Limitations on animal flight performance. *Journal of Experimental Biology*, 91:71–91, 1991.

[21] Graham K Taylor. Mechanics and aerodynamics of insect flight control. *Biol Rev Camb Philos Soc.*, (November 2001):449–471, 2015.

[22] G K Taylor, H G Krapp, and S J Simpson. Sensory systems and flight stability: What do insects measure and why? *Advances in Insect Physiology: Insect Mechanics and Control*, 34:231–316, 2007.

[23] G. A. Horridge. The compound eye of insects. *Scientific American*, 237(1):108–121, 1977.

[24] Martin Wilson. The functional organisation of locust ocelli. *Journal of Comparative Physiology A.*, 124(4):297–316, 1978.

[25] Gert Stange and Jonathon Howard. An ocellar dorsal light response in a dragonfly. *Journal of experimental biology*, 83(1):351–355, 1979.

[26] H. Schuppe and R. Hengstenberg. Optical properties of the ocelli of Calliphora erythrocephala and their role in the dorsal light response. *Journal of Comparative Physiology A*, 173(2):143–149, 1993.

[27] Holger G Krapp and Roland Hengstenberg. Estimation of self-motion by optic flow processing in single visual interneurons. *Nature*, 384:463, 12 1996.

[28] A. L. Eberle, B. H. Dickerson, P. G. Reinhall, and T. L. Daniel. A new twist on gyroscopic sensing: Body rotations lead to torsion in flapping, flexing insect wings. *Journal of the Royal Society Interface*, 12(104), 2015.

[29] Alexandra M. Yarger and Jessica L. Fox. Dipteran Halteres: Perspectives on Function and Integration for a Unique Sensory Organ. *Integrative and Comparative Biology*, 56(5):865–876, 2016.

[30] G. Nalbach. Extremely non-orthogonal axes in a sense organ for rotation: Behavioural analysis of the dipteran haltere system. *Neuroscience*, 61(1):149–163, 1994.

[31] Akiko Mizutani, Javaan S Chahl, and Mandyam V Srinivasan. Motion camouflage in dragonflies. *Nature*, 423:604, 6 2003.

[32] T. S. Collett and M. F. Land. Visual control of flight behaviour in the hoverfly Syritta pipiens L. *Journal of Comparative Physiology - A*, 99(1):1–66, 1975.

[33] T J Wardill, K Knowles, L Barlow, G Tapia, K Nordström, R M Olberg, and P T Gonzalez-Bellido. The Killer Fly Hunger Games: Target Size and Speed Predict Decision to Pursuit. *Brain, Behavior and Evolution*, 86(1):28–37, 2015.

[34] R. M. Olberg, A. H. Worthington, and K. R. Venator. Prey pursuit and interception in dragonflies. *Journal of Comparative Physiology A: Sensory, Neural, and Behavioral Physiology*, 186(2):155–162, 2000.

[35] S. A. Combes, D. E. Rundle, J. M. Iwasaki, and J. D. Crall. Linking biomechanics and ecology through predator-prey interactions: flight performance of dragonflies and their prey. *Journal of Experimental Biology*, 215(6):903–913, 2012.

[36] C J Pennycuick, Mark R Fuller, Jack J Oar, Sean J Kirkpatrick, C J Pennycuick, Mark R Fuller, Jack J Oar, and Sean J Kirkpatrick. Falcon versus Grouse : Flight Adaptations of a Predator and Its Prey. *Journal of Avian Biology*, 25(1):39–49, 2018.

[37] P. T. Gonzalez-Bellido, T. J. Wardill, and M. Juusola. Compound eyes and retinal information processing in miniature dipteran species match their specific ecological demands. *Proceedings of the National Academy of Sciences*, 108(10):4224–4229, 2011.

[38] R. M. Olberg, A. H. Worthington, J. L. Fox, C. E. Bessette, and M. P. Loosemore. Prey size selection and distance estimation in foraging adult dragonflies. *Journal of comparative physiology. A, Neuroethology, sensory, neural, and behavioral physiology*, 191(9):791–797, 2005.

[39] Arash Rashed, Christopher D. Beatty, Mark R. Forbes, and Thomas N. Sherratt. Prey selection by dragonflies in relation to prey size and wasp-like colours and patterns. *Animal Behaviour*, 70(5):1195–1202, 2005.

[40] Rolf Brechbühl, Jérôme Casas, and Sven Bacher. Diet choice of a predator in the wild: overabundance of prey and missed opportunities along the prey capture sequence. *Ecosphere*, 2(12):art133, 2011.

[41] D S Dennis. Ethology of Holcocephala fusca in Virginia (Diptera: Asilidae). In *Proceedings of the Entomological Society of Washington*, pages 366–78, 1979.

[42] A G Scarbrough. Coexistence in two species of Holcocephala (Diptera: Asilidae) in a Maryland habitat: predatory behavior. *Proceedings of the Entomological Society of Washington.*, 84:349–365, 1982.

[43] P L Miller. Visually controlled head Movements in Perched Anisopteran dragonflies. *Odonatologica*, 24(3):301–310, 1995.

[44] Stephan Holger Drukewitz, Nico Fuhrmann, Eivind A.B. Undheim, Alexander Blanke, Julien Giribaldi, Rosanna Mary, Guillaume Laconde, Sébastien Dutertre, and Björn Marcus von Reumont. A dipteran's novel sucker punch: Evolution of arthropod atypical venom with a neurotoxic component in robber flies (asilidae, diptera). *Toxins*, 10(1), 2018.

[45] B V Brown, A Borkent, J M Cumming, D M Wood, N E Woodley, and M A Zumbado. Manual of Central American Diptera. Vol. 1. Ottawa, National Research Council of Canada, 2009.

[46] Yohan Solano-Rojas, Adrian Pont, José De Freitas, Gustavo Moros, and Yaritza Goyo. First record of Coenosia attenuata Stein, 1903 (Diptera: Muscidae) in Venezuela. *Anales de Biología*, 39(39):223–226, 2017.

[47] Todd A. Ugine, Emily J. Sensenbach, John P. Sanderson, and Stephen P. Wraight. Biology and Feeding Requirements of Larval Hunter Flies Coenosia attenuata (Diptera: Muscidae) Reared on Larvae of the Fungus Gnat Bradysia impatiens (Diptera: Sciaridae). *Journal of Economic Entomology*, 103(4):1149–1158, 2010.

[48] Célia Mateus. Bioecology and behaviour of Coenosia attenuata in greenhouse vegetable crops in the Oeste region, Portugal. *Bulletin of Insectology*, 65(2):257–263, 2012.

[49] Truman E. Sherk. Development of the compound eyes of dragonflies (odonata). III. Adult compound eyes. *Journal of Experimental Zoology*, 203(1):61–79, 1978.

[50] Egemen Agi, Marion Langen, Steven J. Altschuler, Lani F. Wu, Timo Zimmermann, and Peter Robin Hiesinger. The evolution and development of neural superposition. *Journal of Neurogenetics*, 28(3-4):216–232, 2014.

[51] Simpla Mahato, Jing Nie, David C. Plachetzki, and Andrew C. Zelhof. A mosaic of independent innovations involving eyes shut are critical for the evolutionary transition from fused to open rhabdoms. *Developmental Biology*, 443(2):188–202, 2018.

[52] M. F. Land. Compound eyes: Old and new optical mechanisms. *Nature*, 287(5784):681–686, 1980.

[53] G.A. Horridge, L. Marcelja, and R. Jahnke. Light guides in the dorsal eye of the male mayfly. *Proceedings of the Royal Society of London, B*, 216:25–51, 1982.

[54] Dan-Eric Nilsson. A new type of imaging optics in compound eyes. *Nature*, 332(3):76–78, 1988.

[55] E. K. Buschbeck, B. Ehmer, and R. R. Hoy. The unusual visual system of the Strepsiptera: External eye and neuropils. *Journal of Comparative Physiology A: Neuroethology, Sensory, Neural, and Behavioral Physiology*, 189(8):617–630, 2003.

[56] W Pix, J M Zanker, and J Zeil. The optomotor response and spatial resolution of the visual system in male Xenos vesparum (Strepsiptera). *The Journal of Experimental Biology*, 203(22):3397–3409, 2000.

[57] Alexander Borst. Drosophila's View on Insect Vision. *Current Biology*, 19(1):R36–R47, 2009.

[58] B. Pick. Specific misalignments of rhabdomere visual axes in the neural superposition eye of dipteran flies. *Biological Cybernetics*, 26(4):215–224, 1977.

[59] A W Snyder, D G Stavenga, and S B Laughlin. Spatial Information Capacity of Compound Eyes. *Journal of Comparative Physiology*, 116(2):183–207, 1977.

[60] Allan W. Snyder. Acuity of compound eyes: Physical limitations and design. *Journal of Comparative Physiology - A*, 116(2):161–182, 1977.

[61] Michael F. Land. Visual Acuity in Insects. *Annual Review of Entomology*, 42(1):147–177, 1997.

[62] L. Levín and H. Maldonado. A fovea in the praying mantis eye - III. The centring of the prey. *Zeitschrift für Vergleichende Physiologie*, 67(1):93–101, 1970.

[63] M. D.L. Brooke, S. Hanley, and S. B. Laughlin. The scaling of eye size with body mass in birds. *Proceedings of the Royal Society B: Biological Sciences*, 266(1417):405–412, 1999.

[64] Matthew F. Gaffney and William Hodos. The visual acuity and refractive state of the American kestrel (Falco sparverius). *Vision Research*, 43(19):2053–2059, 2003.

[65] G. a. Horridge. The separation of visual axes in apposition compound eyes. *Phil. Trans. R. Soc. Lond. B*, 285(2003):1–59, 1978.

[66] Rayleigh. XXXI. Investigations in optics, with special reference to the spectroscope. *Philosophical Magazine Series 5*, 8(49):261–274, 1879.

[67] G. a. Horridge and M. McLean. The Dorsal Eye of the Mayfly Atalophlebia (Ephemeroptera). *Proceedings of the Royal Society B: Biological Sciences*, 200(1139):137–150, 1978.

[68] J. J. Marotta and M. A. Goodale. The role of learned pictorial cues in the programming and control of grasping. *Experimental Brain Research*, 121(4):465–470, 1998.

[69] Suzanne Amador Kane, Andrew H Fulton, and Lee J Rosenthal. When hawks attack: animal-borne video studies of goshawk pursuit and prey-evasion strategies. *The Journal of Experimental Biology*, 218(2):212–222, 1 2015.

[70] Brett R. Fajen and William H. Warren. Visual guidance of intercepting a moving target on foot. *Perception*, 33(6):689–715, 2004.

[71] Robin Mills, Hanno Hildenbrandt, Graham K. Taylor, and Charlotte K. Hemelrijk. Physics-based simulations of aerial attacks by peregrine falcons reveal that stooping at high speed maximizes catch success against agile prey. *PLOS Computational Biology*, 14(4):e1006044, 2018.

[72] Michael P. Jones, Kenneth E. Pierce, and Daniel Ward. Avian Vision: A Review of Form and Function with Special Consideration to Birds of Prey. *Journal of Exotic Pet Medicine*, 16(2):69–87, 2007.

[73] K V Fite and S Rosenfield-Wessels. A Comparative Study of Deep Avian Foveas. *Brain, Behavior and Evolution*, 12(1-2):97–115, 1975.

[74] Oscar Inzunza, Hermes Bravo, Ricardo L. Smith, and Manuel Angel. Topography and morphology of retinal ganglion cells in Falconiforms: A study on predatory and carrion-eating birds. *The Anatomical Record*, 229(2):271–277, 1991.

[75] G. A. Horridge and P. Duelli. Anatomy of the Regional Differences in the Eye of the Mantis Ciulfina. *J. Exp. Biol.*, 80(1):165–190, 1979.

[76] Matteo Mischiati, Huai Ti Lin, Paul Herold, Elliot Imler, Robert Olberg, and Anthony Leonardo. Internal models direct dragonfly interception steering. *Nature*, 517(7534):333–338, 2015.

[77] Trevor J. T.J. Wardill, S.T. Samuel T. Fabian, Ann C. A.C. Pettigrew, D.G. Doekele G. Stavenga, Karin Nordström, and P.T. Paloma T. Gonzalez-Bellido. A Novel Interception Strategy in a Miniature Robber Fly with Extreme Visual Acuity. *Current Biology*, 27(6):854–859, 3 2017.

[78] D G Stavenga. Angular and spectral sensitivity of fly photoreceptors. I. Integrated facet lens and rhabdomere optics. *Journal of comparative physiology. A, Neuroethology, sensory, neural, and behavioral physiology*, 189(1):1–17, 2003.

[79] N Franceschini and K Kirschfeld. [Pseudopupil phenomena in the compound eye of drosophila]. *Kybernetik*, 9(5):159–182, 1971.

[80] Heinrieh Homann. Zum Problem der Ocellenfunktion bei den Insekten. *Zeitschrift für Vergleichende Physiologie*, 1(3-4):541–578, 1924.

[81] J. H. van Hateren. Waveguide theory applied to optically measured angular sensitivities of fly photoreceptors. *Journal of Comparative Physiology A*, 154(6):761–771, 1984.

[82] Eric J. Warrant and Peter D. McIntyre. Strategies for retinal design in arthropod eyes of low F-number. *Journal of Comparative Physiology A*, 168(4):499–512, 1991.

[83] D. G. M. Beersma, B. J. Hoenders, A. M. J. Huiser, and P. Vantoorn. Refractive-Index of the Fly Rhabdomere. *Journal of the Optical Society of America*, 72(5):583–588, 1982.

[84] G. Seitz. Der Strahlengang im Appositionsauge von Calliphora erythrocephala (Meig.). *Zeitschrift für vergleichende Physiologie*, 59(2):205–231, 1968.

[85] Doekele G Stavenga. A.6 Optical Qualities of the Fly Eye — An Approach from the Side of Geometrical, Physical and Waveguide Optics BT - Photoreceptor Optics. In Allan W Snyder and Randolf Menzel, editors, *Photoreceptor Optics*, pages 126–144. Springer Berlin Heidelberg, Berlin, Heidelberg, 1975.

[86] D. G. Stavenga, R. Kruizinga, and H. L. Leertouwer. Dioptrics of the facet lenses of male blowflies Calliphora and Chrysomyia. *Journal of Comparative Physiology A*, 166(3):365–371, 1990.

[87] J. H. van Hateren. The stiles-crawford effect in the eye of the blowfly, Calliphora erythrocephala. *Vision Research*, 25(9):1305–1315, 1985.

[88] Johannes Schindelin, Ignacio Arganda-Carreras, Erwin Frise, Verena Kaynig, Mark Longair, Tobias Pietzsch, Stephan Preibisch, Curtis Rueden, Stephan Saalfeld, Benjamin Schmid, Jean Yves Tinevez, Daniel James White, Volker Hartenstein, Kevin Eliceiri, Pavel Tomancak, and Albert Cardona. Fiji: An open-source platform for biological-image analysis. *Nature Methods*, 9(7):676–682, 2012.

[89] Samuel Rossel. Regional differences in photoreceptor performance in the eye of the praying mantis. *Journal of Comparative Physiology - A*, 131(2):95–112, 1979.

[90] M Okamoto, K Yasuda, and a Azuma. Aerodynamic characteristics of the wings and body of a dragonfly. *The Journal of experimental biology*, 199(Pt 2):281–94, 1996.

[91] J H van Hateren and C Schilstra. Blowfly flight and optic flow. II. Head movements during flight. *Journal of Experimental Biology*, 202:1481–1490, 1999.

[92] Howard Ensign Evans. *Systematics and nesting behavior of Australian Bembix sand wasps (Hymenoptera, Sphecidae)*. American Entomological Institute, Ann Arbor, Mich., 1973.

[93] G. L. Walls. Factors in Human Visual Resolution. *Journal of the Optical Society of America*, 33(9):487–505, 1943.

[94] D H Kelly. Motion and vision. II. Stabilized spatio-temporal threshold surface. *J. Opt. Soc. Am.*, 69(10):1340–1349, 1979.

[95] D C. O'Carroll, N. J. Bidwell, S.B. Laughlin, and E. J. Warrant. Insect motion detectors matched to visual ecology. *Nature*, 382:63–66, 1996.

[96] Karin Nordström, Paul D. Barnett, and David C. O'Carroll. Insect detection of small targets moving in visual clutter. *PLoS Biology*, 4(3):0378–0386, 2006.

[97] Nakayama. Image Processing :. *Time*, 25, 1985.

[98] Mikko Juusola, An Dau, Zhuoyi Song, Narendra Solanki, Diana Rien, David Jaciuch, Sidhartha Dongre, Florence Blanchard, Gonzalo G de Polavieja, Roger C Hardie, and Jouni Takalo. Microsaccadic information sampling provides Drosophila hyperacute vision. *eLife*, 6:e26117, 2016.

[99] Roger C Hardie and K Franze. Photomechanical Responses in Drosophila Photoreceptors. *Science*, 338(6104):260–263, 2012.

[100] Werner Reichardt. Evaluation of optical motion information by movement detectors. *Journal of Comparative Physiology A*, 161(4):533–547, 1987.

[101] Werner Reichardt. Autocorrelation, a Principle for the Evaluation of Sensory Information by the Central Nervous System. In W A Rosenblith, editor, *Sensory Communication*, pages 303–17. The MIT Press, New York/London, 1961.

[102] Steven D Wiederman, Patrick A Shoemaker, and David C O'Carroll. A Model for the Detection of Moving Targets in Visual Clutter Inspired by Insect Physiology. *PLOS ONE*, 3(7):e2784, 7 2008.

[103] S. D. Wiederman, P. A. Shoemaker, and D. C. O'Carroll. Correlation between OFF and ON Channels Underlies Dark Target Selectivity in an Insect Visual System. *Journal of Neuroscience*, 33(32):13225–13232, 2013.

[104] B. R. H. Geurten, K. Nordstrom, J. D. H. Sprayberry, D. M. Bolzon, and D. C. O'Carroll. Neural mechanisms underlying target detection in a dragonfly centrifugal neuron. *Journal of Experimental Biology*, 210(18):3277–3284, 2007.

[105] Karin Nordström. Neural specializations for small target detection in insects. *Current Opinion in Neurobiology*, 22(2):272–278, 2012.

[106] Geoffrey P. Luke, Cameron H.G. Wright, and Steven F. Barrett. A multiaperture bioinspired sensor with hyperacuity. *IEEE Sensors Journal*, 12(2):308–314, 2012.

[107] Huai-Ti Lin and Anthony Leonardo. Heuristic Rules Underlying Dragonfly Prey Selection and Interception. *Current Biology*, 27(8):1124–1137, 4 2017.

[108] Hubert Eichner, Maximilian Joesch, Bettina Schnell, Dierk F. Reiff, and Alexander Borst. Internal Structure of the Fly Elementary Motion Detector. *Neuron*, 70(6):1155–1164, 2011.

[109] M. F. Land and H. Eckert. Maps of the acute zones of fly eyes. *Journal of Comparative Physiology A*, 156(4):525–538, 1985.

[110] Simon B. Laughlin and Roger C. Hardie. Common strategies for light adaptation in the peripheral visual systems of fly and dragonfly. *Journal of Comparative Physiology - A*, 128(4):319–340, 1978.

[111] Ursula Menzi. Visual adaptation in nocturnal and diurnal ants. *Journal of Comparative Physiology A*, 160(1):11–21, 1987.

[112] Ajay Narendra, Birgit Greiner, Willi A. Ribi, and Jochen Zeil. Light and dark adaptation mechanisms in the compound eyes of Myrmecia ants that occupy discrete temporal niches. *The Journal of Experimental Biology*, 219(16):2435–2442, 2016.

[113] M F Day. Pigment Migration in the Eyes of the Moth Ephestia kuehniella Zeller. *The Biological Bulletin*, 80(3), 1941.

[114] C G Bernhard and D Ottoson. Studies on the relation between the pigment migration and the sensitivity changes during dark adaptation in diurnal and nocturnal Lepidoptera. *The Journal of general physiology*, 44(1):205–215, 1960.

[115] K. Kirschfeld and K. Vogt. Calcium ions and pigment migration in fly photoreceptors. *Naturwissenschaften*, 67(10):516–517, 1980.

[116] G. A. Horridge, J. Duniec, and L. Marcelja. A 24-hour cycle in single locust and mantis photoreceptors. *Journal of Experimental Biology*, 91(APR):307–322, 1981.

[117] L. M W Leggett and D. G. Stavenga. Diurnal changes in angular sensitivity of crab photoreceptors. *Journal of Comparative Physiology - A*, 144(1):99–109, 1981.

[118] P V Switzer and P K Eason. Proximate constraints on intruder detection in the dragonfly Perithemis tenera (Odonata : Libellulidae): Effects of angle of approach and background. *Annals of the Entomological Society of America*, 93:333–339, 2000.

[119] C. Gilbert. Visual control of cursorial prey pursuit by tiger beetles (Cicindelidae). *Journal of Comparative Physiology - A Sensory, Neural, and Behavioral Physiology*, 181(3):217–230, 1997.

[120] K Perlin. An Image Synthesizer. *Siggraph*, 19(3), 1985.

[121] Steven D. Wiederman, Joseph M. Fabian, James R. Dunbier, and David C. O'Carroll. A predictive focus of gain modulation encodes target trajectories in insect vision. *eLife*, 6:1–19, 2017.

[122] Darren Pais and Naomi Leonard. Pursuit and Evasion: Evolutionary Dynamics and Collective Motion. In *AIAA Guidance, Navigation, and Control Conference*, Guidance, Navigation, and Control and Co-located Conferences. American Institute of Aeronautics and Astronautics, 8 2010.

[123] Y. C. Ho, A. E. Bryson, and S. Baron. Differential games and optimal pursuit-evasion strategies. *IEEE Transactions on Automatic Control*, 10(4):385–389, 1965.

[124] T Nagata, M Koyanagi, H Tsukamoto, S Saeki, K Isono, Y Shichida, F Tokunaga, M Kinoshita, K Arikawa, and A Terakita. Depth Perception from Image Defocus in a Jumping Spider. *Science*, 335:469–471, 2012.

[125] Matthias Ott and Frank Schaeffel. A negatively powered lens in the chameleon, 1995.

[126] Samuel Rossel. Binocular stereopsis in an insect, 1983.

[127] William E. Cooper and Theodore Stankowich. Prey or predator? Body size of an approaching animal affects decisions to attack or escape. *Behavioral Ecology*, 21(6):1278–1284, 2010.

[128] Norman Owen-Smith and M. G.L. Mills. Predator-prey size relationships in an African large-mammal food web. *Journal of Animal Ecology*, 77(1):173–183, 2008.

[129] Robert M R Barclay. Long- versus short-range foraging strategies of hoary (Lasiurus cinereus) and silver-haired (Lasionycteris noctivagans) bats and the consequences for prey selection. *Canadian Journal of Zoology*, 63(11):2507–2515, 11 1985.

[130] John W. Laundré. How large predators manage the cost of hunting. *Science*, 346(6205):33–34, 2014.

[131] M Milinski. Experiments on the Selection by Predators against spatial Oddity of their Prey. *Zeitschrift für Tierpsychologie*, 325:311–325, 1977.

[132] Keren Embar, Shomen Mukherjee, and Burt P. Kotler. What do predators really want? The role of gerbil energetic state in determining prey choice by Barn Owls. *Ecology*, 95(2):280–285, 2014.

[133] Eleanor M. Caves, Nicholas C. Brandley, and Sönke Johnsen. Visual Acuity and the Evolution of Signals. *Trends in Ecology and Evolution*, 33(5):358–372, 2018.

[134] Samuel T Fabian, Mary E Sumner, Trevor J Wardill, Sergio Rossoni, and Paloma T Gonzalez-Bellido. Interception by two predatory fly species is explained by a proportional navigation feedback controller. *Journal of the Royal Society Interface*, 15, 2018.

[135] Theodore Garland. The relation between maximal running speed and body mass in terrestrial mammals. *Journal of Zoology*, 199(2):157–170, 1983.

[136] G A Horridge. A theory of insect vision : velocity parallax. *Proc. R. Soc. Lond. B*, 229(1254), 1986.

[137] R. M. Noest and Z. Jane Wang. A tiger beetle's pursuit of prey depends on distance. *Physical Biology*, 14(2), 2017.

[138] Erik C. Sobel. The locust's use of motion parallax to measure distance. *Journal of Comparative Physiology A*, 167(5):579–588, 1990.

[139] Michael Poteser and Karl Kral. Visual distance discrimination between stationary targets in praying mantis: an index of the use of motion parallax. *Journal of Experimental Biology*, 198:2127–2137, 1995.

[140] G. K. Wallace. Visual Scanning in the Desert Locust Schistocerca Gregaria Forskal. *J. Exp. Biol.*, 36(3):512–525, 1959.

[141] Ian P Howard, Ian P Howard, and Brian J Rogers. *Binocular vision and stereopsis*. Oxford University Press, USA, 1995.

[142] Robert Patterson and Wayne L Martin. Human Stereopsis. *Human Factors*, 34(6):669–692, 12 1992.

[143] J Packwood and B Gordon. Stereopsis in normal domestic cat, Siamese cat, and cat raised with alternating monocular occlusion. *Journal of Neurophysiology*, 38(6):1485–1499, 11 1975.

[144] W E Stumpf, Methods Cell, M Sar, Fifth Inter, K Larsson, D C Paup, R A Gorski, J M Davidson, P Alsum, R W Goy, D A Keefer, J B Hutchison, C M Haugen, C Beyer, H H Feder, F Naftolin, J Ryan, J T M Ureeburg, and S Huang. Stereopsis in the Falcon. *Science*, 135(1975):79–82, 1976.

[145] N J Marshall, M F Land, and T W Cronin. The ' six-eyed ' stomatopod. *Endeavour*, 18(1):17–26, 1994.

[146] B. Hocking. The intrinsic range and speed of flight of insects. *Transactions of the Royal Entomological Society of London*, 104:223–345, 1953.

[147] J M V Rayner. Mechanical and Ecological Constraints on Flight Evolution. *The Beginnings of Birds: Proceedings of the International Archaeopteryx conference Eichstatt*, pages 279–288, 1985.

[148] Osborne Reynolds. XXIX. An experimental investigation of the circumstances which determine whether the motion of water shall he direct or sinuous, and of the law of resistance in parallel channels. *Philosophical Transactions of the Royal Society of London*, 174:935–982, 1883.

[149] Michael a B Deakin. Formulae for insect wingbeat frequency. *Journal of insect science (Online)*, 10(96):96, 2010.

[150] David N Byrne, Stephen L Buchmann, and Hayward G Spangler. Relationship Between Wing Loading, Wingbeat Frequency and Body Mass in Homopterous Insects. *J. exp. Biol*, 135(1988):9–23, 1988.

[151] B Dey and P S Krishnaprasad. Trajectory smoothing as a linear optimal control problem. In *2012 50th Annual Allerton Conference on Communication, Control, and Computing (Allerton)*, pages 1490–1497, 2012.

[152] Stephen Young and Victoria A. Taylor. Visually guided chases in polyphemus pediculus. *Journal of Experimental Biology*, 137:387–398, 1988.

[153] James R Tresilian. Visually timed action : time-out for ' tau '? *Trends in Cognitive Sciences*, 3(8):301–310, 1999.

[154] Douglas R. Warrick, Tyson L. Hedrick, Andrew A. Biewener, Kristen E. Crandell, and Bret W. Tobalske. Foraging at the edge of the world: low-altitude, high-speed manoeuvering in barn swallows. *Philosophical Transactions of the Royal Society B: Biological Sciences*, 371(1704):20150391, 2016.

[155] Christian C. Voigt, B. Markus Schuller, Stefan Greif, and Björn M. Siemers. Perch-hunting in insectivorous Rhinolophus bats is related to the high energy costs of manoeuvring in flight. *Journal of Comparative Physiology B: Biochemical, Systemic, and Environmental Physiology*, 180(7):1079–1088, 2010.

[156] Wayne A. Wickelgren. Speed-accuracy tradeoff and information processing dynamics. *Acta Psychologica*, 41(1):67–85, 1977.

[157] M. Gries and N. Koeniger. Straight forward to the queen: pursuing honeybee drones (Apis mellifera L.) adjust their body axis to the direction of the queen. *Journal of Comparative Physiology A*, 179(4), 1996.

[158] M. F. Land. Chasing and pursuit in the dolichopodid fly Poecilobothrus nobilitatus. *Journal of Comparative Physiology A*, 173(5):605–613, 1993.

[159] M. F. Land and T. S. Collett. Chasing behaviour of houseflies (Fannia canicularis). *Journal of Comparative Physiology*, 89(4):331–357, 1974.

[160] Christine Trischler. Chasing behaviour and optomotor following in free-flying male blowflies: flight performance and interactions of the underlying control systems. *Frontiers in Behavioral Neuroscience*, 4(May):1–13, 2010.

[161] Michael H. Dickinson. Motor control: How dragonflies catch their prey. *Current Biology*, 25(6):R232–R234, 2015.

[162] Robert M Olberg. Visual control of prey-capture flight in dragonflies. *Current Opinion in Neurobiology*, 22(2):267–271, 4 2012.

[163] T. S. Collett and M. F. Land. How hoverflies compute interception courses. *Journal of Comparative Physiology - A*, 125(3):191–204, 1978.

[164] Caroline H. Brighton, Adrian L. R. Thomas, and Graham K. Taylor. Terminal attack trajectories of peregrine falcons are described by the proportional navigation guidance law of missiles. *Proceedings of the National Academy of Sciences*, page 201714532, 11 2017.

[165] George M Siouris. Missile Guidance and Control Systems. *Applied Mechanics Reviews*, 57(6):B32, 2004.

[166] N.A. Shneydor. *Missile Guidance and Pursuit: Kinematics, Dynamics and Control*. Horwood Publishing, Chichester, 1998.

[167] Kaushik Ghose, Timothy K. Horiuchi, P. S. Krishnaprasad, and Cynthia F. Moss. Echolocating bats use a nearly time-optimal strategy to intercept prey. *PLoS Biology*, 4(5):865–873, 4 2006.

[168] B S Lanchester and R F Mark. Pursuit and prediction in the tracking of moving food by a teleost fish (Acanthaluteres spilomelanurus). *The Journal of Experimental Biology*, 63(3):627–645, 12 1975.

[169] Dennis M Shaffer, Scott M Krauchunas, Marianna Eddy, and Michael K Mcbeath. How Dogs Navigate to Catch Frisbees. *Psychological Science*, 15(7):437–441, 2004.

[170] R. M. Olberg, R. C. Seaman, M. I. Coats, and A. F. Henry. Eye movements and target fixation during dragonfly prey-interception flights. *Journal of Comparative Physiology A: Neuroethology, Sensory, Neural, and Behavioral Physiology*, 193(7):685–693, 2007.

[171] Andreas F Haselsteiner, Cole Gilbert, and Z Jane Wang. Tiger beetles pursue prey using a proportional control law with a delay of one half-stride. *Journal of The Royal Society Interface*, 11(95), 6 2014.

[172] C. Chiu, P. V. Reddy, W. Xian, P. S. Krishnaprasad, and C. F. Moss. Effects of competitive prey capture on flight behavior and sonar beam pattern in paired big brown bats, Eptesicus fuscus. *Journal of Experimental Biology*, 213(19):3348–3356, 2010.

[173] Z. Jane Wang. On the instability and critical damping conditions. *arXiv*, pages 1–4, 2014.

[174] Brett R. Fajen and William H. Warren. Behavioral dynamics of intercepting a moving target. *Experimental Brain Research*, 180(2):303–319, 6 2007.

[175] Brett R. Fajen, William H. Warren, Selim Temizer, and Leslie Pack Kaelbling. A dynamical model of visually-guided steering, obstacle avoidance, and route selection. *International Journal of Computer Vision*, 54:13–34, 2003.

[176] Brett R Fajen and William H Warren. Behavioral dynamics of steering, obstacle avoidance, and route selection., 2003.

[177] Shiao-tong Kong, Foreign Application, and Priority Data. (12) United States Patent, 2011.

[178] Gregory F Bock. Guidance System with Varying Error Correction Gain, 2010.

[179] Caroline H. Brighton, Adrian L. R. Thomas, and Graham K. Taylor. Terminal attack trajectories of peregrine falcons are described by the proportional navigation guidance law of missiles. *Proceedings of the National Academy of Sciences*, page 201714532, 2017.

[180] Rafael Yanushevsky. *Modern missile guidance*. CRC Press, 2007.

[181] M. W. Fossier. The development of radar homing missiles. *Journal of Guidance, Control, and Dynamics*, 7(6):641–651, 1984.

[182] Kaushik Ghose, Timothy K Horiuchi, P S Krishnaprasad, and Cynthia F Moss. Echolocating Bats Use a Nearly Time-Optimal Strategy to Intercept Prey. *PLOS Biology*, 4(5):e108, 4 2006.

[183] Daniel Pohl, Stefan Kühne, İsmail Karaca, and Eckard Moll. Review of Coenosia attenuata Stein and its first record as a predator of important greenhouse pests in Turkey. *Phytoparasitica*, 40(1):63–68, 2 2012.

[184] H Wagner. Flight performance and visual control of flight of the free-flying housefly (Musca domestica L.) II. Pursuit of targets. *Phil. Trans. R. Soc. Lond. B*, 312(1158):553–579, 1986.

[185] M. F. Land. Motion and vision: Why animals move their eyes. *Journal of Comparative Physiology - A Sensory, Neural, and Behavioral Physiology*, 185(4):341–352, 1999.

[186] Anmo J. Kim, Jamie K. Fitzgerald, and Gaby Maimon. Cellular evidence for efference copy in Drosophila visuomotor processing. *Nature Neuroscience*, 18(9):1247–1255, 2015.

[187] Todd E. Shelly. Comparative foraging behavior of Neotropical robber flies (Diptera: Asilidae). *Oecologia*, 62(2):188–195, 1984.

[188] A E Bryson. Linear feedback solutions for minimum effort interception, rendezvous, and soft landing. *AIAA Journal*, 3(8):1542–1544, 1965.

[189] Thomas Alerstam. Radar observations of the stoop of the Peregrine Falcon Falco peregrinus and the Goshawk Accipiter gentilis. *Ibis*, 129:267–273, 2008.

[190] a Hedenström and F Liechti. Field estimates of body drag coefficient on the basis of dives in passerine birds. *The Journal of experimental biology*, 204(Pt 6):1167–75, 2001.

[191] Ludwig Prandtl and Oskar Kark Gustav Tietjens. *Applied hydro-and aeromechanics*. Dover publications, 1957.

[192] James H Marden. Maximum lift production during takeoff in flying animals. *Journal of Experimental Biology*, 130(1):235–238, 1987.

[193] James H Marden. Bodybuilding Dragonflies: Costs and Benefits of Maximizing Flight Muscle. *Physiological Zoology*, 62(2):505–521, 3 1989.

[194] Kenneth R. Morgan, Todd E. Shelly, and Lynn S. Kimsey. Body temperature regulation, energy metabolism, and foraging in light-seeking and shade-seeking robber flies. *Journal of Comparative Physiology B*, 155(5):561–570, 1985.

[195] F O Lehmann and M H Dickinson. The changes in power requirements and muscle efficiency during elevated force production in the fruit fly Drosophila melanogaster. *Journal of Experimental Biology*, 200(7):1133–1143, 1997.

[196] Kaushik Ghose, Jeffrey D Triblehorn, Kari Bohn, David D Yager, and Cynthia F Moss. Behavioral responses of big brown bats to dives by praying mantises. *Journal of Experimental Biology*, 212(5):693 LP – 703, 3 2009.

[197] Aaron J. Corcoran and William E. Conner. How moths escape bats: predicting outcomes of predator–prey interactions. *The Journal of Experimental Biology*, 219(17):2704–2715, 2016.

[198] M. May. Aerial defense tactics of flying insects. *American Scientist*, 79(4):316–328, 1991.

[199] J J Gibson. Visually controlled locomotion and visual orientation in animals. *British Journal of Psychology*, 49:182–194, 1956.

[200] R. M. Robertson and A. G. Johnson. Retinal image size triggers obstacle avoidance in flying locusts. *Naturwissenschaften*, 80(4):176–178, 1993.

[201] Lance F Tammero and Michael H Dickinson. Collision-avoidance and landing responses are mediated by separate pathways in the fruit fly, Drosophila melanogaster. *The Journal of experimental biology*, 205(Pt 18):2785–2798, 2002.

[202] Huai Ti Lin, Ivo G. Ros, and Andrew A. Biewener. Through the eyes of a bird: Modelling visually guided obstacle flight. *Journal of the Royal Society Interface*, 11(96), 2014.

[203] Wesley H Huang, Brett R Fajen, Jonathan R Fink, and William H Warren. Visual navigation and obstacle avoidance using a steering potential function. *Robotics and Autonomous Systems*, 54:288–299, 2006.

[204] David N. Lee, F. R.(Ruud) van der Weel, Tris Hitchcock, Eddie Matejowsky, and John D. Pettigrew. Common principle of guidance by echolocation and vision. *Journal of Comparative Physiology A*, 171(5):563–571, 1992.

[205] David N Lee. A theory of visual control of braking based on information about time-to-collision. *Perception*, 5(1974):437–459, 1976.

[206] Fabien Expert and Franck Ruffier. Flying over uneven moving terrain based on optic-flow cues without any need for reference frames or accelerometers. *Bioinspiration and Biomimetics*, 2015.

[207] D. N. Lee. The optic flow field : the foundation of vision. *Phil. Trans. R. Soc. Lond. B*, 290:169–179, 1980.

[208] Paloma T Gonzalez-Bellido, Hanchuan Peng, Jinzhu Yang, Apostolos P Georgopoulos, and Robert M Olberg. Eight pairs of descending visual neurons in the dragonfly give wing motor centers accurate population vector of prey direction. *Proceedings of the National Academy of Sciences*, 110(2):696 LP – 701, 1 2013.

[209] Sarah Nicholas, Jack Supple, Richard Leibbrandt, Paloma T Gonzalez-bellido, and Karin Nordstrom. Integration of Small- and Wide-Field Visual Features in Target-Selective Descending Neurons of both Predatory and Nonpredatory Dipterans. *J. Neurosci.*, 38(50):10725–10733, 2018.